Bioengineered tumour-targeted cytokines for tolerable immunotherapy combinations in solid tumours

Melanie Pascale Benedicte Herpels

Imperial College London
and
The Institute of Cancer Research
PhD supervisors: Dr. Jun Ishihara, Dr. Anguraj Sadanandam

A thesis submitted for the degree of
Doctor of Philosophy
Department of Bioengineering
Imperial College London
May 2024

Declaration of originality

I Melanie Herpels confirm that the work presented in this thesis is my own. Where information has been derived from other sources, I confirm that this has been indicated in the thesis.

Declaration of Copyright

The copyright of this thesis rests with the author. Unless otherwise indicated, its contents are licensed under a Creative Commons Attribution-Non Commercial-No Derivatives 4.0 International Licence (CC BY-NC-ND).

Under this licence, you may copy and redistribute the material in any medium or format on the condition that; you credit the author, do not use it for commercial purposes and do not distribute modified versions of the work.

When reusing or sharing this work, ensure you make the licence terms clear to others by naming the licence and linking to the licence text.

Please seek permission from the copyright holder for uses of this work that are not included in this licence or permitted under UK Copyright Law.

Abstract

Cytokines are small powerful molecules that allow inter-cellular communication within the tumour microenvironment (TME). Manipulating their levels can promote immune responses against challenging tumour types like triple negative breast cancer (TNBC) and pancreatic ductal adenocarcinoma (PDAC). Both have low survival rates, heterogeneous TMEs, and are mainly treated with toxic chemotherapy. In these tumour types, pro-inflammatory cytokines have failed in the clinic due to toxicity. Therefore, this PhD's overall objective is to bioengineer two pro-inflammatory cytokines (Interleukin-12 (IL-12) and Interferon γ (IFNγ) through both collagen-anchoring and masking to enhance their safety and efficacy. Each cytokine was conjugated to a collagen-binding domain (CBD) which accumulates in collagenous tumour stroma. Furthermore, CBD-IL12 was masked (M-CBD-IL12) to further reduce its toxicity. As such, the aims of this PhD are:

1. To produce a safe bioengineered IL-12 molecule (M-CBD-IL12) to treat immunologically distinct TNBC mouse models.
2. To test M-CBD-IL12 in immunologically distinct PDAC mouse models and understand the role of the *Kras*^{G12D} mutation in determining the observed responses.
3. To produce and test bioengineered CBD-IFNγ as alternative immunotherapy for PDAC.

Using the HEK293F and Expi293F expression systems, I produced the two wild-type cytokines and their novel bioengineered counterparts. I consequently tested their biological activity *in vitro*. I also demonstrated the tumour lysates, but not serum, to cleave the M-CBD-IL12 linker. *In vivo*, M-CBD-IL12 selectively cured murine TNBC in the EMT6 mouse model, but not 4T1. Differences in collagen and Transforming growth factor-β expression likely contributed to this differential response. I similarly observed differential IL-12 responses between PDAC mouse models, which I demonstrated to be *Kras*^{G12D}-related through co-culture systems. Finally, CBD-IFNγ remodelled the landscape of the immune-depleted PDAC model and reduced liver metastases. Overall, this thesis has identified subgroups within challenging tumour types that can be treated with safe and tolerable bioengineered cytokines.

Acknowledgements

I want to thank my supervisors Dr. Anguraj Sadanandam and Dr. Jun Ishihara for supporting me throughout this journey; thank you for allowing me to do a PhD in your laboratories. I have learnt a lot under your supervision.

I am very grateful to the Cancer Research UK Convergence Science Centre for funding this PhD.

A special thank you also goes to my colleagues in both laboratories, particularly Chanthirika Ragulan (The Institute of Cancer Research). She has been an amazing colleague and a fabulous friend. I am eternally grateful for her support throughout this PhD. Similarly, Pooja Kaur (Imperial College London) and Maria Nikolaidi (Imperial College London) were there to support me whenever I needed it. I would also like to put my friends Kiruththika Sivarasan (The Institute of Cancer Research), Rachel Luo (The Institute of Cancer Research), Dr. Yuta Ikami (The Institute of Cancer Research), Dr. Aasia Hussain (The Institute of Cancer Research), Chuyi Wang (Imperial College London), Daniya Edward (The Institute of Cancer Research), and Dr. Koichi Sasaki (Imperial College London) in the spotlight who helped, taught, advised, and encouraged me continuously throughout this PhD.

I would like to express my sincere appreciation to Dr. Aslan Mansurov (The University of Chicago) for his kind help with explaining techniques and providing me with advice whenever I was stuck. Despite the time difference, he always tried to help me out.

Many people have helped me on a technical level to whom I would like to express my sincere gratitude: Hari PS (Institute of Cancer Research) for teaching me about bioinformatics and helping me to prepare the bioinformatics figure, Will Murphy (The Institute of Cancer Research) for his continuous support and kindness in the Biological Services Unit (BSU, The Institute of Cancer Research), Alexis de Haven Brandon (The Institute of Cancer Research) and Claire Dobinson (The Institute of Cancer Research) for the support with the many intravenous injections, Sharon Gowan (The Institute of Cancer Research) for the help with the Wes Simple Western. Dr. Erik Wennerberg (The

Institute of Cancer Research) and Ricardo Sainz (The Institute of Cancer Research) for the help with flow cytometry and splenocyte culture. Finally, thank you to the flow cytometry core facility (Hira Ale, Sitara Ballal, and Dr. Shruti Daga) and the microscopy core facility (Louise Jones and Emma Westlund) for helping me with the setup and analysis of my experiments. At Imperial College, I would also like to thank Sharad Patel (Imperial College London) and Olivier Dubois (Imperial College London) for their advice and help with the animal work. Finally, a big thank you to Charanjit Singh (Imperial College London), who was very kind to help me with my animal study at Imperial College London.

I would also like to thank Dr. Paul O'Sullivan for being the person who introduced me to academia before this PhD and who has continued to provide me with advice, words of encouragement and a listening ear throughout.

My partner and family also played a major role in this PhD. Henry, I could not have completed this PhD without your endless support, words of encouragement, and valuable advice. I would also like to show my immense appreciation for my parents, who both listened to my stories, provided me with advice and comforted me in challenging times. I unfortunately lost my dad throughout the course of this PhD. Since he was so involved in my work, excited by my achievements, and concerned for my wellbeing over these last three years, I would like to dedicate this thesis to him. He always reminded me to never ever give up.

Table of Contents

Abstract **4**
Acknowledgements **5**
Table of Contents **7**
Table of figures **10**
List of tables **13**
Abbreviations **14**
Chapter 1.Introduction **18**
1.1 Tumours are complex and dynamic multicellular entities **19**
1.2 The challenges with manipulating cytokine levels **22**
1.3 Bioengineered immunotherapy for optimal pharmacokinetics and tolerability **23**
1.3.1 Immuno-cytokines 24
1.3.2 Antibody-drug conjugates 27
1.3.3 ECM-binding proteins for payload delivery 29
1.3.4 Modification for enhanced retention 30
1.3.5 Chimeric Antigen Receptor (CAR) T-cells 32
1.3.6 Masked pro-drugs 34
1.4 Masked CBD-IL12 (M-CBD-IL12) and CBD-IFNγ as targeted and tolerable immunotherapy candidates **36**
1.5 Triple negative breast cancer (TNBC) **40**
1.5.1 Epidemiology 40
1.5.2 Histological classification of breast cancer 40
1.5.3 Biological classification of breast cancer 42
1.5.4 Current therapeutic options for TNBC patients 44
1.5.5 The TNBC TME and its role in immunotherapy resistance 57
1.6 Pancreatic Ductal Adenocarcinoma (PDAC) **59**
1.6.1 Epidemiology 59
1.6.2 PDAC classifications and current potential therapeutic targets 60
1.6.3 Immunotherapy in PDAC 70
1.7 Introduction summary and research rationale **85**
1.8 Aims and thesis significance **87**
1.8.1 Aim 1. To produce a safe and tolerable bioengineered version of IL-12 for the treatment of two immunologically distinct TNBC mouse models. 87
1.8.2 Aim 2. To test M-CBD-IL12 in immunologically distinct PDAC mouse models and understand the role of the *KRAS*^{G12D} mutation in determining the observed responses. 87
1.8.3 Aim 3. To produce and test the efficacy of a bioengineered form of IFNγ as an alternative immunotherapy for PDAC. 88
Chapter 2.Materials & Methods **89**
2.1 Cell culture **89**
2.2 Co-culture experiments **89**
2.3 Transformation, bacterial culture, and plasmid amplification **90**
2.4 Transfection for protein production **90**
2.5 Protein purification **91**

2.6 Sodium Dodecyl Sulphate Polyacrylamide gel electrophoresis (SDS-PAGE) 91
2.7 Western blotting 92
2.8 Wes Simple Western 93
2.9 Ribonucleic acid (RNA) extraction and quantitative real time polymerase chain reaction (qRT-PCR) 93
2.10 Nanostring nCounter Transcriptomic profile 94
2.11 Enzyme-linked immunosorbent assay (ELISA) 94
2.12 LEGENDplex Mouse Inflammation Panel 94
2.13 M-CBD-IL12 linker cleaving 95
2.13.1 Western blot quantification 95
2.13.2 pSTAT4 quantification 95
2.14 Flow cytometry 96
2.15 Immunohistochemistry and Picro Sirius Red staining 97
2.15.1 Immunohistochemistry 97
2.15.2 Picro Sirius Red staining 98
2.16 Animal care 98
2.17 Single cell RNA sequencing (scRNA-seq) analysis 99
2.18 Statistical analysis 99
Chapter 3.Bioengineering interleukin 12 for tolerable immunotherapy in triple negative breast cancer 100
3.1 Introduction 100
3.2 Results 104
3.2.1 Mouse model selection 104
3.2.2 Protein production 106
3.2.3 The M-CBD-IL12 linker is cleaved by breast tumour lysate but not serum *in vitro* 114
3.2.4 *In vivo* evaluation of M-CBD-IL12 in the syngeneic EMT6 TNBC mouse model 116
3.2.5 In the syngeneic 4T1 TNBC mouse model, M-CBD-IL12 performs less well as monotherapy than in EMT6 138
3.2.6 Characterisation of the differences in immune landscape between EMT6 and 4T1 mouse models 140
3.2.7 Discussion 146
Chapter 4.The role of the *Kras^{G12D}* mutation in determining response of PDAC to IL-12-based therapy 154
4.1 Introduction 154
4.2 Results 157
4.2.1 The M-CBD-IL12 linker is cleaved by two syngeneic PDAC mouse models, but not by their serum 157
4.2.2 M-CBD-IL12 is significantly less toxic than wild-type IL-12 in non-tumour bearing mice 159
4.2.3 The efficacy of wild-type IL-12 and M-CBD-IL12 differs in two immunologically distinct PDAC mouse models 161
4.2.4 7947 tumours upregulate KRAS G12D protein expression to evade immune responses 167
4.2.5 Cancer cell lines generated from IL-12-treated 7947 tumours express significantly more KRAS G12D than from untreated 7947 tumours .. 171

4.2.6 The upregulated KRAS G12D expression following IL-12 therapy does not make 7947 more sensitive to MRTX1133 therapy 173
4.2.7 KRAS G12D inhibition in 7947 sensitises it to IL-12 therapy in the presence of immune cells 174
4.2.8 *iKras cell lines as an alternative to MRTX1133* 178
4.2.9 AK28385 and AK14838 mouse models respond to IL-12 in a similar manner as the 3275 mouse model 180
4.3 Discussion 184
Chapter 5.Bioengineered murine IFNγ for tolerable PDAC immunotherapy 189
5.1 Introduction 189
5.2 Results 192
5.2.1 Production of wild-type IFNγ and CBD-IFNγ 192
5.2.2 Both wild-type IFNγ and CBD-IFNγ upregulate PD-L1 expression on cancer cells *in vitro* 197
5.2.3 Wild-type IFNγ and CBD-IFNγ moderately prolong the survival of the MC38 CRC mouse model 199
5.2.4 CBD-IFNγ therapy remodels the TME of a syngeneic PDAC mouse model 201
5.3 Discussion 206
Chapter 6.Discussion and future directions 209
6.1 The fine balance between IL-12 and IFNγ efficacy and toxicity 209
6.2 Finetuning the immunosuppressive cytokines and their effect on IL-12 immunotherapy 211
6.3 Immune suppression at a genetic level may reduce the efficacy of IL-12 immunotherapy 214
6.4 Limitations and future directions 215
6.5 Conclusion 217
Reference List 219
Appendix 250
6.6 Permission to reprint 250
6.7 Gating strategy pSTAT4 experiment on $CD8^+$ T-cells 254
6.8 Gating strategy PD-L1 expression on PDAC cells following CBD-IFNγ treatment *in vitro* 254
6.9 Gating strategy EMT6 intervention study 1 255
6.10 Gating strategy EMT6 intervention study 2 256
6.11 Gating strategy 7947 CBD-IFNγ study 257
Publications and awards 258

Table of figures

Figure 1.1 Schematic representing the hallmarks of cancer 19
Figure 1.2 Important immune cell types within the tumour microenvironment 20
Figure 1.3 Schematic representing bioengineering techniques for cancer immunotherapy 23
Figure 1.4 The sources and targets of IL-12 and IFNγ 37
Figure 1.5 Schematic representing the IL-12 and IFNγ signalling pathways 38
Figure 3.1 Immunological characteristics of the immunotype TNBC classification 102
Figure 3.2 Classification of EMT6 as an immunotype 3- and 4T1 as an immunotype 1-dominant model using scRNA-seq 105
Figure 3.3 Wild-type IL-12 was successfully produced in HEK293F cells 108
Figure 3.4 Wild-type IL-12 was successfully producing in Expi293F cells 109
Figure 3.5 M-CBD-IL12 was successfully produced in HEK293F cells 111
Figure 3.6 M-CBD-IL12 production in Expi293F cells was unsuccessful 113
Figure 3.7 The M-CBD-IL12 linker is cleaved by breast tumour lysates but not serum 115
Figure 3.8 M-CBD-IL12 was tolerable *in vivo* and demonstrated anti-tumour effects against the MC38 CRC mouse model and the EMT6 TNBC mouse model 118
Figure 3.9 M-CBD-IL12 remodelled the TME of EMT6 tumours 120
Figure 3.10 M-CBD-IL12 suppressed myeloid cells, Tregs and exhausted $CD8^+$ T-cells in the EMT6 TME 124
Figure 3.11 Both wild-type IL-12 and M-CBD-IL12 increase dendritic cell and reduce T-cell populations in the spleen of EMT6 bearing mice 125
Figure 3.12 Wild-type IL-12, but not M-CBD-IL12 therapy, significantly increased PD-L1 expression in the spleen 126
Figure 3.13 M-CBD-IL12 and wild-type IL-12 significantly increased intratumoural IFNγ and significantly reduced intratumoural TGFβ1 in the EMT6 mouse model 128
Figure 3.14 M-CBD-IL12 triggers significantly less toxicity than wild-type IL-12 .. 131
Figure 3.15 The delayed effects of M-CBD-IL12 on EMT6 in the intervention setting 133

Figure 3.16 Lymphoid immune changes in the EMT6 TME following IL-12 immunotherapy 134
Figure 3.17 M-CBD-IL12 and wild-type IL-12 affect M1 and M2 macrophage proportions differently in the EMT6 TME 136
Figure 3.18 Expression of PD-1 in the EMT6 TME is raised with M-CBD-IL12 over time 137
Figure 3.19 M-CBD-IL12 monotherapy does not prolong the survival of 4T1-bearing mice 139
Figure 3.20 Spatial and RNA analysis of the TME of EMT6 and 4T1 tumours 141
Figure 3.21 4T1 tumours contain significantly less collagen 1 and 3 than EMT6 tumours 143
Figure 3.22 4T1 tumours contain significantly more TGFβ1 compared to EMT6 tumours 145
Figure 4.1 The M-CBD-IL12 linker is cleaved by PDAC tissue lysate but not by mouse serum 158
Figure 4.2 M-CBD-IL12 is significantly less toxic than wild-type IL-12 in non-tumour bearing Fvb/NCrl mice 160
Figure 4.3 M-CBD-IL12 moderately prolongs survival of mice bearing orthotopic 7947 PDAC tumours 163
Figure 4.4 Wild-type IL-12 suppresses 3275 tumour burden to a larger extent than M-CBD-IL12 164
Figure 4.5 The 7947 orthotopic PDAC mouse model is resistant to wild-type IL-12 166
Figure 4.6 7947 tumours express higher KRAS G12D protein levels than 3275 168
Figure 4.7 The TME and IL-12 therapy trigger an increase in KRAS G12D expression in 7947 170
Figure 4.8 ERK phosphorylation does not differ between cell lines generated from IL-12-treated or PBS-treated 7947 tumours 172
Figure 4.9 Both 7947 and 3275 respond similarly to KRAS G12D inhibition using MRTX1133 *in vitro* 174
Figure 4.10 7947 is more responsive to simultaneous IL-12 therapy and KRAS G12D inhibition in the presence of immune cells *in vitro* 176
Figure 4.11 The proportions of adaptive immune cell populations within splenocytes are not affected by MRTX1133 and IL-12 in a co-culture setting 178

Figure 4.12 The AK15376 *iKras* cell line responds similarly to MRTX1133 as 7947-luc/3275-luc *in vitro* 179
Figure 4.13 AK28385 *iKras* PDAC mouse model responds fully to IL-12 immunotherapy 181
Figure 4.14 $Kras^{G12D}$ withdrawal sensitises AK15376 PDAC mouse model to IL-12 therapy 183
Figure 5.1 CBD-IFNγ was successfully produced using the HEK293F expression system 194
Figure 5.2 Murine wild-type IFNγ was successfully produced in Expi293F cells .. 196
Figure 5.3 Both murine wild-type IFNy and CBD-IFNy upregulate PD-L1 expression on PDAC cells 199
Figure 5.4 Wild-type IFNγ and CBD-IFNy prolong survival of the MC38 CRC mouse model 200
Figure 5.5 CBD-IFNy therapy in a syngeneic metastatic PDAC mouse model 202
Figure 5.6 The combination of CBD-IFNγ + anti-PD-1 increases intratumoural T-cells and reduces dendritic cells in the 7947 PDAC mouse model 206

List of tables

Table 1.1 Important cytokines in the TME 21
Table 1.2 Biological subtypes of breast cancer 43
Table 1.3 Overview of therapeutic targets and strategies in TNBC clinical trials ... 44
Table 1.4 Completed immunotherapy clinical trials in TNBC 49
Table 1.5 Examples of currently ongoing TNBC immunotherapy clinical trials 55
Table 1.6 Overview of current therapeutic targets and strategies in PDAC clinical trials. 61
Table 1.7 Overview of clinical trials involving CPIs in PDAC 70
Table 1.8 An overview of clinical trials involving immune stimulatory molecules (agonists & inhibitors) and adoptive T-cell therapies in PDAC 74
Table 1.9 An overview of clinical trials involving cancer vaccines and oncolytic viruses in PDAC. 78
Table 2.1 Primary antibodies for western blotting and Wes Simple Western 92
Table 2.2 List of qRT-PCR primers 94
Table 2.3 List of flow cytometry antibodies used 97
Table 3.1 LEGENDplex cytokines and their roles in the TME 129
Table 3.2 Table demonstrating monocyte populations, their markers, and their functions 149

Abbreviations

Abbreviation	Full name
ADEX	Aberrantly differentiated endocrine exocrine
ALT	Alanine transaminase
AR	Androgen receptor
BL1	Basal-like 1
BL2	Basal-like 2
BAT	Bispecific antibody-targeted T-cells
BSA	Bovine serum albumin
CAF	Cancer-associated fibroblasts
CAR	Chimeric antigen receptor
Cav1	Caveolin-1
CBD	Collagen binding domain
CEA	Carcinoembryonic antigen
CKS2	Cyclin-dependent kinases regulatory subunit 2
CPI	Checkpoint inhibition
CPS	Combined positive score
CRC	Colorectal cancer
CTLA-4	Cytotoxic T-lymphocyte-associated antigen 4
CXCL	C-X-C motif chemokine ligand
CXCR	C-X-C chemokine receptor
DAMP	Damage-associated molecular pattern
DCIS	Ductal carcinoma *in situ*
DNA	Deoxyribonucleic acid
ECM	Extracellular matrix
EDTA	Ethylenediaminetetraacetic acid
EGFR	Epidermal growth factor receptor
ELISA	Enzyme-linked immunosorbent assay
EMT	Epithelial to mesenchymal transition
ER	Oestrogen receptor
EUS	Endoscopic ultrasonography
FAP	Fibroblast activation protein
FDA	Food and drug administration

FOLFOX	Leucovorin calcium (folinic acid), fluorouracil, and oxaliplatin
FOLFIRINOX	5-fluorouracil/leucovorin with irinotecan and oxaliplatin
GAF	Gamma-activated factor
GAP	GTPase-activating proteins
GAS	Gamma-activated site
GEF	Guanine nucleotide exchange factors
GM-CSF	Granulocyte-macrophage colony-stimulating factor
GTP	Guanosine triphosphate
GTPase	Guanosine triphosphatase
HBSS	Hank's balanced salt solution
HER	Human epidermal growth factor receptor
HH	Hedgehog
HLA	Human leukocyte antigen
HRR	Homologous recombinant repair
IDC	Invasive ductal carcinoma
IFNγ	Interferon γ
IGF-1R	Insulin-like growth factor receptor 1
IHC	Immunohistochemistry
iKras	Inducible *Kras*
ILC	Invasive lobular carcinoma
ILs	Interleukins
IL-12	Interleukin 12
IM	Immunomodulatory
IPMN	Intraductal papillary mucinous neoplasms
ISG	Interferon-stimulated gene
IVIS	In vivo imaging system
KO	Knockout
KRAS	Kirsten rat sarcoma virus
LAR	Luminal androgen receptor
LCIS	Lobular carcinoma *in situ*
LDS	Lithium dodecyl sulphate
LRRN3	Leucine rich repeat neuronal 3
M	Mesenchymal

MAPK	Mitogen-activated protein kinase
MCP-1	Macrophage chemoattractant protein 1
MDM2	Mouse double minute 2 homolog
MDSC	Myeloid-derived suppressor cell
MHC	Major histocompatibility complex
MMAE	Monomethyl auristatin E
MMP	Matrix metalloproteinase
mOS	Median overall survival
mPFS	Median progression-free survival
MSA	Mouse serum albumin
MSI-H	Microsatellite instability high
MSL	Mesenchymal stem-like
MST	Mean survival time
M-CBD-IL12	Masked CBD-IL12
NF-κB	Nuclear factor kappa B
NICE	National institute for health and care excellence
NK cells	Natural killer cells
NR	Non-reducing
NSCLC	Non-small cell lung cancer
NST	No special type
ORR	Objective response rate
PanINs	Pancreatic intraepithelial neoplasias
PARP	Poly ADP-ribose polymerase
PDAC	Pancreatic ductal adenocarcinoma
PDGFR	Platelet-derived growth factor receptor
PDX	Patient-derived xenograft
PD-L1	Programmed death ligand 1
PD-1	Programmed cell death protein 1
PEI	Polyethylenimine
PI3K	Phosphoinositide 3-kinase
PR	Progesterone receptor
PSR	Picrosirius red stain
QM	Quasi-mesenchymal

qRT-PCR	Quantitative real-time polymerase chain reaction
R	Reducing
RAF	Rapidly accelerated fibrosarcoma
RNA	Ribonucleic acid
SBRT	Stereotactic body radiation therapy
scFv	Single-chain variable fragment
scRNA-seq	Single cell RNA sequencing
SDS-PAGE	Sodium dodecyl sulphate polyacrylamide gel electrophoresis
shRNA	Short hairpin RNA
SMO	Smoothened
STAT	Signal transducer and activator of transcription
TAM	Tumour-associated macrophage
TAP	Transporter associated with antigen processing
TBS-T	Tris-buffered saline with tween
TDLU	Terminal duct lobular unit
TERT	Human enzyme telomerase reverse transcriptase sequence
TGFβ	Transforming growth factor β
TLR	Toll-like receptor
TMB	Tumour mutational burden
TME	Tumour microenvironment
TNBC	Triple negative breast cancer
TNFα	Tumour necrosis factor α
Treg	T regulatory cell
Trop-2	Trophoblast cell surface antigen 2
T-VEC	Talimogene laherparepvec
UMAP	Uniform manifold approximation and projection
UNS	Unstable
VEGF	Vascular endothelial growth factor
VHH	Variable heavy domain of heavy chain
VWF	Von Willebrand factor

Chapter 1. Introduction

Cancer is an inflammatory process. This was first recognised in 1863 by Virchow who identified abundant immune cells in tumours (1). In 1893, William Coley became the pioneer in exploiting the body's immune system to treat cancer (2). He found that repeated erysipelas infections could suppress the growth of sarcomas (2). Despite demonstrating this proof of concept, practical challenges such as the risk of infections prevented further development of William's idea (1). The question whether immunotherapy would be useful remained a topic of debate until the late 20th century with the approval of interferon (IFN) α2 for different cancer types (3). However, only the pivotal discovery of immune checkpoint inhibitors (CPI) caused cancer immunotherapy to gain significant interest (1). These antibodies, designed to reactivate exhausted T-cells, have revolutionised cancer treatment and have been approved for a plethora of different cancers (1).

However, many have now realised that inflammation in the context of cancer is a double-edged sword (4). On one hand, immunotherapy aims to trigger inflammation resulting in an anti-tumour immune response. On the other hand, intratumoural tumour-promoting inflammation is now recognised as one of the hallmarks of cancer due to its ability to support tumour progression (see Figure 1.1)(5). This is supported by the fact that multiple cancer types are associated with chronic inflammation such as Crohn's disease/ulcerative colitis with colorectal cancer, *H. pylori* infection with gastric cancer, pancreatitis with pancreatic cancer, and human papilloma virus infection with cervical cancer (4). Secondly, if inflammation is not targeted to the tumour in question, it can trigger severe autoimmune-like toxicity and ultimately lethal cytokine storms. The challenge we still face to this day is to modulate and target the inflammation to exclusively the tumour and, more specifically, the cytotoxic cell types within it.

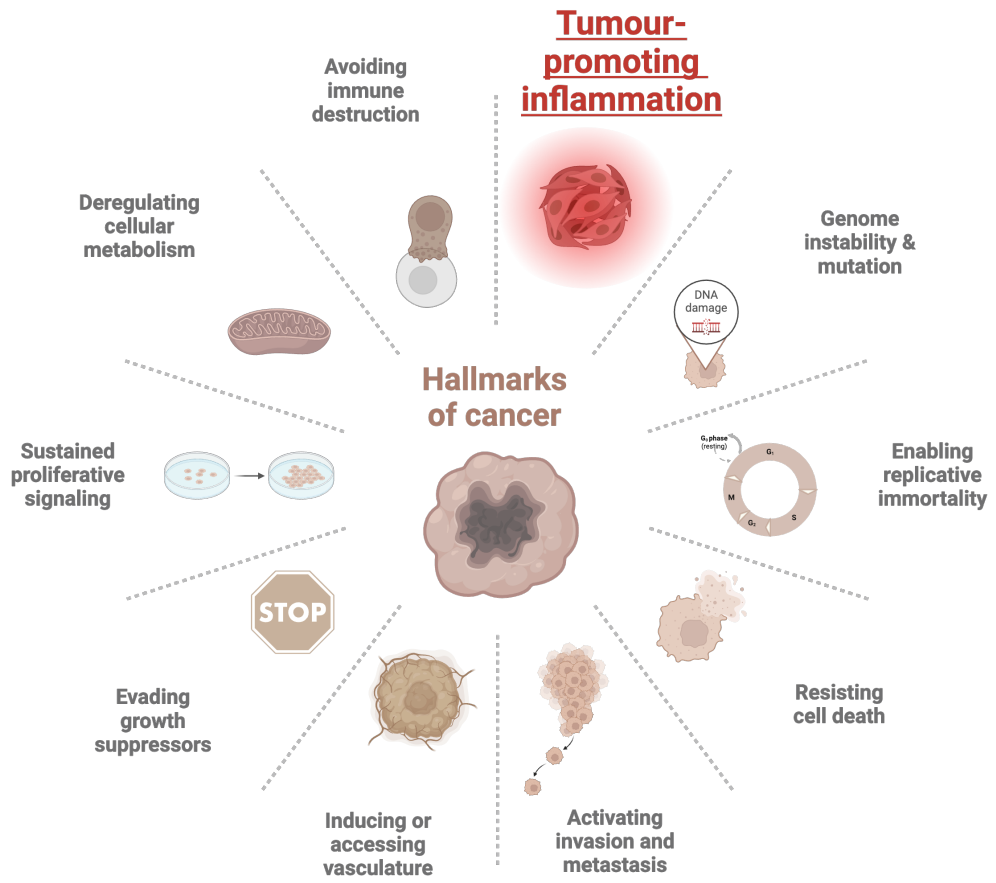


Figure 1.1 Schematic representing the hallmarks of cancer

This schematic is based on (5). Adapted from 'Hallmarks of Cancer (Circle Layout)', by BioRender.com (2024). Retrieved from https://app.biorender.com/biorender-templates

1.1 Tumours are complex and dynamic multicellular entities

Tumours are highly complex and dynamic entities that consist of a plethora of cell types (cancer cells, immune cells, stromal cells) and non-cellular components such as connective tissue, extra-cellular matrix (ECM), and blood vessels (6). Collectively, these are often referred to as the tumour microenvironment (TME) (7). Its exact composition heavily differs between tumour types and this has a large impact on patient outcomes and response to therapy (7). In terms of the non-cellular components of the TME, the ECM is a dense network of proteins and proteoglycans that is continuously remodelled by abundant proteases and eventually contributes to metastasis (7). The stromal cells within a tumour include fibroblasts, adipocytes, stellate cells, and endothelial cells (7).

They are involved in ECM production, a mechanism through which tumour growth can be promoted (7). Therefore, stroma is an umbrella term for stromal cells, immune cells, blood vessels, the basement membrane, lymphatic vessels, and ECM components (7). In more aggressive cancer types like pancreatic cancer, the dense stroma can form a barrier that prevents efficient drug and immune cell infiltration, reduces blood supply to the tumour and plays a major role in promoting metastasis (7, 8). However, in such tumour types, attempts to deplete the ECM have unfortunately also been unsuccessful, highlighting some tumour restrictive effects of the stroma (9).

Dendritic cell 	• Phagocytosis • Antigen presentation to T-cells through MHC class II, T-cell activation • Cytokine release • Co-stimulation
Macrophage 	• Phagocytosis • Antigen presentation to T-cells through MHC class II, T-cell activation • Cytokine release • Some pro-inflammatory, some anti-inflammatory effects
Neutrophil 	• Phagocytosis and digestion • Secretion of growth factors, reactive oxygen species, reactive nitrogen species, proteases • Cytokine release • Can promote angiogenesis
B-cell 	• Phagocytosis • Antigen presentation to T-cells through MHC class II, T-cell activation • Antibody production • Cytokine release
T-cell 	• Helper T-cells develop from naive $CD4^+$ T-cells ◦ Th1: develop upon IL-12 exposure, pro-inflammatory, cause IFNγ production ◦ Th2: develop upon IL-4 exposure, immunosuppressive, produce IL-4, IL-5, IL-13 ◦ Th17: develop upon IL-6 and TGFβ exposure, secrete IL-17, IL-21, IL-22 ◦ Tregs: develop upon TGFβ exposure, immunosuppressive, reduce T-cell cytotoxicity, secrete IL-10/TGFβ • Cytotoxic/memory $CD8^+$ T-cells: eliminate cancer cells through MHC class I
NK cell 	• Target cell lysis through granzymes or perforins • Cytokine production

Figure 1.2 Important immune cell types within the tumour microenvironment

Schematic representing some important immune cell types in the tumour microenvironment and their functions. This schematic was based on (7) and was created on Biorender.com.

The immune cells within a tumour have context-dependent functions that change continuously, some of which have been described in Figure 1.2 (7). Each tumour is unique and may contain these cell types at different proportions which may impact clinical outcomes and response to therapy (7). Particularly patients with tumours that are depleted in pro-inflammatory immune cells like T-cells or where they are exhausted tend to have worse prognoses (7). Therefore, the purpose of immunotherapy is to recruit and activate intratumoural immune cells to enhance their ability to kill cancer cells and shrink the tumour. Since immune cells heavily interact with each other and the stroma through a variety of different molecules such as checkpoints, growth factors, proteases, and cytokines, they offer an opportunity for manipulation (7). Firstly, checkpoints such as PD-1, PD-L1, and CTLA-4 are molecules that are normally expressed on immune cells to prevent excessive immune activation under physiological circumstances (10). In a cancer context, these molecules can be heavily overexpressed to suppress anti-tumour immune cells whereby promoting cancer cell survival (10). Secondly, cytokines are small yet potent proteins that allow inter-cellular communication, either between nearby cells through autocrine and paracrine action or on distant cells (11). Cytokine is an umbrella term for chemokines, monokines, lymphokines, IFNs, and interleukins (ILs) (11). IFNs are mainly known as anti-viral molecules but have demonstrated strong anti-proliferative and inflammatory properties that can suppress tumour growth (11, 12). ILs are cytokines that are generated by leukocytes and serve to act on other leukocytes, with either pro-inflammatory or anti-inflammatory effects (11). An overview of important intratumoural cytokines is given in Table 1.1.

Table 1.1 Important cytokines in the TME

Table explaining important pro- and anti-inflammatory cytokines and their sources and targets. Table is based on (13, 14).

Cytokine	Source	Target
Pro-inflammatory		
IL-12	Macrophages, dendritic cells, monocytes, neutrophils, B-cells	T-cells, NK cells
IFNγ	T-cells, NK cells	Cancer cells, dendritic cells, macrophages, Th1 cells
TNFα	Monocytes, macrophages, dendritic cells, NK cells, T-cells, endothelial cells	Macrophages, fibroblasts, endothelial cells, highly context-dependent
IL-2	$CD4^+$ helper T-cells	T-cells, B-cells, NK cells, monocytes, macrophages

Anti-inflammatory		
IL-10	Helper T-cells, monocytes, macrophages, dendritic cells	Mast cells, $CD8^+$ T-cells, NK cells, B-cells
IL-4	$CD4^+$ T-cells (Th2 cells), NK cells, basophils, mast cells, eosinophils	Mast cells, eosinophils, neutrophils, NK cells, endothelial cells, fibroblasts
TGFβ	Fibroblasts, epithelial cells, M2 macrophages	Tregs, neutrophils, macrophages, NK cells, $CD8^+$ T-cells

1.2 The challenges with manipulating cytokine levels

By adjusting cytokines or checkpoints, we have become capable of altering the TME to promote immune activation and therefore cancer cell death. For example, the discovery of CPIs, antibodies against checkpoints, has allowed boosting of T-cell activity in the tumour (10). These molecules are highly successful and have been approved for a variety of cancer types (10). Administration of recombinant cytokines has also been trialled extensively as a means of triggering an anti-tumour immune response and suppressing tumour burden (11). However, their success has been more limited. Unfortunately, the small size of cytokines results in rapid renal clearance, and they are readily degraded by proteases which leads to a short half-life in the bloodstream (15). This means they usually cannot reach the tumour to exert their desired effect (15). Secondly, their small size also allows them to diffuse across the endothelium into non-cancerous tissues, where they trigger autoimmune-like inflammation (16, 17). This inflammation makes it challenging for patients to tolerate systemic recombinant cytokine therapy (16, 17). Moreover, most clinical trials on solid tumours rely on combination immunotherapy, especially for tumour types with a complex and immunosuppressive TME. It is therefore crucial to acknowledge that combination therapies are usually associated with cumulative toxicity; the combination of durvalumab (anti-PD-L1 antibody) and tremelimumab (anti-CTLA-4 antibody) not only showed minor efficacy, but also triggered significant treatment-induced side effects of grade 3 or higher in 22% of patients compared to 6% in the monotherapy arm (18). In addition, in a phase I study of nivolumab (anti-PD-1 antibody) in combination with gemcitabine and nab-paclitaxel, 96% of patients had at least one treatment-associated adverse event (grade 3/4) and 36% discontinued treatment for this reason (19). Cumulatively, these aforementioned factors have limited the translation of cytokine therapy for solid tumours into the clinic.

1.3 Bioengineered immunotherapy for optimal pharmacokinetics and tolerability

A promising strategy to improve cytokines' half-lives, enhance their efficacy, and reduce their toxicity is through bioengineering. Different bioengineering techniques have been used to develop inventive and novel forms of immunotherapy. Examples are masking of pro-drugs, cytotoxic conjugates, and ECM anchoring of molecules or a combination of multiple techniques (see Figure 1.3). These usually involve tumour-specific localisation and activation which renders the active compounds less toxic. The results of some commonly used bioengineering strategies have been described below.

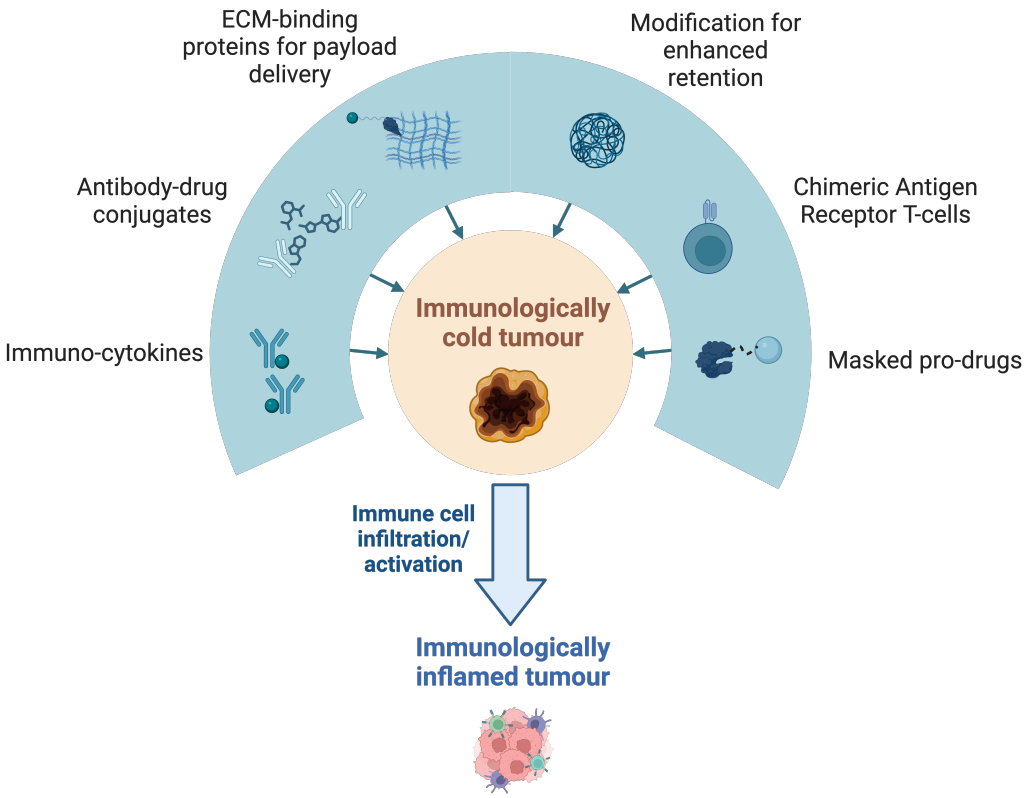


Figure 1.3 Schematic representing bioengineering techniques for cancer immunotherapy

Adapted from 'Mechanisms of Cancer-associated Fibroblast Activation', by BioRender.com (2024). Retrieved from https://app.biorender.com/biorender-templates

1.3.1 Immuno-cytokines

Immuno-cytokines are antibody-cytokine conjugates. By exploiting the affinity of the antibody for its target, it serves as a delivery vehicle for the cytokine (20). The purpose of the cytokine is to trigger a localised anti-tumour immune response by activating or recruiting immune cells into immune-depleted tumours. This conjugation technique should reduce off-target effects of the cytokine by giving it tumour specificity (20). The conjugates can either consist of a full sized or component of an antibody (Fab, scFv) (20). The former will augment the half-life of said cytokine in the bloodstream, yet penetrates the tumour stroma less efficiently, whilst the latter is less stable yet more capable of infiltration (20). Dougan and colleagues conjugated IL-2 and IFNγ, both pro-inflammatory cytokines, to a Variable Heavy domain of Heavy Chain (VHH; nanobody) that targets PD-L1 (21). This compound was promising in pre-clinical models of PDAC; it reduced tumour burden by 50% in contrast with irrelevant VHH-cytokine fusion proteins or anti-PD-L1 monotherapy. IL-2 and IFNγ conjugated to the VHH increased $CD8^+$ T-cells and reduced CD11b+ cells in the TME whilst increasing the M1/M2 ratio of macrophages, respectively (21). However, the lack of specificity of anti-PD-L1 for the tumour stroma could lead to dose-limiting toxicity (21).

A second example is Simlukafusp alfa (FAP-IL2v, RO6874281/RG746) (22). It is an immuno-cytokine that contains an anti-fibroblast activation protein α (anti-FAP) antibody and a form of IL-2 with enhanced affinity for the IL-2Rβγ and reduced affinity for IL-2Rα (22). This modification enhances the cytokine's ability to activate effector $CD4^+$/$CD8^+$ T-cells and Natural Killer (NK) cells whilst reducing T regulatory cell (Treg) activation compared to its wild-type counterpart (22). FAP is a surface glycoprotein and a human cancer-associated fibroblast (CAF) marker that is highly expressed in several solid tumour types and is associated with worse prognosis (23, 24). This is particularly the case if it is expressed on the cancer cells rather than the CAFs (24). The FAP-IL2v immuno-cytokine was administered with anti-PD-L1 weekly for 5 weeks in pancreatic orthotopic syngeneic Panc02 mouse models (22). The combination immunotherapy significantly prolonged median survival compared to anti-PD-L1 or FAP-IL2v monotherapy (22). Similarly, a CD40 agonist in combination with FAP-IL2v significantly prolonged the median survival to 93 days, compared to 45 days with CD40 agonist monotherapy and 40 days with FAP-IL2v monotherapy (22). Finally, for the triple

combination of FAP-IL2v, anti-PD-L1 and anti-CD40, the median survival was not reached due to high efficacy and the surviving animals failed to regrow tumours upon a rechallenge (22).

Cergutuzumab amunaleukin, (CEA-IL2v, RG7813) has a similar structure to FAP-IL2v, however, a bivalent anti-carcinoembryonic antigen (CEA) antibody is used instead of anti-FAP (25). CEA was found to be expressed at high or moderate intensity in 90% of pancreatic cancer, 95% of colorectal cancer (CRC), 40% of breast cancer, and 60% of non-small cell lung cancer (NSCLC) samples compared to normal tissues through immunohistochemistry (IHC), making it a suitable target (25). The same IL-2 variant (IL2v) was used as in FAP-IL2v, which lacks the ability to bind to CD25 to reduce IL-2 toxicity and vascular leak syndrome (22). CEA-IL2v monotherapy was found to significantly prolong median survival from 42 days in controls to 63 days in a CEA-expressing MC38 cell line. It was also tested in orthotopic CEA-expressing Panc02 mouse models as monotherapy and median survival was significantly prolonged to 42 days compared to 30 days in mice with vehicle control (25). The molecule was also found to accumulate preferentially in CEA-expressing areas within the pancreatic tumour over healthy pancreas (25). Again, the addition of anti-PD-L1 further improved median survival to 57 days in contrast with the 29 days of vehicle control mice (25).

A fourth immune-cytokine example is L19-IL2, where L19 is a human single chain Fv (fragment crystallisable) antibody, which targets the fibronectin extradomain B, linked to human IL-2 (26). Fibronectin is an ECM component and its extradomain B is associated with tumour growth and neoangiogenesis (26). It is absent in most healthy tissues and may be introduced into fibronectin in tissues undergoing rapid remodelling and neoangiogenesis such as tumours (26). As such, the extradomain B of fibronectin offers a degree of tumour specificity (26). Nude mice bearing orthotopic DanG pancreatic tumours were treated with either wild-type IL-2 or L19-IL2 for 10 days (26). Contrary to IL-2 therapy, which only demonstrated a mild therapeutic benefit at high doses, a significant reduction in tumour volume was noted with L19-IL-2 therapy. At the lower dose, tumour volume was reduced to 21.4%, while at the higher dose, it was further decreased to just 2.7% compared to the control group. No off-target effects of the therapy were noted, whilst an increase in CD11b+ cells (>4-fold) and NK cell (>70-fold) infiltration was noted in the tumours following L19-IL2 therapy (26). NK cell

depletion completely obliterated the observed anti-tumour response, suggesting the response is NK-cell-mediated (26). This same molecule was also tested in CRC mouse models in combination with radiotherapy. L19-IL2 in combination with 15Gy caused an abscopal effect that led to cure in 20% of mice, which was dependent on T-cells (27).

The safety of L19-IL2 was confirmed in a phase I/II clinical trial in solid tumours (28). The expansion phase involved 12 patients with metastatic renal cell carcinoma who received the recommended phase II dose (28). The toxicities could be controlled appropriately and the median progression-free survival (mPFS) was found to be 8 months (28). Around 50% of patients has stable disease (28). Finally, L19-IL2 was then combined with gemcitabine for PDAC patients in a phase I clinical trial (NCT01198522). Unfortunately, the trial was terminated due to lack of recruitment.

Bintrafusp Alfa (M7824) is more of a bifunctional antibody that has been heavily studied in a clinical setting (29). It consists of an anti-PD-L1 monoclonal antibody and the extracellular domain of the Transforming growth factor (TGF)β receptor II (29). The latter is meant to operate as a TGFβ trap (29). M7824 had promising anti-tumour effects in mouse models, and it was therefore trialled in advanced solid tumour patients as a monotherapy in a dose-escalation trial (NCT02517398) (29). Unfortunately, three of the nineteen patients stopped the course of M7824 prematurely due to treatment-related side effects like colitis, bullous pemphigoid, and gastroparesis, which meant that the maximum tolerated dose was not reached (29). One of the patients who discontinued treatment with metastatic human papillomavirus-positive cervical cancer had a complete response (29). A second patient with pancreatic cancer demonstrated a durable partial response out of the 5 PDAC patients enrolled in the study (29). Another PDAC patient had prolonged stable pancreatic cancer (29). The partially responding patient had a mismatch repair deficient PDAC, making it more susceptible to CPIs and representative of only ~1% of all PDACs (29). Unfortunately, the partial response was observed at 4.5 months, but the disease progressed after 10.5 months into the study suggesting resistance to therapy (29).

In another trial, M7824 was clinically tested in combination with gemcitabine in heavily pre-treated PDAC patients, but this trial was terminated prematurely due to a treatment-related death (NCT03451773) (30). In another trial (NCT04327986), M7824 was

combined with Stereotactic Body Radiation Therapy (SBRT) and the NHS-IL12 (M9241) immuno-cytokine (30). The latter consists of two recombinant human IL-12 heterodimers, that have each been conjugated to the human monoclonal NHS76 antibody (31). This antibody binds exposed histone/DNA complexes, which are highly prevalent in areas of tissue necrosis, mainly located in the tumour stroma (31). However, this trial was similarly terminated prematurely due to the worsening risk:benefit ratio for the M7824 group (30).

In a phase 1b/II trial on advanced gastric cancer patients, it was tested in combination with paclitaxel (32). The mPFS was 3.8 months with an objective response rate (ORR) of 28%, making it a modest efficacy (32). M7824 was also trialled in a variety of other cancer types such as triple negative breast cancer (TNBC)(33), advanced squamous cell carcinoma of the head and neck (34), NSCLC (35), and oesophageal adenocarcinoma (36).

A fusion protein (SHR-1701) with similar targets, PD-L1 and TGFBR2, was administered to patients with recurrent or metastatic cervical cancer. These patients had an ORR of 15.6% and a disease control rate of 50% with limited adverse events (NCT05179239)(37). It was also trialled in combination with gemcitabine/nab-paclitaxel in patients with advanced or metastatic PDAC (NCT04624217)(30, 38). There was a 92.9% incidence of SHR-1701-related adverse events, with even an SHR-1701-related death following gastrointestinal bleeding (30, 38). The ORR of patients having undergone one or more post-baseline radiographic assessments was 36.5%, suggesting a degree of efficacy (30, 38). Further results of this trial are pending.

1.3.2 Antibody-drug conjugates

Antibody-drug conjugates allow for targeted delivery of drugs into the tumour stroma. They operate in a similar way to immuno-cytokines yet with a cytotoxic drug instead of a cytokine, again to reduce toxicity of the drug whilst maintaining its cytotoxic effect towards cancer cells. A humanised anti-Epidermal Growth Factor Receptor (EGFR) monoclonal antibody (RC68) and Monomethyl Auristatin E (MMAE), a molecule that exerts cytotoxicity by affecting microtubules, have been conjugated through two

cleavable linkers (39). Both at low (5 mg/kg) and high (10 mg/kg) doses, the conjugate had a more profound effect on the growth of BXPC-3 PDAC xenografts than gemcitabine hydrochloride (60 mg/kg) (39). The high dose resulted in a significant reduction in tumour volume when compared to gemcitabine, suggesting a dose-dependent efficacy (39). In a non-small cell lung cancer mouse model H125, this molecule significantly suppressed tumour burden at the 10 mg/kg dose to an even larger extent than docetaxel (40). Unlike with docetaxel, the body weight of the mice was however not affected by this drug, highlighting the importance of bioengineering to reduce toxicity (40).

The anti-EGFR antibody (cetuximab) has also been used to deliver chemotherapy agents packaged into nanoparticles into the tumour stroma of solid tumours. The use of nanoparticles prevents rapid degradation, toxicity, or clearance from the circulation (41). This technique was applied to deliver temozolomide-loaded nanoparticles into glioblastoma, CRC, and melanoma cell lines using EGFR-receptor-mediated endocytosis *in vitro* (42). In a mouse model bearing a PANC-1 tumour, a cetuximab-nanoparticle conjugate was administered intravenously on 5 different occasions (41). By day 28 following tumour inoculation, the conjugate had significantly suppressed tumour volume; a 50% difference was observed between cetuximab-nanoparticle conjugate treated tumours and blank-nanoparticles or IgG-nanoparticle controls (41).

A third example is the anetumab ravtansine antibody-drug conjugate, that was developed using an anti-mesothelin antibody and the maytansinoid DM4 drug, a potent cytotoxic drug (43). Mesothelin is overexpressed in a variety of solid tumours and its expression is restricted in healthy tissues (43). This makes it an attractive anti-tumour target (43). Due to encouraging pre-clinical study findings in patient-derived xenografts, this anetumab ravtansine antibody-drug conjugate was tested in a phase I clinical trial involving patients with different solid tumours (NCT01439152) (43). Among 148 patients with either mesothelioma, ovarian, pancreatic, non-small cell lung, or breast cancer, a single complete response, 11 partial responses and 66 cases of stable disease were observed (43). A phase Ib trial has been completed on the conjugate in combination with gemcitabine in multiple solid tumour types, however, the results have not yet been reported (NCT03102320)(44). In ovarian cancer, anetumab ravtansine was tested in combination with pegylated liposomal doxorubicin (NCT02751918)(45). One complete

and 17 partial responses were observed out of the 65 patients and the ORR was 27.7% (45).

1.3.3 ECM-binding proteins for payload delivery

A third engineering technique to enhance efficacy of immunotherapy in solid tumours has been the conjugation of a cytokine to a protein with high affinity for an ECM component. Therefore, the cytokine payload can accumulate locally in the tumour stroma, whereby prolonging its half-life and enhancing its efficacy. This technique allows the compound to be injected intravenously rather than intratumourally. Both IL-2 and IL-12 were conjugated to lumican and mouse serum albumin (MSA). Lumican is a proteoglycan in the ECM with a high affinity for collagens type I/IV (46). Due to the abundance of collagen in the stroma of several solid tumour types, lumican should enhance the cytokines' retention in the stroma and prevent dissemination following intratumoural injection (46). Addition of the MSA increases the molecular weight of the molecule leading to enhanced retention in the tumour stroma (46). Lumican-MSA-IL2 was tested in B16F10 tumours in combination with the TA99 antibody, a monoclonal antibody that targets tyrosinase-related protein 1, which is a glycoprotein and differentiation marker expressed in melanoma cells (47). The TA99 antibody is known to be effective in the treatment of B16F10 melanomas in combination with other immunotherapy modalities (48). This combination immunotherapy (lumican-MSA-IL2 + TA99) was found to significantly reduce tumour burden with 15 out of 17 mice achieving a complete response (46). In contrast, only 4 out of 17 mice treated with MSA-IL2 + TA99 were cured, highlighting the role of the lumican in enhancing the efficacy of the cytokine (46). Similarly, either of the components as monotherapies only moderately impacted tumour burden (46). Despite this molecule being a great candidate for intratumoural administration into easily accessible tumours, intravenously injected immunotherapy is considerably less invasive for the patients.

Many have therefore attempted to bioengineer cytokines for targeted delivery into the tumour stroma following intravenous injection. An example is the TNFα-CSG fusion protein, consisting of the anti-tumour cytokine TNFα and the CSG peptide ligand (49). CSG targets laminin-nidogen complexes in the ECM, and it does not tend to localise into non-cancerous tissues (49). Following intravenous injection, TNFα-CSG

significantly prolonged survival of mice bearing breast tumours (4T1/RT5), triggered intratumoural infiltration of cytotoxic T-cells and altered tumour stiffness (49). These findings were achieved with less toxicity than normally expected from TNFα (49). This proof-of-concept study demonstrates the ability of CSG to bind tumour ECM and thereby reduce peripheral toxicity. This drug delivery system could be translated to other pro-inflammatory cytokines and cancer types.

Similarly, the Ishihara laboratory designed a collagen-binding domain (CBD) from the A3 domain of Von Willebrand Factor (VWF) which binds to collagens type I and III with high affinity (50, 51). The conjugation of this CBD to anti-tumour cytokines allows for rapid delivery of the cytokines into multiple solid tumour mouse models (50, 51). This technique has successfully suppressed tumour growth and prolonged survival for CPI therapy, IL-2, CCL4, and IL-12 in breast cancer, melanoma, and CRC models (50-52). The CBD conjugation technique also significantly suppressed the concentration of circulating IFNγ and ALT (liver toxicity marker), suggesting this technique reduces peripheral toxicity (51).

1.3.4 Modification for enhanced retention

A strategy to increase the half-life and alter the hydrophobicity and conformation of compounds is to conjugate them to polymers (53). This increases the molecule's molecular weight and can help with solubility and therefore drug administration (53). By increasing the molecular weight of a compound, it can be more easily retained in the tumour stroma after for example intratumoural injection and prevents rapid renal clearance from the system. It however does not render the compound specific to the tumour stroma meaning modified compounds still require intratumoural administration, which is often not feasible in clinical practice. Polyethylene glycol (PEGylation) is a commonly used polymer in multiple solid tumours; an example is the approval of PEGylated IFN-α-2b for the adjuvant treatment of melanoma (54, 55). IL-10 is a commonly PEGylated cytokine since it has been shown to play a role in mediating cytotoxic T-cell infiltration and IFNγ and granzyme expression in $CD8^+$ T-cells, despite some controversy due to its known role as an anti-inflammatory cytokine (56).

In a Human Epidermal Growth Factor Receptor 2 (HER2) transgenic breast cancer mouse model, PEGylated IL-10 (PEG-IL10, pegilodecakin) suppressed tumour growth and induced a significant increase in $CD8^+$ T-cells (56). A phase Ib clinical trial assessed the safety of PEG-IL10 as monotherapy or in combination with either FOLFOX (in PDAC)(57, 58) or CPIs in multiple cancer types (NSCLC, melanoma, renal cell carcinoma, TNBC)(59, 60) (NCT02009449). In the advanced cancer types, PEG-IL10 monotherapy triggered an overall response rate of 27% in patients with renal cell carcinoma and a partial response was observed in a patient with uveal melanoma (60). In a later study, PEG-IL10 was combined with pembrolizumab or nivolumab (anti-PD-1 antibodies)(59). Toxicity was common with grade 3 or 4 events being noted in 66% of patients and an objective response was seen in 43% of patients with NSCLC, 10% of melanoma patients and 40% of renal cell carcinoma patients (59). In the PDAC patients, the overall response with the combination immunotherapy (PEG-IL10+FOLFOX) was 14%, with a complete response in 2 patients (57, 58). Interestingly, a reduction in the PDAC tumour marker CA19-9 was noted in 66.7% of patients, of which 41.7% had a reduction of ≥ 60% (57, 58). Anaemia and thrombocytopenia were noted in almost half of the patients (57, 58). This was improved by adjusting the dosing schedule and introducing a 2-day rest (57, 58).

As a result of these promising findings a phase III clinical trial (SEQUOIA trial, NCT02923921) was initiated comparing FOLFOX alone to FOLFOX + PEG-IL10 as a second-line therapy for PDAC patients who did not respond to prior gemcitabine-based therapy (61). Within of the 567 participants, virtually no difference was seen between the treatment arms in terms of median overall survival (mOS), PFS, and ORR and toxicity was not drastically altered (61). These findings could potentially be attributed to IL-10's immunosuppressive role and potential differences in the immune landscape in previously treated late-stage PDACs. This technique could however be translated to other pro-inflammatory cytokines to enhance their retention in tumour tissues and reduce toxicity.

The conjugation of IL-12 to aluminium hydroxide, a compound commonly used in the production of vaccines, lead to retention of the cytokine in the tumour stroma for over a week (62). A single intratumoural dose of modified IL-12-ABP-p + alum lead to a significantly prolonged survival of mice with Ag104A, B16F10, and MC38 tumours either

as monotherapy or when combined with other immunotherapy modalities such as anti-PD-1 (B16F10/MC38) or TA99 (B16F10) (62). The difficulty with such bioengineered compounds that have enhanced retention is that they require intratumoural injection, which is not feasible for many cancer types. Molecules suitable for intravenous or subcutaneous injection are usually small and targeted to the tumour stroma for easy infiltration.

1.3.5 Chimeric Antigen Receptor (CAR) T-cells

Adoptive T-cell therapy involves the collection of a patient's T-cells, their amplification, and reintroduction back into the patient. This could be particularly useful for treating immune-depleted tumours. Although this expanded T-cell population may help mount an anti-tumour immune response, these T-cells lack tumour specificity (63). A possible method to enhance the efficacy of T-cell therapy is by transducing T-cells with a Chimeric Antigen Receptor (CAR), a bioengineering technique that causes T-cells to recognise tumour antigens as foreign (63). This triggers an anti-tumour immune response, which leads to the elimination of cancer cells and consequently an increased release of tumour antigens and enhanced T-cell activity (63). The high response rate of B-cell malignancies and leukaemia to CAR T-cell therapy has led to its approval (64). For optimal efficacy of CAR T-cells, the CAR is normally designed to target tumour antigens, an example of which are immune checkpoints. Therefore, third-generation CAR T-cells were designed to target the abundant PD-L1 on cancer cells (65). They either fused the extracellular domain of the PD-1 immune checkpoint or the single chain variable fragment (scFv) of the anti-PD-L1 monoclonal antibody (both bind to PD-L1 on cancer cells) to intracellular signalling domains (CD3ζ, CD28, 4-1BB) (65). These two types of CAR T-cells killed CFPAC1 PDAC cells *in vitro* and induced a tumour regression over 80% in both xenograft/orthotopic pre-clinical mouse models of PDAC (65). This proof-of-concept study allows translation to other immunomodulatory pathways such as LAG3 and CTLA-4. Unfortunately, the extensive PD-L1 expression on myeloid-derived suppressor cells (MDSCs) and macrophages could lead to non-specific effects of the CAR-T-cells and therefore it may create autoimmune-like toxicity (65).

Using a more tumour-specific target for CAR T-cells could avoid non-specificity. An example is mesothelin, a surface molecule that is expressed at low levels on mesothelial cells in, for example the pleura or pericardium (66). It is however highly overexpressed in PDACs, ovarian tumours, and mesotheliomas (66). Haas and colleagues developed a lentiviral-transduced CAR that is specific to mesothelin (CART-meso) (67). In a phase I clinical trial, a single infusion of the CART-meso resulted in stable disease in 11/15 patients with various chemotherapy-unresponsive tumours (67). A reduction in tumour burden was seen in a patient with ovarian adenocarcinoma, although the effect was still too mild to be considered a partial response (67). The therapy triggered toxicity in one of the PDAC patients, particularly worsening jaundice, abdominal pain, which was later attributed to *Klebsiella* bacteraemia (67). The patient passed away shortly after with multiple PDAC metastases upon autopsy (67).

Beatty and colleagues then bioengineered mesothelin-targeted CAR T-cells that employ *in vitro* transcribed mRNA encoding the CAR, making it transiently expressed and less toxic (68). In a first phase I clinical trial they tested the CAR on a single mesothelioma and a single PDAC patient (NCT01355965) (68). The efficacy in the PDAC patient was limited to stable disease and a reduction in the maximum standardised uptake was seen on PET/CT in the primary tumour and metastases (68). They therefore explored the same CAR T-cells in a second phase I clinical trial on PDAC patients and 2 out of 6 patients had stable disease and progression-free survival times of 3.8 and 5.4 months (NCT01897415) (69). Since a reduction was seen in the metastases in some of the patients, it would be worth further investigating this technique in combination with standard of care chemotherapy (69).

Beside a CAR, patient T-cells could be transduced with other proteins or receptors; an example is the conjugation of cetuximab to a murine anti-CD3 mAb (bispecific antibody). T-cells armed with this bispecific antibody are referred to as bispecific antibody-targeted T-cells (BATs) and are also reinfused back into the patient (70). Both the BATs and cetuximab significantly delayed the growth of pancreatic COLO 356/FG xenografts in SCID/beige mice compared to vehicle or unmodified T-cells (70). The cetuximab group however showed signs of toxicity upon necropsy such as raised liver and spleen weights in contrast with the other groups (70). The anti-CD3xanti-EGFR BATs molecule entered a phase I clinical trial involving five PDAC patients

(NCT01420874)(71). No dose-limiting toxicities were noted and mOS was 31 months, which is highly promising for PDACs (71). In the phase II clinical trial, BATs were combined with IL-2 and granulocyte-macrophage colony-stimulating factor (GM-CSF) (NCT02620865) (71). However, this trial only included 2 participants who survived 12.2 months and 38.5 months (71).

1.3.6 Masked pro-drugs

Several studies have attempted to incorporate the 'prodrug' strategy, where the active substance is released exclusively upon entering the tumour stroma, usually through protease activity. The benefits of this technique are a reduction in toxicity and improved tissue penetration. Wang and colleagues developed a matrix metalloproteinase (MMP)-sensitive synthetic protein-polypeptide conjugate (PEP20-M-IFN) that consists of a synthetic polypeptide, an MMP2-cleavable peptide, as well as an interferon (72). This conjugate triggered considerable anti-tumour efficacy in murine ovarian OVCAR3 xenograft cancer models; PEP20-M-IFN significantly suppressed tumour volume compared to the uncleavable PEP20-IFN control (72). A benefit of this design is that the cytokine and the cleavable MMP linker can easily be translated/adapted to other tumour types.

For example, using a linker that is cleaved by both MMPs and serine protease could release the cytokine more efficiently (73). Mansurov and colleagues masked IL-12 using such linkers, where the mask abolished virtually all IL-12 associated toxicity and displayed strong anti-tumour effects in colon adenocarcinoma, melanoma, and breast cancer mouse models (73). A human version of the masked IL-12 molecule was designed and its linker was readily cleaved by human tumour lysate (73).

A similar concept was recently explored by Xue and colleagues (74). They initially developed an IL-12-Fc conjugate with an extended half-life and great anti-tumour efficacy in B16 and MC38 mouse models (74). The IL-12-Fc consists of two murine IL-12 molecules linked to an immunoglobulin Fc (74). However, a mask was later introduced due to heavy toxicity of the molecule (74). The mask consisted of a unit of the IL-12 receptor and it was conjugated to the IL-12-Fc through an MMP-14 cleavable

linker (74). The mask successfully suppressed toxicity, which was reflected in reduced serum IFNγ levels and maintenance of body weight compared to the unmasked variant in an MC38 mouse model (74). The masked IL-12-Fc (Pro-IL-12) significantly prolonged survival and suppressed tumour growth in B16, MC38, and 4T1 models (74).

1.4 Masked CBD-IL12 (M-CBD-IL12) and CBD-IFNγ as targeted and tolerable immunotherapy candidates

Each bioengineering technique has its own benefits and limitations. For example, although powerful, CAR T-cells lack affinity for the tumour stroma leading to reduced penetration into solid tumours. This explains why the success of CAR T-cells remains mainly limited to blood cancers (64). Antibody-drug conjugates and immuno-cytokines tend to lack specificity and have difficulty penetrating the tumour stroma due to their size. This PhD focuses on two tumour types with a dense stroma and highly complex TME (TNBC and PDAC). Hence, the aforementioned techniques are unlikely to be successful. Since PDACs and TNBCs contain abundant collagen, I decided to exploit this by collagen-anchoring and masking two pro-inflammatory cytokines (IL-12 and IFNγ).

IL-12 and IFNγ are closely linked as the two major T helper (Th)1 cytokines and have previously shown promising results in preclinical models of multiple cancer types (see Figure 1.5/Figure 1.4)(21, 51). They are therefore suitable candidates for promoting a Th1-based response in a complex, immunosuppressive TME. In addition, these pro-inflammatory cytokines are small making it easier for them to manoeuvre through the leaky vasculature of the tumour. IL-12 is a heterodimeric cytokine, consisting of a p35 and p40 subunit, that is mainly secreted by monocytes, macrophages, and dendritic cells, all of which play a role in antigen presentation (Figure 1.4). IL-12 can trigger a Th1-based response upon binding to its receptor (see Figure 1.5) (13). The IL-12 receptor (IL-12R), comprising of a β1 and β2 subunit, is mainly expressed on the surface of T-cells and NK cells (13). Upon binding of IL-12 to its receptor, signal transducer and activator of transcription 4 (STAT4) is phosphorylated by the non-receptor protein tyrosine kinases JAK2 and TYK2 (13). Two phosphorylated STAT4 molecules then dimerise and are translocated into the nucleus, where they upregulate the transcription of IFNγ-encoding genes through regulators of transcription such a Tbet (13). Therefore, IL-12 receptor signalling results in the production of IFNγ (13).

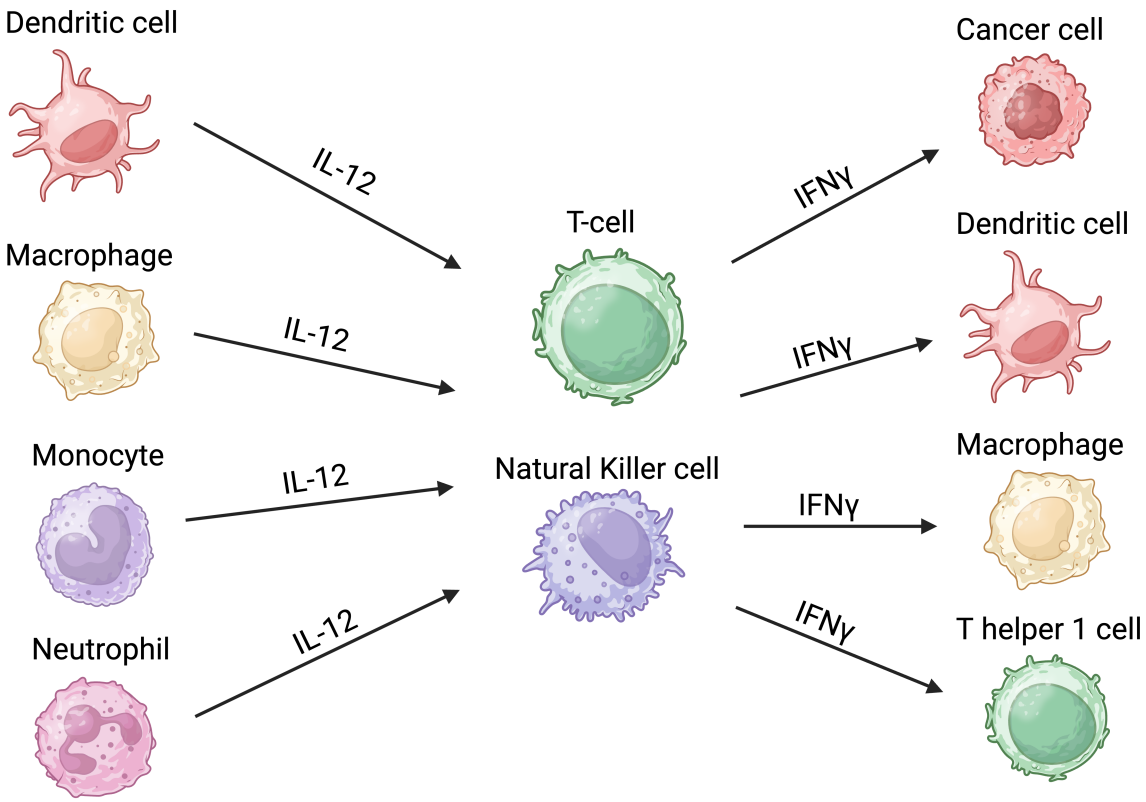


Figure 1.4 The sources and targets of IL-12 and IFNγ

Schematic representing the cell types that produce IL-12 and IFNγ and which ones are targeted by these molecules. Schematic was created on Biorender.com.

IFNγ then binds the IFNγR, also consisting of an R1 and an R2 subunit, which results in oligomerisation and transphosphorylation of their intracellular domains (12). Whilst the former is expressed at an intermediate level on a wide variety of cells, the latter's expression is strictly controlled and highly dependent on a cell's differentiation state and exposure to IFNγ (12). Although interesting, this means that IFNγ seems to control the expression of its own receptor to an extent which could ultimately lead to desensitisation (12). Unlike IL-12, IFNγ signalling triggers JAK1 and JAK2 to phosphorylate STAT1. Two phosphorylated STAT1s, also referred to as gamma-activated factors (GAFs), then dimerise and are translocated into the nucleus (12). In the nucleus, GAFs bind to gamma-activated site (GAS) elements, that form a part of the promoters of interferon-stimulated genes (ISGs). Tbet is the main transcription factor that regulates IFNγ expression, meaning that a positive feedback loop is present (12).

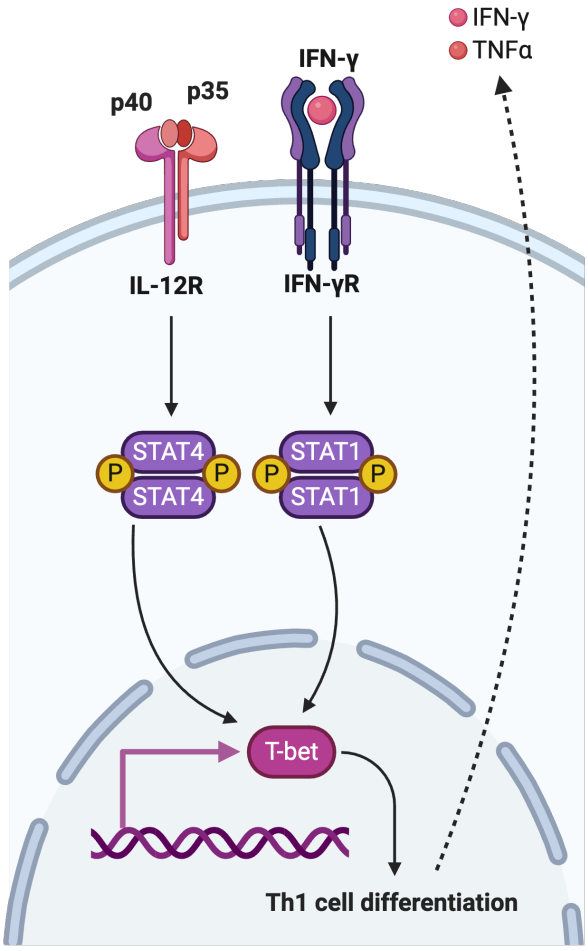


Figure 1.5 Schematic representing the IL-12 and IFNy signalling pathways

Adapted from 'T Cell Differentiation into Various Functional Subtypes', by BioRender.com (2024). Retrieved from https://app.biorender.com/biorender-templates

Bioengineering these cytokines to anchor onto the collagenous ECM enhances their tumour infiltration whilst reducing their peripheral toxicity. Hence, they were both conjugated to a collagen-binding domain (CBD), which as discussed earlier, is a protein derived from the A3 domain of VWF (50-52). Therefore, it has a high affinity for collagens type 1 and 3 (50-52). By adding the CBD to these cytokines, their molecular weight is increased which therefore prolongs their half-life and prevents their diffusion across the endothelium into healthy tissues which causes toxicity (50-52). Instead, the cytokines exclusively have access to tissues that are undergoing necrosis or have leaky vasculature, both of which are typical for the stroma of most solid tumours. Since these tumours usually contain abundant collagen, the CBD-conjugated cytokines tend to accumulate intratumourally (50-52). Choosing a rarer ECM molecule instead of collagen

would reduce the affinity of the bioengineered cytokines for the tumour stroma whereby limiting such accumulation.

In addition, the protease sensitive masking strategy offers tumour specificity to further suppress any residual toxicity of the CBD-IL12. The mask consists of the β1 subunit of the IL-12 receptor and temporarily inactivates IL-12 whilst in the blood stream following intravenous injection (73). This mask is conjugated to the p35 subunit of the IL-12 heterodimer through a protease-sensitive linker. Once the molecule has accumulated in the tumour stroma, MMPs 1, 2, and 9 and matriptase, legumain and urokinase can cleave the linker to remove the mask (73). Since these proteases are overexpressed in a variety of solid tumours compared to healthy tissues, this molecule offers a degree of tumour specificity which reduces toxicity even further.

Protease sensitive linkers were chosen over temperature or pH sensitive linkers due to their straightforward production and purification process and enhanced stability allowing long-term storage. They also provide easy adaptation of the linker sequence to other proteases, which is more limited with temperature or pH-sensitive linkers. Therefore, the molecule could be easily adjusted and personalised depending on which proteases are most abundantly expressed in a particular tumour. The masking was only applied to CBD-IL12 since unmasked CBD-IL12 was previously shown to be highly effective and the mask serves to reduce its toxicity further (51). However, CBD-IFNγ is a completely novel molecule of which the efficacy and biological activity in different cancer types was unknown. Therefore, this PhD focused on testing the efficacy of unmodified CBD-IFNγ without a mask first.

1.5 Triple negative breast cancer (TNBC)

1.5.1 Epidemiology

In 2020, 11.7% of all newly diagnosed cancers comprised of female breast cancer (75). This means it has now replaced lung cancer (11.4% of all cancer diagnoses) as the most commonly diagnosed cancer worldwide (75). However, lung cancer still remains more lethal; it is responsible for 18% of all cancer deaths, whilst female breast accounts for 6.9% (75). This is likely due to a combination of extensive breast cancer screening programs and increased public awareness leading to earlier breast cancer diagnosis and treatment (75). Breast cancer rates are considerably higher in high-income countries compared to low-income countries, most likely due to a combination of hormonal risk factors like contraceptives and age of menarche, as well as lifestyle risk factors like alcohol and obesity (75). The problem remains TNBC, which forms 10-15% of all new breast cancer diagnoses (76). They contribute to a large proportion of the breast cancer-related deaths due to their highly proliferative and tumorigenic nature (76). TNBC incidence is the highest young females, particularly of African American and Hispanic origin; it is more commonly diagnosed in women aged 20-39 compared to oestrogen receptor (ER)+/ progesterone receptor (PR)+, HER2- cancers (76, 77). Secondly, TNBC development is also linked to oestrogen exposure; in particular, women diagnosed within the 2 years following pregnancy are more likely to have TNBCs compared to other breast cancer types (78). Oestrogen's crucial role in the development of ER-negative tumours and the stromal changes and angiogenesis within them has been demonstrated in mouse xenografts (79).

1.5.2 Histological classification of breast cancer

Around 95% of breast cancers are adenocarcinomas (80). Invasive ductal carcinoma (IDC) is the most common form of breast adenocarcinoma (80). The rarer alternative is lobular carcinoma (80). Originally, it was thought that ductal carcinomas originated from the epithelium lining the milk duct and the lobular carcinoma from the lobules that produce the milk (81). However, it was later shown that both types arise in the terminal duct lobular unit (TDLU) (81). The two subtypes are now differentiated based on cell morphology: lobular carcinomas contain small, non-polarised cells similar in

appearance to the luminal cells of breast acini, whilst the ductal carcinoma contains larger, polarised cells, that take after normal ductal cells (80, 81). Both types of breast cancer have a non-invasive form characterised by early neoplastic proliferation that may develop into invasive breast cancer, referred to as '*in situ*' (80). The *in situ* forms of breast cancer are often referred to as stage 0 (76). Stages I-III are collectively referred to as invasive carcinoma (either ductal or lobular), but the three stages differ in tumour size; in stage I, tumours remain under 2 cm in size but have spread into the breast tissue from the TDLU (76). Stage II tumours are between 2-5 cm diameter and stage III tumours exceed 5 cm with spread to the axillary lymph nodes (76). Finally, stage IV tumours are referred to as metastatic breast cancer and have spread to organs distant from the mammary tissue (76).

1.5.2.1 Ductal carcinoma in situ (DCIS)

Ductal carcinoma *in situ* (DCIS) is an excessive proliferation of cancerous epithelial ductal-like cells that have not yet invaded local breast tissue (76, 80). DCIS is usually rather heterogeneous, meaning they are usually classified into 5 histological subtypes: comedo, solid, cribiform, papillary, micropapillary (80). In addition, they exist in low-grade (monomorphic cells, round nuclei, small increase in nuclear-cytoplasmic ratio), intermediate-grade (like low-grade but with potentially some necrosis in the ducts or the presence of nucleoli and coarse chromatin), or high-grade (atypical cells, high grade nuclei, prominent nucleoli) (80). The risk of progression to an invasive ductal carcinoma is determined by the DCIS grade (80).

1.5.2.2 Lobular carcinoma in situ (LCIS)

Similar to DCIS, LCIS is a precursor and risk factor for invasive lobular carcinoma (80). It differs from DCIS because it is positive for high molecular weight keratin and negative for E-cadherin and β-catenin (80). The exact opposite pattern can be found in DCIS for those markers (80).

1.5.2.3 Invasive ductal carcinoma (IDC)

IDC is the most common form (around 55% of all breast cancers) (80) and is an umbrella term for a wide range of histological subtypes: tubular, mucinous, invasive cribiform, medullary, invasive papillary, invasive micropapillary, apocrine, neuroendocrine, metaplastic, lipid-rich, secretory, oncocytic, adenoid cystic and acinic cell. The most common subtype remains the No Special Type (NST) which includes a broad variety or morphologies, margins, sizes, grades, and growth patterns (80).

1.5.2.4 Invasive lobular carcinoma (ILC)

Invasive lobular carcinomas (ILC) form around 5-15% of breast carcinomas and their incidence is increasing in post-menopausal women, potentially due to increased use of hormone replacement therapy (80). Their cells are usually small, round and rather uniform and they invade the stroma in a single-file pattern (80). They have five histological subtypes: classic type, pleiomorphic lobular carcinoma, histocytoid carcinoma, signet ring carcinoma, and tubulolobular carcinoma (80).

1.5.3 Biological classification of breast cancer

Since the histological classification of breast cancers is often not representative of the complex genetic background and behaviour of breast tumours, many have attempted to use gene expression data to classify breast cancers biologically. Perou and colleagues collected 65 tumour specimens from 42 patients who had previously been treated with neoadjuvant doxorubicin (82). Using hierarchical clustering they were able to identify two major subsets: ER-positive and ER-negative tumours (82). The ER-positive tumours were enriched for genes usually expressed by breast luminal cells (e.g. luminal cytokeratins) which resulted in them being called the luminal group (82). In contrast, the ER-negative group was rather heterogenous; some tumours stained for basal keratins and they resembled basal epithelial cells (82). These tumours were therefore referred to as the basal-like group. A second subset expressed abundant Erb-B2 and were called Erb-B2+ (82). Finally, a third subset contained samples that were grouped together with three normal breast samples (82). They expressed high levels of basal epithelial cell genes and adipose cell genes but very few luminal epithelial genes

(82). They were referred to as the normal-like group. Sørlie et al. then analysed the prognostic value of this classification in 78 breast cancer patients and found the ErbB2+ and the basal-like subtypes to have the worst survival rates (83). They also further classified luminal tumours into luminal A, luminal B, and luminal C with the former having the best prognosis and higher ER expression (83). Finally, Hu et al. combined datasets from multiple studies, including those discussed above (83-85) and confirmed the existence of two luminal-like subgroups with unique survival patterns (86). Over time, this classification has been adjusted and a version of the current breast cancer classification is shown below (see Table 1.2). TNBCs lack the expression of the ER, PR, and HER2, and they overlap largely, but not fully, with the claudin-low and basal-like subtypes (87). For example, 15-20% of TNBC lack the expression of basal markers, whilst 15-20% of non-TNBCs express basal markers (87). This highlights the vast heterogeneity within TNBCs. The Sadanandam laboratory addressed this heterogeneity by classifying TNBCs into 3 distinct subtypes (immunotypes) based on the expression of cancer, stromal, and immune genes (88). Patients bearing immunotype 1 tumours usually have better survival rates since the tumours are more acutely inflamed with enhanced T-cell infiltration (88). On the other hand, women diagnosed with immunotype 3 tumours tend to have shorter survival rates, most likely due to the heavy myeloid infiltration that results in chronic inflammation (88). This classification and its use in selecting patients for the immunotherapy agents in this PhD thesis will be discussed in more detail in section 3.1 of Chapter 3.

Table 1.2 Biological subtypes of breast cancer

The contents of this table are adapted from (76), (89). HER2 = Human epidermal growth factor receptor 2, ER = oestrogen receptor, PR = progesterone receptor, AR = androgen receptor, CK = cytokeratin.

Biological subtypes	Proportion of all breast cancers	Histological subtypes	Prognosis	Molecular markers
Luminal A-like	50-60%	Lobular, classical, tubular, cribiform	Good	ER+, PR+, HER2-, low Ki67
Luminal B-like	15-20%	Micropapillary	Intermediate to poor	ER+, PR±, HER2±, high Ki67
HER2 overexpressed	15-20%	Pleomorphic	Poor	ER-, PR-, HER+, CK5/6 +/-, EGFR+/-, high Ki67
Triple negative	10-15%	Metaplastic, adenoid, cystic, secretory	Poor	ER-, PR-, HER2-, AR+, CK5/6 +/-, EGFR+/-, high Ki67

Claudin low	7-14%	Metaplastic, medullary	Poor	Claudin 3,4 and 7 low, E-cadherin low, ER-, PR-, HER2-, high Ki67
Basal-like	8-37%	Metaplastic, medullary, adenoid cystic, secretory	Poor	ER-, PR-, CK5+, CK6+, CK14+, CK17+, EGFR+, high Ki67
Normal-like	5-10%	Medullary, metaplastic	Intermediate	ER+, PR±, HER2-, CK5+, CK6+, EGFR+, high Ki67

1.5.4 Current therapeutic options for TNBC patients

Similar to other breast cancers, the primary therapeutic option for TNBC remains surgical removal of the lump (lumpectomy) or the entire breast (mastectomy), usually followed with (adjuvant) or preceded by systemic chemotherapy (neo-adjuvant) (76). The preferable chemotherapeutics are anthracyclines, taxanes, and platinum-based chemotherapies (76). However, these toxic chemotherapy regimens have limited efficacy in TNBC patients (90). Radiotherapy can be useful for treatment of both the primary tumour, as well as its associated symptoms (76). It is also a tool to eradicate remaining cancer cells following surgery (76). This could help prevent relapse, which TNBC is particularly notorious for (90). Although it is challenging to pinpoint the culprit, certain pathways within TNBCs are overactive and drive tumorigenesis. They are therefore being explored as therapeutic targets and have been described below as well as in Table 1.3.

Table 1.3 Overview of therapeutic targets and strategies in TNBC clinical trials

Cancer cell	**Stroma**	**Immune**
BRCA	Androgen pathway	CPIs
PI3K/Akt/mTOR	Hedgehog	Oncolytic viruses
Wnt/β-catenin		Antibody-drug conjugates
		Agonistic and antagonistic antibodies
		Cancer vaccines

1.5.4.1 BRCA1/2 and PARP inhibitors

Women with TNBC usually have a family history of breast or ovarian cancers, suggesting the existence of a genetic link (76). This is particularly relevant for the

BRCA1/2 germline mutations, that are responsible for around 10% of TNBC (87, 91). In addition, mutations in *BRIP1, BARD1, RAD51D* and *PALB2* are frequent in TNBC patients compared to other breast cancers (91). In *BRCA1* mutation carriers, 70% of breast tumours are TNBC, whilst around 16-23% of breast cancers in *BRCA2* mutation carriers are TNBC (87).

Poly(ADP-ribose) polymerase (PARP) is an enzyme that functions to repair single-strand DNA breaks (92, 93). If inhibited, PARP is unable to fix these breaks which then become double strand breaks (92, 93). In that case, the homologous recombinant repair (HRR) DNA repair pathway fixes DNA double strand breaks. However, mutations in *BRCA1/2* or other genes such as *ATM*, *PALB2*, or *RAD51* (these mutations cause the 'BRCAness' phenotype) result in the deficiency of HRR (92, 93). In tumours that are HRR deficient, these double strand breaks cannot be repaired, which results in the elimination of cancer cells (92, 93). Therefore, PARP inhibitors are effective only against *BRCA1/2* mutant tumours or tumours high in 'BRCAness' (mutant in for example *ATM*, *PALB2*, or *RAD51*) (92, 93). 'BRCAness' refers to the concept of a defective HRR pathway leading to a BRCA-like phenotype, yet this phenotype is not caused by *BRCA1/2* mutations but by other mutations (92, 93).

In the 10% of TNBCs that are *BRCA* mutant, the PARP inhibitors olaparib and talazoparib have recently been approved based on the results of two phase III clinical trials: OlympiAD (NCT02000622) (94) and EMBRACA (NCT01945775) (95). OlympiAD included both metastatic BRCA-mutant TNBC (49.8%) and ER+PR+HER- tumours (50.2%) (94). The trial revealed the olaparib group to have a significantly longer mPFS than the chemotherapy group (94). Interestingly, the overall survival did not differ between treatment arms (94). In the EMBRACA trial, advanced or metastatic *BRCA*-mutant breast tumours, of which 40% were TNBCs, were treated with either talazoparib or chemotherapy (95). In this trial, the mPFS was significantly higher in the talazoparib arm compared to chemotherapy (95). Once again, no difference in overall survival was observed between treatment arms. Despite the approval of PAPR inhibitors for *BRCA*-mutant TNBC, 50% of patients still progress whilst receiving treatment (96). Other PARP inhibitors such as rucaparib, niraparib and veliparib are currently being tested in TNBC patients (97).

Due to the small proportion of TNBC that are *BRCA*-mutant and the degree of resistance these patients demonstrate against PARP inhibitors, other tumorigenic pathways in TNBC have been explored as potential therapeutic targets.

1.5.4.2 PI3K/Akt pathway

The PI3K/Akt pathway is overactive in about 50% of TNBCs due to mutations in for example *PIK3CA, mTOR*, or *AKT1* (76, 98). This was the rationale behind clinical trials using the PI3Kα inhibitor alpelisib (BYL719) (76, 99). In the phase 1a clinical trial on multiple solid tumour types including breast tumours with *PIK3CA* mutations, alpelisib was found to be safe with a manageable safety profile (NCT01219699)(99). Alpelisib is currently being tested in a phase III trial in combination with nab-paclitaxel in advanced TNBC patients with *PIKC3A* mutations or *PTEN* loss (NCT04251533) (76). AKT1, AKT2, and AKT3 are crucial downstream components of the PI3K pathway that can be inhibited through pan-AKT inhibitors such as capivasertib or ipatasertib (100, 101). In combination with paclitaxel in the phase II trials PAKT and LOTUS, they showed significant improvements in progression-free and overall survival in patients with metastatic TNBC compared to placebos (100, 101).

1.5.4.3 Hedgehog (HH) pathway

The hedgehog (HH) pathway is involved in tissue repair and cellular growth (102, 103). Its activation promotes the proliferation and invasiveness of TNBC cells by increasing angiogenesis and the expression of matrix-degrading proteases (102, 103). Tumours in which this pathway is dysregulated have a more aggressive phenotype (76). Since HH pathway components are more abundantly expressed in TNBC compared to other breast cancers, its dysregulation could be contributing to the poor TNBC survival rates (76, 102, 103). Within TNBCs, a higher expression of HH pathway components is also associated with poorer survival (76).

This pathway also plays a role in resistance to chemotherapy; resistance of TNBC cells to chemotherapy was found to be mediated by GLI1, a major HH effector protein (104). This protein can upregulate the transcription of drug resistance efflux transporters

(MDR1, BCRP) that cause resistance to taxanes (104). This makes the HH pathway an attractive target for TNBC therapy.

The easiest to target component of this pathway is Smoothened (SMO), against which a variety of inhibitors exist. Their success in other cancer types is varied with promising results in basal cell carcinomas (105) and medulloblastomas (106), yet disappointing results in colorectal (107), pancreatic (108) or lung cancer (109). In breast cancer, three clinical trials using SMO inhibitors have been organised (NCT01071564, NCT01757327, and NCT02027376) of which the latter (EDALINE study) has results available on TNBC patients; a complete response was observed in a single patient out of twelve but this patient was eventually excluded from the study due to docetaxel-related cumulative toxicity (110). Stable disease was noted in three other patients. Further trials are required to draw conclusions on the efficacy of this SMO inhibitor in advanced TNBC (110). GLI inhibitors have also been identified but have only been tested in pre-clinical models (111). Therefore, the information on their pharmacokinetics is currently still limited and uncertainty exists around their suitability as a cancer drug due to extensive post-translation modifications leading to a variety of truncated GLI isoforms (111).

1.5.4.4 Wnt/β-catenin pathway

The Wnt/β-catenin pathway is also involved in cell proliferation, migration and invasion (76). When the pathway is activated by Wnt ligands, β-catenin accumulates in the cytoplasm and gets translocated into the nucleus to regulate gene expression (76). In the Wnt-off state in the absence of Wnt ligands, β-catenin gets degraded in the cytoplasm (76). Various genes involved in this pathway (*FZD7, TCF, LRP6*) are highly upregulated in TNBC samples in microarray analysis (112). Using immunohistochemistry, the differential expression between normal breast cancers and TNBCs was confirmed (112). Knocking down *FZD7* in human TNBC cell lines reduced their invasiveness and proliferation *in vitro* and their tumour growth rate *in vivo* (112). Monoclonal antibodies against Wnt ligands exist yet a pan-Wnt ligand inhibitor is thought to be more suitable due to the large number of existing ligands. This type of

inhibitor performed well against murine mammary tumours (113) but its use in TNBC clinical trials remains currently limited.

1.5.4.5 Androgen pathway

The androgen receptor (AR) is a steroid hormone receptor that contributes to cell proliferation and migration (98). Around 10-15% of TNBCs are AR-positive and these tumours tend to have a poor prognosis and are unresponsive to chemotherapy (98).

Instead, in tumours where the androgen signalling pathway is active, AR inhibitors can be efficacious (114). In a phase II trial on AR-positive TNBCs, the AR inhibitor enzalutamide was well tolerated and showed some efficacy (114); especially in patients with a nuclear AR expression over 10%, the mOS was 17.6 months compared to 12.7 months in the intent-to-treat population (114). However, in contrast, in a second phase II trial using bicalutamide, no clear efficacy was observed against metastatic AR-positive (>10% AR expression) TNBCs (115). The mPFS was only 12 weeks (115). The cytochrome P450 17 alpha-hydroxylase (CYP17) blocker abiraterone acetate reduces androgen production and is often used for the therapy of prostate cancers (116). In combination with prednisone, it performed similarly to enzalutamide in a phase II trial, especially in patients with 10% or more AR expression (116). The mPFS was 2.8 months with few adverse events. Overall, a select set of TNBC patients seem to benefit from androgen pathway inhibition but the identification of this patient subset is currently still suboptimal.

1.5.4.6 Immunotherapy in TNBC

Immunotherapy either as monotherapy or in combination with other agents has been widely explored in TNBC (see Table 1.4). IMpassion130 was a phase III trial assessing nab-paclitaxel either with placebo or atezolizumab (anti-PD-L1 antibody). In the ITT population, the mOS was 18.7 months for placebo and 21.0 for atezolizumab, suggesting a slight improvement (117). In the PD-L1+ subgroup, the atezolizumab arm had a significantly longer mOS of 25.4 months, compared to placebo with 17.9 months (117). Following the results of this trial, in 2020, National Institute for Health and Care

Excellence (NICE) guidelines were published recommending atezolizumab in combination with nab-paclitaxel for PD-L1+ (≥1%) unresectable locally advanced or metastatic TNBCs that have not been treated with prior chemotherapy (118).

In the KEYNOTE-355 study, chemotherapy in combination with pembrolizumab (C+PE) (anti-PD-1 antibody) was compared to chemotherapy with placebo (C+PL) (119, 120). They analysed groups in terms of Combined Positive Score (CPS), which refers to the number of cancer cells, lymphocytes and macrophages that stain positive for PD-L1, divided by the total number of live tumour cells, multiplied by 100. In the CPS-1 group, little difference was observed between groups in terms of mOS (C+PE 17.6 vs. C+PL 16.0 months) (119, 120). In contrast, in the CPS-10 group, mOS in the C+PE group was 23.0 months whilst the C+PL group mOS remained 16.1 months (119, 120). Therefore, in June 2022, a second recommendation was published revealing patients with untreated, unresectable or metastatic TNBC (no prior chemotherapy, PD-L1 CPS of ≥10, immune cell staining <1%) to benefit from pembrolizumab (anti-PD-1 antibody) in combination with (nab-)paclitaxel (121). Later in 2022, this advice was also extended to patients with early or locally advanced TNBC as neoadjuvant treatment with chemotherapy and consequently as adjuvant therapy following surgery (122). As a consequence of these approvals, a variety of immunotherapy clinical trials combining the targeted therapies described above (PARP inhibitors, Akt inhibitors, etc.) with CPIs and chemotherapy in TNBC have been completed in an attempt to further prolong these survival rates (see Table 1.4).

Table 1.4 Completed immunotherapy clinical trials in TNBC

ITT = Intention to treat population. VEGFR2 = vascular endothelial growth factor receptor 2, mOS = median overall survival. Table is based on (123). Trial registration numbers have been underlined for trials that tested a combination of immunotherapy with other agents that was eventually approved by NICE in the UK.

Study name	Trial arms	N=	Phase	mOS (months)	Trial registration	Ref.
KEYNOTE-012	anti-PD-1 antibody (pembrolizumab)	32	Ib	11.2	NCT01848834	(124)
KEYNOTE-086-A	anti-PD-1 antibody (pembrolizumab)	170	II	9.0	NCT02447003	(125)
KEYNOTE-086-B	anti-PD-1 antibody (pembrolizumab)	84	II	18.0	NCT02447003	(126)
KEYNOTE-119	A: anti-PD-1 antibody (pembrolizumab) B: chemotherapy	622	III	PD-L1 score ≥10: A: 12.7 B: 11.6	NCT02555657	(127)

TOPACIO/KEYNOTE-162	PARP inhibitor (niraparib) + anti-PD-1 antibody (pembrolizumab)	55	II	/	NCT02657889	(128)
JAVELIN	anti-PD-L1 antibody (avelumab)	168 (58 TNBC)	Ib	TNBC: 9.2	NCT01772004	(129)
JAVELIN PARP	anti-PD-L1 antibody (avelumab) + PARP inhibitor (talazoparib)	233 (22 TNBC)	Ib/II	/	NCT03330405	(130)
/	anti-PD-L1 antibody (atezolizumab)	116	I	17.6	NCT01375842	(131)
KEYNOTE-150/ENHANCE-1	anti-PD-1 antibody (pembrolizumab) + microtubule inhibitor (eribulin mesylate)	167	Ib/II	16.1	NCT02513472	(132)
IMpassion130	A: placebo + nab-paclitaxel B: anti-PD-L1 antibody (atezolizumab) + nab-paclitaxel	902	III	ITT population A: 18.7 B: 21.0 PD-L1+ A: 17.9 B: 25.4	NCT02425891	(117)
IMpassion131	A: placebo + paclitaxel B: anti-PD-L1 antibody (atezolizumab) + paclitaxel	651	III	PD-L1+: A: 28.3 B: 22.1	NCT03125902	(133)
IMpassion132	A: placebo + chemotherapy (investigator selected, either gemcitabine + carboplatin or capecitabine) B: anti-PD-L1 antibody (atezolizumab) + chemotherapy	/	III	Not available yet	NCT03371017	(134)
KEYNOTE-173	anti-PD-1 antibody (pembrolizumab) + chemotherapy (nab-paclitaxel, carboplatin, doxorubicin, cyclophosphamide)	60	Ib	/	NCT02622074	(135)
GeparNuevo	A: anti-PD-L1 antibody (durvalumab) + nab-paclitaxel B: placebo + nab-paclitaxel	174	II	/	NCT02685059	(136)
FUTURE-C-PLUS	nab-paclitaxel + receptor tyrosine kinase inhibitor (famitinib) + anti-PD-1 antibody (camrelizumab)	48	II	Not reached	NCT04129996	(137)
/	A: carboplatin + gemcitabine B: carboplatin + gemcitabine + anti-CSF-1 antibody (lacnotuzumab)	49	II	/	NCT02435680	(138)
SAFIR02-BREAST IMMUNO	A: anti-PD-L1 antibody (durvalumab) B: chemotherapy	199 (82 TNBC)	II	TNBC: A: 21.2 B: 14.0	NCT02299999	(139)
/	nab-paclitaxel + anti-PD-L1 antibody (atezolizumab)	33	Ib	14.7	NCT01633970	(140)
COLET	Cohort I: A: paclitaxel + placebo B: paclitaxel + MAPK/MEK inhibitor (cobimetinib) Cohort II: cobimetinib + atezolizumab + paclitaxel Cohort III: cobimetinib + atezolizumab + nab-paclitaxel	Cohort I: 106 Cohort II/III: 63	II	I: A: 19.6 B: 16.0 II: 11.0 III: NE	NCT02322814	(141)
/	anti-PD-1 antibody (camrelizumab) + VEGFR2 inhibitor (apatinib) Either continuously or intermittently dosed	40	II	Cont.: 8.1 Interm: 9.5	NCT03394287	(142)

/	anti-PD-L1 antibody (durvalumab) + anti-CTLA-4 antibody (tremelimumab)	18 (7 TNBC)	II	Not reached	NCT02536794	(143)
/	anti-PD-L1 antibody (atezolizumab) + talimogene laherparepvec (T-VEC, herpes simplex oncolytic virus)	11	Ib	19.2	NCT03256344	(144)
I-SPY2, arm 2	A: anti-PD-L1 antibody (durvalumab) + PARP inhibitor (olaparib) + paclitaxel B: paclitaxel	372 (40 TNBC)	II	Not available yet	NCT01042379	(145)
I-SPY2, arm 1	A: paclitaxel + anti-PD-1 antibody (pembrolizumab) B: paclitaxel	250 (82 TNBC)	II	/	NCT01042379	(146)
TORCHLIGHT	A: nab-paclitaxel + placebo B: nab-paclitaxel + anti-PD-1 antibody (toripalimab)	531	III	ITT: A: 23.5 B: 33.1 PD-L1+ A: 19.5 B: 32.8	NCT04085276	(147)
IMPRIME 1	anti-PD-1 antibody (pembrolizumab) + Imprime PGG (soluble yeast β-glucan)	44	II	16.4	NCT02981303	(148)
KEYNOTE-355	A: chemotherapy + anti-PD-1 antibody (pembrolizumab) B: chemotherapy + placebo	847	III	CPS-1: A: 17.6 B: 16.0 CPS-10: A: 23.0 B: 16.1	NCT02819518	(119), (120)
ALICE	A: cyclophosphamide + pegylated liposomal doxorubicin + placebo B: cyclophosphamide + pegylated liposomal doxorubicin + anti-PD-L1 antibody (atezolizumab)	68	II	/	NCT03164993	(149)
KEYNOTE-522	A: anti-PD-1 antibody (pembrolizumab) + chemotherapy (paclitaxel, carboplatin) B: placebo + chemotherapy	1174	III	Not yet available	NCT03036488	(150)
NeoPACT	carboplatin + docetaxel + anti-PD-1 antibody (pembrolizumab)	115	II	/	NCT03639948	(151)
NeoTRIPaPDL1	A: carboplatin + nab-paclitaxel + anti-PD-L1 antibody (atezolizumab) B: carboplatin + nab-paclitaxel	280	III	/	NCT02620280	(152)
IMpassion031	A: chemotherapy (nab-paclitaxel + doxorubicin + cyclophosphamide) + anti-PD-L1 antibody (atezolizumab) B: chemotherapy + placebo	333	III	Not yet available	NCT03197935	(153)
/	anti-PD-L1 antibody (durvalumab) + PARP inhibitor (olaparib)	54 (43 TNBC)	I/II	Not yet available	NCT03594396	(154)
DORA	anti-PD-L1 antibody (durvalumab) + PARP inhibitor (olaparib)	45	II	/	NCT03167619	(155)
/	anti-PD-1 antibody (pembrolizumab) + radiotherapy	17	II	Not yet available	NCT02730130	(156)
/	anti-PD-1 antibody (pembrolizumab) + antibody drug conjugate (ladiratuzumab vedotin)	51	Ib/II	/	NCT03310957	(157)
SYNERGY	A: anti-PD-L1 antibody (durvalumab) + anti-CD73	127	Ib/II	A: 25.1 B:19.3	NCT03616886	(158)

	monoclonal antibody (oleclumab) + paclitaxel + carboplatin B: durvalumab + paclitaxel + carboplatin					
/	bispecific antibody against PD-L1 and CTLA-4 (KN046) + nab-paclitaxel	27	Ib/II	30.92	NCT03872791	(159)
AZTEC	anti-PD-L1 antibody (atezolizumab) + radiotherapy	50	II	Not yet available	NCT03464942	(160)
/	Talimogene laherparepvec (T-VEC, herpes simplex oncolytic virus) + anti-PD-1 antibody (nivolumab) + anti-CTLA-4 antibody (ipilimumab)	6	I	/	NCT04185311	(161)
/	anti-PD-1 antibody (camrelizumab) + VEGFR2 inhibitor (apatinib) + eribulin	46	II	Not reached	NCT04303741	(162)
/	nab-paclitaxel + anti-PD-L1 antibody (atezolizumab)	37	II	/	NCT02530489	(163)
OlympiA	A: PARP inhibitor (olaparib) B: placebo	1836 (1509 TNBC)	III	/	NCT02032823	(164)
MEDIOLA	PARP inhibitor (olaparib) + anti-PD-L1 antibody (durvalumab)	34	I/II	21.5	NCT02734004	(165)
PIVOT 02	CD122 agonist (NKTR-214) + anti-PD-1 antibody (nivolumab)		I/II	/	NCT02983045	(166)
/	anti-PD-1 antibody (pembrolizumab) + androgen receptor modulator (enobosarm)	18	II	25.5	NCT02971761	(167)
161O VIOLETTE	A: PARP inhibitor (olaparib) B: ATR inhibitor (ceralasertib) + olaparib C: WEE1 inhibitor (adavosertib) + olaparib	273	II	/	NCT03330847	(168)
CO41101, IPATunity170	paclitaxel + anti-PD-L1 antibody (atezolizumab) + AKT inhibitor (ipatasertib)	317	III	15.7-28.3	NCT04177108	(169)
CO40016, IPATunity 130			III		NCT03337724	(169)
CO40151			Ib		NCT03800836	(169)

1.5.4.6.1 Currently ongoing immunotherapy clinical trials in TNBC

In Table 1.5 I have described currently ongoing TNBC clinical trials, which, similarly to Table 1.4, are also starting to include some more creative forms of immunotherapy such as oncolytic viruses (talimogene laherparepvec, pelareorep, CF33-hNIS-antiPDL1), antibody drug conjugates (ladiratuzumab vedotin, sacituzumab govitecan), agonistic antibodies (CD122 agonist (NKTR-214)), antagonistic antibodies (anti-CD47 monoclonal antibody (AK117)), cytokine-based therapy (IL-12 gene therapy, IL-6 receptor antagonist (sarilumab), tavokinogene telseplasmid), and cancer vaccines (PVX-410 vaccine, DNA vaccine, AE37 peptide vaccines, ADV/HSV-tk).

1.5.4.6.1.1 Oncolytic viruses

Oncolytic viruses are viruses that are engineered to infect cancer cells and induce their lysis which simultaneously releases tumour antigens to trigger an anti-tumour immune response (170). Talimogene laherparepvec (T-VEC) is an oncolytic herpes virus that generates GM-CSF (171). It has been approved for the treatment of unresectable melanoma as an intratumoural injection and has been shown to have a synergistic effect with CPIs (171). It has already been trialled in two separate clinical trials in TNBC (see Table 1.4). In the first, it was combined with an anti-PD-L1 antibody (atezolizumab) in 11 patients (NCT03256344) (144). Their mOS was 19.2 months. In the second, an anti-CTLA-4 antibody (ipilimumab) was added to this combination, yet the mOS was not reported (NCT04185311) (161).

A second example is the chimeric oncolytic virus CF33-hNIS-antiPDL1, which consists of the orthopoxvirus (CF33), a sodium iodide symporter (hNIS), and an anti-PD-L1 antibody (172). Its safety is currently being tested in a phase I TNBC trial (NCT05081492) (see Table 1.5).

1.5.4.6.1.2 Antibody drug conjugates

Ladiratuzumab vedotin consists of a humanised antibody against LIV-1 which has been conjugated to MMAE (cytotoxic drug) through a protease-cleavable linker (157). This conjugate induces immunogenic cell death (157). It has thus far been studied in a phase Ib/II clinical trial in combination with an anti-PD-1 antibody (pembrolizumab)(NCT03310957) (see Table 1.4) (157). The ORR in the 26 patients that are currently still involved was 54% and two patients seem to have a partial response (157). However, 86% of patients reported adverse events (157).

Sacituzumab govitecan consists of an antibody against trophoblast cell surface antigen 2 (Trop-2), as well as an active irinotecan metabolite and a topoisomerase I inhibitor (involved in DNA replication) (173). The Food and Drug Administration (FDA) approved this conjugate in 2020 for TNBC, but it currently not yet recommended by NICE in the England for TNBC (173). However, this approval sparked four more clinical trials in which sacituzumab govitecan is combined with either anti-PD-1 (pembrolizumab,

NCT05382286, NCT04468061), or anti-PD-L1 (avelumab/atezolizumab, NCT04434040, NCT03971409) (see Table 1.5). These trials are all currently still ongoing.

1.5.4.6.1.3 Agonistic and antagonistic antibodies

In the PIVOT 02 trial (NCT02983045) the CD122 agonist NKTR-214 was combined with an anti-PD-1 antibody (nivolumab) in patients with multiple advanced cancers including TNBC (166) (see Table 1.4). CD122 is the IL-2 receptor subunit β and a component of the IL-15 receptor, suggesting an agonistic CD122 antibody aims to trigger cytotoxic T-cell activation (174). Although the trial is still ongoing, the authors could already conclude that the safety profile is manageable and within the three TNBC patients, the ORR is 33% (166). Although promising, this compound's efficacy requires testing in a much larger cohort (166).

Secondly, CD47 is a macrophage immune checkpoint which can be inhibited through the anti-CD47 monoclonal antibody AK117 (175). In a currently ongoing trial, AK117 is combined with both chemotherapy and AK112 (a dual anti-PD-1 and anti-vascular endothelial growth factor (VEGF) antibody) (NCT05227664) (see Table 1.5). Using this macrophage CPI in combination with standard CPIs may also be a promising strategy for TNBC.

1.5.4.6.1.4 Cancer vaccines

Cancer vaccines usually involve the introduction of exogenous tumour antigens or cells, either unmodified or pulsed/pre-treated, into the patient to increase the antigenic strength of the tumour (176). This causes an anti-tumour immune response (176) The PVX-410 vaccine is an example that is currently being tested in two clinical trials (see Table 1.5). It is a human leukocyte antigen (HLA) A2-restricted peptide vaccine (177) and is combined with an anti-PD-1 antibody (pembrolizumab, NCT03362060) and in the second trial with an anti-PD-L1 antibody (durvalumab, NCT02826434).

Finally, another cancer peptide vaccine AE37 is currently being tested in combination with an anti-PD-1 antibody (pembrolizumab) in the NSABP FB-14 trial (NCT04024800). The AE37 vaccine is a HER2-based vaccine which consists of a hybrid peptide (AE36), comprising of the intracellular component of HER2 and the major histocompatibility complex (MHC) class II invariant chain, co-administered with GM-CSF adjuvant (178). This vaccine is meant to prime $CD4^+$ T-cells against HER2 causing future HER2-expressing cells to be eliminated (178). However, due to the lack of HER2 expression, it may not be sufficiently efficacious in TNBC.

1.5.4.6.1.5 Cytokine-based therapy

The EMPOWER trial (NCT04333706) involves the use of an IL-6 receptor antagonist (sarilumab) in combination with capecitabine. Sarilumab is normally used as an anti-inflammatory drug and has been approved for rheumatoid arthritis in combination with methotrexate (179). Its use in cancer immunotherapy is currently limited. However, it may be involved in suppressing cancer-promoting intratumoural inflammation. This phase I trial is currently recruiting (see Table 1.5).

However, other trials have used pro-inflammatory IL-12 to trigger inflammation instead. To minimise toxicity, IL-12 has been used as part of gene therapy. The first example is tavokinogene telseplasmid, which is an IL-12-encoding plasmid that is injected intratumourally and results in transient localised cytokine production (180). A trial (KEYNOTE-890) using this plasmid together with chemotherapy and an anti-PD-1 antibody (pembrolizumab) is currently ongoing (NCT03567720) (see Table 1.5). Finally, the INTEGRAL trial using adenoviral-mediated IL-12 (ADV/IL-12) gene therapy in combination with docetaxel and an anti-PD-1 antibody (pembrolizumab) has currently been suspended and further review is required prior to enrolling again (NCT04095689) (see Table 1.5).

Table 1.5 Examples of currently ongoing TNBC immunotherapy clinical trials

Table is based on (123).

Study name	Trial arms	Phase	Trial registration
INTEGRAL	docetaxel + anti-PD-1 antibody (pembrolizumab) + adenoviral mediated IL-12 (ADV/IL-12)	II	NCT04095689
/	chemotherapy + anti-PD-1 antibody (HLX10)	III	NCT04301739

/	carboplatin + anti-PD-1 antibody (spartalizumab) + LAG3 inhibitor (LAG525)	II	NCT03499899
OXEL	A: capecitabine B: anti-PD-1 antibody (nivolumab) C: capecitabine + nivolumab	II	NCT03487666
A-BRAVE	All pts. had prior surgery and chemotherapy A: anti-PD-L1 antibody (avelumab) B: observation	III	NCT02926196
SWOG 1418	A: anti-PD-1 antibody (pembrolizumab) B: observation	III	NCT02954874
/	anti-CD20 antibody (carilizumab) + nab-paclitaxel + cisplatin	II	NCT04537286
	A: carboplatin + gemcitabine B: carboplatin + gemcitabine + anti-PD-1 antibody (pembrolizumab)	II	NCT02755272
TONIC	chemotherapy/radiotherapy induction + anti-PD-1 antibody (nivolumab)	II	NCT02499367
TONIC-2	doxorubicin, cisplatin + anti-PD-1 antibody (nivolumab)	II	NCT04159818
GIM25-CAPT	anti-PD-L1 antibody (atezolizumab) + nab-paclitaxel + carboplatin	II	NCT05266937
EL1SSAR	anti-PD-L1 antibody (atezolizumab) + nab-paclitaxel	III	NCT04148911
/	A: chemotherapy + anti-PD-1 antibody (camrelizumab) B: chemotherapy + placebo	III	NCT04613674
NSABP B-59	A: chemotherapy + anti-PD-L1 antibody (atezolizumab) B: chemotherapy + placebo	III	NCT03281954
Impassion030	A: chemotherapy B: chemotherapy + anti-PD-L1 antibody (atezolizumab)	III	NCT03498716
MIRINAE trial	A: capecitabine B: capecitabine + anti-PD-L1 antibody (atezolizumab)	II	NCT03756298
/	anti-PD-L1 antibody (atezolizumab) + radiotherapy	II	NCT03483012
KEYLINK-009	A: anti-PD-1 antibody (pembrolizumab) + PARP inhibitor (olaparib) B: pembrolizumab + carboplatin + gemcitabine	II/III	NCT04191135
ASCENT-04	A: anti-PD-1 antibody (pembrolizumab) + antibody drug conjugate (sacituzumab govitecan) B: pembrolizumab + physician's choice therapy	III	NCT05382286
/	A: anti-PD-1 antibody (pembrolizumab) + antibody drug conjugate (sacituzumab govitecan) B: Sacituzumab govitecan	II	NCT04468061
ASPRIA	anti-PD-L1 antibody (atezolizumab) + antibody drug conjugate (sacituzumab govitecan)	II	NCT04434040
/	anti-PD-1 antibody (camrelizumab) + VEGFR2 inhibitor (apatinib) + chemotherapy	II	NCT05447702
/	anti-PD-1 antibody (pembrolizumab) + receptor tyrosine kinase inhibitor (lenvatinib)	I	NCT04427293
/	A: anti-PD-1 antibody (carelizumab) + nab-paclitaxel + VEGFR2 inhibitor (apatinib) B: carelizumab + nab-paclitaxel C: nab-paclitaxel	III	NCT04335006
/	A: anti-PD-L1 antibody (atezolizumab) + AKT inhibitor (ipatasertib) + paclitaxel/doxorubicin/cyclophosphamide B: anti-PD-L1 antibody (atezolizumab) + paclitaxel/doxorubicin/cyclophosphamide	II	NCT05498896
/	anti-PD-L1 antibody (atezolizumab) + anti-TIGIT monoclonal antibody (tiragolumab) + chemotherapy	Ib	NCT04584112
/	A: anti-CD47 monoclonal antibody (AK117) + (nab-)paclitaxel B: anti PD-1/anti-VEGF dual antibody (AK112) + (nab-)paclitaxel C: AK117 + AK112 + (nab-)paclitaxel	II	NCT05227664
/	anti-PD-1 antibody (pembrolizumab) + PVX-410 vaccine	I	NCT03362060
/	anti-PD-L1 antibody (durvalumab) + PVX-410 vaccine	I	NCT02826434
/	A: chemotherapy + anti-PD-L1 antibody (durvalumab) + anti-CTLA-4 antibody (tremelimumab) + vaccine B: chemotherapy + durvalumab + tremelimumab	II	NCT03606967
/	A: anti-PD-L1 antibody (durvalumab) + DNA vaccine B: DNA vaccine	I	NCT03199040
NSABP FB-14	AE37 peptide vaccine + anti-PD-1 antibody (pembrolizumab)	II	NCT04024800

QUILT-3.067	NANT TNBC Vaccine combination immunotherapy	Ib/II	NCT03387085
/	anti-PD-1 antibody (retifanlimab) + oncolytic reovirus (pelareorep)	II	NCT04445844
/	Radiotherapy + anti-PD-1 antibody (pembrolizumab) + ADV/HSV-tk	II	NCT03004183
/	CF33-hNIS-antiPDL1	I	NCT05081492
KEYNOTE-890	anti-PD-1 antibody (pembrolizumab) + tavokinogene telseplasmid + electroporation + chemotherapy	II	NCT03567720
BreastImmune03	A: radiotherapy + anti-PD-1 antibody (nivolumab) + anti-CTLA-4 antibody (ipilimumab) B: radiotherapy + capecitabine	II	NCT03818685
/	PLK4 inhibitor (CFI-400945) + anti-PD-L1 antibody (durvalumab)	II	NCT04176848
Morpheus-panBC	Multiple targeted therapy combinations	Ib/II	NCT03424005
InCITe	A: MEK inhibitor (binimetinib) + anti-PD-L1 antibody (avelumab) + liposomal doxorubicin B: antibody drug conjugate (sacituzumab govitecan) + anti-PD-L1 antibody (avelumab) C: Liposomal doxorubicin + anti-PD-L1 antibody (avelumab)	II	NCT03971409
EMPOWER	IL-6 receptor antagonist (sarilumab) + capecitabine	I/II	NCT04333706
NIMBUS	anti-CTLA-4 antibody (ipilimumab) + anti-PD-1 antibody (nivolumab)	II	NCT03789110
/	PARP inhibitor (olaparib) + anti-PD-L1 antibody (durvalumab)	II	NCT03801369
PHOENIX	anti-PD-L1 antibody (durvalumab) + PARP inhibitor (olaparib) + ATR inhibitor (ceralasertib)	II	NCT03740893
MARIO-3	PI3K inhibitor (eganelisib) + anti-PD-L1 antibody (atezolizumab) + nab-paclitaxel + anti-VEGF (bevacizumab)	II	NCT03961698

1.5.5 The TNBC TME and its role in immunotherapy resistance

Under ideal circumstances, the cancer-immunity cycle results in the efficacious elimination of cancer cells by T-cells. Unfortunately, as is the case in many solid tumour types, evasion mechanisms and immunosuppressive cell types in TNBC can render the cancer-immunity cycle ineffective (181). Both the innate and the adaptive components of the immune system contribute to this cycle, each of which harbour pro- and anti-tumorigenic cell types. Some important cell types and their role in the TNBC TME have been described below:

1.5.5.1 Immunosuppressive components of the TNBC TME

Immunosuppressive macrophages (often called M2 macrophages), MDSCs, Tregs, Th2/Th17 cells are usually considered pro-tumorigenic in the TME. For example, M2 macrophages promote tumour progression by secreting immunosuppressive cytokines, promoting cancer cell proliferation, and inducing EMT (182, 183). Secondly, MDSCs are more common in TNBCs compared to other breast cancer types (184) and in TNBC

mouse models, their adoptive transfer resulted in the formation of significantly more pulmonary metastasis compared to controls (185). They achieve this by inhibiting the anti-tumour activity of $CD8^+$ T-cells (185). Finally, Th2 cells, Th17 cells and Tregs develop from naïve $CD4^+$ T-cells (186). Following the encounter of the naïve $CD4^+$ T-cell with its antigen through MHC class II on antigen presenting cells, cytokines determine the population of Th cells that arises (186). For example, Th2 cells develop upon exposure to IL-4 and they consequently express IL-4, IL-5, and IL-13, largely involved in allergic reactions (187). They tend to promote a polarisation of macrophages towards the M2 phenotype and therefore rapid tumour progression (188). Meanwhile, Th17 cells require TGFβ and IL-6 for their development and consequently secrete IL-17, IL-21, and IL-22 (186, 189). Whether Th17 cells are purely pro- or anti-tumorigenic remains a topic of debate; some have shown them to promote angiogenesis, MMP secretion, enhanced invasiveness of cancer cells, and suppressed $CD8^+$ T-cell activity (186, 189). On the other hand, their presence has been associated with smaller breast tumour size, lower tumour stage and longer survival (186, 190, 191).

Tregs develop upon exposure to TGFβ and they secrete more TGFβ, IL-10, and IL-35 (192). They have been shown to comprise a large proportion of the T-cell population in claudin-low TNBCs and their depletion renders the tumours responsive to CPI therapy (193). Their absence has been associated with favourable TNBC survival rates (194).

1.5.5.2 Immunogenic components of the TNBC TME

In contrast with the immunosuppressive Th cell subsets, Th1 cells arise following exposure to IL-12 and they secrete IFNγ and TNFα (195). Th1 cells are generally considered pro-inflammatory. In TNBC, these Th1 cytokines are crucial in triggering cancer cell apoptosis and senescence, particularly in combination with EGFR inhibition (195). The IFNγ secreted by Th1 cells promotes the activation of both macrophages and $CD8^+$ T-cells (196). $CD8^+$ T-cells are a crucial component of anti-tumour immunity since they exert direct cytotoxicity towards cancer cells (197). $CD8^+$ T-cell scores are higher in TNBC compared to other breast cancer types (197). Within TNBC, a raised $CD8^+$ T-cell score is associated with significantly longer patient survival (197). However,

raised $CD8^+$ T-cell scores are also associated with raised checkpoint expression and therefore exhaustion of such T-cells (197).

Due to the ability of M1 macrophages to phagocytose, secrete inflammatory cytokines, and recruit more T-cells through CXCL9 and CXCL10, they are usually considered anti-tumorigenic (196). However, some have demonstrated them to promote carcinogenesis by secreting IL-1 and TNFα which results in cancer cell proliferation through Nuclear Factor kappa B (NF-κB) (196).

Finally, NK cells are also capable of cancer cell destruction in TNBCs (198) and they produce large amounts of pro-inflammatory cytokines such as IFNγ (199). These cytokines in turn can induce dendritic cell maturation (199). However, their function is determined by their developmental status (198). For example, a subset of immature NK cells with reduced capacity for granzyme-mediated toxicity within the TNBC TME has been linked to tumour progression and metastasis (198).

Although these are general cell types that exist and exert similar functions across a variety of solid tumour types such as PDAC, the proportions of these cell types are highly heterogeneous within and between TNBC tumours. I have described this heterogeneity further in the introduction of chapter 3 (see section 3.1).

1.6 Pancreatic Ductal Adenocarcinoma (PDAC)

1.6.1 Epidemiology

Despite only being the 14th most common cancer type, pancreatic cancer still remains the 7th most frequent cause of cancer death (75). Due to its increasing incidence, by 2030, it is likely to become the second leading cause of cancer death (75, 200). The incidence is highest in Europe and North America and the lowest in Africa and Asia (75). Males (5.7 per 100 000) are also more commonly affected than females (4.1 per 100 000) (75).

Pancreatic ductal adenocarcinomas (PDACs) originate from the exocrine part of the pancreas and are the most common and aggressive form of pancreatic cancer (201).

90% of PDAC deaths have been documented in people aged 55 years or older, suggesting this disease is associated with not only genetics and environmental factors, but also age (202). Unfortunately, the PDAC 5-year survival rate is an abysmal 10.2% (202). This can be attributed to a variety of factors; firstly, it is a highly aggressive tumour type that metastasises rapidly, mainly to the liver (201). Secondly, PDAC patients usually remain symptomless until very late stages, which means the tumours often have metastasised at the point of diagnosis (201). Therefore, the majority of patients are not eligible for curative surgery. Furthermore, out of the patients that undergo surgery, 80% relapse following resection (203, 204). Thirdly, the non-surgical therapeutic options for advanced PDAC are limited to toxic chemotherapy regimens such as gemcitabine/nab-paclitaxel and 5-fluorouracil/leucovorin with irinotecan and oxaliplatin (FOLFIRINOX), the former being the slightly more tolerable alternative for patients with insufficient performance status (205). The efficacy of these agents against this disease remains limited; the response rates vary from 23% to 31% with overall survival rates of 8.5 to 11 months (205). Finally, we currently lack a reliable diagnostic and monitoring biomarkers, meaning we heavily rely on imaging to monitor treatment response.

1.6.2 PDAC classifications and current potential therapeutic targets

The PDAC TME is highly heterogeneous on a cancer cell, immunological and stromal level. Many have attempted to classify PDACs into multiple subtypes that aim to guide therapy selection. Collisson and Sadanandam et al. reported three unique PDAC cancer cell subtypes using gene expression analysis: classical (enriched with adhesion and epithelial genes), quasi-mesenchymal (QM, enriched with mesenchymal genes), and exocrine-like (enriched with digestive enzyme genes) (206). Classical cell lines were more sensitive to erlotinib (epidermal growth factor receptor inhibitor) therapy whilst QM cell lines responded better to gemcitabine (206). Secondly, Bailey et al. defined a system that shows abundant overlap with Collisson and Sadanandam: pancreatic progenitor and immunogenic correspond to classical, squamous to QM and aberrantly differentiated endocrine exocrine (ADEX) to exocrine-like (207). Finally, Moffitt et al. identified the classical and basal-like PDAC subtypes and simultaneously revealed considerable heterogeneity within the stromal PDAC compartment (208). They therefore labelled two stromal subtypes as either normal or activated (208). Overall, the

PDACs with high degrees of epithelial to mesenchymal transition, that are resistant to CPIs due to their sparse T-cell population fall within the QM subtype by Collisson and Sadanandam, squamous by Bailey and basal-like by Moffitt. In contrast, T-cell infiltrated PDACs are considered classical by Collisson and Sadanandam and Moffitt and progenitor by Bailey. Further work is required to understand how these classifications can offer insight into therapy guidance for PDACs.

Due to the ample number of genetic mutations in PDACs (in for example *KRAS, VEGF, TP53,* and *Sonic Hedgehog*), defects in downstream signalling pathways are common (209). Many have attempted to target these defects described in Table 1.6 with the aim of suppressing PDAC progression. However, very few targeted therapies have been approved for PDACs.

Table 1.6 Overview of current therapeutic targets and strategies in PDAC clinical trials.

Cancer cell	**Stroma**	**Immune**
KRAS	TGFβ	CPIs
RAF/MEK/ERK	Hedgehog	Oncolytic viruses
PI3K/Akt/mTOR	Hyaluronic acid and MMPs	Cancer vaccines
TP53	VEGF	Immunomodulation
EGFR/ERBB		Adoptive T-cell therapy
IGF-1R		
PARP		
JAK-STAT pathway		
Notch		

1.6.2.1 Kirsten Rat Sarcoma Virus (KRAS)

The human RAS family is a group of oncoproteins of which HRAS, NRAS, and KRAS are the most well-known members (210). The proteins all share a main activity that revolves around guanosine triphosphate (GTP) binding and hydrolysis (210). They structurally consist of two domains: a G-domain and a membrane-targeting domain (211). The G-domain attaches and hydrolyses GTP, whilst the membrane-targeting domain is involved in membrane anchoring (211). The *KRAS* gene encodes the KRAS GTPase, which functions as part of an on-off system for downstream signalling events

that result in growth and proliferation (211). The KRAS protein can be bound to either GDP or GTP, with the former resulting in its deactivation whilst the latter causes it to be active (211). This is also referred to as GTP-GDP cycling, a process controlled by guanine nucleotide exchange factors (GEFs) and GTPase-activating proteins (GAPs) that enhance the hydrolytic activity of KRAS (211). When KRAS is switched on, it triggers pathways involving over 80 effector proteins such as the mitogen-activated protein kinase (MAPK), phosphoinositide 3-kinase (PI3K) or rapidly accelerated fibrosarcoma (RAF) pathways (211). Through the activation of transcription factors, these pathways trigger proliferation, survival, migration, and differentiation.

Mutations in the *KRAS* gene generate some of the most aggressive cancer types (212). 90% of PDACs have oncogenic *KRAS* mutations and it is one of the four most commonly mutated genes in pancreatic cancer besides *TP53, SMAD4, CDKN2A* (209). These are usually point mutations that take place on codon 12, but can also exist on codons 11, 13, 16 or 146, albeit less frequently (211). The most common mutations are the G12D mutation (40% of PDACs), the G12V mutation (33% of PDACs), the G12R mutation (15% of PDACs), or the G12A, G12S, and G12C mutations (211). Examples of much rarer mutations on other codons are G13D, G13C, G13S, and G13R, Q61H, Q61L, Q61K, and Q61R (211). In the G12D mutation the glycine is swapped for an aspartic acid on codon 12 of exon 2 as a consequence of a single nucleotide change (209). The GTPase activity of KRAS is hindered by these point mutations which means GAPs cannot convert GTP to GDP, causing downstream pathways to be continuously active (211). Interestingly, oncogenic mutations in *KRAS* tend to be associated with inactivation of tumour suppressor genes (*INK4a*, *TP53*, and *SMAD4*) in most PDACs.

Besides directly encouraging continuous cancer cell growth, the $KRAS^{G12D}$ mutation also indirectly promotes tumour progression by allowing the cancer cells to escape from the immune system, particularly $CD8^+$ T-cells (212). Studies have identified multiple ways in which the mutation has led to reduced efficacy of CPIs in PDAC, the relevance of which will be discussed further in 4.1 (212-214). However, studying this relationship was challenging since KRAS was considered an undruggable target for a long time. Instead, KRAS was therefore indirectly suppressed through the inhibition of farnesylation, a process crucial for RAS activation (205). A farnesyltransferase inhibitor was trialled in a phase II trial (SWOG9924) in metastatic PDAC patients, yet the benefit

was very limited (215). Alternatively, exosomes or vesicles loaded with small interfering RNA against *KRAS*^{G12D} were trialled to treat *KRAS* mutant PDACs. A clinical trial using these exosomes is currently ongoing (NCT03608631). A revolutionary turning point in targeted cancer therapy was the discovery of sotorasib, a small molecule *KRAS*^{G12C} inhibitor, which was approved in 2021 in the US and 2022 in Europe for the treatment of non-small cell lung cancer patients harbouring the *KRAS*^{G12C} mutation (216). This was shortly followed by the discovery of the selective small molecule *KRAS*^{G12D} inhibitor MRTX1133 (217). It has demonstrated significant anti-tumour effects and a phase I/II trial to test MRTX1133 in advanced solid tumours (including PDAC) with a *KRAS*^{G12D} mutation (NCT05737706) is currently recruiting participants. Due to the important immunomodulatory role of KRAS (212), future studies involving MRTX1133 and how it may improve the efficacy of various immunotherapy modalities are promising.

1.6.2.2 RAF/MEK/ERK pathway

Downstream of KRAS exist a variety of different downstream pathways, one of which is the RAF/MEK/ERK signalling pathway that is crucial for proliferation, differentiation, and angiogenesis (218). Inhibition of any of its components has unfortunately been unsuccessful in PDAC, through for example MEK inhibitors (CI-1040 (219), selumetinib (220), pimasertib (221), trametinib (222)). This can most likely be explained through the compensatory effects of the other pathways downstream of KRAS such as the PI3K/AKT/mTOR pathway. However, even when selumetinib is combined with other agents such as afatinib (pan-human epidermal growth factor receptor inhibitor)(223) or an Akt inhibitor (224) to overcome these compensatory mechanisms, it still has little effect on patient survival.

1.6.2.3 PI3K/Akt/mTOR pathway

Akt is overexpressed in around 40% of PDAC patients (225). Its effects are similar to the RAF/MEK/ERK pathway described above. In certain cancer types, Akt inhibition triggers apoptosis and a reduction in tumour burden (226). The mTOR inhibitor everolimus had little clinical activity in gemcitabine refractory PDAC patients with a mOS of 4.5 months (227). However, with everolimus in combination with capecitabine this

survival improved to 8.9 months, which is similar to what can be achieved with gemcitabine monotherapy (228). Other mTOR inhibitors (Temsirolimus), PI3K inhibitors (BKM120 and BYL179) and dual PI3K/mTOR inhibitors (BEZ235) are currently being studied in clinical trials (NCT03662412, NCT02155088).

1.6.2.4 TP53 tumour suppressor pathway

In contrast with the proto-oncogene *KRAS*, *TP53* is a tumour suppressor gene that is inactivated in around 70% of PDACs leading to tumorigenesis (229). The p53 transcription factor normally maintains normal cell proliferation and apoptosis (229). *TP53* function can be restored and stabilised using reactivators such as Zn2+ chelators (COTI-2) (205). A clinical trial using COTI-2 in patients with *TP53* mutations is currently ongoing (NCT02433626). The p53 antagonist Mouse Double Minute 2 homolog (MDM2) can also be inhibited to restore *TP53* activity (205). A selective MDM2 inhibitor (Milademetan) is currently being tested in a phase II clinical trial (MANTRA-2) on metastatic solid tumours including PDAC (NCT05012397).

1.6.2.5 EGFR/ERBB family

EGFR (ErbB1, HER1) is one of the members of the human epidermal growth factor receptor family (205). It is a receptor that operates upstream of, and therefore to an extent regulates, the RAS/RAF/MEK/ERK and PI3K/AKT/mTOR pathways (205). It is therefore crucial for cell proliferation, survival, and growth (205). EGFR is overexpressed in around 30-50% of PDACs (230) and it is essential for tumorigenesis of the pancreas (205). The small molecule EGFR tyrosine kinase inhibitor erlotinib remains currently the only FDA-approved targeted therapy in combination with gemcitabine for patients with metastatic, locally advanced PDAC patients (231, 232). This combination improved overall survival by 0.33 months (around 10 days).

The monoclonal antibody against EGFR (nimotuzumab) in combination with gemcitabine significantly prolonged mOS to 8.6 months from 6.0 months with gemcitabine monotherapy (233). A consecutive phase III trial on nimotuzumab in combination with gemcitabine confirmed the significant impact of this combination

therapy on mOS (10.9 months for gemcitabine+nimotuzumab vs. 8.5 months for gemcitabine+placebo) (234). Similarly, the EGFR inhibitors matuzumab and panitumumab in combination with gemcitabine and erlotinib have demonstrated promising results (235, 236). However, for cetuximab in combination with gemcitabine the benefit was limited compared to gemcitabine monotherapy (237).

The second member of the HER family is HER2 (ErbB2) (205). Trastuzumab is an anti-HER2 humanised antibody that is often used for HER2+ breast cancer therapy. However, its effects in PDAC are disappointing (238). The previously discussed pan-HER inhibitor (EGFR and HER2 inhibitor) afatinib was combined with gemcitabine and compared to gemcitabine monotherapy in patients with metastatic PDACs (239). However, apart from augmenting the toxicity, addition of the afatinib to gemcitabine did not contribute to the anti-tumour effects of gemcitabine in these patients and mPFS was the same in both groups (239).

1.6.2.6 Insulin-like growth factor receptor 1 (IGF-1R)

Similarly to EGFR and HER2, IGF-1R is a tyrosine kinase that is overexpressed in PDAC which causes enhanced cell proliferation and reduced apoptosis (240). An IGF-1R inhibitor ganitumab in combination with gemcitabine did not prolong survival in a phase III trial; mOS was 7.2 months in the placebo+gemcitabine arm and 7.0 months in the ganitumab+gemcitabine arm (241). Simultaneous inhibition of IGF-1R (MK-0646) and EGFR/HER2 (erlotinib) with gemcitabine in PDAC showed a slight prolongation in overall survival but not in PFS compared with gemcitabine with erlotinib (242).

1.6.2.7 VEGF

VEGF overexpression in PDAC triggers more rapid tumour progression and poor prognosis (243). However, anti-angiogenic therapy has been unsuccessful for PDAC (244, 245) and its withdrawal induces a more aggressive tumour phenotype (246). The same effects were observed with other VEGF inhibitors axitinib, aflibercept, and sorafenib (247-249). The single outlier is anlotinib, a tyrosine kinase inhibitor affecting VEGFR, fibroblast growth factor receptor, platelet-derived growth factor receptor

(PDGFR) and c-kit (205). It is highly promising in lung cancer (250) and is currently being studied in a phase II trial in combination with toripalimab (anti-PD-1) and nab-paclitaxel (NCT04718701) in patients with advanced/metastatic PDAC.

1.6.2.8 PARP

The *BRCA* mutations are autosomal dominant germline mutations that increase susceptibility to breast, gastro-intestinal and gynaecological malignancies (205). Families that carry germline *BRCA2* mutations have a relative risk of pancreatic cancer of 3.5% (251). Tumours that are *BRCA1/2* mutant tend to be susceptible to PAPR inhibition, since they lack a crucial DNA repair pathway, which leads to the elimination of cancer cells (205). As discussed in 1.3.4.1 'BRCA1/2 and PARP inhibitors', PARP inhibitors are commonly used in *BRCA*-mutant TNBC. In PDAC, olaparib monotherapy was surprisingly effective and triggered a mOS of 9.8 months (252). At the 1-year mark, 40.9% of the PDAC patients in this trial were still alive (252). Furthermore, in a phase III trial (POLO, NCT02184195) on metastatic germline *BRCA*-mutant PDAC patients, differences in the PFS following olaparib monotherapy sparked interest in the ability of PARP inhibitors to suppress tumour progression (253). The olaparib group had a significantly longer mPFS (7.4 months) than the placebo (3.8 months) group, whilst mOS did not differ between groups (253). Since these were metastatic, heavily pre-treated patients, their survival was expected to be shorter than usual. Nevertheless, it is important to highlight these were patients who had not progressed after 16 weeks of platinum-based induction chemotherapy, which suggests they may have had less aggressive tumours at baseline.

Evidently, variation exists between PARP inhibitors because veliparib was not as effective in a group of PDAC patients with similar baseline characteristics (254). Their mOS was extremely low at 3.1 months (254). Interestingly, rucaparib was trialled in the RUCAPANC study involving 19 previously treated participants (255). The investigators observed two partial responses and a complete, which is highly promising for PDAC (255).

1.6.2.9 JAK/STAT pathway

Inhibition of components of the JAK/STAT pathway such as STAT3 has been shown to result in an increased sensitivity to chemotherapy and delayed tumour growth (256). Results of a trial involving STAT3 inhibitors in combination with chemotherapy in PDAC are yet to be uploaded (NCT02231723). The JAK1 inhibitor itacitinib in combination with nab-paclitaxel and gemcitabine caused an ORR of 24% across multiple solid tumour types including PDAC (257). However, a de-escalation was required due to multiple grade 3/4 adverse events such as severe neutropenia (257). Unfortunately, in the phase III JANUS trial the combined JAK1/2 inhibitor ruxolitinib in combination with capecitabine did not demonstrate any clinical activity which led to study termination (NCT02117479, NCT02119663). Therefore, the evidence supporting JAK/STAT pathway inhibition in PDAC remains limited.

1.6.2.10 Notch pathway

Notch pathway upregulation is associated with enhanced tumorigenesis in PDAC (205). It has been shown to play a role in the regulation of cancer stem cells and it closely interacts with other pathways such as KRAS and the HH pathway (205). Notch signalling is triggered by γ-secretase and an inhibitor of this molecule (RO4929097) was unfortunately discontinued due to uncontrollable toxicity (258). Nevertheless, it caused a mOS of 4.1 months in patients with metastatic PDAC (258). A second γ-secretase inhibitor MK-0752 was combined with gemcitabine and triggered a singular partial response and stable disease in 13 out of 19 evaluable patients (259). Finally, an anti-Notch2 and Notch3 receptor antibody (tarextumab) in combination with gemcitabine/nab-paclitaxel failed to prolong both overall and progression-free survival (260).

1.6.2.11 TGFβ

The TGFβ pathway was named after its ability to transform tumour-stomal interactions and mediate epithelial to mesenchymal transition (205). Some evidence shows TGFβ inhibition to lead to reduced tumour growth and metastasis in mouse models (261, 262). The TGFβ receptor I kinase inhibitor galunisertib has been combined with gemcitabine

(263) and durvalumab (anti-PD-L1 antibody) (264). In the former, the combination of gemcitabine and galunisertib prolonged survival slightly (median survival times 8.9 months for galunisertib+gemcitabine vs. 7.1 months for placebo+gemcitabine) (263). The combination of durvalumab and galunisertib generated a mOS of 5.72 months, highlighting the need for chemotherapy (264). Due to the limited clinical activity of galunisertib in PDAC, other TGFβ receptor inhibitors or TGFβ traps have been developed. An example is NIS793 which is a human monoclonal antibody against TGFβ, which is currently in a phase III trial on previously untreated metastatic PDAC patients (NCT04935359). More examples are bintrafusp alfa (M7824) and SHR-1701, both of which have been described under 1.1.1 ‘Immuno-cytokines”. Many of the trials involving these molecules were unfortunately terminated prematurely due to inefficacy.

1.6.2.12 Hedgehog (HH)

The HH pathway plays a crucial role in the regulation of CAFs, epithelial to mesenchymal transition, and the formation of the dense PDAC stroma (205). IPI-926 inhibits Smoothened, a major component of the HH pathway (205). In combination with gemcitabine, IPI-926 suppressed tumour burden by increasing the vascular network within the tumours and therefore the intratumoural gemcitabine concentration in mouse models of PDAC (265). However, others have demonstrated the sonic hedgehog ligand, a crucial activator of the hedgehog pathway, to restrain tumour growth. Its deletion in a PDAC mouse model led to a more aggressive tumour phenotype with increased vascularity (266). Interestingly, these effects were partially reversed upon administration of an anti-VEGF antibody (266). Whether tumour vascularity is pro- or anti-tumorigenic in PDAC remains a heavily debated topic. Nevertheless, IPI-926 was still combined with gemcitabine in a clinical trial (NCT01130142), but it was not found to decrease the survival rates when compared to the gemcitabine+placebo group (267). A consecutive trial (NCT01383538) on IPI-926+FOLFIRINOX was terminated due to the disappointing results from the previous trial, despite the ORR being 67% (268).

Vismodegib is a second Smoothened inhibitor, which, in combination with gemcitabine, improved mPFS but not mOS (269, 270). These findings were confirmed in a second trial (NCT01088815) (269, 270). Due to the disappointing results of vismodegib, its

development has been halted (205). Overall, results of HH pathway inhibition in PDAC have been disappointing.

1.6.2.13 Hyaluronic acid and MMP inhibitors

Hyaluronic acid is a glucosaminoglycan and a crucial ECM component (271). It is largely produced by CAFs and its presence in the stroma has been linked with a poor prognosis, minimal $CD8^+$ T-cell infiltration, and enhanced tumour cell invasion (271). Pegylated hyaluronidases (PEGPH20) have been used to dissolve the hyaluronic acid in the PDAC stroma (205). PEGPH20 in combination with gemcitabine and nab-paclitaxel (HALO 202 trial) considerably improved mOS compared to chemotherapy alone (11.5 months for combination therapy vs. 8.5 months for chemotherapy monotherapy) in patients with tumours with a high hyaluronic acid (>50% staining) load (272). However, others have demonstrated disappointing results; the HALO109-301 phase III trial was terminated prematurely due to inefficacy (NCT02715804). Finally, in the phase II SWOG S1313 trial, modified FOLFIRINOX was combined with PEGPH20 and this combination reduced mOS in comparison with modified FOLFIRINOX alone (7.7 months for combination, 14.4 months for FOLFIRINOX alone) (273). Finally, in the MORPHEUS trial, PEGPH20 + atezolizumab (anti-PD-L1 antibody) demonstrated limited clinical activity (274).

MMPs are overexpressed in PDACs and continuously remodel the PDAC stroma and basement membrane to aid tumour progression and metastasis (275). The MMP inhibitor marimastat was compared to gemcitabine and the 1-year survival rates were similar between the groups (276). Similarly, in combination with gemcitabine, marimastat did not prolong survival beyond what could be achieved with gemcitabine monotherapy (277). The results of the phase III trial on tanomastat (BAY 12-9566), an alternative MMP inhibitor, were similarly disappointing; gemcitabine was significantly superior to tanomastat and the study was terminated prematurely (278). Andecaliximab is an anti-MMP9 antibody that seemed promising in combination with gemcitabine and nab-paclitaxel in a phase I trial in advanced PDAC (279). Median PFS was found to be 7.8 months (279).

1.6.3 Immunotherapy in PDAC

1.6.3.1 The PDAC TME and its role in the lack of success of CPI in PDAC

PDACs are notorious for their highly complex immunosuppressive TME and dense stromal barrier (8). Especially the dynamic interactions between cancer cells, immune cells, CAFs and the ECM have made it challenging to target PDACs with a singular or a combination of two to three immunotherapy agents (8, 280-282). Therefore, despite the numerous clinical trials on immunotherapy in PDAC patients, no immunotherapy agents have been approved for PDAC by NICE in the UK thus far.

CPIs are antibodies that prevent checkpoints on T-cells, cancer cells, and myeloid cells from interacting (10). The interaction of checkpoints normally functions as a safety mechanism to prevent excessive unnecessary immune activation by inducing T-cell anergy (10). Cancer cells exploit this mechanism by overexpressing checkpoints to suppress the anti-tumour immune response (10). Inhibiting checkpoint axes releases the brakes on T-cells, meaning they can once again exert their anti-tumour effects (10). CPIs have revolutionised the cancer immunotherapy field and have been successfully introduced into the clinic for melanoma, lung cancer, renal cell carcinoma, and urothelial carcinoma (283-286). Unfortunately, they have demonstrated limited efficacy in PDAC (see Table 1.7); intravenous ipilimumab (anti-CTLA-4 antibody) triggered a delayed response in a single patient out of 27 in a phase II clinical trial (see Table 1.7) (287). Instead, severe adverse events were noted in three participants (287). In another phase II trial, metastatic PDAC patients were administered the combination of durvalumab (anti-PD-L1 antibody) and tremelimumab (anti-CTLA-4 antibody), yet the ORR was 3.1% (see Table 1.7) (18). In the durvalumab monotherapy group, no responses were observed (18).

Table 1.7 Overview of clinical trials involving CPIs in PDAC

Unless stated otherwise, median overall survival has been reported in months. Where applicable, the different treatment arms have been displayed as A and B. mOS = median overall survival, ITT = intention to treat. Table is from (288). Trial registration numbers have been underlined for trials that tested a combination of immunotherapy with other agents that was eventually approved by NICE in the UK.

Author, year	Immunotherapy treatment arms	Enrolled patients	PDAC stage	mOS (months (95% CI))	Trial phase	Trial registration	Ref.

Royal et al., 2010	Anti-CTLA-4 (Ipilimumab, MDX-010)	27	Locally advanced or metastatic	Not reported	II	NCT00112580	(287)
O'Reilly et al., 2019	A: concurrent anti-PD-L1 (Durvalumab) + anti-CTLA-4 (Tremelimumab), then Durvalumab B: Durvalumab	65	Metastatic, pre-treated with fluorouracil/gemcitabine-based therapy	A: 3.1 (2.2-6.1) B: 3.6 (2.7-6.1)	II	NCT02558894	(18)
Brahmer et al., 2012	Anti-PD-L1 (BMS-936559)	207 (14 PDAC)	Advanced cancers	Not reported	I	NCT00729664	(289)
Aglietta et al., 2014	Anti-CTLA-4 (Tremelimumab, CP-675,206) + gemcitabine	34	Chemotherapy naïve metastatic	7.4 (5.8-9.4)	Ib	NCT00556023	(290)
Kamath et al., 2020	Anti-CTLA-4 (Ipilimumab) + gemcitabine	21	Locally advanced or metastatic	6.9 (2.63-9.57)	Ib	NCT01473940	(291), (292), (293)
Weiss et al., 2017 (PembroPlus)	All groups anti-PD-1 (Pembrolizumab) A: + gemcitabine B: + gemcitabine + docetaxel C: + gemcitabine + nab-paclitaxel D: + gemcitabine + vinorelbine E: + irinotecan F: + liposomal doxorubicin	49 (11 PDAC)	Advanced or metastatic	Not reported	Ib	NCT02331251	(294)
Weiss et al., 2018	Arm C Weiss et al, 2017	17	Metastatic, 12 chemotherapy-naïve	15 (6.8-23.2) for chemotherapy-naïve	Ib/II	NCT02331251	(295)
Marabelle et al., 2020 (KEYNOTE-158)	Anti-PD-1 (Pembrolizumab)	233 (22 PDAC)	MSI-H/dMMR advanced non-colorectal cancers	For all tumour types combined: 23.5 (13.5-not reached)	II	NCT02628067	(296)
Hong et al., 2019	Anti-PD-L1 (Durvalumab) + BTKI (Ibrutinib)	124 (50 PDAC)	Relapsed/refractory solid tumours	PDAC: 4.2 (2.6-6.4)	Ib/II	NCT02401048	(297)
Wainberg et al., 2020	A: Anti-PD-1 (Nivolumab) + nab-paclitaxel B: Anti-PD-1 (Nivolumab) + nab-paclitaxel + gemcitabine	61	Locally advanced or metastatic	B: 9.9 (6.74-12.16) PD-L1<5%: 9.7 PD-L1≥5%: 11.6	I	NCT02309177	(19)
Rahma et al., 2021	A: Anti-PD-1 (Pembrolizumab) + chemoradiation (capecitabine) B: Chemoradiation only	37	Resectable or borderline resectable	A: 27.8 B: 24.3	Ib/II	NCT02305186	(298)
Parikh et al., 2021	Anti-PD-1 (Nivolumab) + anti-CTLA-4 (Ipilimumab) + radiotherapy	65 (25 PDAC)	Microsatellite stable (MSS), metastatic	ITT/PDAC: 4.2 (2.1-6.4) Per	II	NCT03104439	(299)

				- protocol/PDAC: 6.1 (4.0-7.0)			
Xie et al., 2020	All arms anti-PD-L1 (Durvalumab) A1: + SBRT (8 Gy, 1 fraction) A2: + SBRT (25 Gy, 5 fractions) B1: + anti-CTLA-4 (Tremelimumab) + SBRT (8 Gy, 1 fraction) B2: + anti-CTLA-4 (Tremelimumab) + SBRT (25 Gy, 5 fractions)	59	Metastatic, pre-treated with chemotherapy	A1: 3.3 (1.2-6.6) A2: 9.0 (0.5-18.4) B1: 2.1 (1.1-4.3) B2: 4.2 (2.9-9.3)	I	NCT02311361	(300)

A variety of factors contributed to the failure of CPIs in PDAC. Firstly, PDACs have a low tumour mutational burden (TMB), which results in a limited repertoire of tumour neoantigens (301, 302). Consequently, the PDAC tumour stroma harbours few T-cells that recognise these tumour antigens, making it usually a T-cell depleted cancer type (303). This means most PDACs do not tend to respond to CPIs due to the absence of a target T-cell population for them to act on. Abundant evidence supports this theory; cancer types with higher TMB (melanomas, non-small cell lung cancer) than PDACs respond better to anti-PD-1 therapy (304, 305). Responding melanoma patients also harbour more abundant $CD8^+$ T-cells, express more PD-1 and PD-L1 and have a more clonally diverse T-cell receptor repertoire than non-responders (306). PD-1 and PD-L1 expression are often considered biomarkers for response to therapy with anti-PD-1 and anti-PD-L1. Secondly, a small subset (around 1%) of PDACs have abundant mutational burden, namely those that lack mismatch repair (MMR) and therefore show high microsatellite instability (MSI-H) (307). Interestingly, these tumours do respond to CPI therapy (307). This suggests that the low mutational burden of the majority of PDACs makes them challenging to treat with immunotherapy.

Besides the lack of antigenic strength of PDACs, a whole network of other immunosuppressive factors prevents the efficacy of immunotherapy in PDACs (8). Examples are activation of the TGFβ pathway, Tregs, Tumour-associated macrophages (TAMs), CAFs and MDSCs that communicate through an intricate mechanism of immunosuppressive cytokines (8). Particularly the transformation of fibroblasts into CAFs through the presence of TGFβ can result in the production of

desmoplastic stroma (8). This stroma prevents efficient blood flow into the tumour core and therefore also infiltration of immune cells and therapeutic agents (8).

Therefore, in this rapidly advancing field, researchers have had to rely on creativity to develop agents that are capable of rectifying the low mutational burden, T-cell depletion, and immune suppression that all contribute to the failure of CPI in PDACs. Some examples have been described below and in Table 1.8.

1.6.3.2 Immunomodulatory therapy

The immunosuppressive PDAC TME calls for strategies that reactivate the cancer-immunity cycle. Examples like agonistic antibodies against CD40, GITR, or 4-1BB all promote T-cell activation (308, 309). Sotigalimab is a CD40 agonistic antibody that, in combination with chemotherapy in untreated metastatic PDAC patients, demonstrated dose-dependent effects; the patients receiving the higher dose survived 7 months longer than those administered the lower dose (see Table 1.8) (310). When nivolumab (anti-PD-1 antibody) was added to the combination of low dose sotigalimab and chemotherapy, mOS was prolonged by 3 months in contrast with sotigalimab and chemotherapy alone (310). Despite this improvement with the addition of nivolumab (anti-PD-1 antibody), a consecutive phase II trial demonstrated that nivolumab+sotigalimab+chemotherapy did not prolong mOS (311). Interestingly, the chemotherapy+nivolumab group had longer mOS and better ORR than any of the sotigalimab groups (311). It is important to mention that the authors describe the benefits to be short-lasting and for them to lack radiological evidence (311). This makes it challenging to draw conclusions on the efficacy of these combinations.

IMM-101 is toll-like receptor (TLR) agonist that is produced from heat-killed *Mycobacterium obuense* (312). This too was tested in a phase II trial in combination with gemcitabine, where it demonstrated a small benefit (mOS 6.7 months) in contrast with gemcitabine monotherapy (mOS 5.6 months) (see Table 1.8) (312). The combination therapy however significantly prolonged mOS in a separate sub-group that had a particularly high metastatic burden (312).

Instead of agonists, the immune system can also be reactivated through inhibition of immunosuppressive pathways. An example is the CCR2-CCL2 axis. The CCR2 inhibitor (PF-04136309) was assessed in two separate trials, one in combination with gemcitabine/nab-paclitaxel (313) and the other with FOLFIRINOX (314). Gemcitabine/nab-paclitaxel together with 500 mg of PF-04136309 triggered pulmonary toxicity in a quarter of the participants (313). The authors were unable to justify this level of toxicity for little benefit gained over standard of care chemotherapy (313). Similar toxicity was observed with FOLFIRINOX, yet this was attributed to FOLFIRINOX rather than PF-04136309 (314). In this trial, patients administered the combination therapy had an ORR of 49%, compared to 0% in the FOLFIRINOX group (314). Therefore, PF-04136309 and FOLFIRINOX may be a useful combination to target TAMs in the PDAC TME.

Table 1.8 An overview of clinical trials involving immune stimulatory molecules (agonists & inhibitors) and adoptive T-cell therapies in PDAC

Survival has been described as median overall survival in months, unless stated otherwise. Where applicable, if the median overall survival data was not accessible, median survival time has been reported instead. mOS = median overall survival, MST = median survival time. Table is from (288). Trial registration numbers have been underlined for trials that tested a combination of immunotherapy with other agents that was eventually approved by NICE in the UK.

Author, year	Immunotherapy treatment arms	Enrolled patients	PDAC stage	mOS (months (95% CI))	Trial phase	Trial registration	Ref.
Immune Stimulatory molecules (agonists)							
O'Hara et al., 2021	All groups: gemcitabine + nab-paclitaxel + B1: 0.1 mg/kg CD40 mAb (APX005M) B2: 0.3 mg/kg APX005M C1: same as B1 + 240 mg Anti-PD-1 (Nivolumab) C2: same as B2 + 240 mg Anti-PD-1 (Nivolumab)	30	Untreated metastatic	B1: 12.7 B2: 20.1 C1: 15.9 C2: not estimable	Ib	NCT03214250	(310)
Padron et al., 2022 (PRINCE trial)	All groups: gemcitabine + nab-paclitaxel + A: Anti-PD-1 (Nivolumab) B: 0.3 mg/kg APX005M C: 0.3 mg/kg APX005M + Anti-PD-1 (Nivolumab)	99	First-line metastatic	A: 16.7 (9.8-18.4) B: 11.4 (7.2-20.1) C: 10.1 (7.9-13.2)	II	NCT03214250	(311)

Beatty et al., 2011	CD40 monoclonal antibody (CP-870,893) + gemcitabine	21	Locally advanced or metastatic	7.4 (5.5-12.8)	I		(315)
Beatty et al., 2013	CD40 monoclonal antibody (CP-870,893) + gemcitabine	22	Chemotherapy-naïve, advanced	8.4 (5.3-11.8)	I	NCT00711191	(316)
Dalgleish et al., 2016	A: TLR2/1 agonist (IMM-101) + gemcitabine B: gemcitabine	110	Advanced	A: 6.7 (5.4-7.5) B: 5.6 (3.2-7.2)	II	NCT01303172	(312)
Wang-Gillam et al., 2013	A: gemcitabine B: gemcitabine + IMP321 (0.5 mg) C: gemcitabine + IMP321 (2 mg)	18	Locally advanced or metastatic	A: 72.7 weeks B: 24.5 weeks C: 28.0 weeks	I		(317)
Hecht et al., 2018	Pegilodecakin (AM0010, LY3500518, PEGylated recombinant human IL-10) + FOLFOX	21	Heavily pretreated metastatic	10.2	Ib	NCT02009449	(57)
Hecht et al., 2021	Pegilodecakin (AM0010, LY3500518, PEGylated recombinant human IL-10) + FOLFOX	39 (29 PDAC)	Heavily pretreated metastatic	AM0010 at 5 μg/kg: 6.8 (2.6-14.6)	Ib	NCT02009449	(58)
Hecht et al., 2021 (SEQUOIA)	A: Pegilodecakin + FOLFOX B: FOLFOX alone	567	Metastatic with progression following gemcitabine	A: 5.8 B: 6.3	III	NCT02923921	(61)
Immune Stimulatory molecules (inhibitors)							
Hassan et al., 2020	Anetumab ravtansine (anti-mesothelin antibody + maytansinoid DM4 cytotoxic drug)	148 (9 PDAC)	Advanced or metastatic solid tumours, mesothelin expressing	Not reported	I	NCT01439152	(43)
Adjei et al., 2018	Anetumab ravtansine + gemcitabine	350	Unresectable locally advanced or metastatic solid tumours	Not yet reported	Ib	NCT03102320	(44)
Noel et al., 2020	PF-04136309 (CCR2 inhibitor) + nab-paclitaxel + gemcitabine	21	Untreated metastatic	Not reported	Ib	NCT02732938	(313)
Nywening et al., 2016	A: FOLFIRINOX alone B: FOLFIRINOX + PF-04136309 (CCR2 inhibitor)	47	Borderline resectable or locally advanced	Not reported	Ib	NCT01413022	(314)
Doi et al., 2019	Anti-PD-1 (Nivolumab) + anti-CCR4 (Mogamulizumab)	96 (15 PDAC)	Immunotherapy-naïve advanced/ metastatic	PDAC: 6.5 (3.5-10.8)	I	NCT02476123	(318)

Bockorn y et al., 2020 (COMB AT)	A: Anti-PD-1 (Pembrolizumab) + anti-CXCR4 (BL-8040) B: Anti-PD-1 (Pembrolizumab) + anti-CXCR4 (BL-8040) + chemotherapy	59	Metastatic	3.3 months in the ITT population, 7.5 months with second-line therapy	IIa	NCT02826486	(319), (320)
Melisi et al., 2018	A: TGFβ Receptor I Kinase inhibitor (Galunisertib) + gemcitabine B: placebo + gemcitabine	156	Locally advanced or metastatic, untreated	A: 8.9 (7.3-11.1) B: 7.1 (5.8-9.0)	Ib/II		(263)
Melisi et al., 2021	TGFβ Receptor I Kinase inhibitor (Galunisertib) + anti-PD-L1 (Durvalumab)	79	Recurrent/ refractory metastatic	5.72 (4.01-8.38)	Ib	NCT02734160	(264)
Strauss et al., 2018	M7824 (bintrafusp alfa, fusion protein of anti-PD-L1 and a TGFβ ligand)	19 (5 PDAC)	Heavily pre-treated	Not reported	I	NCT02517398	(29)
/	M7824 (bintrafusp alfa) + gemcitabine	7	Heavily pre-treated advanced	Terminated after treatment-related death	I/II	NCT03451773	/
/	M7824 (bintrafusp alfa) + SBRT + M9241 (NHS-IL12)	3	Locally advanced	Terminated due to worsening risk:benefit ratio	I/II	NCT04327986	/
Zhou et al., 2022	SHR-1701 (fusion protein targeting PD-L1 and TGFBR2) + gemcitabine/nab-paclitaxel	56	Untreated locally advanced or metastatic	Not yet available	Ib/II	NCT04624217	(38)
Adoptive T-cell therapy							
Aoki et al., 2017	A: Vγ9Vδ2 T-cells + gemcitabine B: gemcitabine alone	56	Curatively resected	Not reported	I	UMIN000000931	(321)
Kumai et al., 2021	A: αβ T-cells B: αβ T-cells + chemotherapy/chemoradiation	77	Previously treated, unresectable advanced	MST: 18.7			(322)
Beatty et al, 2014	Mesothelin-specific mRNA CAR-T-cells (4-1BB and CD3ζ signalling domains)	2 (1 PDAC)	Metastatic	Not reported	I	NCT01355965	(68)
Beatty et al., 2018	Mesothelin-specific mRNA CAR-T-cells	6	Chemotherapy-refractory metastatic	Not reported	I	NCT01897415	(69)
Haas et al., 2019	Mesothelin-specific lentiviral-transduced CAR-T-cells ± cyclophosphamide	15 (5 PDAC)	Chemotherapy-refractory	Not reported	I	NCT02159716	(67)
Thistlethwaite et al., 2017	Carcinoembryonic Antigen (CEA)-specific CAR-T-cells	14 (1 PDAC)	Previously treated,	Not reported	I	NCT01212887	(323)

	(CAECAM5) + IL-2 + fludarabine		CEACAM5+				
Katz et al, 2020 (HITM-SURE)	anti-CEA CAR-T-cells	1	Liver metastases, previously treated	23.2	Ib	NCT02850536	(324)
Lum et al., 2020	Anti-CD3 x anti-EGFR bispecific antibody armed T-cells (+IL-2 + G-CSF)	7	Locally advanced and metastatic	31	I/II	NCT01420874 NCT02620865	(71)

1.6.3.3 Adoptive T-cell therapy

Due to the sparsity of T-cells in the PDAC tumour stroma, many have attempted to use adoptive T-cell therapy for PDAC. This involves the extraction, expansion and reintroduction of a patient's T-cells, either with or without modifications (325). The peripheral human blood contains both αβ and γδ T-cells, the former of which are more common, are activated through MHC molecules and express the T-cell receptor αβ (326, 327). The γδ T-cells are much rarer (1-5%) and do not rely on MHC molecules for their activation (326, 327). Vγ9Vδ2 T-cells are the most prevalent type of γδ T-cells (327) and Aoki and colleagues administered them in combination with gemcitabine to PDAC patients who had undergone a curative surgical resection (see Table 1.8) (321). In comparison with gemcitabine monotherapy, the Vγ9Vδ2/gemcitabine combination did not improve overall or recurrence-free survival (321). The number of autologous T-cells remained high in the patients that remained stable whilst they were reduced in those that progressed (321). In another trial, autologous αβ T-cell monotherapy yielded a median survival time of 18.7 months, which is beyond what can be achieved with gemcitabine (322).

T-cells that are transduced *ex vivo* with a novel exogenous receptor to make them targeted are referred to as Chimeric Antigen Receptor (CAR)-T-cells. Lum and colleagues have transduced T-cells with bispecific antibodies (against both CD3 and EGFR) and these resulted in a mOS of 31 months in late-stage PDAC patients (see Table 1.8) (71). Although this is extremely encouraging, a larger sample would be required to confirm these findings (71). This technique could potentially be translated to other surface receptors; for example, for breast cancer anti-CD3 x anti-HER2 bispecific antibody armed T-cells have been generated (328).

Table 1.9 An overview of clinical trials involving cancer vaccines and oncolytic viruses in PDAC.

Unless stated otherwise, survival is written as median overall survival in months. If this was not available, median survival time has been reported instead. mOS = median overall survival, MST = median survival time, HLA = human leukocyte antigen, KRAS = Kirsten rat sarcoma viral oncogene, CEA = carcinoembryonic antigen, CIK = cytokine-induced killer cell therapy, TLR = toll-like receptor, hTERT = human telomerase reverse transcriptase, VEGFR = vascular endothelial growth factor receptor, WT1 = Wilms tumour 1. Table is from (288). Trial registration numbers have been underlined for trials that tested a combination of immunotherapy with other agents that was eventually approved by NICE in the UK.

Author, year	Immunotherapy treatment arms	Enrolled patients	PDAC stage	mOS (months (95% CI))	Phase	Registration	Ref.
Vaccination							
Rojas et al., 2023	Cevumeran (individualised neoantigen vaccine) + mFOLFIRINOX + Atezolizumab (anti-PD-L1)	34	Surgically resected	Not reached	I	NCT04161755	(329)
Yanagimoto et al., 2010	Personalised peptide vaccine + gemcitabine	21	Untreated, unresectable	MST: 9.0 (6.0-15.5)	II		(330)
Bernhardt et al., 2006	Telomerase peptide vaccination (GV1001 112 μg, 560 μg, 1.87 mg) + GM-CSF	48	Unresectable, untreated	112 μg: 4.0 560 μg: 8.6 1.87 mg: 5.1	I/II		(331)
Middleton et al., 2014 (TeloVac)	A: chemotherapy B: chemotherapy + sequential telomerase peptide vaccination (GV1001) C: chemotherapy + concurrent GV1001	1062	Untreated locally advanced or metastatic	A: 7.9 (7.1-8.8) B: 6.9 (6.4-7.6) C: 8.4 (7.3-9.7)	III	ISRCTN43821338	(332)
Zheng et al., 2021	A: GVAX (neoadjuvant) B: GVAX + IV cyclophosphamide C: GVAX + oral cyclophosphamide	87	Resectable	A: 34.2 (21.6-45.7) B: 15.4 (13.2-26.5) C: 16.5 (11.3-25.2)	II	NCT00727441	(333)
Laheru et al., 2008	A: CG8020/CG2505 (GM-CSF-secreting pancreatic cancer cell line) B: cyclophosphamide + CG8020/CG2505	50	Metastatic	A: 2.3 B: 4.3			(334)
Jaffee et al., 2001	GM-CSF-secreting tumour vaccine + radiation/chemotherapy	14	Resected	Not reported	I		(335)
Lutz et al., 2011	GM-CSF-secreting tumour vaccine + 5-FU-based chemoradiation	60	Resected	24.8 (21.2-31.6)	II	NCT00084383	(336)
Le et al., 2012	ANZ-100 (live-attenuated double deleted *Listeria monocytogenes* strain), IV administration single dose	9 (2 PDAC)	Treatment resistant with liver metastases	Not reported	I	NCT00327652	(337)

Le et al., 2012	CRS-207 (ANZ-100, engineered to express human mesothelin) 4 intravenous doses	17 (7 PDAC)	Treatment resistant	Not reported	I	NCT00585845	(337)
Le et al., 2015	A: 2 doses Cy-GVAX + 4 doses CRS-207 (Listeria-encoding human mesothelin vaccine) B: 6 doses Cy-GVAX	90	Previously treated metastatic	A: 6.1 B: 3.9	II	NCT01417000	(338)
Le et al., 2019 (ECLIPSE)	A: Cy-GVAX + CRS-207 B: CRS-207 C: single agent chemotherapy	Primary cohort: 213 Secondary cohort: 90	Previously treated metastatic	Primary cohort: A: 3.7 (2.9-5.3) B: 5.4 (4.2-6.4) C: 4.6 (4.2-5.7) Secondary cohort: A: 4.3 B: 4.1 C: 9.1	IIb	NCT02004262	(339)
Tsujikawa et al., 2020	A: Cy-GVAX + CRS-207 + anti-PD-1 (Nivolumab) B: Cy-GVAX + CRS-207	93	Previously treated metastatic	A: 5.9 (4.7-8.6) B: 6.1 (3.5-7.0)	II	NCT02243371	(340)
Wu et al, 2020	A: GVAX + anti-CTLA-4 (Ipilimumab) B: FOLFIRINOX	82	Previously treated metastatic	Stopped for futility A: 9.38 (5.0-12.2) B: 14.7 (11.6-20.0)	II	NCT01896869	(341)
Le et al., 2013	A: anti-CTLA-4 (Ipilimumab) B: GVAX + anti-CTLA-4 (Ipilimumab)	30	Previously treated, advanced	A: 3.6 B: 5.7	Ib	NCT00836407	(342)
Lee et al., 2021	Cyclophosphamide, anti-PD-1 (Pembrolizumab), GVAX + SBRT + surgical resection/irreversible electroporation/biopsy	58	Locally advanced	Not reported	II	NCT02648282	(343)
Geynisman et al., 2013	CEA peptide (CAP1-6D)/montanide/GM-CSF vaccine A: 10 μg B: 100 μg C: 1000 μg	19	PS 0-1, HLA-A2+ and CEA-expressing, previously treated	334 days	I	NCT00203892	(344)
Weden et al., 2011	KRAS peptide vaccine + GM-CSF	23	Resected	MST: 27.5	I/II	CTN-95002 CTN-98010	(345)
Abou-Alfa et al., 2011	Adjuvant 21-mer KRAS peptide vaccine + GM-CSF	24	Resected, KRAS mutated	20.3 (11.6-45.3)			(346)
Kubuschok et al., 2012	KRAS vaccine (Ras-transfected EBV-transformed lymphoblastoid cell line)	7	Relapsed or metastatic	Not reported	I	DeReG-Nr.1001	(347)
Palmer et al., 2020	KRAS peptide vaccine (TG01) (A: high antigen burden, B: modified	32	Resected, KRAS mutated	A: 33.1 B: 34.3	I/II	NCT02261714	(348)

	version with lower antigenic burden) + GM-CSF + gemcitabine						
Bassani-Sternberg et al., 2019	Autologous dendritic cells with personalised neoantigen peptide vaccine (PEP-DC) + chemotherapy + anti-PD-1 (Nivolumab) + aspirin	3	Resected	Not reported	Ib	CHUV-DO-0017_PC-PEPDC_2017	(349)
Bauer et al., 2011	Autologous dendritic cell vaccine loaded with tumour lysate + gemcitabine	12	Recurrent/palliative	10.5			(350)
Kimura et al., 2012	Dendritic cell-based vaccine (±lymphokine-activated killer cell therapy) + gemcitabine +S-1	49	Treatment unresponsive, unresectable	360 days			(351)
Yutani et al., 2013	A: Personalised peptide vaccine (based on pre-existing IgG responses) + chemotherapy B: Personalised peptide vaccine	41	Chemotherapy resistant, advanced	MST: A: 9.6 B: 3.1	II	UMIN #08167	(352)
Qiu et al., 2013	Dendritic cell-based and cytokine-induced killer cell-based therapy	14	Unresectable, advanced	24.7			(353)
Lin et al., 2015	Pancreatic cancer stem cell vaccination	90	Resectable	Not reported	I/II	NCT02074046	(354)
Zhang et al., 2016	A: dendritic cell vaccine, cytokine-induced killer cell therapy (CIK) B: no immunotherapy	407 (150 PDAC)	Previously treated	MST: A: 134 days B: 115 days			(355)
Mehrotra et al., 2017	Dendritic cell vaccine (pulsed with A2-restricted peptides: hTERT, CEA, survivin) + TLR-3 agonist	12	Locally advanced or metastatic	7.7	I	NCT01410968	(356)
Asahara et al., 2013	A: KIF20A-66 peptide vaccine (HLA-A*2402 restricted)	29	Metastatic, chemotherapy resistant	MST: 142 days	I/II	UMIN000004919	(357)
Suzuki et al., 2014	KIF20A-derived peptide vaccine (RAB6KIFL) + gemcitabine	9	Previously treated locally advanced	MST: 173 days	I		(358)
Suzuki et al., 2017 (VENUS-PC)	KIF20A-66/VEGFR1-1084/VEGFR2-169 peptide vaccination (all restricted with HLA-A*2402) + gemcitabine	68	Chemotherapy naïve	HLA-matched: 9 HLA-unmatched: 10	II	UMIN000008082	(359)
Miyazawa et al., 2010	VEGFR2 peptide vaccine (VEGFR2-169) (elpamotide) + gemcitabine	18	Unresectable metastatic	MST: All patients: 7.7 No prior chemotherapy: 8.7	I	NCT00622622	(360)
Miyazawa et al., 2017	OCV-C01 (KIF20A/VEGFR1/VEGF	30	Resected	Not reached	II	UMIN000007991	(361)

	R2) peptide vaccination + gemcitabine						
Yamaue et al., 2015 (PEGASUS-PC)	A: VEGFR2 peptide vaccine (elpamotide) + gemcitabine B: placebo + gemcitabine	153	Locally advanced or metastatic	MST A: 8.36 (7.46-10.18) B: 8.54 (7.33-10.84)	II/III	UMIN000001664	(362)
Kameshima et al., 2013	Survivin-2B80-88-derived peptide vaccine + IFNα	6	Advanced	Not reported		UMIN000000905	(363)
Shima et al., 2019	A: Survivin-2B peptide vaccine + IFNβ B: Survivin-2B vaccine only C: placebo Later all patients received the Survivin vaccine + IFNβ	94	Pre-treated advanced, HLA-A24+	A: 102 days (77-144) B: 96.5 days (66-131 C: 111 days (63-150)	II	UMIN 000012146	(364)
Rong et al., 2012	MUC1 peptide-pulsed dendritic cell vaccine	7	Advanced, MUC1-positive	Not reported	I		(365)
Kaida et al., 2011	WT1 peptide vaccine + gemcitabine	25 (9 PDAC)	Unresectable, HLA-A 2402-positive	MST, PDAC: 259 days	I		(366)
Nishida et al., 2014	WT1 peptide vaccine + gemcitabine	32	Advanced, metastatic or recurrent, HLA-A 2402-positive	MST: 8.1 (6.3-10.0)	I	UMIN000001187	(367)
Nishida et al., 2018	A: WT1 peptide vaccine + gemcitabine B: Gemcitabine	91	Advanced, HLA-A*02:01– or HLA-A*24:02–positive	A: 9.6 B: 8.9	II	UMIN000005248	(368)
Koido et al., 2014	Dendritic cell vaccine pulsed with WT1-specific MHC class I/II epitopes + gemcitabine	11 (10 PDAC)	Stage IV, HLA-positive for A*02:01, A*02:06, A*24:02, DRB1*04:05, DRB1*08:03, DRB1*15:01, DRB1*15:02, DPB1*05:01, DPB1*09:01	Not reported	I	UMIN000004063	(369)
Mayanagi et al., 2015	WT1-pulsed dendritic cell vaccine + gemcitabine	10	Advanced, HLA-A 2402-positive	243 days	I	UMIN-000004855	(370)
Yanagisawa et al., 2018	WT1-pulsed dendritic cell vaccine + gemcitabine	8	Resected	Not reported	I		(371)

Hanada et al., 2019	WT1-pulsed dendritic cell vaccine, chemotherapy, radiation and/or surgery	6	Resected, recurrent, or metastatic	1796.5 days			(372)
Nagai et al., 2020	WT1/MUC1-pulsed dendritic cell vaccine + gemcitabine	10	Resected	46.4	I/IIa		(373)
Hardacre et al, 2013	Algenpantucel-L (irradiated allogenic pancreatic cancer cells) + chemotherapy and chemoradiotherapy	73	Resected	Not reached	II	NCT00569387	(374)
Hewitt et al., 2022	A: chemotherapy + chemoradiation B: chemotherapy + algenpantucel-L	303	Borderline resectable or locally advanced unresectable	A: 14.9 (12.2-17.8) B: 14.3 (12.6-16.3)	III	NCT01836432	(375)
Oncolytic viruses							
Aguilar et al., 2015	A: aglatimagene besadenovec (AdV-tk, adenoviral vector expressing HSV-tk gene) + anti-herpetic pro-drug adjuvant to surgery B: aglatimagene besadenovec + anti-herpetic pro-drug adjuvant to 5-FU chemoradiation	24	Resected, locally advanced or metastatic	B: 12	I	NCT00638612	(170)
Lee et al., 2020	Ad5-yCD/mutTK(SR39)rep-ADP (Ad5-DS, replication-competent adenovirus-mediated double suicide gene therapy) + gemcitabine	11	Locally advanced	Not reported	I	NCT02894944	(376)
Muscher et al, 2022	LOAd703 (a TMZ-CD40L/4-1BBL-armed oncolytic adenovirus) + gemcitabine + nab-paclitaxel	22	Unresectable/metastatic	8.7	I/II	NCT02705196	(377)
Bazan-Peregrino et al., 2021	VCN-01 (intratumoural) + gemcitabine + nab-pacitaxel	8	Locally advanced/metastatic	Not reported	I	NCT02045589	(378)
Garcia-Carbonero et al., 2022	For PDACs: A: 1 dose of VCN-01 (intravenous) + nab-paclitaxel + gemcitabine (concurrent) B: 1 dose of VCN-01 (intravenous) + nab-paclitaxel + gemcitabine (7 days after VCN-01)	42 (26 PDAC)	Locally advanced/metastatic, unresectable	A: 11.0 (5.03-48.43) B: 13.47 (2.6-29.6)	I	NCT02045602	(379)
Nakao et al., 2011	HF10 (Herpes Simplex Virus)	6	Unresectable	Not reported	I		(380)
Kasuya et al., 2014	HF10 (Herpes Simplex Virus)	17 (8 PDAC)	Unresectable	Not reported	I		(381)

Hirooka et al., 2018	HF10 (Herpes Simplex Virus) + erlotinib + gemcitabine	12	Unresectable, locally advanced	15.5	I	UMIN000010150	(382)
Hashimoto et al., 2019	Canerpaturev (C-REV, HF10) + gemcitabine + nab-paclitaxel	6	Unresectable, late stage	Not reported	I	NCT03252808	(383)
Noonan et al., 2016	A: Pelareorep (reovirus) + carboplatin/paclitaxel B: carboplatin/paclitaxel	73	Untreated metastatic	A: 7.31 (4.80-11.24) B: 8.77 (6.60-11.76)	II	NCT01280058	(384)
Mahalingam et al., 2018	Pelareorep (Reolysin, reovirus) + gemcitabine	34	Advanced chemotherapy-naïve	10.2 (4.8-17.4)	II	NCT00998322	(385)
Mahalingam et al., 2020	Pelareorep (Reolysin, reovirus) + chemotherapy + anti-PD-1 (Pembrolizumab)	11	Relapsed metastatic	3.1 (0-8.7)	Ib	NCT02620423	(386)

1.6.3.4 Cancer vaccines and oncolytic viruses

A strategy of indirectly attracting T-cells into the tumour stroma is by increasing PDACs' antigenic strength. This refers to increasing the number tumour antigens that can be recognised by the immune system as foreign, which will lead to the formation of tumour-targeted T-cell populations (176). This can be achieved using two different techniques: cancer vaccines and oncolytic viruses (see Table 1.9) (176). The former relies on the introduction of exogenous tumour antigens to reactivate the cancer-immunity cycle (176). The tumour antigens can be either standardised or personalised, which will be based on the expression of for example HLA, KRAS, WT-1 and MUC1. The vaccines can also consist of patient cancer cells or dendritic cells that have been pulsed with peptides or RNA to prime them. Despite this being the more personalised form of immunotherapy, it is a labour intensive and expensive strategy.

Many types of cancer vaccines have been tested in PDAC patients, one of which is GV1001. This peptide vaccine contains the human enzyme telomerase reverse transcriptase (TERT) sequence (387). It was tested in a phase I/II trial where it triggered an immune response in 24 of the 38 participants (331). Interestingly, those that mounted an immune response survived significantly longer than those that did not (331). However, when combined with chemotherapy in the phase III TeloVac trial, the combination generated poorer survival rates (mOS 6.9 months) than chemotherapy alone (mOS 7.9 months) (332). This reduction led to trial termination and its failure was attributed to the dense desmoplastic PDAC stroma.

GVAX is another cancer vaccine that consists of granulocyte-macrophage colony-stimulating factor (GM-CSF)-generating cancer cells, which have been irradiated (341). They are also modified to express GM-CSF to enhance the maturation of dendritic cells (341). To enhance its efficacy, cyclophosphamide if often co-administered with GVAX, which is referred to as Cy-GVAX (334, 340, 341). However, patients with resectable PDAC who were administered neoadjuvant GVAX monotherapy survived longer than patients treated with neoadjuvant Cy-GVAX (333). In contrast in late-stage metastatic patients, the opposite pattern was observed (334). This highlights how the efficacy of certain immunotherapies differs with tumour stage, most likely due to time-dependent changes in the TME.

Due to the prominence of KRAS mutations in PDAC, KRAS peptide vaccines are a promising strategy that in combination with chemotherapy has demonstrated encouraging survival rates with raised T-cell activity (348). However, as monotherapy, KRAS vaccines have yielded conflicting results; all 7 treated metastatic PDAC patients had progressed by the 4-month mark (347). Further research in larger cohorts is required to draw valid conclusions.

Finally, neoantigen mRNA vaccines have been developed as a personalised form of PDAC immunotherapy (329). An example is Cevumeran, which was tested in combination with modified FOLFIRINOX and atezolizumab (anti-PD-L1 antibody) in resected PDAC patients (329). Half of the patients developed a neoantigen-targeted T-cell population and they were labelled ‘the responders’ (329). The responders had a significantly longer median recurrence-free survival than the non-responders (329). If the neoantigen repertoire of the vaccine could be adapted to each patient, the heterogeneity in the patient responses may be suppressed.

Oncolytic viruses have been designed to infect cancer cells whereby triggering cancer cell lysis, a process which triggers the release of tumour antigens and consequently an anti-tumour immune response (170). Clinical trials have been hindered by challenges such as the production of neutralising antibodies against the viruses that prevent successful infection, as well as difficulties with systemic administration of the viruses (170). Hence, oncolytic viruses are frequently injected intratumourally using endoscopic ultrasonography (EUS) or CT (170, 376, 377). Although the safety of oncolytic

adenoviruses has been confirmed in combination with chemotherapy, further studies are required to determine their efficacy.

An oncolytic virus example is the VCN-01 adenovirus which has been modified to express hyaluronidase to digest the hyaluronic acid component of the stroma (378, 379). This compound has been injected both intratumourally (378) and intravenously (379). The intratumoural injection VCN-01 study caused all lesions to remain stable or shrink (378). Along with this, raised levels of serum hyaluronidase and reduced tumour stiffness were noted following VCN-01 therapy (378). Despite increasing the immune cell accessibility, this softening of the tumour stroma may also lead to enhanced metastasis. Intravenously administered VCN-01 was able to infiltrate into the tumour (379). When it was co-administered with chemotherapy, 50% of patients responded (survival >12 months), regardless of chemotherapy timing (379). VCN-01 with delayed chemotherapy improved survival by 2 months in comparison with concurrent chemotherapy. However, patients require selection prior to starting therapy based on pre-existing baseline neutralising antibody levels against the virus. As discussed, intratumoural administration of the virus may reduce its exposure to neutralising antibodies.

1.7 Introduction summary and research rationale

Overall, the overview of clinical trials has demonstrated that for both TNBC and PDAC, very few targeted agents and immunotherapy agents are currently successful. Hence, both tumour types are still mainly treated with unselected chemotherapy. The current clinical trial landscape in TNBC seems to have heavily revolved around CPIs which lead to their recent approval in combination with chemotherapy. However, the CPIs were approved only for a select subset of TNBC patients with sufficient PD-L1 expression (119, 120). This highlights how the efficacy of immunotherapy may be improved by carefully selecting patients based on the tumour immune landscape. Secondly, it also highlights the need for novel agents, beyond CPIs, to treat for example PD-L1 low TNBCs. The promising preclinical findings of some immunotherapy strategies discussed in 1.3, have encouraged their gradual introduction into TNBC clinical trials. Two ongoing trials utilise IL-12 administered through gene therapy to prevent IL-12-

mediated toxicity. This demonstrates the promise of IL-12 as a candidate for TNBC immunotherapy and the importance of exploring alternative bioengineering techniques to reduce its toxicity whilst allowing for intravenous administration.

The results of the clinical trials in PDAC have reminded us of its aggressiveness and challenging TME. In contrast with TNBC, an even smaller proportion of PDAC patients have benefited from CPIs (only MSI-H patients, ≈1%). As discussed, the failure of CPIs in PDACs is largely related to their immune-depleted TME. Therefore, extensive efforts have gone into developing agents that induce immune cell infiltration into these tumours, including CAR T-cells, modified oncolytic viruses, and cancer vaccines. Their success has unfortunately been very limited, suggesting other avenues may need to be explored. Due to the ability of pro-inflammatory cytokines to induce T-cell infiltration, their bioengineered variants are promising, yet preclinical research is currently limited. Moreover, it is crucial to identify mechanisms that drive resistance to immunotherapy in this complex tumour type to overcome them in future experiments.

1.8 Aims and thesis significance

1.8.1 Aim 1. To produce a safe and tolerable bioengineered version of IL-12 for the treatment of two immunologically distinct TNBC mouse models.

Although the therapies for breast cancer have greatly evolved in the last two decades with the discovery of CPIs, TNBC remains a challenge to treat in the clinic. Despite the large cancer cell and immunological heterogeneity that exists within TNBC, most patients currently receive unselected toxic chemotherapy. IL-12 is a potent pro-inflammatory cytokine that has been unsuccessful in the clinic due to its severe autoimmune-like toxicity. Therefore, my first aim was to produce a bioengineered tolerable version of IL-12 and test its efficacy and toxicity in immunologically distinct TNBC subgroups (immunotypes). These immunotypes were previously discovered in bulk TNBC human tumours and were defined using gene signatures in the Sadanandam laboratory. Consequently, I am aiming to identify mouse models that are representative of the different immunotypes and to test their responsiveness to the bioengineered M-CBD-IL-12 molecule. This aim therefore furthers our understanding of how the immune landscape of TNBCs directly influences responsiveness to IL-12-based immunotherapy. Finally, it will allow me to identify potential resistance mechanisms towards this therapy by performing downstream analysis on the harvested tumours. Using such classification systems for therapy selection allows personalisation of immunotherapy and may be key to improving the survival rates of patients with TNBC.

1.8.2 Aim 2. To test M-CBD-IL12 in immunologically distinct PDAC mouse models and understand the role of the *KRAS*^{G12D} mutation in determining the observed responses.

Similarly to TNBC, PDAC is a highly lethal cancer type with very few therapeutic options available. The Sadanandam laboratory has a repertoire of PDAC mouse models available which are well characterised within the laboratory. Therefore, my second aim is focused on testing the bioengineered M-CBD-IL-12 immunotherapy in two immunologically distinct PDAC mouse models. Very few immunotherapeutic agents have demonstrated success in PDAC and understanding the reasons behind this failure is crucial. The available PDAC models not only differ in their immune composition and

morphology but also their *Kras*^{G12D} expression. The *Kras*^{G12D} mutation has been shown to determine the immune composition of PDAC tumours and play a role in immune evasion mechanisms. This means it likely contributes to the unresponsiveness of PDACs to immunotherapy. I therefore decided to focus my second aim on investigating the relationship between the *Kras*^{G12D} mutation and response to IL-12 immunotherapy in these PDAC mouse models. With the recent discovery of the small molecule KRAS G12D inhibitor MRTX1133, this cutting-edge topic remains an important problem to address in PDAC.

1.8.3 Aim 3. To produce and test the efficacy of a bioengineered form of IFNγ as an alternative immunotherapy for PDAC.

IFNγ is an inflammatory cytokine that operates downstream of the IL-12 receptor and triggers a Th1-based response. On the basis that IFNγ is responsible for a large proportion of IL-12's pro-inflammatory effects, a safer version of IFNγ could be a suitable alternative therapeutic candidate for PDAC, yet with a more direct and potent effect. The IL-12 receptor expression is largely limited to T-cells and NK cells, both of which are very sparse in the PDAC TME. Instead, IFNγ has more pleiotropic effects on cancer cells, as well as both the innate and adaptive immune system. This makes it an attractive drug candidate to target an immune-depleted mesenchymal and highly metastatic PDAC model, which has sparse adaptive immune cells in its TME for IL-12 to act on. Therefore, my third aim was focused on producing collagen-anchored IFNγ and testing its ability to prolong the survival of mice bearing immune-depleted highly metastatic PDAC tumours. This aim focuses on opening avenues towards IFNγ immunotherapy that have thus far been closed due to its severe dose-limiting toxicity through bioengineering.

Chapter 2. Materials & Methods

2.1 Cell culture

All cells were cultured under standard tissue culture conditions (humidified incubators at 37 °C and 5% CO_2). I cultured HEK293F and Expi293F cells in serum-free HEK293F Freestyle (Gibco, 12338018) or Expi293F Expression Medium (Gibco, A1435101), respectively, in vented Erlenmeyer flasks (Corning, 431145). The cells were continuously shaken at 130 rpm. EMT6 and 4T1 cells were cultured in DMEM, 10% FBS whilst 7947, 3275, Panc02, AK28385, AK15376, and AK14838 cells were cultured in RPMI 10% FBS. The AK28385, AK15376, and AK14838 inducible *Kras*^{G12D} cells were kindly supplied by Dr. Haoqiang Ying from MD Anderson Cancer Centre, University of Texas (388). Doxycycline hyclate (Merck, D9891) was added to the inducible *Kras*^{G12D} cell culture media at a final concentration of 1 µg/ml. Cells were regularly tested for mycoplasma infections using an in-house nested PCR method.

2.2 Co-culture experiments

For co-culture experiments, a 6-well plate was coated with 3 µg/ml of murine anti-CD3 (clone 17A2, Bioxcell) in PBS and was left overnight at 4 °C. The mice were sacrificed, their spleen was collected and mechanically homogenised using a strainer. Red blood cells were lysed using ACK lysis buffer (Fisher Scientific, 11509876). Finally murine anti-CD28 (clone 37.51, Biolegend), recombinant murine IL-2 (final concentration 30 ng/ml, Peprotech, 212-12) and pen/strep was added to the splenocyte media and the splenocytes were left in culture to activate for 48 hours. The cancer cells were seeded at a concentration of 1000 cells/well in 100 µl and 24 hours later the cancer cell media was removed from the wells and activated splenocytes were added in 100 µl into the wells at a 1:15 Cancer:Effector ratio. The cancer cells and splenocytes were left overnight in the incubator and MRTX1133 (Mirati Therapeutics) was diluted serially and added into the correct wells. The plates were imaged 72 hours after treatment with MRTX1133 using CellTiter-Glo Cell Viability Assay (Promega, G9242).

2.3 Transformation, bacterial culture, and plasmid amplification

The amino acid sequences of murine p35, p40, CBD-p40, mask-linker-p35, wild-type IFNγ, CBD-IFNγ were subcloned into mammalian expression vector pcDNA 3.1(+) by Genscript Biotech. A $(His)_6$ tag sequence was introduced on the N-terminus of p35 and wild-type IFNγ, which allowed me to perform immobilised metal affinity chromatography protein purification. To produce M-CBD-IL12, a sequence that encodes the mask and the linker was introduced at the N-terminus of p35. To generate any of the IL-12-based molecules, I co-transfected the different variations of the p35 and p40 plasmids. To amplify the plasmids, I transformed the plasmid into competent *E. coli* using the heat shock technique (42 °C for 1 minute), followed by spreading the bacteria onto agar plates containing 100 µg/L of ampicillin using an inoculation loop. Following an overnight incubation at 37 °C, I collected a colony and let it grow in 2YT broth containing 100 µg/L of ampicillin overnight on a shaker (220 rpm, 37 °C). The plasmid was consequently extracted from the bacteria using a NucleoBond Xtra Midi kit for transfection-grade plasmid DNA (Machary-Nagel, 740410.50) using the manufacturer's recommendations. The plasmid was finally resuspended in ultrapure water and I used a Nanodrop (Thermo Fisher Scientific) to determine the plasmid concentration.

2.4 Transfection for protein production

Proteins were either produced using HEK293F cells (cultured and transfected at 1 million cells/ml) or Expi293F cells (cultured and transfected at 3 million cells/ml). I passaged both cell lines 24 hours prior to transfection. For a 200 ml flask of the HEK293F cells, I dissolved 400 µg of Linear Polyethylenimine (PEI transfection grade, MW 25 000, 23966-1, final concentration 2 mg/L) into 3.6 ml of Optipro SFM (12309019). In another 4 ml of Optipro SFM, I dissolved 200 µg of plasmid, which I then filtered using a syringe filter Millex-HA Syringe Filter Unit, 0.45 µm, mixed cellulose esters, 33 mm (Merck, SLHA0033SS). When co-transfecting plasmids, I used 200 µg of each plasmid instead (total 400 µg). For the production of M-CBD-IL12, His-mask-linker-p35 and p40-CBD were co-transfected. I combined the PEI-Optipro mixture with the plasmid-Optipro mixture and incubated this at room temperature for 10 minutes. Whilst swirling the Erlenmeyer flask, the mixture was then added in a dropwise manner

to the cells. Expi293F cells were transfected in batches of 125 ml of cell culture media for which I used 2.2 ml of Optipro supplied with 800 µg of linear PEI and 125 µg of DNA dissolved in 2.5 ml of Optipro. For both cell lines, the transfected flasks were shaken for 5 days in a humidified incubator. On day 5 following transfection, the culture was centrifuged at 3000 g, 4 °C for 30 minutes. I filtered the cell culture supernatant using Nalgene Rapid-Flow Sterile Disposable Filter Units (Thermo Fisher Scientific, 166-0045) and adjusted the pH to >8 using 1M Tris.

2.5 Protein purification

I loaded the filtered culture media onto the HisTrap HP His Tag protein purification column (5 ml, Cytiva, 17524801) on the ÄKTA start protein purification system with buffer A (0.5M of NaCl, 20mM of NaH2PO4, titrated with NaOH for pH to rise to 7.2-8.5). I then used buffer B to elute the trapped protein from the column (0.5M of NaCl, 20mM of NaH2PO4, 250mmol of Imidazole). The fractions containing the protein were then loaded onto the size exclusion HiLoad 16/600 Superdex 200pg SEC column (120 ml, Cytiva, 28989335) were analysed using SDS-PAGE under reducing and non-reducing conditions to confirm the purity and the identity of the protein. The correct fractions were then combined and stored at -80 °C.

2.6 Sodium Dodecyl Sulphate Polyacrylamide gel electrophoresis (SDS-PAGE)

Following protein purification, each tube was analysed using 4x reducing (Alfa Aesar, J60015) or 4x non-reducing (Alfa Aesar, J63615) sample buffer and the samples were heated to 95 °C for 5 minutes. They were then loaded into a 4-15% Mini-PROTEAN TGX Precast Protein Gel (Biorad, 4561084) and the gel was run at 150 V, 0.4 Amps and 300 Watts using 1x running buffer (Tris/Gly/SDS buffer)(Biorad, 1610772). The gel was then incubated in Novex Simply Blue Safe Stain (Novex Life Technologies, LC6065) for 2 hours and consequently 3 hours in ultrapure water for destaining. The gel was then imaged using Azure 280 chemiluminescent Imaging system.

2.7 Western blotting

For cell lines, cells were lysed using NP40 buffer (Sigma, 74385-1L) with a protease and phosphatase inhibitor tablet, EDTA-free (Thermo Fisher Scientific, A32961) on ice for 20 minutes. For snap-frozen tumours, a small piece of around 50 mg was placed in a Precellys Lysing tubes (P000911-LYSK0-A.C) with around 100 µl of NP40 buffer (Sigma, 74385-1L)/T-PER buffer (Thermo Fisher Scientific, 78510). Total protein levels were then quantified using the Pierce Bicinchoninic Acid Protein Assay (Thermo Fisher Scientific, 23225) in 96-well flat-bottom microplates according to the manufacturer's instructions. Protein concentration was then standardised in the presence of 4x Laemmli sample buffer (Biorad, 1610747) and samples were heated to 95 °C for 5 minutes prior to sample loading. Samples were then loaded onto a 4-15% Mini-PROTEAN TGX Precast Protein Gel (Biorad, 4561084). The protein was separated at 150V, 0.4 Amps and 300 Watts for 45 minutes in running buffer 10x (Tris/Gly/SDS buffer) (Biorad, 1610772). An activated PVDF membrane was used to transfer proteins onto using the Transblot Turbo Transfer System (Biorad) and it was consequently blocked in 5% milk in Tris Buffered Saline-Tween 0.1% (TBS-T) at room temperature for 1 hour. It was incubated overnight in primary antibody diluted in 5% milk in TBS-T 0.1% on a shaker at 4 °C. Following incubation in secondary antibody, diluted in 5% milk in TBS-T 0.1% for an hour at room temperature, the proteins were detected using Immobilon Crescendo Western HRP Substrate (Merck, WBLUR0500). For primary antibody dilutions, see Table 2.1.

Table 2.1 Primary antibodies for western blotting and Wes Simple Western

Target	Host	Cat. number	Western blot	Simple Western
Murine IL-12	Rat	ab80682	1:200	
Cleaved caspase 3 (Asp175)	Rabbit	9664	1:1000	
Caspase 3 (3G2)	Mouse	9668	1:1000	
Vinculin	Mouse	V9131	1:200	1:10 000
ERK1/2 p44/42 MAPK	Rabbit	4695	1:1000	
p-ERK (T202/Y204) p44/42 MAPK	Rabbit	9101	1:1000	
KRAS G12D	Rabbit	MA5-36256		1:500

2.8 Wes Simple Western

Cells were lysed using NP40 buffer (Sigma, 74385-1L) with a protease and phosphatase inhibitor tablet, EDTA-free (Thermo Fisher Scientific, A32961) on ice for 20 minutes. For snap-frozen tumours, a small piece of around 50 mg was placed in a Precellys Lysing tubes (P000911-LYSK0-A.C) with around 100 µl of NP40 buffer (Sigma, 74385-1L)/T-PER buffer (Thermo Fisher Scientific, 78510). Total protein levels were then quantified using the Pierce Bicinchoninic Acid Protein Assay (Thermo Fisher Scientific, 23225) in 96-well flat-bottom microplates according to the manufacturer's instructions. Simple Western analysis was then performed on the Wes machine using a 12-230 kDa separation module (Biotechne, SM-W001). Per run 0.0625 µg of protein was used per sample and the primary antibodies were diluted as described in Table 2.1. Data was analysed and normalised to Vinculin in the Compass for SW software.

2.9 Ribonucleic acid (RNA) extraction and quantitative real time polymerase chain reaction (qRT-PCR)

Following the harvesting and flash freezing of tumours, they were homogenised in Precellys Lysing tubes (P000911-LYSK0-A.C) that contained TRIzol. Consequently, an miRNeasy Kit (Qiagen, 217084) was used to extract RNA from the tissue homogenate according to the manufacturer's instructions. The RNA product concentration was determined using NanoDrop (Thermo Fisher Scientific). cDNA was synthesised using the Superscript Double-Stranded cDNA synthesis kit (Thermo Fischer Scientific, 11917010) according to manufacturer's instructions. Power SYBR Green PCR master mix (Thermo Fischer Scientific, A25742) was used in combination with murine primers (see Table 2.2) and the data was obtained using the QuantStudio 6 Real-Time PCR System. Mouse PPIA was used as a housekeeping gene to standardise samples using the $2^{\Delta\Delta Ct}$ method.

Table 2.2 List of qRT-PCR primers

Mouse PPIA Forward	AGC ATA CAG GTC CTG GCA TC
Mouse PPIA Reverse	TTC ACC TTC CCA AAG ACC AC
Mouse total KRAS Forward	CAA GAG CGC CTT GAC GAT ACA
Mouse total KRAS Reverse	CCA AGA GAC AGG TTT CTC CAT C
Mouse KRAS G12D Forward 1	GCT TAT CGA TAC CGT CGA TCG
Mouse KRAS G12D Reverse 1	GGT CGT ACT CAT CCA CAA AGT G
Mouse COL1A1 Forward 2	GAC CGA TGG ATT CCC GTT CG
Mouse COL1A1 Reverse 2	GAT AGG TGA TGT TCT GGG AGG C
Mouse COL1A2 Forward 1	TAG TCG ATG GCT GCT CCA AAA
Mouse COL1A2 Reverse 1	GGT GCA ATG TCA AGG AAC GG
Mouse COL3A1 Forward 2	CCC ATG ACT GTC CCA CGT AA
Mouse COL3A1 Reverse 2	AGG GCC ATA GCT GAA CTG AAA A

2.10 Nanostring nCounter Transcriptomic profile

The nCounter Max analysis system (Nanostring Technologies) was used to run a mouse immune panel (custom made in the laboratory) on 100 ng of RNA from tumour samples. The custom assay was performed according to the published protocol by Ragulan et al., 2019 (389). nsolver 4.0 was used to normalise data.

2.11 Enzyme-linked immunosorbent assay (ELISA)

I performed ELISAs in a flat-bottom, clear medium-binding microplate (Greiner Bio-one, 655001). A mouse IFNγ, ELISA kit (Thermo Fisher Scientific, 88-7314-88), a mouse Granzyme B kit (R&D Systems, DY1865), human/mouse TGFβ1 ELISA kit (Thermo Fisher Scientific, 88-8350-88) was used according to the manufacturer's recommendations. Plasma was diluted 1:16, whilst for tumour analysis 50 µg of protein was loaded for mouse IFNγ, 20 µg for granzyme B, and 50 µg for TGFβ1.

2.12 LEGENDplex Mouse Inflammation Panel

Tumours were homogenised using T-PER buffer (Thermo Fisher Scientific, 78510) which was supplemented with 5 mM of EDTA and a protease inhibitor (Roche, 5892791001). Total protein concentration was quantified using the Pierce Bicinchoninic

Acid Protein Assay (Thermo Fisher Scientific, 23225). The kit (Biolegend, 740446) was then used according to the manufacturer's recommendations. Data was analysed on FlowJo and cytokine levels were normalised to protein concentration for the tumour samples.

2.13 M-CBD-IL12 linker cleaving

Tissues were homogenised in the presence of cleaving buffer (150 mM NaCl, 50 mM Tris, 10 mM $CaCl_2$, 0.05% Brij-35, 50 µM $ZnCl_2$) and protein concentrations were determined using the Pierce Bicinchoninic Acid Protein Assay (Thermo Fisher Scientific, 23225). The recombinant murine MMP2 was diluted to 8 µg/ml in buffer (150 mM NaCl, 50 mM Tris, 10 mM $CaCl_2$, 0.05% Brij-35) and this was stored in 20 µl aliquots at -80 °C. On the day of the experiment, an aliquot was activated using 1 µl of 7 mg/ml phenylaminomercuric acetate (Merck, A9563-5G) dissolved in DMSO for 2 hours at 37 °C.

2.13.1 Western blot quantification

Tumour lysates (final concentration of 2 mg/ml) or plasma (diluted 1:5) were incubated with M-CBD-IL12 (final concentration of 0.84 µM) for either 30 minutes, 3 hours or 5 hours at 37 °C. The active MMP2 was incubated with M-CBD-IL12 for 45 minutes at 37 °C. Of each mixture, 10 µg of protein was loaded onto a 4-15% Mini-PROTEAN TGX Precast Protein Gel (Biorad, 4561084). For untreated M-CBD-IL12, I loaded 0.0625 µg of protein and for the MMP2 incubation, I loaded 1 µg of protein onto the gel. I performed a western blot according to 2.8 Western blotting for murine IL-12 (1:500, Abcam, ab80682).

2.13.2 pSTAT4 quantification

Spleens were processed according to 2.2 Co-culture experiments and $CD8^+$ T-cells were isolated using the Mouse $CD8a^+$ T cell Isolation Kit (Miltenyi Biotec, 130-104-075) according to the manufacturer recommendations. The isolated $CD8^+$ T-cells were then activated according to 2.2 Co-culture experiments using anti-CD3 and anti-CD28 in the

presence of 30 ng/ml of murine IL-2 for 72 hours. Tumour lysate (final concentration of 2 mg/ml) was incubated with M-CBD-IL12 (final concentration of 0.84 μM) or wild-type IL-12 (final concentration of 0.84 μM) overnight at 37 °C. On the day of the experiment, 50 000 $CD8^+$ T-cells were seeded per well of a V-bottom plate and they were left to rest in the incubator. Meanwhile, the active MMP2 was incubated with M-CBD-IL12 for 45 minutes at 37 °C. The cytokine mixtures were serially diluted and were added onto the activated $CD8^+$ T-cells for 15 minutes at 37 °C, which was immediately followed by cell fixation using 1x Lyse/fix buffer (diluted in ultrapure water, BD Biosciences, 558049) for 10 min at 37 °C. Following centrifugation at 600 g, 5 min, 4 °C, the supernatant was removed and Permeabilisation buffer III (BD Biosciences, 558050) was added on ice for 30 min. This was followed by 2 washes with Stain buffer (BD Biosciences, 554656) and incubation with CD16/CD32 Fc block (BD Biosciences, 553141, diluted 1:200 in stain buffer) for 15 minutes at 4 °C. Finally, the anti-pSTAT4 antibody (BD Biosciences, 558137, clone 38) incubation (diluted 1:50 in stain buffer) was performed overnight at 4 °C. Cells were then resuspended in 100 μl of stain buffer for flow cytometric analysis.

2.14 Flow cytometry

Tumours were collected in MACS tissue storage solution. A single cell suspension was generated through mechanical dissociation using gentleMACS C tubes (Miltenyi Biotech, 130-093-237) in a gentleMACS Dissociator. Dissociation enzymes from the Tumour Dissociation Kit (Miltenyi Biotech, 130-096-730) were used to chemically dissociated the tumours. In the presence of these enzymes, the tumours were incubated in a 37 °C water bath for 30 minutes, followed by straining through 70 μm strainers and centrifugation (600 g, 5 min 4 °C). The cell suspension was then stained with fixable viability dye in PBS (eBioscience, 65-0865-14), followed by incubation with antibody for 20 minutes at 4 °C. For the antibodies used in flow cytometry experiment see Table 2.3. All antibodies were diluted 1:200. Cells were then washed and resuspended in 150 μl of staining buffer for flow cytometric analysis. Data was analysed on Flowjo and statistical tests were performed using GraphPad Prism.

Table 2.3 List of flow cytometry antibodies used

Marker	Fluorophore	Clone
FOXP3	PE	MF-14
Gr1 (Ly6G/Ly6C)	APC/Cy7	RB6-8C5
PD-1	BB700	J43
PD-L1	BV711	MIH5
F4/80	FITC	BM8
CD45	BUV805	30-F11
CD45	Pacific blue	30-F11
CD3	BUV395	145-2C11
CD4	BV785	RM4-5
CD8	AF700	53-6.7
CD11b	BUV737	M1/70
CD11c	PE-Cy7	N418
CD335	BUV563	29A1.4
IA/IE (MHC II)	BV480	M5/114.15.2
CD206	BV605	C068C2
CD86	BUV805	PO3

2.15 Immunohistochemistry and Picro Sirius Red staining

After 48 hours of fixation in 10% neutral buffered formalin, tumours were embedded in paraffin. Sections of 4 μm thickness were cut and left to dry overnight at room temperature. The sections were then baked at 65 °C for 5 minutes, deparaffinised, processed, and rehydrated using xylene, graded alcohol and water, respectively.

2.15.1 Immunohistochemistry

For immunohistochemistry, antigens were retrieved using a pressure cooker in citrate buffer (pH 6.0) or EDTA buffer (pH 9.0). Following an hour of blocking with 3% Bovine Serum Albumin, slides were coated with primary antibody overnight at 4 °C. The three washes with TBS-T 0.025% Tween were then followed by a 15-minute endogenous peroxidase block (Dako) and a 1-hour secondary antibody incubation at room temperature. The DAB staining was performed (Dako Real Envision kit), immediately followed by haematoxylin counterstaining, dehydration, and mounting of the slides.

2.15.2 Picro Sirius Red staining

For Picro Sirius red staining a 10-minute iron haematoxylin stain was performed first at room temperature, followed by a 10-minute wash. The Picro Sirius Red stain (abcam, ab150681) was consequently added onto the slides and left to incubate at room temperature for 1 hour. The slides were consequently dipped in 0.5% acetic acid, rehydrated, and mounted.

2.16 Animal care

All the protocols under which animal experiments were performed were approved by the UK Home Office Regulations as part of the Animals Scientific Procedures Act 1986. 6-7-week-old female immunocompetent mice were purchased from Charles River Laboratory. Cells were resuspended in 50% Hank's balanced salt solution (HBSS)/50% Matrigel (Corning, 354234) and we injected either subcutaneously in the right flank or orthotopically into the 4th nipple mammary fat pad for breast cancer studies. The diameter of tumours was measured thrice weekly using digital callipers. Tumour volume was calculated using the following formula: $Volume = 4.19 * (\frac{D}{4} + \frac{d}{4})^3$ (D and d represent the large and small diameters of the tumours respectively). Once tumours reached between 50-100 mm^3, mice were randomised into their respective treatment groups. For orthotopic pancreatic injections, mice were anaesthetised using isoflurane and their left flank was shaved and disinfected. Using sterile tools under aseptic conditions, I performed a laparotomy to expose the pancreas. Cancer cells (20 µl) were injected into the pancreas and the abdomen was closed using sutures and skin clips were used to close the skin. Tumour growth was monitored using palpation and mice were randomised using In Vivo Imaging System (IVIS). For survival study, mice were sacrificed when they reach maximum tumour burden, severe ulceration, or the humane endpoint. For intervention studies, all mice in the study were sacrificed once the first animal reaches maximum tumour burden, ulcerates severely, or reaches the humane endpoint. Where possible, tumours were harvested and divided into four pieces for different purposes: flow cytometry, formalin-fixed, two flash frozen in liquid nitrogen for protein and RNA. Where applicable other organs such as the spleen, liver, brain or lung were collected to record number of metastases.

2.17 Single cell RNA sequencing (scRNA-seq) analysis

Raw scRNA-seq data from the GSE191246 (390) dataset was processed through the R Seurat package by Hari PS, a bioinformatician in the Sadanandam laboratory. He performed quality control using nFeature_RNA criteria (between 200-2500) and mitochondrial content (<20%). Doublet cells were removed using the scDblFinder() function of the scDblFinder package. SCTransform method was performed to batch correct samples of different batches. Anchor features of 10000 were selected. Nearest neighbours were calculated using FindNeighbors function with default parameters followed by FindClusters function. This followed by the generation of Uniform Manifold Approximation and Projection (UMAP). Cells were assigned to specific cell types using the celldex package. Centroid from Korlimarla et al. (88) was used as part of correlation assigner to predict the immunotype each cell belongs to. Ensembl biomaRt was used to convert mouse to human gene symbols.

2.18 Statistical analysis

Data are presented as mean ± standard deviation for technical repeats or mean ± standard error of the mean for biological repeats. All *in vitro* experiments were repeated three times independently unless stated otherwise in the figure legends. *In vivo* experiments were performed only once usually with 7 mice per group (n=7), as was previously determined suitable for these experiments through a priori power analysis in the Sadanandam laboratory. Where the number of mice differs from this, this has been specified in the figure legends. All statistical analyses were performed on GraphPad Prism 10 and results were considered statistically significant with a p-value<0.05. For statistically significant results (referred to in the text as ‘significant’), the p-value is shown in the figure and has also been written out in the main text. Two-tailed student’s t-tests were used for the comparison of two independent groups, whilst one-way analysis of variation (ANOVA) or two-way ANOVA tests were used to compare more than 2 different groups. Tukey’s multiple comparison analysis was used to reduce potential error in experiments containing more than 2 groups. For survival curves, the Kaplan Meier technique was applied with a Mantel Cox test.

Chapter 3. Bioengineering interleukin 12 for tolerable immunotherapy in triple negative breast cancer

3.1 Introduction

TNBCs lack the ER, PR, and HER2 making them virtually unresponsive to hormone therapy and targeted therapies such as trastuzumab (anti-HER2 antibody) (391). They are therefore usually treated with unselected chemotherapy, with or without radiation, despite their high degree of heterogeneity (391). Many have attempted to classify TNBC to better understand its complex TME and to identify immunotherapeutic targets. Seven TNBC subtypes were identified based on gene expression data from 21 breast cancer data sets including 587 TNBCs by Lehmann and colleagues: basal-like 1 (BL1), basal-like 2 (BL2), immunomodulatory (IM), mesenchymal (M), mesenchymal stem-like (MSL), luminal androgen receptor (LAR), and unstable (UNS) (392, 393). Cell lines representing each of these subtypes were used to determine the ability of the classification to aid therapy selection (392, 393). Cell lines representative of BL1 and BL2 subtypes were most sensitive to cisplatin. BL1 tumours highly expressed genes related to the cell cycle and DNA damage response, whilst the BL2 subtype is enriched for metabolic pathways (392, 393). Epithelial to mesenchymal transition genes and growth factor pathways were highly expressed in M and MSL tumours. Their representative cell lines responded most to PI3K/mTOR and abl/src inhibitors. LAR tumours had increased androgen receptor signalling and the representative cell lines therefore responded to anti-androgenic medication (bicalumatide) (392, 393). However, they were found to be the least prognostically favourable. Finally, the IM subtype is immunologically inflamed with raised T-cell and B-cell receptor signalling, upregulated cytokine pathways and antigen presentation (392, 393). This subtype has the best prognosis and would most likely be responsive to immunotherapy. Many more TNBC classification systems followed based on transcriptomic and gene expression analysis such as by Burnstein et al. (394) and Jiang et al. (395). However, these are general classifications that do not specifically represent the TME of TNBCs.

To select TNBC patients specifically for immunotherapy, a robust classification system that addresses the immunological heterogeneity in TNBCs is key. Some have achieved

this such as Hu et al. (396) with the immune subtypes 1-3 (IS1, IS2, IS3) based on 299 TNBC samples. IS3 tumours are associated with a better prognosis and have significantly more $CD8^+$ T-cells, Th1 cells, immature and activated B-cells compared to IS1 (396). The authors predict these tumours to respond better to anti-PD-1 therapy and chemotherapy. In contrast, IS1 tumours have a significantly worse prognosis (396).

A second example is the classification into Immunity High, Immunity Medium, and Immunity Low by He et al. (397). As its name suggests, the former subtype has higher immune scoring, lymphocyte infiltration, and expression of HLA genes (397). The expression of *CD8A*, *CD20* and more inflammatory genes was also raised in the Immunity High subtype compared to the Immunity Low subtype, but this was also true for *PD-L1* and *FOXP3* (397). Overall, these factors contributed to the Immunity High subtype being the most prognostically favourable compared to the other two (397).

Finally, our laboratory categorised TNBC into three immunologically distinct immunotypes based on 730 immune genes from 88 human TNBC samples using the non-negative matrix factorisation machine learning technique (see Figure 3.1) (88). The samples were assigned to an immunotype based on which immunotype gene expression pattern (centroid) the sample's gene expression pattern most closely aligned with. After having identified the different immunotypes, they were characterised immunologically. Immunotype 1 was found to be the most prognostically favourable potentially due to its more acutely inflamed nature with raised immune activation (88). Secondly, immunotype 3 is more myeloid enriched with innate immune gene expression patterns and a worse prognosis. Immunotype 2 tumours were enriched with a Th2 response and Tregs and had an intermediate prognosis (88). Due to the sparsity of immunotype 2 cells in comparison with the other two immunotypes, I decided to focus mainly on immunotypes 1 and 3 in this thesis. More such immunological classifications have been developed (398, 399). Although some of them prognosticate and suggest potential therapies that may be effective in each of the subtypes, few have translated these theories to select mouse models for pre-clinical immunotherapy studies.

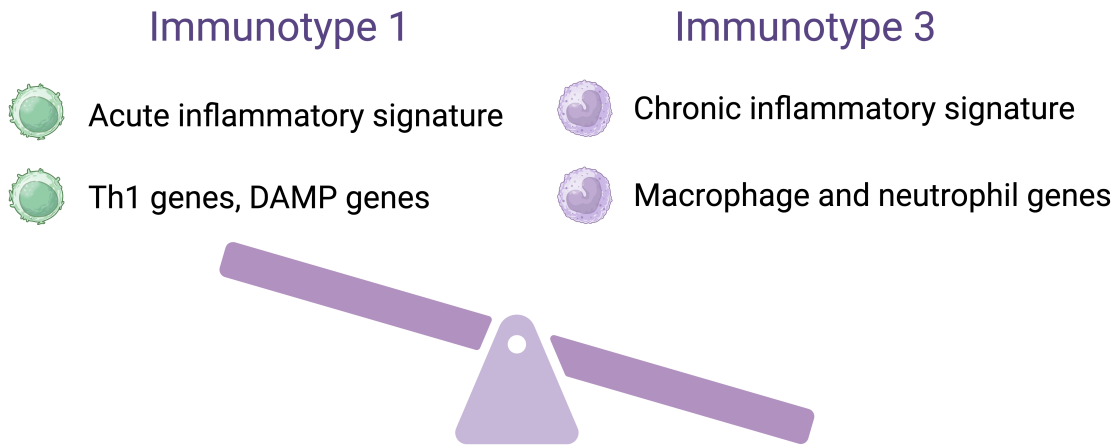


Figure 3.1 Immunological characteristics of the immunotype TNBC classification

Schematic representing characteristics of the immunotype classification by Korlimarla et al. (88). Schematic was created on Biorender.com. DAMP = Damage-associated molecular patterns.

Recently, certain CPIs were approved for TNBC in combination with chemotherapy, as extensively discussed in the introduction (see section 1.5.4.6) (400, 401). However, these are effective in only a small subset of TNBC patients (see section 1.5.4.6), highlighting the need for novel immunotherapeutic agents. Cytokine therapy involving IL-6 and IL-12 has also made an appearance into TNBC clinical trials (98). IL-12 is an example of a highly potent pro-inflammatory anti-tumour cytokine that holds great potential in cancer therapy (13). This cytokine operates through the IL-12 receptor, which consists of IL-12Rβ1 and IL-12Rβ2, and is expressed on mainly T-cells and NK cells (13). IL-12 receptor signalling results in the phosphorylation of STAT4 by the non-receptor protein tyrosine kinases JAK2 and TYK2 (13). Two phosphorylated STAT4 molecules then dimerise and are translocated into the nucleus, where they upregulate the transcription of IFNγ encoding genes through regulators of transcription such a Tbet (13). Therefore, IL-12 receptor signalling results in the production of IFNγ (13). IFNγ is the single member of the type II interferon family with pro-inflammatory effects on both the innate and adaptive immune system (12, 402). It plays an important role in anti-viral defence and tumour immune surveillance by upregulating the expression of MHC to promote antigen presentation (12, 402). Through a positive feedback loop, it also promotes and maintains a Th1-based response and directly prevents differentiation into Th2 cells (403).

A frequently encountered issue with IL-12-based cytokine therapy is its inability to penetrate the tumour stroma and consequently high degrees of peripheral toxicity (17). Therefore, the majority of IL-12 based immunotherapies in TNBC clinical trials have been injected intratumourally (98). Examples are IL-12 monotherapy, a recombinant adenovirus encoding IL-12 (AdIL-12) and the combination of the IL-12-encoding tavokinogene telseplasmid with electroporation and an anti-PD-1 antibody (pembrolizumab)(Table 1.4) (98). Although intratumoural injections for breast cancer are possible, there is still a need to develop therapies that allow intravenous injection with little to no toxicity (98).

Conjugation of IL-12 to a CBD was highly successful in murine models of breast cancer, CRC and melanoma (51). The CBD is a protein, derived from the A3 domain of VWF, with a high affinity for collagen types 1 and 3 (50, 52). In contrast with wild-type IL-12, CBD-IL12 has a much higher molecular weight. This reduces the diffusion of CBD-IL12 across the endothelium into healthy tissues, a process that causes peripheral toxicity (50, 52). However, upon tumour necrosis and an increase in the leakiness of the tumour vasculature, CBD has access to the TME to deliver its cargo (50, 52). This heavily increased the half-life and efficacy of the molecule, whilst suppressing the toxicity (51). Here, I have masked CBD-IL12 to even further reduce the IL-12 associated toxicity. The mask is attached to the p35 subunit of IL-12 through a protease-sensitive linker. The linker is selectively cleaved by MMP1, 2 and 9, as well as the serine proteases urokinase, legumain, and matriptase. These proteases are highly expressed in the tumour stroma and to a lesser degree in the bloodstream. Therefore, the linker should be preferentially cleaved by the tumour leading to a tumour-specific activation of this bioengineered molecule. The aim of this chapter is to establish an association between the TNBC immune landscape of mouse models through immunotyping and the success of M-CBD-IL12 therapy.

3.2 Results

3.2.1 Mouse model selection

The immunotype centroid from Korlimarla et al. (88) was applied (by Hari PS, a bioinformatician in the Sadanandam laboratory) to a murine tumour scRNA-seq dataset (GSE191246) (390) to find whether EMT6 and 4T1 are representative mouse models of the immunotypes (1, 2, and 3). Based on the scRNA-seq data, the 4T1 and EMT6 models seem to closely overlap with immunotypes 1 and 3, respectively, but some immunotype 2 cells are present (see Figure 3.2a,d). EMT6 is a more heterogeneous model than 4T1 since it also expresses immunotype 1 and 2 genes (see Figure 3.2a). In contrast, 4T1 is a predominant immunotype 1 model with very little immunotype 3 influence (see Figure 3.2b).

In terms of the cell types that populate the tumours, EMT6 contains mostly monocytes, in particular the $CD14^+$ and $CD16^+$ monocytes (see Figure 3.2b,c). It simultaneously also harbours few B-cells and Th17 cells, albeit to a lesser extent (see Figure 3.2b,c). In contrast, 4T1 is more T-cell inflamed (see Figure 3.2e,f), particularly Th17 $CD4^+$ T-cells and also B-cells, yet contains few myeloid cells. Since the TME of tumours largely determines their response to immunotherapy, I decided to produce and test wild-type IL-12 and M-CBD-IL12 proteins as cytokine therapies in both mouse models.

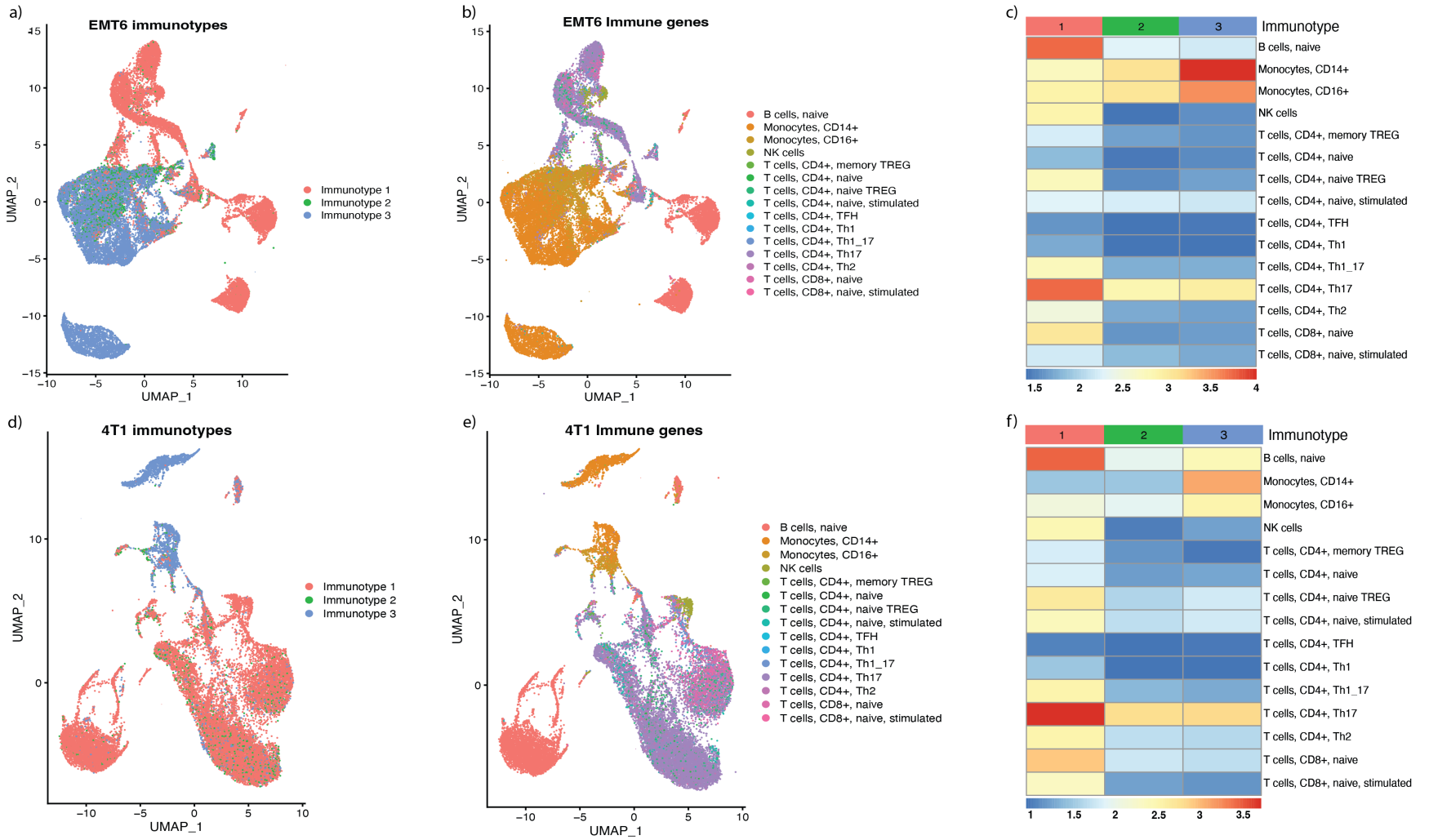


Figure 3.2 Classification of EMT6 as an immunotype 3- and 4T1 as an immunotype 1-dominant model using scRNA-seq

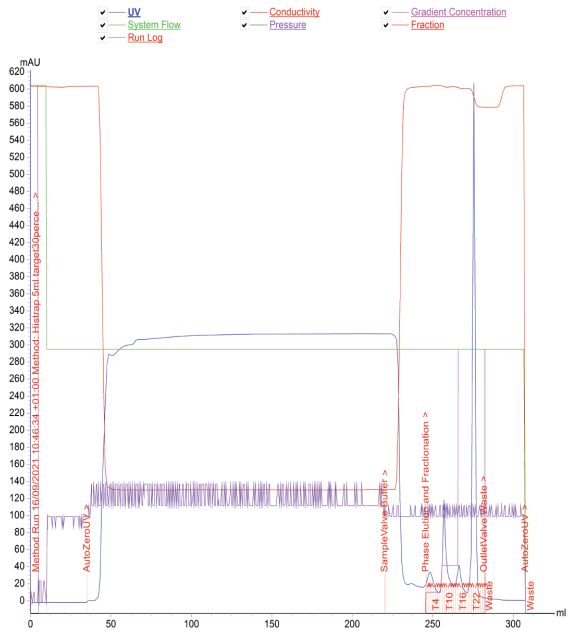
The centroid from Korlimarla et al., 2022 was used on scRNA-seq data of a-c) EMT6 or d-f) 4T1 tumours from GSE191246 from Carpen et al., 2022 to classify the cells into immunotypes a/d). The cell populations were labelled using the celldex package and have been presented as UMAPS in b/e) and heatmaps in c/f). The contents of this figure were generated by Hari PS.

3.2.2 Protein production

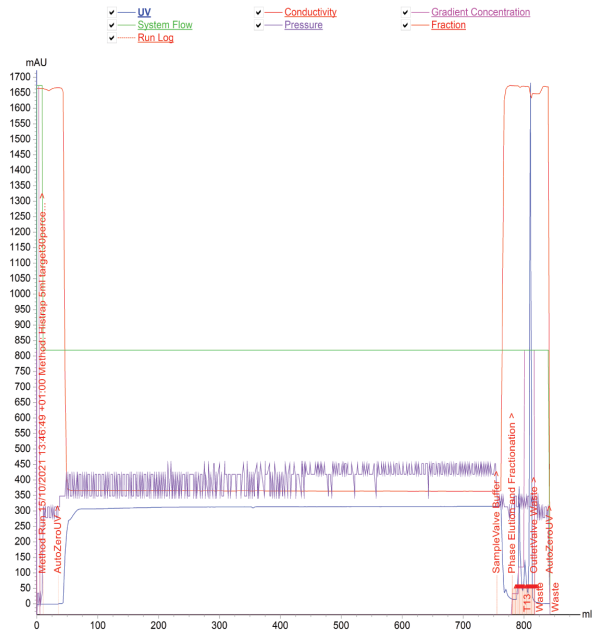
3.2.2.1 Wild-type IL-12

To produce wild-type IL-12, I transfected both HEK293F (batches 1 and 2) and Expi293F cells (batch 3) using linear PEI. These transfections for batches 1 and 2 were successful with UV absorbance peaks (blue curve) of 600 milliabsorbance units (mAU) (batch 1) and 1650 mAU (batch 2) on HisTag purification (see Figure 3.3a,b). The size exclusion chromatograms demonstrate clear UV absorbance peaks (see Figure 3.3c,d) and the fractions corresponding to the protein were consequently analysed using SDS-PAGE under reducing (R) and non-reducing (NR) conditions (see Figure 3.3e,f). Using the former, I observed two distinct bands representing the p35 (35 kDa) and p40 (40 kDa) subunits of IL-12 (see Figure 3.3e,f) as a consequence of the reducing agent β-mercaptoehtanol disrupting the disulphide bonds between the IL-12 subunits (404). In contrast, the non-reducing conditions represent IL-12 with intact disulphide bonds and therefore a molecular weight of 70 kDa (see Figure 3.3e,f). These SDS-PAGEs allowed me to confirm the successful production and purification of the target protein.

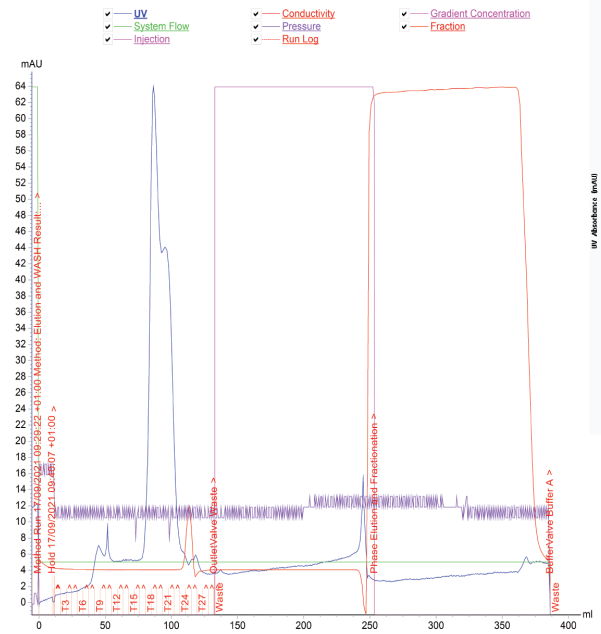
a)


UV
System Flow
Run Log
Conductivity
Pressure
Gradient Concentration
Fraction
mAU
ml
Method Run: 16/09/2021 10:46:34 +01:00 Method: Histrap 5ml target30perce... >
AutoZeroUV >
SampleValve Buffer >
Phase Elution and Fractionation >
OutletValve Waste >
AutoZeroUV >
Waste

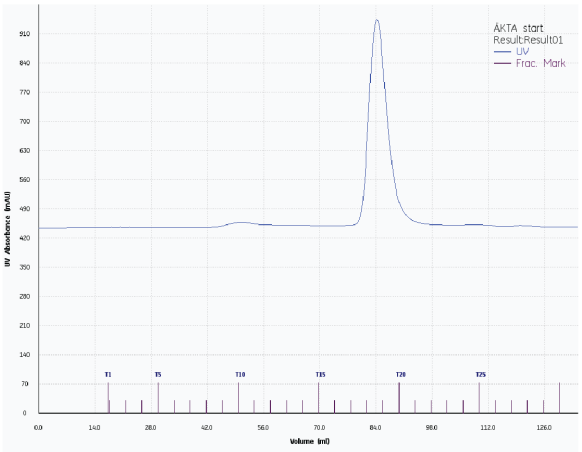
b)


UV
System Flow
Run Log
Conductivity
Pressure
Gradient Concentration
Fraction
mAU
ml
Method Run: 15/10/2021 13:46:49 +01:00 Method: Histrap 5ml target40perce... >
AutoZeroUV >
SampleValve Buffer >
Phase Elution and Fractionation >
OutletValve Waste >
AutoZeroUV >
Waste

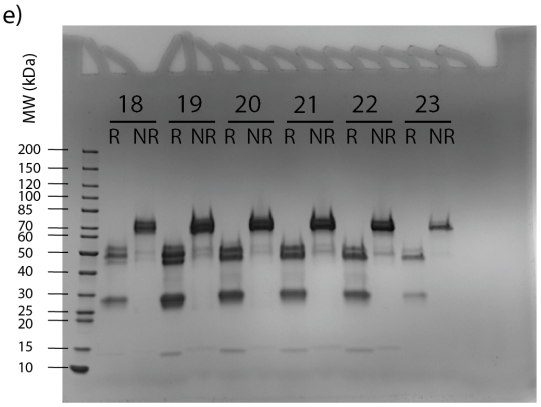
c)


UV
System Flow
Injection
Conductivity
Pressure
Run Log
Gradient Concentration
Fraction
mAU
ml
Method Run: 17/09/2021 09:29:22 +01:00 Method: Elution and WASH Result... >
Hold 17/09/2021 09:48:07 +01:00 >
OutletValve Waste >
Phase Elution and Fractionation >
BufferValve Buffer A >
Waste

d)


ÄKTA start
ResultResult01
UV
Frac. Mark
UV Absorbance (mAU)
Volume (ml)

e)


MW (kDa)
18 19 20 21 22 23
R NR R NR R NR R NR R NR R NR
200
150
120
100
85
70
60
50
40
30
25
20
15
10

f)

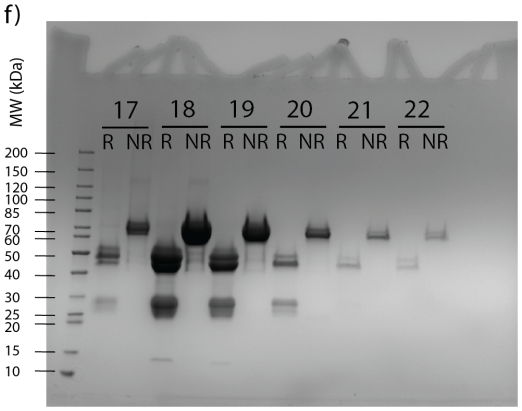

MW (kDa)
17 18 19 20 21 22
R NR R NR R NR R NR R NR R NR
200
150
120
100
85
70
60
50
40
30
25
20
15
10

Figure 3.3 Wild-type IL-12 was successfully produced in HEK293F cellsHEK293 cells were used for IL-12 production using PEI in both batches 1 a/c/e) and 2 b/d/f). Five days following transfection according to 2.4 of the Methodology, the filtered cell media was loaded onto the HisTrap HP HisTag protein purification column on the ÄKTA start protein purification system and the immobilised metal affinity chromatograms are displayed in a) for batch 1 and b) for batch 2. In these chromatograms, the blue curve represents the UV absorbance of the protein and is displayed as milliabsorbance units (mAU) on the y-axis, whilst the x-axis represents the volume of purified media. The consecutive size exclusion chromatograms are displayed in c) for batch 1 and d) for batch 2. The fractions corresponding with the peak were then analysed on SDS-PAGE e) for batch 1 and f) for batch 2 under reducing (R) and non-reducing (NR) conditions. The chromatograms were generated on Cytiva Unicorn.

Due to the cell concentration of Expi293F cells at transfection being three-fold higher than with HEK293F cells, I hypothesised the concentration of PEI should be tripled. I therefore optimised the protocol by transfecting two 125 ml cultures of Expi293F cells using 125 µg of plasmid DNA and either 600 µg (see Figure 3.4a) or 800 µg (see Figure 3.4b) of PEI for my batch 3 of murine wild-type IL-12. The histogram UV absorbance peak increased from 650 mAU at 600 µg (see Figure 3.4a) to 1100 mAU with 800 µg of PEI (see Figure 3.4b). Using this protocol, the Expi293F cell line was therefore the more efficient cell line for the production of wild-type IL-12. The obtained protein from Expi293F cells was also relatively purer compared to HEK293F cells as can be seen on the SDS-PAGE (see Figure 3.4d).

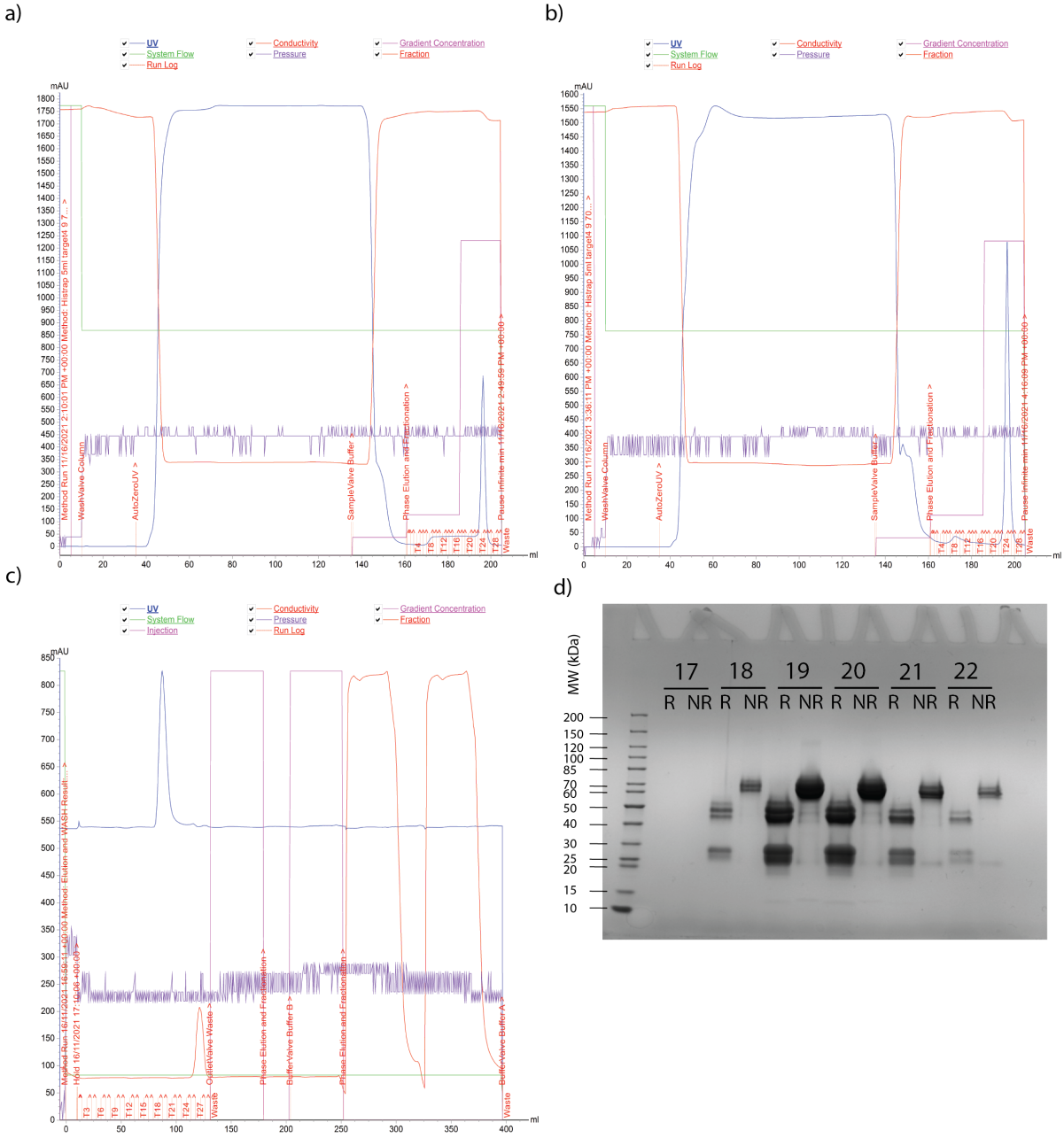


Figure 3.4 Wild-type IL-12 was successfully producing in Expi293F cells Expi293F cells were transfected with either 600 µg a) and 800 µg b) of linear PEI for 125 µg of DNA. Five days following transfection according to 2.4 of the Methodology, the filtered media was loaded onto the HisTrap HP HisTag protein purification column on the ÄKTA start protein purification system and the immobilised metal affinity chromatograms are displayed in a) and b). In these chromatograms, the blue curve represents the UV absorbance of the protein and is displayed as milliabsorbance units (mAU) on the y-axis, whilst the x-axis represents the volume of purified media. The consecutive size exclusion chromatogram is also displayed in c). Finally, the fractions containing this peak were analysed through SDS-PAGE d). The chromatograms were generated using Cytiva Unicorn.

3.2.2.2 M-CBD-IL12

M-CBD-IL12 protein was produced in a similar fashion to its wild-type counterpart. Following initial confirmation that the co-transfection protocol was successful for these plasmids, a large 2 litre culture of HEK293F cells was transfected and purified, which yielded the majority of the M-CBD-IL12 used in this thesis (see Figure 3.5a-c); this transfection generated a peak of 2000 mAU on the metal affinity chromatogram (see Figure 3.5a). Similarly to wild-type IL-12 (see Figure 3.3e,f), the intact M-CBD-IL12 molecule (112 kDa) can be seen as a single band in the non-reducing conditions (see Figure 3.5c). However, under reducing conditions, the separated mask-linker-p35 and p40-CBD proteins are visible as overlapping bands (see Figure 3.5c).

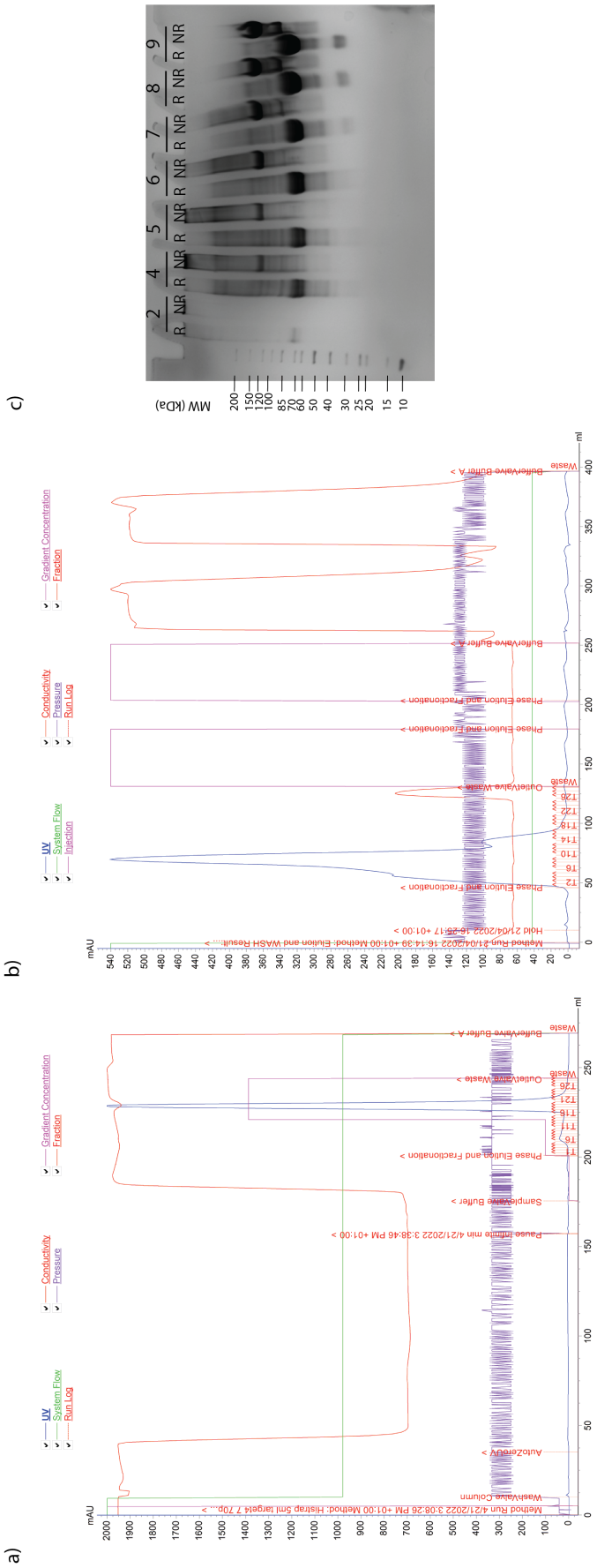


Figure 3.5 M-CBD-IL12 was successfully produced in HEK293F cells

The immobilised metal affinity chromatogram of M-CBD-IL12 produced in HEK293F cells according to 2.4 of the Methodology, are shown in a). In this chromatogram, the blue curve represents the UV absorbance of the protein and is displayed as milliabsorbance units (mAU) on the y-axis, whilst the x-axis represents the volume of purified media. The b) size exclusion chromatogram and c) SDS-PAGE are displayed. The chromatograms were generated using Cytiva Unicorn.

Unfortunately, Expi293F cell transfections were unsuccessful for M-CBD-IL12 (see Figure 3.6); during the elution and fractionation phase of the protein from the HisTrap HP column, only a very small peak can be observed in the UV absorbance (blue curve)(see Figure 3.6). Similarly to HEK293F cells, the Expi293F cells can secrete proteases into the culture media following transfection. Due to the cell concentration of Expi293 cells at transfection being three-fold larger than HEK293F, the quantity of proteases may have been considerably larger in these transfections. These proteases can cleave the linker of M-CBD-IL12 prior to harvesting the protein. Therefore, we ensured the His tag was located within the amino acid sequence in between the IgG kappa signal sequence and the mask sequence. This means the HisTag purification process will ensure the proteins being trapped in the HisTrap HP column are masked and intact and not contaminated with unmasked CBD-IL12. Therefore, the protein yield following HisTag purification with Expi293 cells was much lower than with HEK293F cells. This also meant a small proportion of cleaved off mask may have collected in the HisTrap HP column along with M-CBD-IL12. This was however easily separated from M-CBD-IL12 during the consecutive size exclusion purification due to its much lower molecular weight.

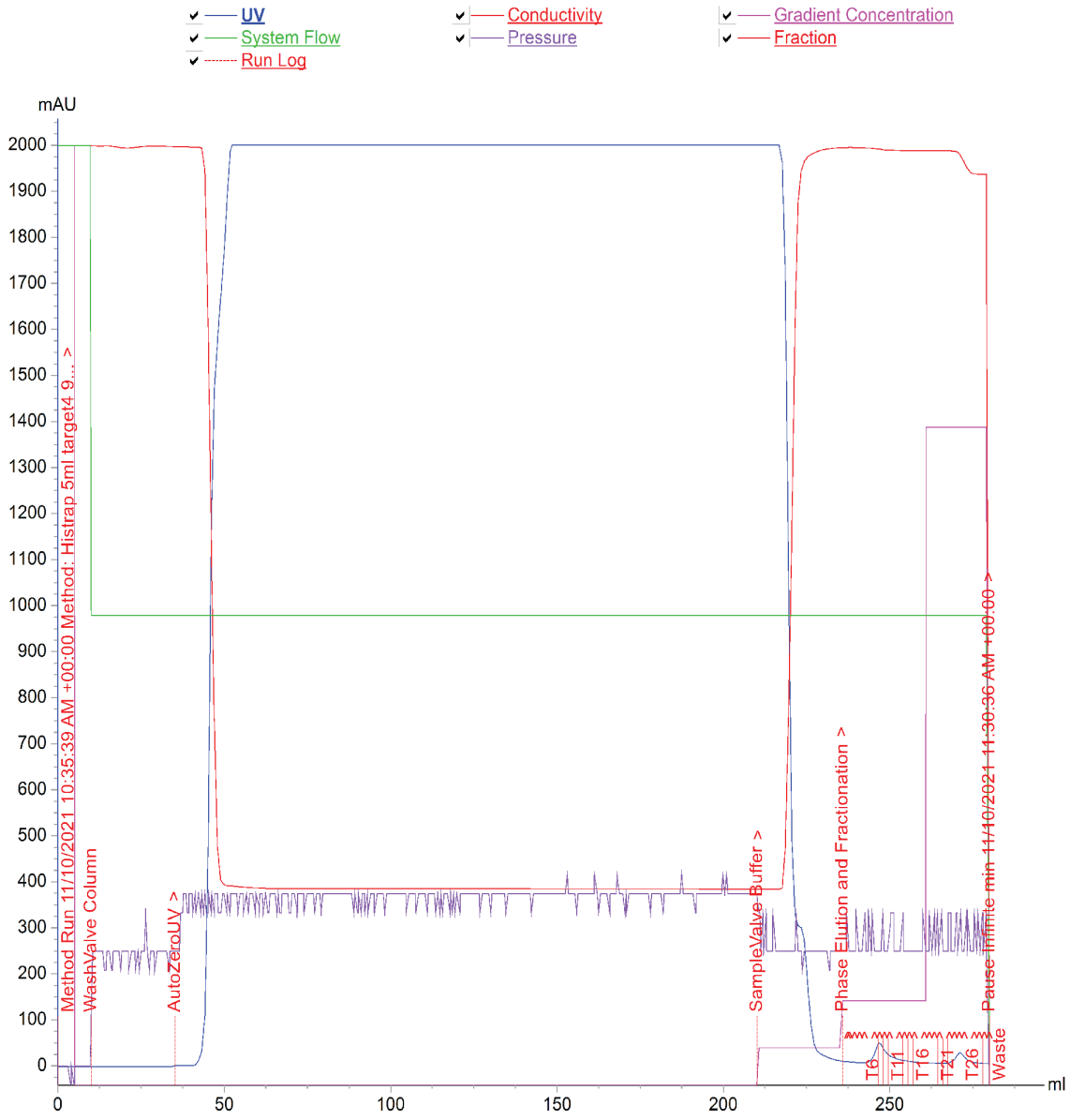


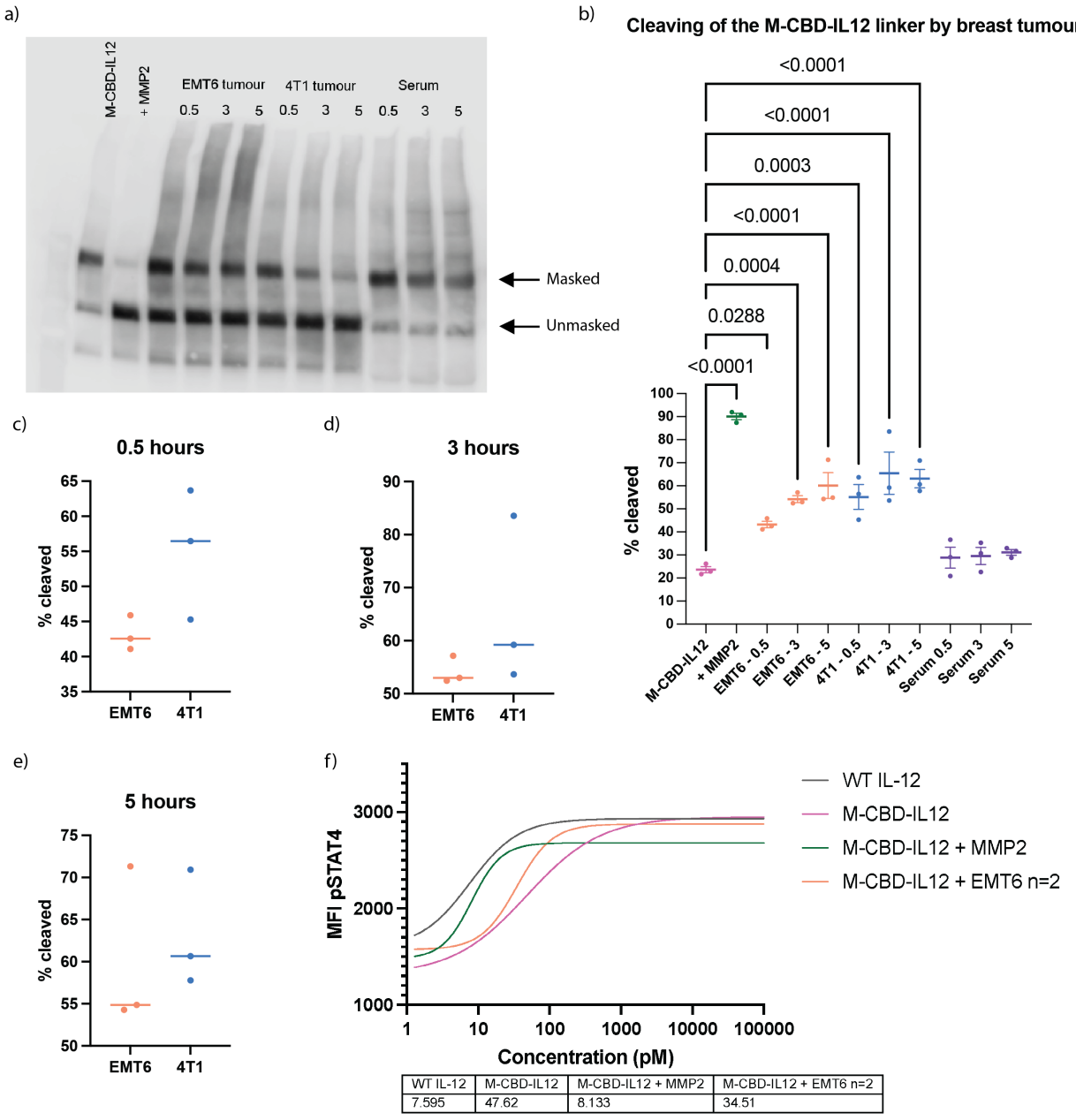
Figure 3.6 M-CBD-IL12 production in Expi293F cells was unsuccessful

The immobilised metal affinity chromatogram of M-CBD-IL12 in Exp293F cells using PEI. In these chromatograms, the blue curve represents the UV absorbance of the protein and is displayed as milliabsorbance units (mAU) on the y-axis, whilst the x-axis represents the volume of purified media. The chromatogram was generated using Cytiva Unicorn.

3.2.3 The M-CBD-IL12 linker is cleaved by breast tumour lysate but not serum *in vitro*

Following the production of the proteins, I proceeded to test the cleaving of the linker in an *in vitro* setting using mouse tissues. I firstly performed this by incubating M-CBD-IL12 with tumours lysates and serum as described in the methodology section 2.13.1, followed by a western blot for murine IL-12 (see Figure 3.7a). Due to the larger molecular weight of M-CBD-IL12 (112 kDa) compared to CBD-IL12 (102 kDa), I was able to differentiate between the two to quantify the cleaving of the linker (see Figure 3.7a). The majority of untreated M-CBD-IL12 was masked, whilst incubation with active murine recombinant MMP2 significantly increased the cleaving of the linker to 90% ($p<0.0001$)(see Figure 3.7b). EMT6 and 4T1 tumour lysates cleaved around 50-60% of the linker (see Figure 3.7b-e). The percentages cleaved were not significantly different between the two tumour models at any of the time points (see Figure 3.7c-e). Interestingly, incubating M-CBD-IL12 with serum did not increase the cleaving of the mask compared to the untreated M-CBD-IL12 (see Figure 3.7b), suggesting the molecule should remain masked in the bloodstream and therefore be less toxic than wild-type IL-12.

To support these findings, a second experiment was performed that aimed to measure whether removal of the mask restored the ability of IL-12 to trigger signalling downstream of the IL-12 receptor, in particular the phosphorylation of STAT4 in primary $CD8^+$ T-cells (see Figure 3.7f). Since the mask with an intact linker suppresses the biological activity of IL-12, the EC50 of untreated M-CBD-IL12 was six-fold higher compared to wild-type IL-12 (see Figure 3.7f). The wild-type IL-12 and M-CBD-IL12 + MMP2 conditions had virtually the same EC50 suggesting recombinant murine MMP2 completely restores the biological activity of M-CBD-IL12 by removing the mask (see Figure 3.7f). Incubating M-CBD-IL12 with EMT6 tumour lysate confirmed that the molecule's biological activity increased following cleaving of the mask, albeit less than with the recombinant murine MMP2 (see Figure 3.7f). These experiments suggests that the tumour lysate restores a portion of M-CBD-IL12 biological activity, though its signalling ability remains lower than wild-type IL-12.



WT IL-12	M-CBD-IL12	M-CBD-IL12 + MMP2	M-CBD-IL12 + EMT6 n=2
7.595	47.62	8.133	34.51

Figure 3.7 The M-CBD-IL12 linker is cleaved by breast tumour lysates but not serum

a) Western blot of murine IL-12 representing the cleaving of the linker following incubation of M-CBD-IL12 with tumour lysates and serum for 0.5, 3 or 5 hours and 37 °C as described in 2.13.1 of the Methodology. Of the incubation mixtures, 10 µg of protein was loaded onto a gel, except for 0.0625 µg of untreated M-CBD-IL12 and 1 µg of the murine MMP2 mixture. The top band represents M-CBD-IL12 whilst the bottom band represents unmasked CBD-IL12 b) Three independent experiments were performed and blots were quantified. c-e) Comparison of the cleaving of the linker at each of the time points for the different tumour lysates. f) Quantification of the *in vitro* activity of M-CBD-IL12 on pre-activated primary $CD8^+$ T-cells through measurements of pSTAT4 MFI using flow cytometry as described in 2.13.2 of the Methodology. The EC50 values have been displayed in the table. Experiment was performed once for confirmation of biological activity. Flow cytometry data was analysed using Flowjo.

Statistical analyses were performed using a two-tailed student's t-test or one-way ANOVA with Tukey's multiple comparison test on GraphPad Prism.

3.2.4 *In vivo* evaluation of M-CBD-IL12 in the syngeneic EMT6 TNBC mouse model

The study design used to evaluate the toxicity of wild-type and M-CBD-IL12 in non-tumour bearing mice is shown in Figure 3.8a. No significant changes in body weights were observed over time and between the conditions (see Figure 3.8b). Murine IFNγ in the plasma was quantified using ELISA as a toxicity marker (see Figure 3.8c,d). Plasma IFNγ on day 2 was significantly higher in the mice treated with wild-type IL-12 (350 pg/ml) than those treated with M-CBD-IL12 ($p=0.0005$), whose plasma IFNγ concentration was virtually zero (see Figure 3.8c,d). Interestingly, by day 6, the plasma IFNγ levels in the wild-type IL-12 group had decreased to around 3 pg/ml, at which point it was still significantly higher than with M-CBD-IL12 ($p=0.0473$) (see Figure 3.8d). This suggests that in non-tumour bearing mice, M-CBD-IL12 was considerably less toxic than wild-type IL-12 and that plasma IFNγ concentrations decreased rapidly over time.

As an *in vivo* pilot study, my colleague Dr. Aslan Mansurov at the University of Chicago previously tested the anti-tumour effects of both produced proteins in the MC38 CRC mouse model (see Figure 3.8e), which the Ishihara laboratory has previously shown to be highly responsive to IL-12 (73). The MC38 tumours fully responded to either molecule, albeit more delayed in response to M-CBD-IL12 compared to wild-type IL-12 (see Figure 3.8f). These findings confirmed this molecule was biologically active *in vivo*.

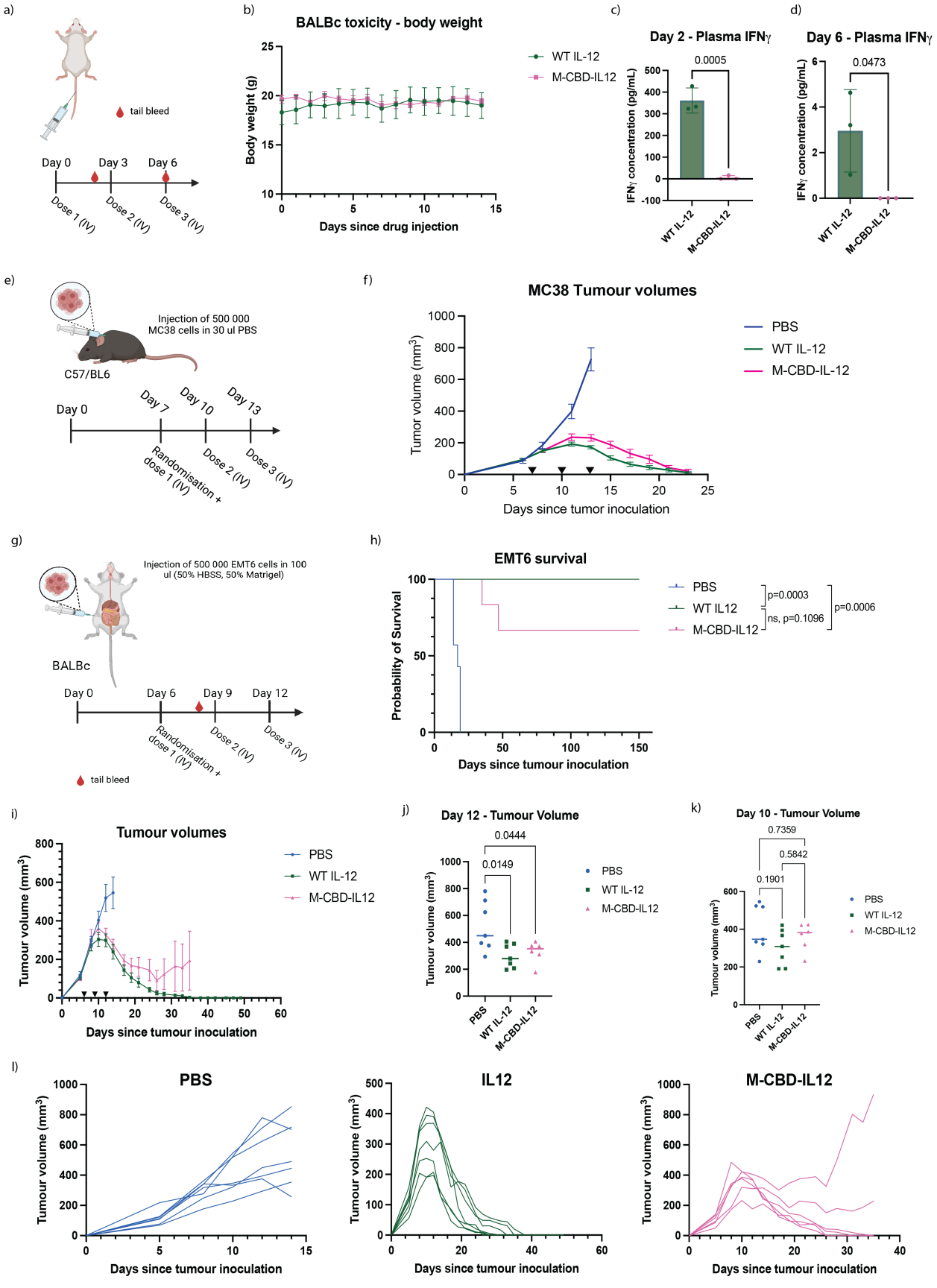

a)
tail bleed
Day 0
Day 3
Day 6
Dose 1 (IV)
Dose 2 (IV)
Dose 3 (IV)
b)
BALBc toxicity - body weight
Body weight (g)
Days since drug injection
WT IL-12
M-CBD-IL12
c)
Day 2 - Plasma IFNγ
0.0005
IFNγ concentration (pg/mL)
WT IL-12
M-CBD-IL12
d)
Day 6 - Plasma IFNγ
0.0473
IFNγ concentration (pg/mL)
WT IL-12
M-CBD-IL12
e)
Injection of 500 000 MC38 cells in 30 ul PBS
C57/BL6
Day 0
Day 7
Day 10
Day 13
Randomisation + dose 1 (IV)
Dose 2 (IV)
Dose 3 (IV)
f)
MC38 Tumour volumes
Tumor volume (mm3)
Days since tumor inoculation
PBS
WT IL-12
M-CBD-IL-12
g)
Injection of 500 000 EMT6 cells in 100 ul (50% HBSS, 50% Matrigel)
BALBc
Day 0
Day 6
Day 9
Day 12
Randomisation + dose 1 (IV)
Dose 2 (IV)
Dose 3 (IV)
tail bleed
h)
EMT6 survival
Probability of Survival
Days since tumour inoculation
PBS
WT IL12
M-CBD-IL12
p=0.0003
ns, p=0.1096
p=0.0006
i)
Tumour volumes
Tumour volume (mm3)
Days since tumour inoculation
PBS
WT IL-12
M-CBD-IL12
j)
Day 12 - Tumour Volume
0.0444
0.0149
Tumour volume (mm3)
PBS
WT IL-12
M-CBD-IL12
k)
Day 10 - Tumour Volume
0.7359
0.5842
0.1901
Tumour volume (mm3)
PBS
WT IL-12
M-CBD-IL12
l)
PBS
IL12
M-CBD-IL12
Tumour volume (mm3)
Days since tumour inoculation

Figure 3.8 M-CBD-IL12 was tolerable *in vivo* and demonstrated anti-tumour effects against the MC38 CRC mouse model and the EMT6 TNBC mouse model

a) Study design of the tolerability study of wild-type (WT) IL-12 and M-CBD-IL12 in non-tumour bearing BALB/c mice. Non-tumour-bearing 6-7-week-old BALB/c mice (n=3) were treated with 83 pmol of wild-type IL-12 or 250 pmol of M-CBD-IL12 intravenously (IV) on days 0, 3, and 6. b) The mice's body weight was recorded for 13 days following the first dose. Plasma IFNγ quantification through ELISA from days 2 c) and 6 d) following the first dose of the respective drugs. e) Study design of the pilot mouse study on the MC38 mouse model, performed by my colleague Dr. Aslan Mansurov. C57/BL6 mice (n=7) were injected with 500 000 MC38 cells subcutaneously and were then administered 3 doses of either 83 pmol of wild-type IL-12 or 250 pmol of M-CBD-IL12 intravenously (IV) on days 7, 10, and 13 following tumour inoculation. f) Tumour growth curve of MC38 tumours. g) Study design of the survival study of wild-type IL-12 and M-CBD-IL12 in the EMT6 mouse model. 6-7-week-old BALB/c mice (n=7 for PBS and wild-type IL-12, n=6 for M-CBD-IL12 group) were injected with 500 000 EMT6 cells in the 4th nipple mammary fat pad and were administered 3 doses of either 83 pmol of wild-type IL-12 or 250 pmol of M-CBD-IL12 intravenously on days 6, 9, and 12. h) Kaplan-Meier survival curve and i) tumour growth curve of both wild-type IL-12 and M-CBD-IL12 in EMT6-bearing mice. Differences in EMT6 tumour volume between treatment groups on days j) 12 and k) 10 following tumour inoculation. l) individual tumour growth curves for the EMT6 survival study. Each mouse experiment was performed only once. Statistical analyses were either performed with two-tailed student's t-test, one-way ANOVA with Tukey's multiple comparison tests or Mantel Cox test for Kaplan Meier survival curves on GraphPad Prism. Schematics were designed on Biorender.com

I then evaluated the anti-tumour effects of M-CBD-IL12 in EMT6-bearing mice (see Figure 3.8g). EMT6-bearing mice treated with wild-type IL-12 survived significantly longer compared to PBS-treated mice (p=0.0003) (see Figure 3.8h). These mice all exhibited complete responses (see Figure 3.8i,l). During a monitoring period of 150 days following tumour inoculation, they all remained tumour-free (see Figure 3.8i,l). Similarly, complete tumour regressions were observed in four out of the six mice that received M-CBD-IL12 (see Figure 3.8i,l). These mice also survived significantly longer than PBS controls (p=0.0006) and remained tumour-free throughout the consecutive 248 days following tumour inoculation (see Figure 3.8h). No significant difference was observed between wild-type IL-12 and M-CBD-IL12 treatment groups in terms of survival, however as observed in *in vitro* studies, it seems the mask and CBD minimally dampen the biological activity of IL-12 (see Figure 3.8h,i). Between days 10 and 12 post-tumour inoculation, the difference in tumour volume between the treatment groups and the PBS group became significant (p=0.0149 for wild-type IL-12, p=0.0444 for M-

CBD-IL12), which suggested this was a suitable time point to analyse the immunological changes inside the tumour (see Figure 3.8j,k).

3.2.4.1 Immunological composition of the EMT6 tumour following M-CBD-IL12 therapy

I therefore proceeded to visualise the immunological mechanisms that may be responsible for reducing the tumour burden in the EMT6 mouse model following M-CBD-IL12 treatment. To achieve this, I performed an intervention study with a similar design as the survival study, yet all mice were terminated using cardiac punctures on day 11 and tumours and spleens were collected for flow cytometric analysis (see Figure 3.9a). At this point, the tumour volume in the treatment groups was reduced compared to PBS, albeit not yet significant (see Figure 3.9b). Interestingly, the spleen weight was significantly higher in the wild-type IL-12 group compared to the PBS ($p<0.0001$) and M-CBD-IL12 ($p=0.0041$) groups (see Figure 3.9c). This splenomegaly could suggest the mice treated with wild-type IL-12 were experiencing significantly more toxicity than the M-CBD-IL12 group.

Flow cytometric analysis of the tumours revealed a significant decrease in intratumoural immune cells ($CD45^+$)($p=0.0295$)(see Figure 3.9d) and a significant increase in intratumoural non-immune cells ($CD45^-$)($p=0.0341$)(see Figure 3.9e) in the tumours of mice treated with wild-type IL-12 compared to PBS. A similar trend was visible in the mice treated with M-CBD-IL12 to an extent, but not at a statistically significant level (see Figure 3.9d,e). Although overall NK cells (see Figure 3.9j) and T-cell numbers (see Figure 3.9f) remained largely unaltered, $CD4^+$ T-cells significantly decreased in the wild-type IL-12 group compared to PBS ($p=0.0213$) (see Figure 3.9g). $CD4^+$ T-cells comprise of multiple different subsets, such as Th1, Th2, Th17 and Treg cells. Although specific changes in Th1, Th2, and Th17 subsets were not included in this flow cytometry panel due to the limited availability of tissue in the treated tumours, the treatment-induced changes in Tregs will be discussed as part of the next figure. Interestingly, $CD8^+$ T-cells significantly increased in the M-CBD-IL12 group in comparison with PBS mice ($p=0.0406$) (see Figure 3.9h,i). This suggests M-CBD-IL12 is somewhat remodelling the EMT6 TME.

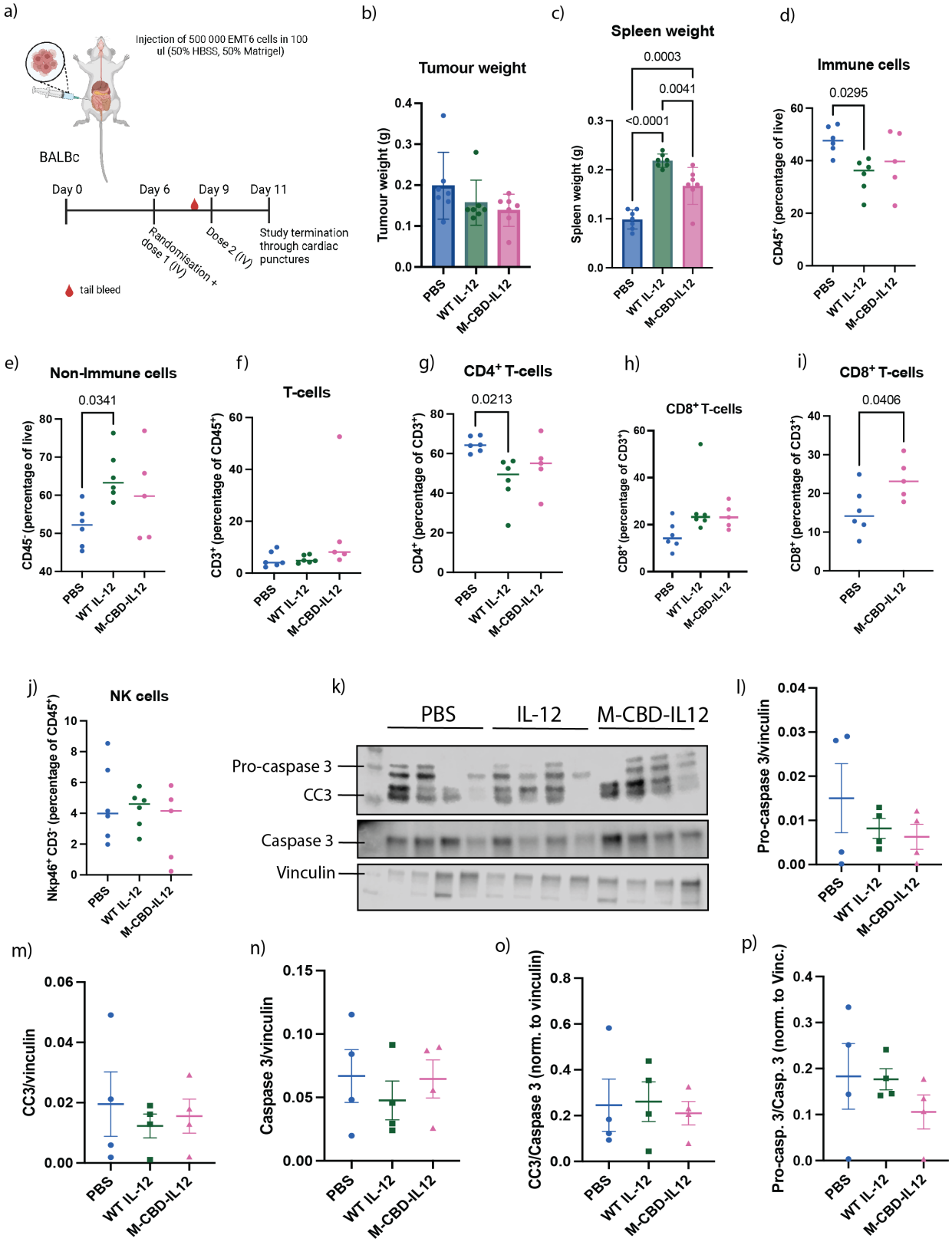


Figure 3.9 M-CBD-IL12 remodelled the TME of EMT6 tumours

a) Study design of the intervention study of M-CBD-IL12 and wild-type (WT) IL-12 in the EMT6 mouse model. 6-7-week-old BALB/c mice (n=7) were inoculated with 500 000 EMT6 cells in the 4th nipple mammary fat pad and treated with 83 pmol of wild-type IL-12 or 250 pmol of M-CBD-IL12 intravenously (IV) on days 6 and 9 following tumour inoculation. All mice were sacrificed through a cardiac puncture on day 11. Mouse tumour b) and spleen c) weights at study termination on day 11. d-j) Flow cytometric analysis of the tumours was performed. k-p) From each group, 4 tumours were lysed, and protein levels were standardised to 10 µg and a western blot was performed for the expression of cleaved caspase 3, pro-caspase, and total caspase 3. Blots were quantified and normalised to the loading control. Each mouse experiment was performed only once. Tumour samples with poor quality on flow cytometry were excluded from the study and flow cytometry data was analysed on Flowjo. Statistical analyses were performed with either a two-tailed student's t-test or one-way ANOVA with Tukey's multiple comparison test on GraphPad Prism. Schematics were designed on Biorender.com

Cytotoxic CD8$^+$ T-cells can exert their cytotoxic effect towards cancer cells by inducing cancer cell apoptosis (405). Due to the observed increase in CD8$^+$ T-cells, I therefore also quantified the intratumoural expression of a commonly used marker and the major effector of apoptosis (406), using western blotting (see Figure 3.9k-p). A slight reduction in pro-caspase 3 (see Figure 3.9l) and in the proportion of pro-caspase 3 to total caspase 3 (see Figure 3.9p) was observed, although neither of these differences were significant. No major changes were observed elsewhere (see Figure 3.9m-o). This suggests IL-12 may be inducing cancer cell apoptosis through an alternative effector to caspase 3 in the EMT6 model.

For the enlarged population of CD8$^+$ T-cells within EMT6 tumours to be active, they require antigen presentation by antigen presenting cells, an example of which are dendritic cells. Although dendritic cells seemed to be showing an increasing trend, particularly for the wild-type IL-12 group, this change was not significant (see Figure 3.10a). In contrast, a significant reduction in other cell types, of which some are considered immunosuppressive, was also observed following wild-type IL-12 and M-CBD-IL12 therapy. Particularly macrophages ($p=0.0457$)(see Figure 3.10b,c), neutrophils ($p=0.0062$)(see Figure 3.10d,e), Tregs ($p=0.0005$)(see Figure 3.10f,g), and PD-1$^+$ CD8$^+$ T-cells ($p=0.0171$)(see Figure 3.10k) were significantly decreased with M-CBD-IL12 compared to PBS. Notably, the latter two are crucial resistance mechanisms to IL-12 that seem to be relieved with therapy in this case.

Due to the ability of IL-12, and particularly its downstream effector IFNγ, to induce checkpoint upregulation which can lead to resistance (407), I also quantified their expression on various cell types. Wild-type IL-12, but not M-CBD-IL12, seemed to be triggering an increase in PD-L1 on $CD8^+$ T-cells (see Figure 3.10l) and $CD45^-$ cells (see Figure 3.10o), and increases in PD-1 expression on NK cells (see Figure 3.10m). Therefore, subtle differences exist between wild-type IL-12 and M-CBD-IL12 activity in inducing immunosuppressive mechanisms.

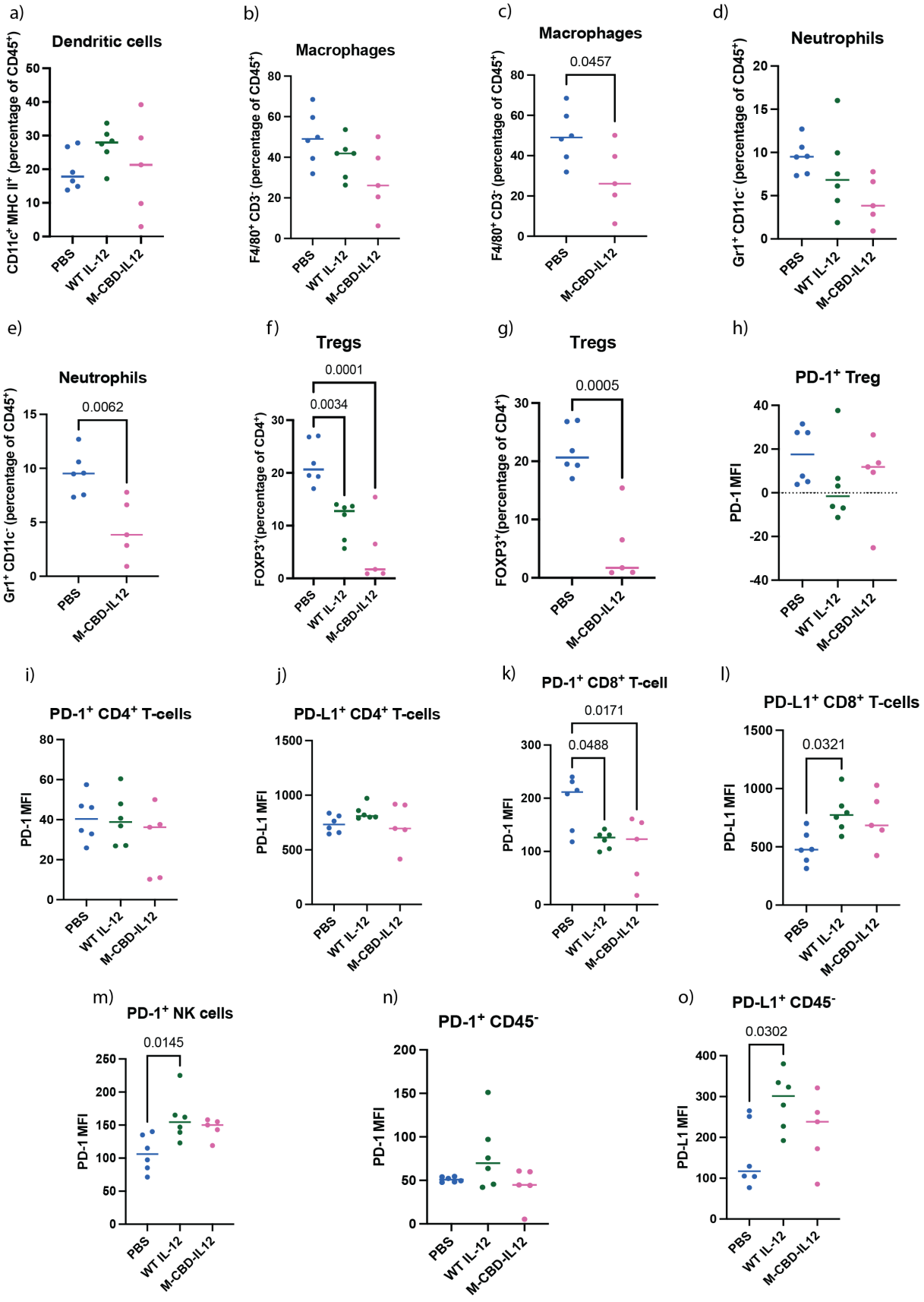

a)
Dendritic cells
CD11c+ MHC II+ (percentage of CD45+)
b)
Macrophages
F4/80+ CD3- (percentage of CD45+)
c)
Macrophages
0.0457
F4/80+ CD3- (percentage of CD45+)
d)
Neutrophils
Gr1+ CD11c- (percentage of CD45+)
e)
Neutrophils
0.0062
Gr1+ CD11c- (percentage of CD45+)
f)
Tregs
0.0001
0.0034
FOXP3+(percentage of CD4+)
g)
Tregs
0.0005
FOXP3+(percentage of CD4+)
h)
PD-1+ Treg
PD-1 MFI
i)
PD-1+ CD4+ T-cells
PD-1 MFI
j)
PD-L1+ CD4+ T-cells
PD-L1 MFI
k)
PD-1+ CD8+ T-cell
0.0171
0.0488
PD-1 MFI
l)
PD-L1+ CD8+ T-cells
0.0321
PD-L1 MFI
m)
PD-1+ NK cells
0.0145
PD-1 MFI
n)
PD-1+ CD45-
PD-1 MFI
o)
PD-L1+ CD45-
0.0302
PD-L1 MFI
PBS
WT IL-12
M-CBD-IL12

Figure 3.10 M-CBD-IL12 suppressed myeloid cells, Tregs and exhausted CD8$^+$ T-cells in the EMT6 TME

6-7-week-old BALB/c mice (n=7) were inoculated with 500 000 EMT6 cells in the 4th nipple mammary fat pad and treated with 83 pmol of wild-type (WT) IL-12 or 250 pmol of M-CBD-IL12 intravenously (IV) on days 6 and 9 following tumour inoculation. All mice were sacrificed through a cardiac puncture on day 11. Tumours were processed and stained for flow cytometry. Each mouse experiment was performed only once. Tumour samples with poor quality on flow cytometry were excluded from the study and flow cytometry data was analysed on Flowjo. Statistical analyses were performed using two-tailed student's t-tests or one-way ANOVA with Tukey's multiple comparison tests on GraphPad Prism.

3.2.4.2 Immunological composition of the spleen following M-CBD-IL12 therapy

Due to the crucial role of the spleen as a secondary lymphoid organ in mice, analysing its immune composition may help understand the effects of M-CBD-IL12 therapy in EMT6 mouse models. I noted that mice treated with wild-type IL-12 harboured fewer intra-splenic CD45$^+$ cells than the M-CBD-IL12 group (see Figure 3.11a). This suggests the CD45$^+$ cells in wild-type IL-12 mice were scarce both in the tumour (see Figure 3.9d) and in the spleen (see Figure 3.11a).

Intra-splenic T-cells were significantly reduced in both wild-type IL-12 (p=0.0002) and M-CBD-IL12 (p=0.0162) groups in comparison with PBS (see Figure 3.11c). However, no differences were observed between conditions in CD4$^+$ and CD8$^+$ T-cells (see Figure 3.11d,e). A slight reduction in NK cells in both treated groups could also be seen (see Figure 3.11f), along with an increase in Tregs (see Figure 3.11g). Neither of these trends were however statistically significant. Meanwhile, I observed a significant increase in splenic dendritic cells with both wild-type IL-12 (p=0.0004) and M-CBD-IL12 (p=0.0027), suggesting enhanced antigen presentation is taking place (see Figure 3.11h). A second cell type with antigen presenting abilities are macrophages, which were significantly higher with wild-type IL-12 therapy compared to PBS (p=0.0005) and M-CBD-IL12 (p=0.0022) treatment (see Figure 3.11i). Due to the extensive heterogeneity within macrophage populations, further experiments are required to understand which subtypes in particular are altered by IL-12 immunotherapy, which will be discussed later in this chapter. Splenic neutrophil populations did not differ between the therapy groups (see Figure 3.11j). Overall, a lot of variation however existed between the different mice for these cell types.

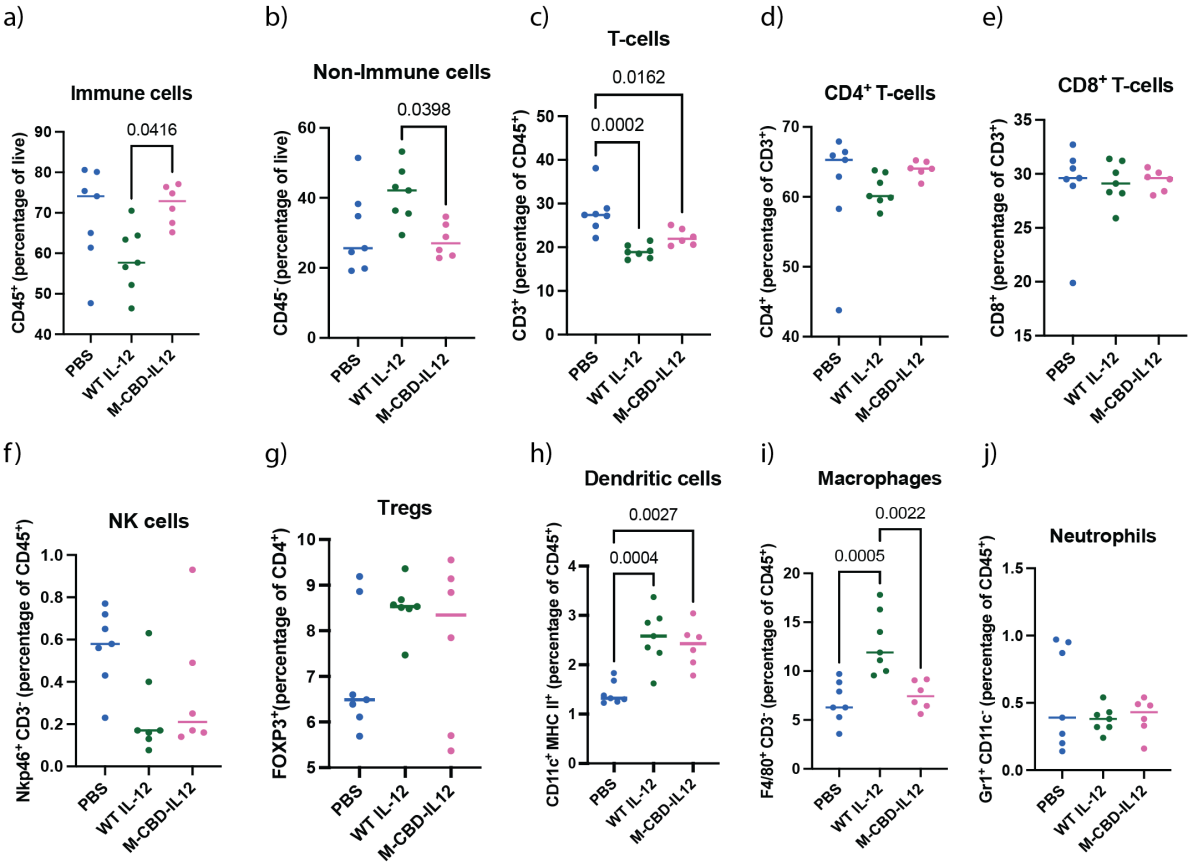


Figure 3.11 Both wild-type IL-12 and M-CBD-IL12 increase dendritic cell and reduce T-cell populations in the spleen of EMT6 bearing mice

6-7-week-old BALB/c mice (n=7) were inoculated with 500 000 EMT6 cells in the 4th nipple mammary fat pad and treated with 83 pmol of wild-type (WT) IL-12 or 250 pmol of M-CBD-IL12 intravenously (IV) on days 6 and 9 following tumour inoculation. All mice were sacrificed through a cardiac puncture on day 11. Spleens were processed and stained for flow cytometry. Each mouse experiment was performed only once. Spleen samples with poor quality on flow cytometry were excluded from the study and flow cytometry data was analysed on Flowjo. Statistical analyses were performed using one-way ANOVA with Tukey's multiple comparison tests on GraphPad Prism.

In contrast with the tumour, the expression of PD-1 in the spleen did not differ between groups on any of the cell types shown (see Figure 3.12a-d). However, PD-L1 expression on CD4$^+$ and CD8$^+$ T-cells and CD45$^-$ cells was significantly raised with wild-type IL-12 in comparison with the M-CBD-IL12 and PBS groups (see Figure 3.12e-g). This increase in checkpoint expression only in the wild-type IL-12 group, but not with M-CBD-IL12, was also previously observed in the tumour (see Figure 3.10l,m,o), This

once again confirms that differences in immunosuppressive mechanisms exist between wild-type IL-12 and M-CBD-IL12.

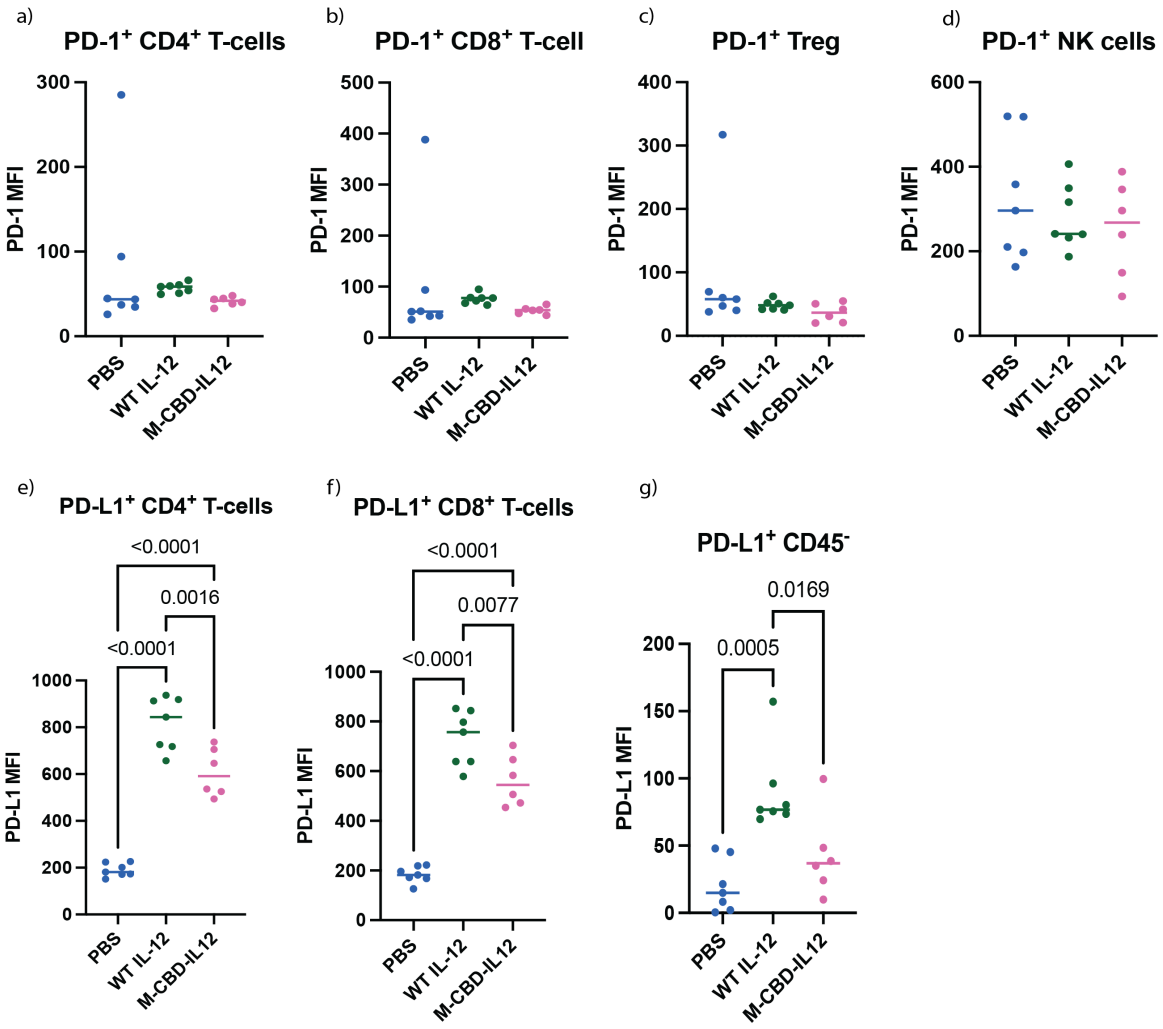


Figure 3.12 Wild-type IL-12, but not M-CBD-IL12 therapy, significantly increased PD-L1 expression in the spleen

6-7-week-old BALB/c mice (n=7) were inoculated with 500 000 EMT6 cells in the 4th nipple mammary fat pad and treated with 83 pmol of wild-type (WT) IL-12 or 250 pmol of M-CBD-IL12 intravenously (IV) on days 6 and 9 following tumour inoculation. All mice were sacrificed through a cardiac puncture on day 11. Spleens were processed and stained for flow cytometry. Each mouse experiment was performed only once. Spleen samples with poor quality on flow cytometry were excluded from the study and flow cytometry data was analysed on Flowjo. Statistical analyses were performed using one-way ANOVA with Tukey's multiple comparison tests on GraphPad Prism.

3.2.4.3 M-CBD-IL12 and wild-type IL-12 significantly increased intratumoural IFNγ and significantly reduce TGFβ1 expression in EMT6 tumours

Since immune cell differentiation, particularly T-cell differentiation, is strongly governed by cytokine levels (408), I measured the intratumoural cytokine levels in the different treatment groups using ELISA and a cytokine quantification kit (LEGENDplex Mouse Inflammation Panel (13-plex)). Intratumoural IFNγ was significantly higher in both the wild-type IL-12 ($p=0.0010$) and M-CBD-IL12-treated ($p=0.0136$) tumours when measured through ELISA compared to PBS (see Figure 3.13a). The increase with M-CBD-IL12 was less drastic than with wild-type IL-12, confirming there is a slight suppression of the activity of IL-12 by the mask. This increase in IFNγ was validated through the LEGENDplex Mouse Inflammation Panel (13-plex) cytokine quantification kit (see Figure 3.13d).

I proceeded to quantify intratumoural levels of TGFβ1 (see Figure 3.13b) and granzyme B (see Figure 3.13c) using ELISA. With both wild-type IL-12 ($p=0.0027$) and M-CBD-IL12 ($p=0.0003$), TGFβ1 levels were decreased significantly in EMT6 tumours compared to PBS, but this decrease was slightly larger in the M-CBD-IL12 group (see Figure 3.13b). This suggests M-CBD-IL12 and wild-type IL-12 may be reducing tumour burden by relieving this crucial immunosuppressive pathway. Overall, there seemed to be an increasing trend in the cytotoxic granzyme B levels in the M-CBD-IL12 group, yet this change was not significant (see Figure 3.13c). This suggests cancer cells are eliminated by M-CBD-IL12 relieving TGFβ1-mediated immune suppression rather than through direct granzyme B-mediated cytotoxicity towards cancer cells in the EMT6 model.

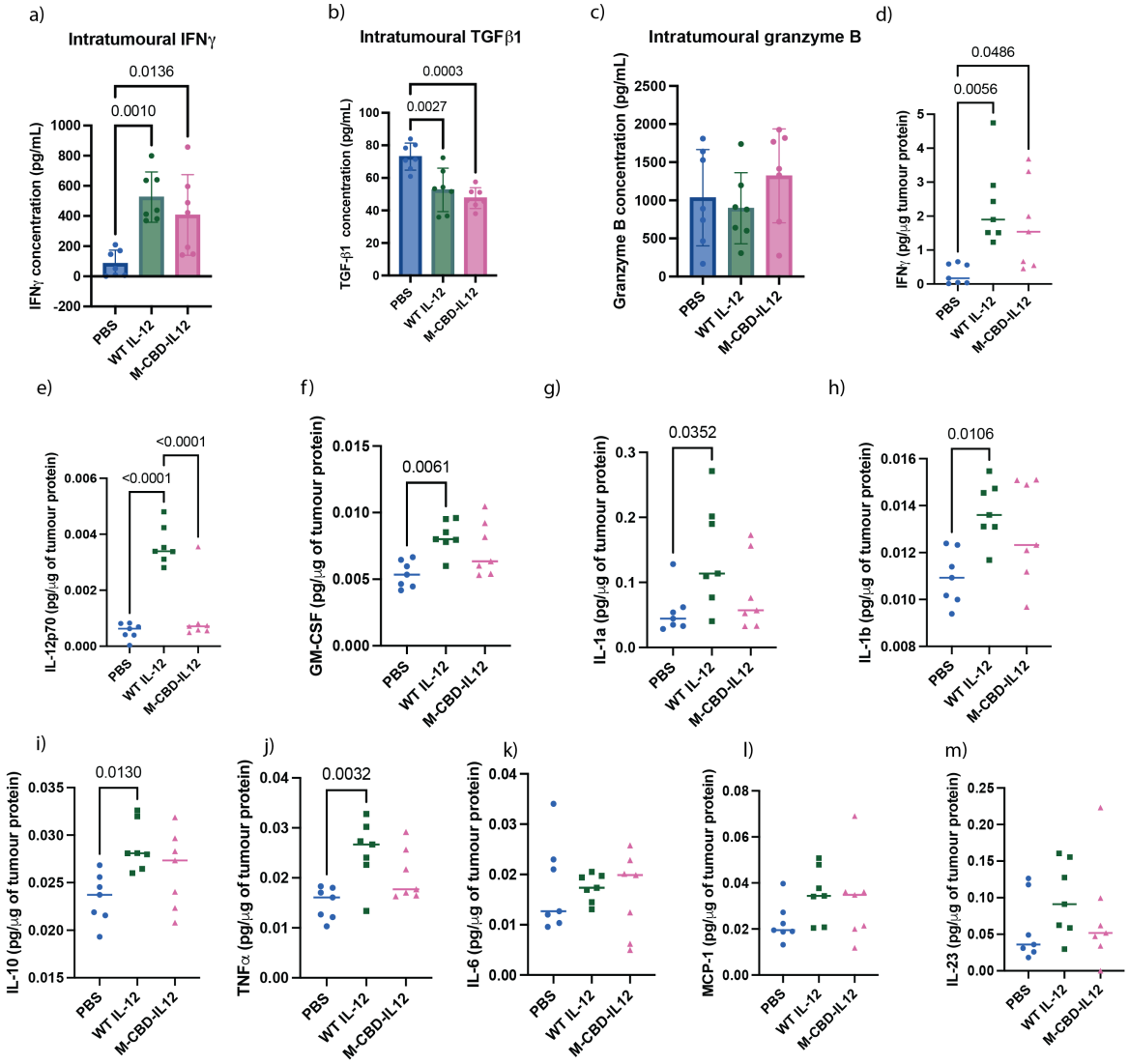


Figure 3.13 M-CBD-IL12 and wild-type IL-12 significantly increased intratumoural IFNγ and significantly reduced intratumoural TGFβ1 in the EMT6 mouse model

6-7-week-old BALB/c mice (n=7) were inoculated with 500 000 EMT6 cells in the 4th nipple mammary fat pad and treated with 83 pmol of wild-type (WT) IL-12 or 250 pmol of M-CBD-IL12 intravenously (IV) on days 6 and 9 following tumour inoculation. All mice were sacrificed through a cardiac puncture on day 11. Tumours were collected for cytokine analysis. Intratumoural a) IFNγ b) TGFβ1 c) granzyme B were quantified using ELISA. Consequently, other intratumoural cytokines were quantified using the LEGENDplex kit. Cytokine concentrations determined using this kit were normalised to protein concentration in the samples. Each mouse experiment was performed only once. Statistical analyses were performed using one-way ANOVA with Tukey's multiple comparison tests on GraphPad Prism.

A wide variety of other intratumoural cytokines were quantified using the LEGENDplex kit, one of which was IL-12 (see Figure 3.13d-m). The kit was able to detect the raised intratumoural IL-12 in the wild-type IL-12 group, but not M-CBD-IL12 due to the

presence of the mask preventing the interaction with the beads in the kit (see Figure 3.13e). A statistically significant increase was seen in GM-CSF (p=0.0061)(see Figure 3.13f), IL-1a (p=0.0352)(see Figure 3.13g), IL-1b (p=0.0106)(see Figure 3.13h), IL-10 (p=0.0130)(see Figure 3.13i), and TNFα (p=0.0032)(see Figure 3.13j) in the wild-type IL-12 group compared to PBS. The function, place of origin, and targets of these cytokines has been described in Table 3.1. Several of these cytokines also seem to be raised with M-CBD-IL12 but not to the same extent as wild-type IL-12 and more variability exists between the mice. This again highlights the dampening effect of the mask.

Table 3.1 LEGENDplex cytokines and their roles in the TME

Cytokine	Sources	Effects in breast cancer	Ref
GM-CSF	Lymphocytes, macrophages, fibroblasts, endothelial cells, cancer cells	Promotes the generation of neutrophils, monocytes, macrophages, dendritic cells, inhibited by IL-10, IL-4, IFNγ, can enhance cancer cell lysis, but can also promote EMT and Treg, TAM, and MDSC formation	(409)
IL-1a	Endothelial cells, epithelial cells, fibroblasts, macrophages, dendritic cells, T-cells	Maintains cancer stem cells by promoting NF-κB and STAT3 signalling in breast cancer, can suppress cancer cell proliferation	(410)
IL-1b	Myeloid cells, fibroblasts, cancer cells	Increases IL-6 and Fibroblast growth factor receptor 1 production, both of which can support cancer aggressiveness. Increases MDSC population and IL-10 production.	(411)
IL-10	Th2 cells, Th17 cells, Tregs, dendritic cells, monocytes, macrophages	Immunoregulatory, suppresses the production of pro-inflammatory cytokines and chemokines and antigen presentation by downregulating MHC class II and co-stimulatory molecules, some pro-inflammatory effects such as activation of B-cells and the promotion of T-cell survival	(412)
TNFα	Macrophages, B-cells, T-cells, NK cells	Activates NF-κB (anti-apoptotic) and c-Jun N-terminal kinase (pro-apoptotic) signalling, therefore has both pro- and anti-tumorigenic effects	(413, 414)

3.2.4.4 M-CBD-IL12 is a safer and more tolerable alternative to wild-type IL-12

To test the ability of the mask to suppress peripheral toxicity, I collected plasma from the EMT6-bearing mice through both a tail bleed on day 8 and a cardiac puncture when terminating the intervention study on day 11. I analysed this plasma using both ELISA and the LEGENDplex kit to observe time-dependent changes in plasma cytokine production in response to M-CBD-IL12 therapy. In the day 8 plasma, IFNγ was already significantly raised to 300 pg/ml (3-fold higher than M-CBD-IL12) with wild-type IL-12 compared to PBS controls ($p<0.0001$) and M-CBD-IL12 ($p=0.0001$) (see Figure 3.14a). These IFNγ levels further increased to over 4000 pg/ml (4-fold higher than M-CBD-IL12) in the wild-type IL-12-treated mice on day 11 (see Figure 3.14b). In contrast, M-CBD-IL12 therapy triggered significantly less plasma IFNγ than wild-type IL-12 ($p<0.0001$) suggesting a clear reduction in toxicity at either of the time points (see Figure 3.14a,b). These findings were validated using the LEGENDplex kit, which is able to detect a larger range of cytokine concentrations, meaning some wild-type IL-12 mice were found to reach plasma IFNγ concentrations of 8000 pg/ml using this kit (see Figure 3.14c).

Plasma macrophage chemoattractant protein (MCP-1, CCL2) showed a similar pattern to IFNγ with significantly raised levels with wild-type IL-12 compared to both M-CBD-IL12 ($p=0.0217$) and PBS ($p=0.0020$)(see Figure 3.14d). Similarly to the intratumoural IL-12p70 levels, plasma M-CBD-IL12 was most likely not detected by the LEGENDplex beads due to the effects of the mask (see Figure 3.14e). TNFα levels were significantly raised with wild-type IL-12 therapy compared to PBS ($p=0.0037$), but not with M-CBD-IL12 (see Figure 3.14f). Although not significant, IL-10 levels were also slightly raised in the wild-type IL-12-treated mice compared to the other groups (see Figure 3.14j). Other cytokines were not gravely affected by either therapy (see Figure 3.14g-l). Overall, these findings confirm the mask's ability to suppress the accumulation of other toxic inflammatory cytokines in the plasma.

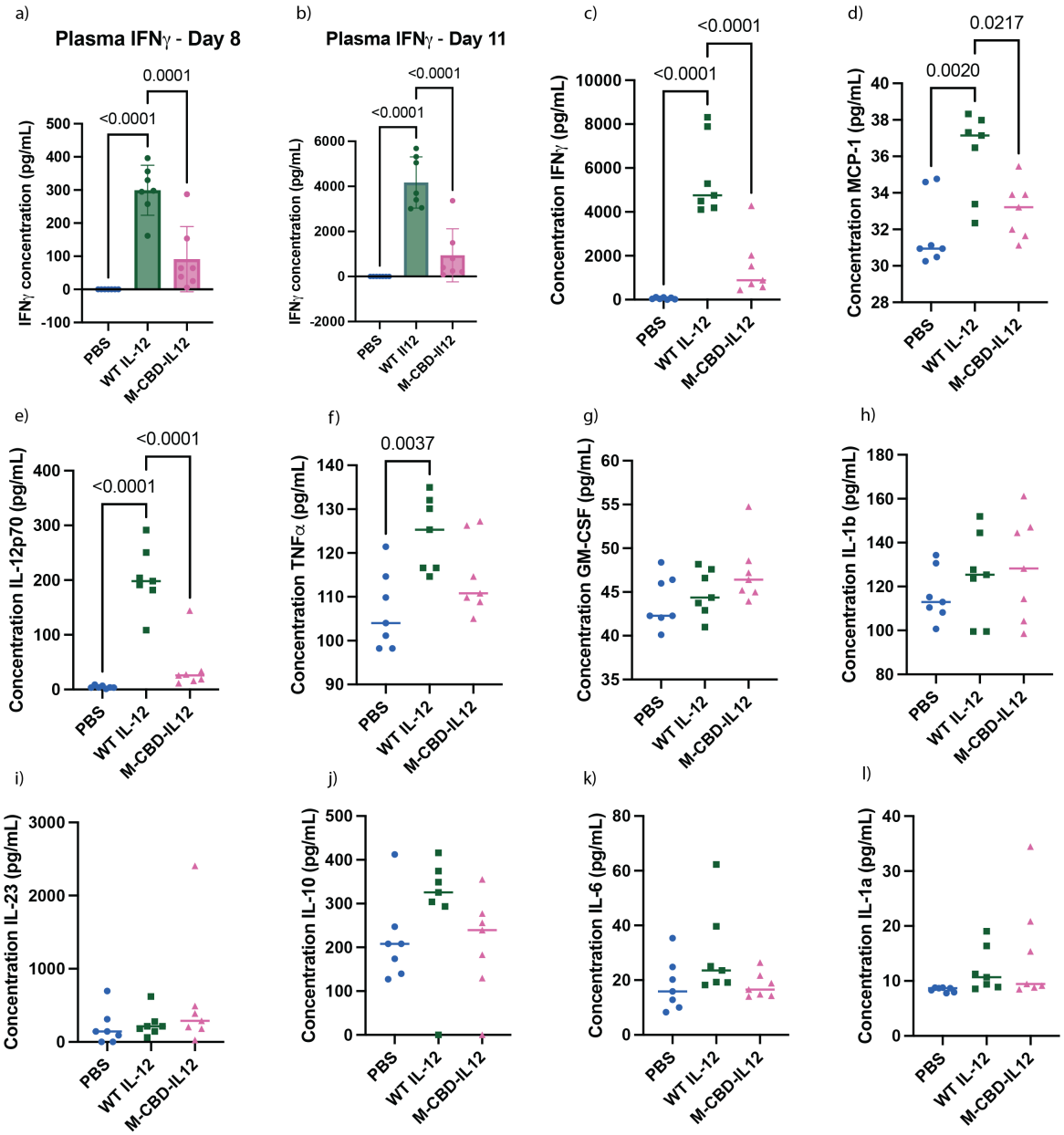


Figure 3.14 M-CBD-IL12 triggers significantly less toxicity than wild-type IL-12

6-7-week-old BALB/c mice (n=7) were inoculated with 500 000 EMT6 cells in the 4th nipple mammary fat pad and treated with 83 pmol of wild-type (WT) IL-12 or 250 pmol of M-CBD-IL12 intravenously (IV) on days 6 and 9 following tumour inoculation. All mice were sacrificed through a cardiac puncture on day 11. Plasma was collected through a tail bleed on day 8 (2 days following dose 1) and through a cardiac puncture on day 11 (2 days following dose 2) following tumour inoculation and was analysed for cytokine levels using ELISA and LEGENDplex cytokine kit. Each mouse experiment was performed only once. Statistical analyses were performed using one-way ANOVA with Tukey's multiple comparison tests on GraphPad Prism.

3.2.4.5 The time-dependent immunological changes in EMT6 tumours following IL-12 therapy

In the first intervention study, I sacrificed the mice at a point where tumour burden was reduced, but not yet significantly (day 11 following tumour inoculation) (see Figure 3.9b). This time point was chosen for optimal visualisation of intratumoural and plasma cytokine levels based on existing literature (51, 73). However, this study design was not suitable for visualising the delayed immunological changes caused by M-CBD-IL12. The control mice had reached maximum tumour burden before the volume of the treated tumours started to shrink. To overcome this problem, I performed a second intervention study where I injected only 100 000 cells instead of 500 000 to reduce the speed of tumour growth (see Figure 3.15a). Both wild-type IL-12 and M-CBD-IL12 suppressed tumour burden considerably compared to PBS controls (see Figure 3.15b), as demonstrated in the previous intervention study (see Figure 3.9). All the mice were terminated on day 18 following tumour inoculation, at which point the treated tumours were significantly smaller ($p=0.0028$ for wild-type IL-12, $p=0.0024$ for M-CBD-IL12) and weighed significantly less ($p=0.0018$ for wild-type IL-12, $p=0.0036$ for M-CBD-IL12) than the PBS controls (see Figure 3.15c,d). These findings closely align with my previous EMT6 mouse studies. Interestingly, the difference in spleen weight I had observed between the wild-type IL-12 group and PBS and M-CBD-IL12 groups in the first intervention study (see Figure 3.9c) was not as striking in this study (see Figure 3.15e). This suggests that the mice gradually recovered from acute wild-type IL-12 toxicity over time.

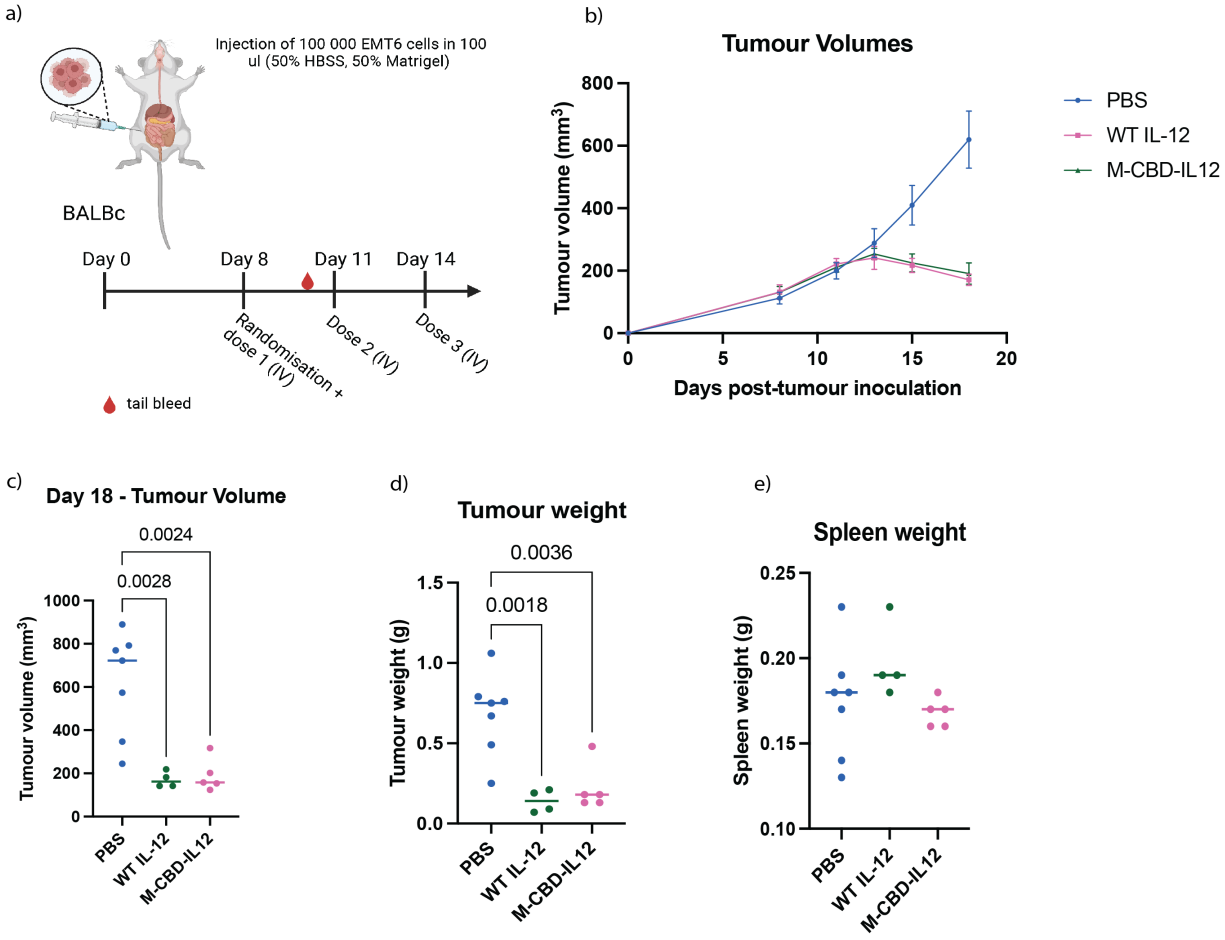


Figure 3.15 The delayed effects of M-CBD-IL12 on EMT6 in the intervention setting

a) 6-7-week-old BALB/c mice (n=7 for PBS, n=5 for M-CBD-IL12, and n=4 for wild-type IL-12 group) were inoculated with 100 000 EMT6 cells into the 4th nipple mammary fat pad and were treated with either 83 pmol of wild-type (WT) IL-12 or 250 pmol of M-CBD-IL12 intravenously (IV) on days 8, 11, and 14 following tumour inoculation. b/c) Tumour volumes were recorded throughout the study. All mice were sacrificed on day 18 and d) tumour and e) spleen weights are displayed. Tumours were processed for flow cytometric analysis. Mouse experiments were performed only once. Flow cytometry data was analysed on Flowjo. Statistical tests were performed using one-way ANOVA with Tukey's multiple comparison tests on GraphPad Prism. Schematics were designed on Biorender.com.

The tumours were once again analysed for immunological changes using flow cytometry. Since the day of study termination was later in relation to the last therapy dose compared to the first intervention study (see Figure 3.9a, Figure 3.15a), the immunological changes were not as apparent as previously shown. For example, I had previously observed a reduction in immune cells in the treated tumours in the first intervention study, yet this reduction was only statistically significant in the wild-type IL-12 group compared to PBS (p=0.0295)(Figure 3.9d). Here, the immune and non-

immune cell populations in the wild-type IL-12-treated tumours have normalised again and the wild-type IL-12 tumours do not have significantly fewer intratumoural immune cells anymore (see Figure 3.16a,b). The overall T-cells are low in both treated groups, yet this change is not statistically significant (see Figure 3.16c). No major differences could be observed between treatment groups for $CD4^+$ and $CD8^+$ T-cells and NK cells (see Figure 3.16d,e,g). Within T-cells, Tregs seemed to start to increase in the treated groups, although this was not significant either (see Figure 3.16f). However, despite this increasing trend, the tumour burden remained suppressed in the prior survival study (see Figure 3.8I,l). This suggests the emerging Treg population did not trigger tumour recurrence in this model.

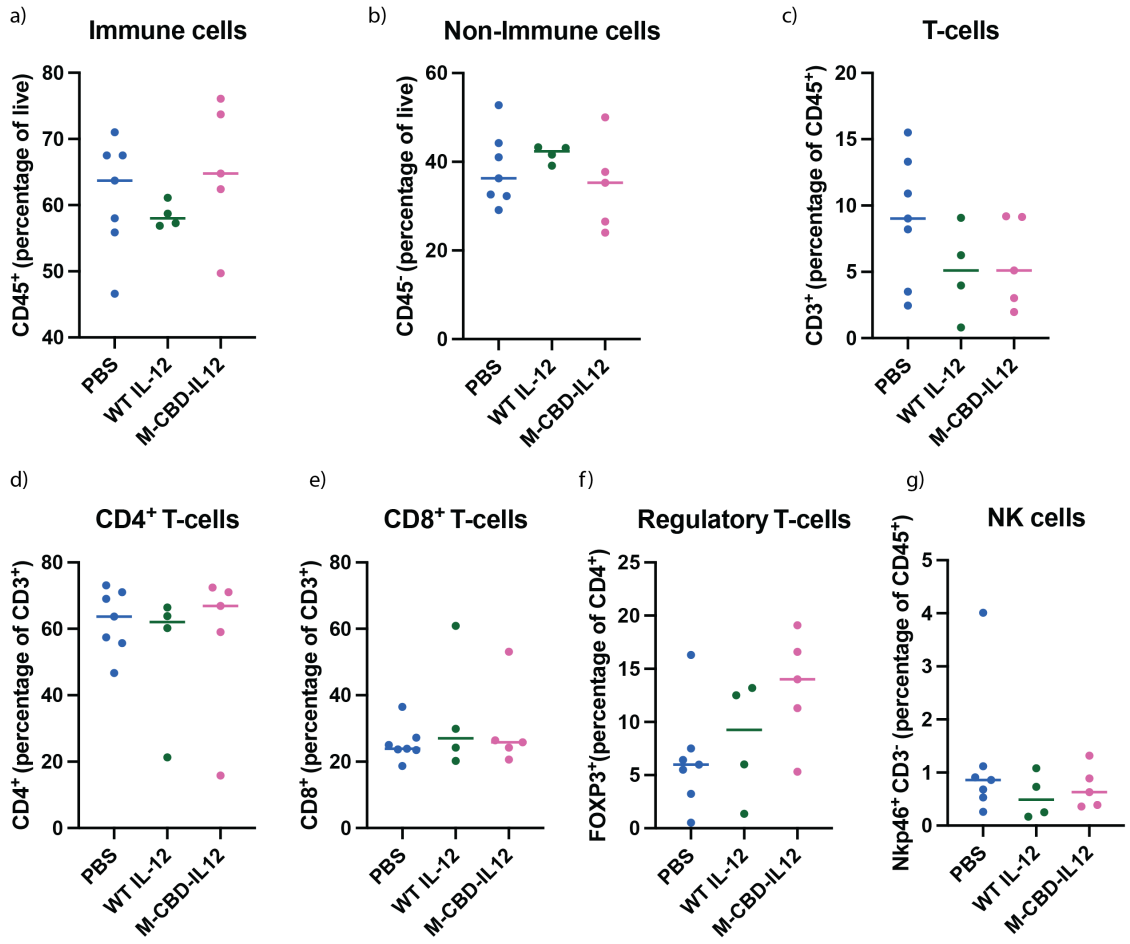


Figure 3.16 Lymphoid immune changes in the EMT6 TME following IL-12 immunotherapy

6-7-week-old BALB/c mice (n=7 for PBS, n=5 for M-CBD-IL12, and n=4 for wild-type IL-12 group) were inoculated with 100 000 EMT6 cells into the 4th nipple mammary fat pad and were treated with either 83 pmol of wild-type (WT) IL-12 or 250 pmol of M-CBD-IL12 intravenously (IV) on days 8, 11, and 14 following tumour inoculation. All

mice were sacrificed on day 18 and tumours were processed for flow cytometric analysis. Mouse experiments were performed only once. Flow cytometry data was analysed on Flowjo. Statistical tests were performed using one-way ANOVA with Tukey's multiple comparison tests on GraphPad Prism.

In terms of myeloid cells, an important change in macrophages was observed, in particular changes in $CD86^+$ (M1) and $CD206^+$ (M2) macrophages, the former of which is usually considered pro-inflammatory whilst the latter anti-inflammatory (415). Whilst total macrophages were not greatly affected (see Figure 3.17a), M1 macrophages were increased in the M-CBD-IL12 group compared to the wild-type IL-12 group (see Figure 3.17b). M2 macrophages were significantly raised with wild-type IL-12 compared to both PBS ($p<0.0001$) and M-CBD-IL12 ($p<0.0001$)(see Figure 3.17c). Hence, the M1/M2 ratio was significantly higher with M-CBD-IL12 than wild-type IL-12 ($p=0.0144$)(see Figure 3.17d). A lot of variation was observed between mice within the same groups for other cell types and no clear patterns were visible (see Figure 3.17e-g). Overall, these findings confirm that differences exist in the way in which wild-type IL-12 and M-CBD-IL12 induce resistance mechanisms.

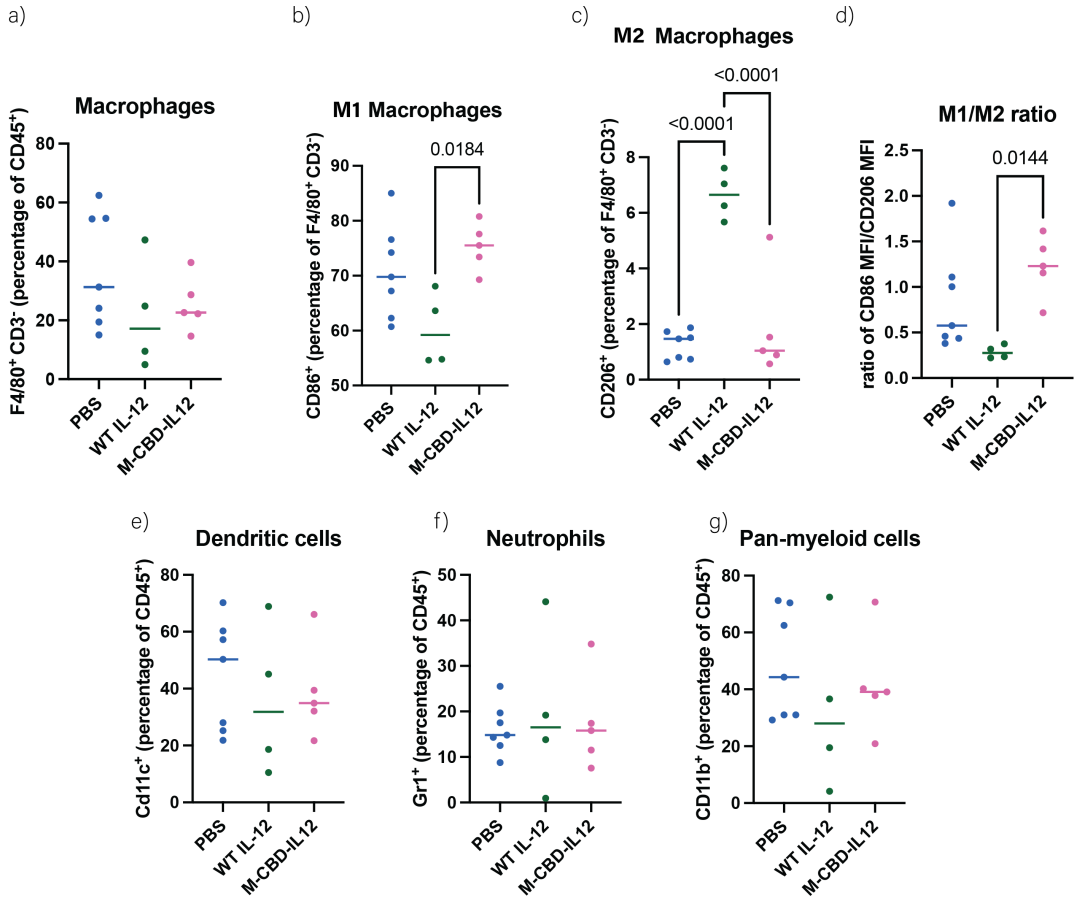


Figure 3.17 M-CBD-IL12 and wild-type IL-12 affect M1 and M2 macrophage proportions differently in the EMT6 TME

6-7-week-old BALB/c mice (n=7 for PBS, n=5 for M-CBD-IL12, and n=4 for wild-type IL-12 group) were inoculated with 100 000 EMT6 cells into the 4th nipple mammary fat pad and were treated with either 83 pmol of wild-type (WT) IL-12 or 250 pmol of M-CBD-IL12 intravenously (IV) on days 8, 11, and 14 following tumour inoculation. All mice were sacrificed on day 18 and tumours were processed for flow cytometric analysis. Mouse experiments were performed only once. Flow cytometry data was analysed on Flowjo. Statistical tests were performed using one-way ANOVA with Tukey's multiple comparison tests on GraphPad Prism.

In terms of the expression of checkpoints, a significant increase in PD-1 expression was noted on CD45^{+} cells (p=0.0260)(see Figure 3.18a) and NK cells (p=0.0404)(see Figure 3.18j) with M-CBD-IL12 therapy compared to PBS controls. Little change was observed in the expression of PD-L1 and PD-1 on other cell types (see Figure 3.18b-i).

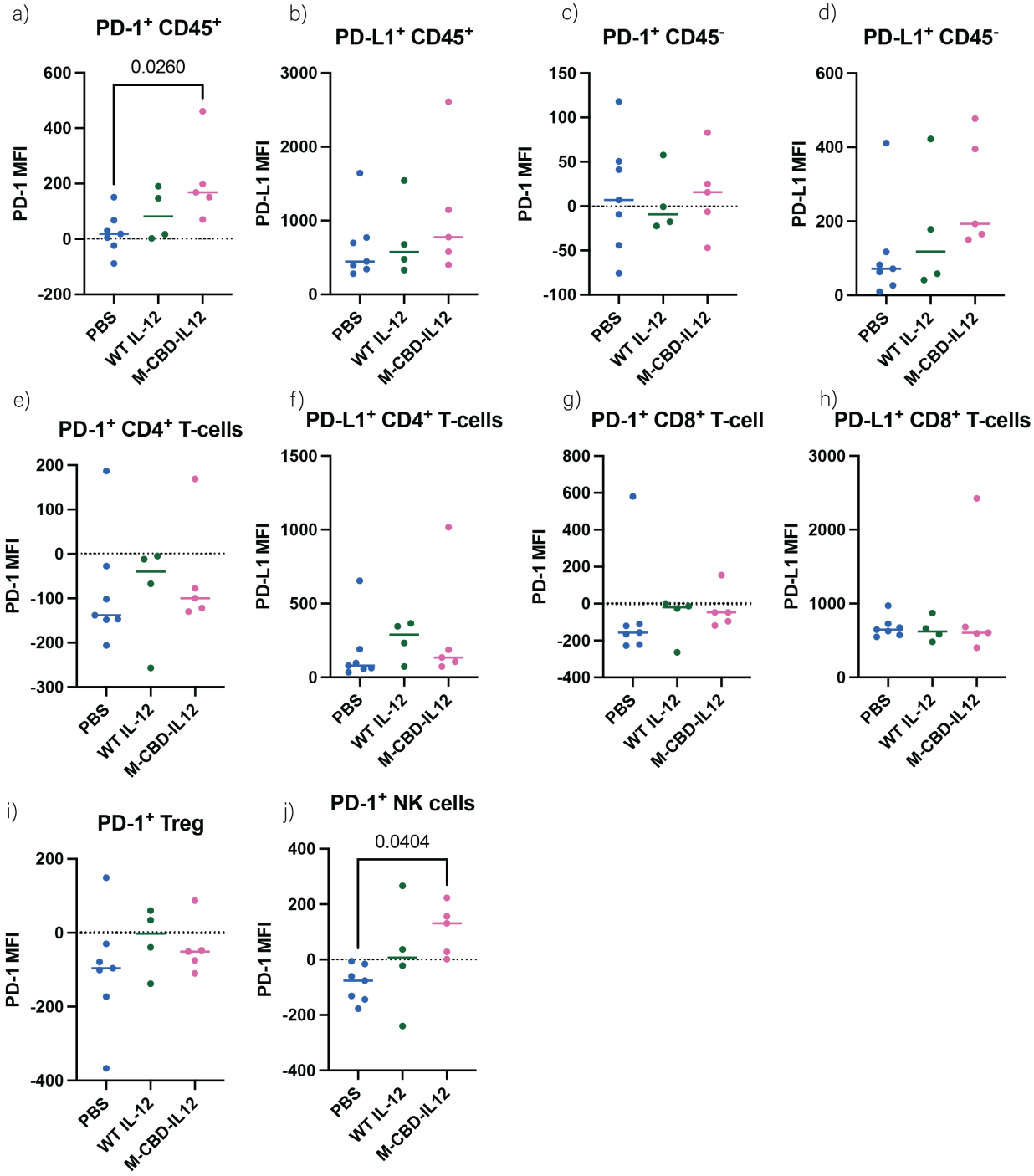


Figure 3.18 Expression of PD-1 in the EMT6 TME is raised with M-CBD-IL12 over time

6-7-week-old BALB/c mice (n=7 for PBS, n=5 for M-CBD-IL12, and n=4 for wild-type IL-12 group) were inoculated with 100 000 EMT6 cells into the 4th nipple mammary fat pad and were treated with either 83 pmol of wild-type (WT) IL-12 or 250 pmol of M-CBD-IL12 intravenously (IV) on days 8, 11, and 14 following tumour inoculation. All mice were sacrificed on day 18 and tumours were processed for flow cytometric analysis. Mouse experiments were performed only once. Flow cytometry data was analysed on Flowjo. Statistical tests were performed using one-way ANOVA with Tukey's multiple comparison tests on GraphPad Prism.

3.2.5 In the syngeneic 4T1 TNBC mouse model, M-CBD-IL12 performs less well as monotherapy than in EMT6

Next, I proceeded to test M-CBD-IL12 in a mouse model of TNBC with a completely different immune landscape (see Figure 3.2d-f). As previously mentioned, 4T1 harbours a much larger pre-existing population of T-cells, making it a more immunologically inflamed tumour at baseline. This means introducing IL-12 into the picture may not have the same impact as in a predominantly myeloid-infiltrated model like EMT6 (see Figure 3.2a-c). Due to the large pre-existing T-cell population, of which a proportion could be Tregs or exhausted T-cells, I included a combination treatment arm of M-CBD-IL12 with anti-PD-1 (to reactivate exhausted T-cells) and anti-CTLA-4 (to deplete Tregs) (see Figure 3.19a). In contrast with EMT6 (see Figure 3.8h), M-CBD-IL12 as monotherapy in this model only modestly improved survival (see Figure 3.19b). The combination immunotherapy significantly prolonged survival compared to PBS controls ($p=0.0009$)(see Figure 3.19b), but the effect on tumour burden was only modest with no complete responses (see Figure 3.19c). Wild-type IL-12-treated tumours remained smaller but ulcerated very rapidly, meaning they were sacrificed due to ulceration prior to reaching the maximum tumour burden. I collected some plasma from the tail vein of these mice on day 6 following tumour inoculation to measure plasma IFNγ as a measure of toxicity. As demonstrated in other models, M-CBD-IL12 also triggered significantly less plasma IFNγ compared to wild-type IL-12 ($p=0.0239$), suggesting toxicity is significantly reduced (see Figure 3.19d). Upon sacrificing the animals, brain and lung were collected to spot for metastases. I then visualised the number of metastases in the brain and lung sections using haematoxylin & eosin staining. However, I was unable to identify any metastases in the chosen brain and lung sections and can therefore not draw conclusions on the impact of M-CBD-IL12 on metastasis formation in this model. Overall, both wild-type IL-12 and M-CBD-IL12 seem to modestly prolong the survival of 4T1-bearing mice, yet not to the same extent as in EMT6.

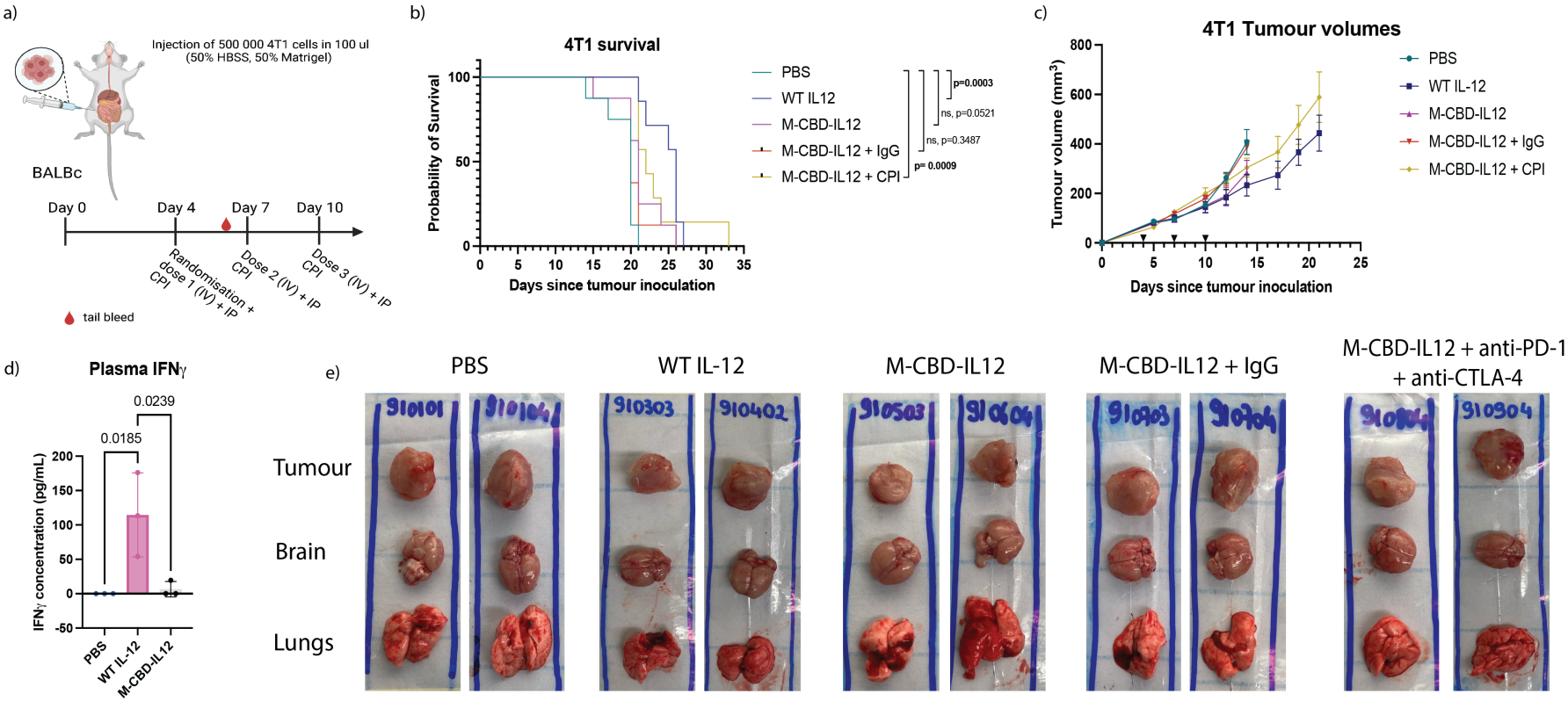


Figure 3.19 M-CBD-IL12 monotherapy does not prolong the survival of 4T1-bearing mice

6-7-week-old BALB/c mice (n=7) were inoculated with 500 000 4T1 cells and were treated three times with 83 pmol of wild-type (WT) IL-12 or 250 pmol of M-CBD-IL12 intravenously (IV), on days 4, 7, and 10 following tumour inoculation, either with or without the checkpoint inhibitors anti-PD-1 and anti-CTLA-4 (100 µg each, intraperitoneal injection (IP)) or their corresponding IgG controls. Their b) survival Kaplan-Meier curve and c) tumour volume curves have been displayed. d) Plasma was collected from 3 mice per group on day 6 following tumour inoculation through a tail bleed and this plasma was analysed for IFNγ using ELISA. e) Upon necropsy, the brain and lungs were collected, and H&E staining was performed to observe changes in metastasis. This mouse experiment was performed only once. Statistical analyses were performed using a one-way ANOVA with Tukey's multiple comparison tests or Mantel Cox test for Kaplan Meier survival curves on Graphpad prism. Schematics were designed on Biorender.com

3.2.6 Characterisation of the differences in immune landscape between EMT6 and 4T1 mouse models

3.2.6.1 Immunohistochemistry and RNA

To understand the differential response seen between EMT6 and 4T1 models with M-CBD-IL12 treatment, I performed downstream analysis on the PBS-treated tumours from both survival studies (EMT6: Figure 3.8, 4T1: Figure 3.19). Firstly, immunohistochemistry analysis supported the findings of the previously discussed scRNA-seq data (see Figure 3.2). I found the 4T1 model to have higher overall T-cell levels and specifically $CD8^+$ T-cells (see Figure 3.20a,b). Conversely, EMT6 is more myeloid infiltrated with raised F4/80 levels (total macrophage marker) (see Figure 3.20c). It is important to highlight that these trends were not significantly different. With the help of Emma Westlund at the Institute of Cancer Research microscopy core facility, we overlayed the CD8 and F4/80 serial sections of EMT6 tumours and identified areas of co-localisation of macrophages and $CD8^+$ T-cells using QuPath (see Figure 3.20d). The co-localisation of these cells could be indicative of their interaction, in particular T-cell priming. Secondly, together with my colleague Chanthirika Ragulan, I extracted RNA from the tumours and performed Nanostring nCounter transcriptomic profiling. We saw a differential expression of a variety of genes between EMT6 and 4T1 untreated tumours (see Figure 3.20e). The expression of *Ly6c* (p=0.0070)*, Cxcl13* (p=0.0264)*, Colec12* (p=0.0007)*, Lrrn3* (p=0.0001)*, Cav1* (p=0.0107)*,* and *Cks2* (p=0.0145) were significantly higher in the EMT6 tumours compared to 4T1 (see Figure 3.20f,h-l), whilst the basal/myoepithelial marker *Keratin 14* was significantly higher in 4T1 tumours (p=0.0017) (see Figure 3.20g). These experiments have helped identify potential culprits for the reduced efficacy of M-CBD-IL12 in 4T1 compared to EMT6, although pinpointing the exact mechanism remains challenging.

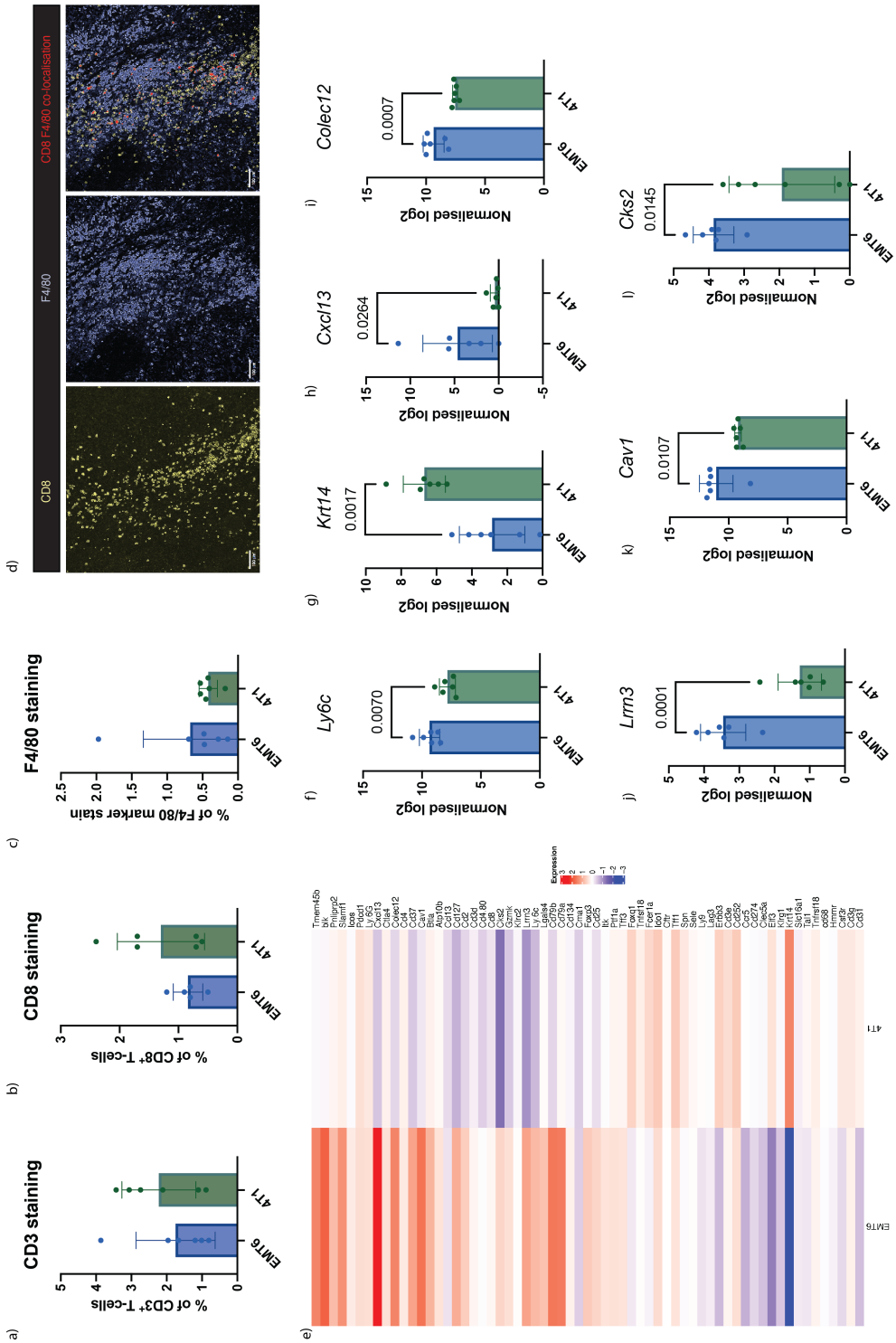


Figure 3.20 Spatial and RNA analysis of the TME of EMT6 and 4T1 tumours

PBS-treated EMT6 and 4T1 tumours from survival studies (EMT6: Figure 3.8, 4T1: Figure 3.19) were stained for CD3, CD8 and F4/80 using immunohistochemistry (n=6). The CD8 and F4/80-stained sections were quantified and overlayed on QuPath. The RNA was also extracted from the tumours (n=6) and Nanostring analysis was performed. Statistical tests were performed using two-tailed student's t-tests on Graphpad prism.

3.2.6.2 Intratumoural collagen (1 and 3) content is significantly higher in EMT6 tumours compared to 4T1 tumours

I hypothesised that, besides spatial or transcriptomic immunological differences, the differential response between EMT6 and 4T1 may be related to their collagen contents. The CBD in M-CBD-IL12 has a high affinity for collagen type 1 and 3. Thus, if insufficient collagen type 1 and 3 is present in the tumour stroma, M-CBD-IL12 may not have sufficient scaffold on which it can anchor itself, whereby hindering intratumoural accumulation of M-CBD-IL12. I therefore quantified the expression of collagen 1 (*Col1a1, Col1a2*) and collagen 3 (*Col3a1*) using qRT-PCR (see Figure 3.21a-c) (51). I observed 4T1 to express lower levels of both, particularly significantly lower *Col1a2* ($p=0.0050$) and *Col3a1* ($p=0.0280$)(see Figure 3.21b,c). Consequently, I performed Picro Sirius Red staining (PSR) which highlights collagen 1 and 3 fibres in tissues as bright pink, along with haematoxylin and eosin staining (see Figure 3.21d). With the support of Emma Westlund from the Institute of Cancer Research microscopy core facility, we quantified the degree of PSR staining on these sections using QuPath (see Figure 3.21d,e). Similarly to what I demonstrated using the qRT-PCR, 4T1 is significantly less collagen enriched than EMT6 ($p=0.0449$), which may have contributed to its unresponsiveness to M-CBD-IL12 therapy.

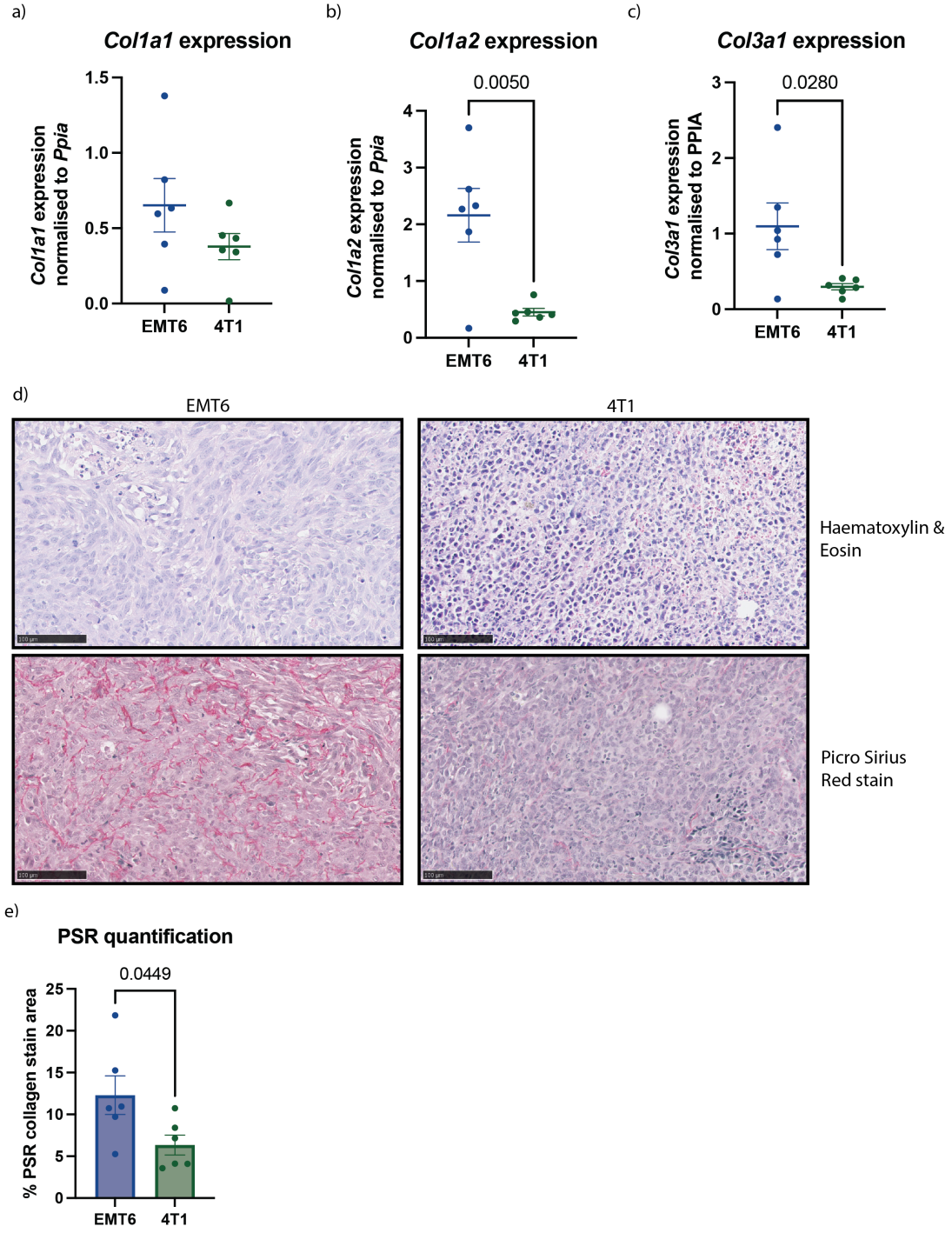


Figure 3.21 4T1 tumours contain significantly less collagen 1 and 3 than EMT6 tumours

Tumours from the PBS-treated survival studies of the EMT6 and 4T1 tumour models (EMT6: Figure 3.8, 4T1: Figure 3.19) were homogenised and their RNA was extracted (n=6). The expression of *Col1a1, Col1a2, and Col3a1* within them was measured using qRT-PCR. Sections of these tumours were stained with Picro sirius red (PSR) stain as well as haematoxylin and eosin. PSR staining was quantified using QuPath by Emma Westlund. Statistical tests were performed using a two-tailed student's t-test on GraphPad Prism.

3.2.6.3 Intratumoural cytokines

I proceeded to measure the levels of intratumoural TGFβ1 levels using ELISA, as well as the set of cytokines discussed in section 3.2.4.3 of this chapter in both models. This allowed me to observe whether the differential response to M-CBD-IL12 was caused by differences in cytokine levels between EMT6 and 4T1 tumours. The levels of TGFβ1 were significantly higher in the 4T1 tumours compared to EMT6 ($p=0.0012$)(see Figure 3.22a), suggesting that this cytokine may also be reducing the efficacy of M-CBD-IL12 in this model. Few differences were observed in the levels of other cytokines (see Figure 3.22b-k), potentially since these tumours were obtained from a survival study. This meant that the tumours were late stage with ulceration, which can influence the immune microenvironment and the secretion of cytokines.

Overall, the promising response observed in EMT6-bearing mice and the lack thereof in 4T1-bearing mice may be attributed to the following: a myeloid-enriched TME along with high collagen content and little TGFβ1 in EMT6 compared to little collagen, abundant T-cells that are potentially suppressed by the excessive TGFβ1 in 4T1. This highlights how the TME in its entirety, which we have visualised through the immunotype classification, determines responsiveness to M-CBD-IL12 in TNBC.

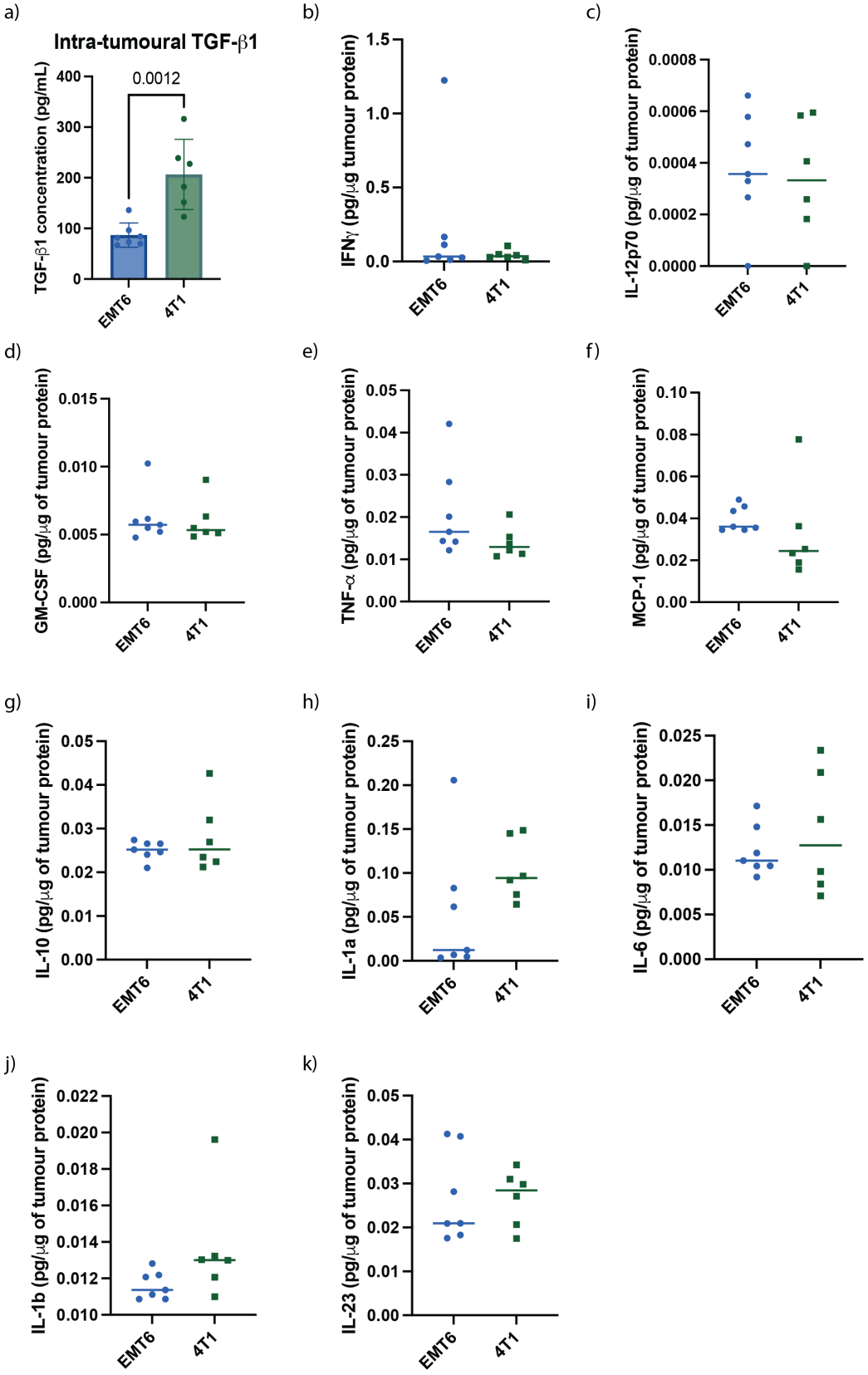


Figure 3.22 4T1 tumours contain significantly more TGFβ1 compared to EMT6 tumours

Tumour tissue from the PBS-treated mice in EMT6 (n=7) and 4T1 (n=6) survival studies (EMT6: Figure 3.8, 4T1: Figure 3.19) were homogenised and cytokine levels were quantified using a) TGFβ1 ELISA or b-k) the LEGENDplex kit. For the kit, cytokine levels were normalised to total protein content. This kit and the ELISAs were run only once. Statistical tests were performed using a two-tailed student's t-test on GraphPad Prism.

3.2.7 Discussion

TNBC remains a challenge to treat in the clinic due to its heterogeneity and limited targeted therapeutic options. Many have classified TNBC into immunologically relevant subtypes, however, these classifications have offered little guidance on therapy selection. In this chapter, TNBC mouse models were categorised into immunotypes by our laboratory in which I tested a safe and tolerable form of immunotherapy, M-CBD-IL12. I found EMT6 to be highly sensitive to this molecule, but not 4T1. This could potentially be attributed to EMT6's higher collagen content, enlarged myeloid population with simultaneously reduced levels of TGFβ1 compared to 4T1. Therefore, the immunotypes seem to have the ability to guide patient selection for M-CBD-IL12 therapy in TNBC.

3.2.7.1 IL-12 at the crossroad between oncology and immunology: the cancer immunity cycle

The cancer immunity cycle is a collection of steps that, under ideal circumstances, lead to the effective elimination of cancer cells by T-cells (416). The initial step of the cycle is that cancer cells release neoantigens upon their death, which the immune system considers 'foreign' due to a lack of tolerance. Secondly, antigen presenting cells, usually dendritic cells, engulf and process these cancer antigens and present them on their MHC class II (416). They then recirculate to secondary lymphoid organs such as lymph nodes and the spleen to encounter T-cells for priming. These T-cells then recirculate through the bloodstream to extravasate into the cancerous tissues. Finally, the T-cells kill cancer cells that express the antigens on their MHC class I that the T-cells have been primed against (416). Further tumour antigens are released from the dying cancer cells which enhances the extent of the immune response throughout the consecutive cycles (416). M-CBD-IL12 therapy aims to activate the T-cells within this cycle to

promote effective cancer cell elimination, without triggering the toxicity of wild-type IL-12.

I observed certain aspects of the cancer-immunity cycle in the first EMT6 intervention study. For example, both treated groups had significantly larger dendritic cell populations in the spleen compared to PBS controls. Following their encounter with the tumour antigens in the tumour, they recirculate to the spleen to encounter T-cells. Simultaneously, intrasplenic T-cells were significantly lower in both treated groups compared to PBS treated mice. These could represent T-cells that have been activated and therefore migrate back towards the tumour for cancer cell elimination (416). Interestingly, an increase in intratumoural $CD8^+$ T-cells was only noted in M-CBD-IL12 mice. This could be related to the timing of study termination, because my flow cytometry results only represent a snapshot at a single time point within the study. However, since wild-type IL-12 causes raised plasma IFNγ compared to M-CBD-IL12, it is more likely to recruit T-cells and other immune cells into the bloodstream rather than into the tumour. This theory was supported by the fact that tumours treated with wild-type IL-12 harboured significantly fewer intratumoural immune ($CD45^+$) cells compared to M-CBD-IL12. Wild-type IL-12 may have triggered an efflux of immune cells out of the tumour. Therefore, different biodistribution patterns between wild-type IL-12 and M-CBD-IL12 may influence the nature of the immune cell types that populate the tumours.

The differences between the molecules also affected resistance mechanisms and intratumoural cytokine levels. In the first EMT6 intervention study, $PD\text{-}1^+$ NK cells, $PD\text{-}L1^+CD8^+$ T-cells, and $PD\text{-}L1^+CD45^-$ cells in the tumour were significantly increased with wild-type IL-12, but not with M-CBD-IL12. In contrast, in the second intervention study, where I studied the delayed immunological responses, $PD\text{-}1^+CD45^+$ and $PD\text{-}1^+$ NK cells were significantly more prominent in the M-CBD-IL12 group compared to wild-type IL-12 and PBS groups. This could suggest that the same resistance mechanisms arise in the M-CBD-IL12 group at a later time point than with wild-type IL-12 since the unmasking may delay its effects. Further experiments would need to be performed where the study is terminated at a later time point to confirm this theory.

When measuring the intratumoural cytokine levels, GM-CSF, IL-1a, IL-10, and TNFα were all significantly raised with wild-type IL-12 therapy compared to PBS controls. This was not the case for M-CBD-IL12-treated mice. Due to the role of these cytokines in recruiting TAMs and MDSCs (409, 411), their increase following wild-type IL-12 therapy could have induced the shift in M1/M2 ratio. The M1/M2 ratio is significantly higher in mice treated with M-CBD-IL12 than those treated with wild-type IL-12. Therefore, the localisation of the IL-12 and the downstream intratumoural cytokines it triggers can be directly reflected in the myeloid compartment of the tumours. Due to the dampening effect of the mask, the strength of the IL-12 signalling that results in the production of these cytokines may be considerably lower and even delayed for M-CBD-IL12. Nevertheless, none of these resistance mechanisms impeded the suppression of tumour burden by either molecule in EMT6.

3.2.7.2 Remodelling the myeloid compartment of EMT6 tumours using M-CBD-IL12

As demonstrated using the scRNA-seq data, EMT6 seems to be much more monocyte/macrophage infiltrated than the T-cell infiltrated 4T1 model, particularly $CD14^+$ and $CD16^+$ monocytes. CD14 and CD16 are human monocyte markers that are also expressed in mice, but at much lower levels (417). $CD16^-CD14^+$ monocytes are referred to as 'classical' monocytes (418). $CD16^+$ monocytes are of a more pro-inflammatory nature and can be further categorised by CD14 expression, which is often considered a continuum: $CD16^+CD14^{high}$ (intermediate) or $CD16^+CD14^{low}$ (non-classical) monocytes (418). The roles of these monocytes in the TME remain controversial; classical monocytes mainly produce IL-10, which is considered an anti-inflammatory cytokine (419). However, some have demonstrated classical monocytes to also express abundant MHC class II that allows them to induce T-cell proliferation (419). Intermediate monocytes are raised in patients with cholangiocarcinoma and decrease following resection (420). Hence, in this study, the authors suggested intermediate monocytes to promote tumorigenicity (420). However, in breast cancer patients, abundant intermediate and non-classical monocytes that express MHC class II have been shown to significantly correlate with response to neoadjuvant

chemotherapy (421). This highlights how the proportions of different monocyte populations may have influenced the efficacy of M-CBD-IL12 in EMT6.

Table 3.2 Table demonstrating monocyte populations, their markers, and their functions

Table is based on (415, 418, 419).

Human monocyte subsets		**Corresponding mouse monocytes**	**Macrophages they differentiate into**	**Function**
$CD16^{-}CD14^{+}$	Classical	Ly6c+	M1	PHAGOCYTIC - Produce IL-10, reactive oxygen species - Largely phagocytic subtype that express MHC class II
$CD16^{+}CD14^{high}$	Intermediate	Ly6c+	M1	INFLAMMATORY - Can secrete TNFα, IL1β - Express high MHC class II - Are potent T-cell stimulators - Can promote tumorigenicity and angiogenesis
$CD16^{+}CD14^{low}$	Non-classical	Ly6c-	M2	PATROLLING - Monitor the endothelium for signs of inflammation - Can secrete TNFα - Express high MHC class II

$CD14^{+}$ monocytes were more abundant in EMT6 in the scRNA-seq analysis than $CD16^{+}$ monocytes. Therefore, EMT6 is likely to contain more classical and intermediate monocytes than non-classical monocytes. Classical and intermediate monocytes are thought to overlap with $Ly6c^{+}$ monocytes (415). These eventually differentiate into M1 macrophages once inflammation takes place (415). Therefore, although EMT6 is heavily monocyte-infiltrated, these cells may be of a pro-inflammatory nature.

Interestingly, I observed a significant decrease in overall macrophages and a change in the M1/M2 ratio, albeit not significant, with M-CBD-IL12 therapy compared to PBS in EMT6. However, many consider the M1/M2 classification to be overly simplistic. Therefore, to understand whether the myeloid compartment of EMT6 made it more responsive to M-CBD-IL12 than 4T1, further experiments are required that capture the

multiple subsets of various myeloid cell populations within these tumours. Unfortunately, the number of different flow cytometry panels in my experiments was restricted by the limited tissue available for analysis in the treated groups.

3.2.7.3 The fine balance between pro- and anti-inflammatory cytokines in determining the therapeutic benefit of IL-12 therapy

The reduction in macrophages I observed in EMT6 following M-CBD-IL12 therapy was associated with a significant increase in $CD8^+$ T-cells, which can exert cytotoxic effects towards cancer cells. Due to the prolonged effect of M-CBD-IL12 and the long-term protection it offers, a subset of memory effector T-cells has most likely formed. To quantify their cytotoxicity in response to M-CBD-IL12 therapy, I measured intratumoural IFNγ and granzyme B through ELISA. Although the cytotoxic granzyme B was largely unaltered, I found IFNγ to be significantly increased in the tumours treated with wild-type IL-12 and M-CBD-IL12 compared to PBS controls. Apart from its ability to upregulate MHC expression or to induce apoptosis (12), IFNγ is often referred to as the macrophage-activating molecule; IFNγ can skew macrophages towards a pro-inflammatory phenotype by enhancing their ability to phagocytose (422). The raised levels of intratumoural IFNγ following M-CBD-IL12 and wild-type IL-12 therapy in EMT6 may have been responsible for the reduction in total macrophages as well as the increased M1/M2 ratio in the M-CBD-IL12 group.

IFNγ has also been shown to counteract the effects of immunosuppressive cytokines like IL-10 (423) and TGFβ (424) . I therefore also quantified both those cytokines in EMT6 tumours through LEGENDplex and ELISA, respectively. Firstly, intratumoural IL-10 levels significantly increased with wild-type IL-12 therapy, but not with M-CBD-IL12, as previously mentioned in this discussion under section 3.2.7.1. Secondly, I quantified TGFβ1, the most abundant of the three TGFβ proteins in the TME (425). It is predominantly produced by cancer cells, MDSCs, M2 macrophages and stromal CAFs (425). This immunosuppressive cytokine is known to support and promote tumorigenesis by stimulating angiogenesis, epithelial to mesenchymal transition (EMT), and breast cancer metastasis (425). TGFβ also enhances the ‘stemness’ of cancer cells, which refers to their ability to form tumours and maintain their survival by

interacting with their environment (425). This concept usually goes hand in hand with EMT, although the exact mechanism remains unclear (425). Immunologically, the TGFβ-induced EMT suppresses antigen presentation through MHC class I on cancer cells, which is required for the cytotoxic effects of $CD8^+$ T-cells (425). Finally, TGFβ also promotes differentiation of T-cells into Tregs and enhances checkpoint expression on cancer cells (425). Interestingly, with M-CBD-IL12 therapy I observed a significant reduction in TGFβ1, Tregs and PD-1 expression on $CD8^+$ T-cells. Whether these three factors are associated is yet to be determined.

3.2.7.4 The biology behind differential responses to M-CBD-IL12 therapy

As a means of understanding the mechanism behind the differential response to M-CBD-IL12 therapy between TNBC models, I also quantified IL-10 and TGFβ1 levels in both EMT6 and 4T1 tumours. I observed no difference in IL-10 levels, whilst TGFβ1 was significantly higher in 4T1 tumours compared to EMT6. This cytokine may therefore have contributed to 4T1's unresponsiveness to M-CBD-IL12. In addition, I found 4T1 to be significantly less collagen enriched than EMT6, more specifically collagens 1 and 3. Since these form the scaffold onto which CBD can anchor itself, their reduced presence in 4T1 tumours could have made 4T1 less responsive to M-CBD-IL12. However, since wild-type IL-12 is also less efficacious in 4T1 compared to EMT6, the collagen is probably not the main source of 4T1's unresponsiveness.

At a transcriptomic level, I found a significant difference in the expression of a variety of genes in EMT6 and 4T1 tumours. A first example is *Keratin 14*, a basal epithelial gene and a marker of cancer cells, specialised in invasion and metastasis (426). The expression of this gene was significantly higher in 4T1 than in EMT6 tumours. Since its expression has been correlated with poor survival in breast cancer, irrespective of hormone receptor expression or tumour staging (426), this gene may also have contributed to 4T1's resistance to M-CBD-IL12. In addition, knocking down *Keratin 14* in orthotopically implanted organoids led to a strong reduction in invasiveness at the border between tumour and stroma, despite tumour growth not being significantly reduced (427). Therefore, this gene has been associated with metastasis, which is also known to be a problem with 4T1 tumours.

The second differentially expressed gene was *Cxcl13*, the role of which has been debated over the years; this B-cell-attracting chemokine is overexpressed in breast cancer tissues and is raised in serum of patients with metastatic disease compared to patients with localised disease (428), but has also been associated with favourable distant disease-free survival in other studies (429). Ma and colleagues developed a *Cxcl13*-overexpressing strain of 4T1 (430). They demonstrated tumours from the *Cxcl13*-overexpressing cells to grow significantly slower than normal 4T1 cells with increased immune cell infiltration ($CD4^+$ and $CD8^+$ T-cells, $CD11b^+CD11c^+$ dendritic cells) in immunocompetent mouse models (430). In immunocompromised mice, this *Cxcl13*-enhanced effect was impaired (430). This highlights the role of this chemokine in attracting pro-inflammatory immune cells into the TME to suppress tumour burden. Since this chemokine-encoding gene was expressed at significantly higher levels in EMT6 compared to 4T1 tumours, it could have supported the mounting of an anti-tumour immune response in EMT6 following treatment with M-CBD-IL12.

Colec12 is a gene encoding a pattern recognition molecule, which forms a crucial part of complement activation (431). It has been shown to play a role in activation of the alternative complement pathway and leukocyte recruitment (431). Its high expression in EMT6 tumours may suggest innate immunity plays an important role in EMT6 tumours, potentially through complement-mediated activation of the adaptive immune system.

The *Lrrn3* gene encodes the leucine rich repeat neuronal 3 (LRRN3) protein, one of the markers of Th1 cells (432). Low *LRRN3* gene expression has been correlated with $CD8^+$ T-cell senescence (432). However, when expressed at low levels, *LRRN3* has been shown to negatively impact survival in patients with neuroblastomas (433). In contrast, another study on uveal melanoma revealed *LRRN3* to be a negative prognostic biomarker for overall survival (432). Since this gene's expression was significantly higher in EMT6 tumours compared to 4T1, it could suggest that the small population of T-cells in EMT6 are more of a Th1 nature, whilst its low expression in 4T1 may suggest the T-cells in 4T1 to be senescent.

Caveolin-1 (*Cav1*) is a well-recognised driver of breast cancer and affects multiple events in the breast cancer microenvironment such as apoptosis, autophagy, and metastasis (434, 435). This gene encodes a membrane protein that is highly expressed in the caveolae of human breast tissue (434, 435). Caveolae are microdomains on the plasma membrane of various cell types with high cholesterol and caveolin protein content (434, 435). Its role is highly pleiotropic and context-dependent; it both promotes and suppresses cancer cell proliferation, apoptosis, and migration by interacting with multiple targets in the EGFR, HER2, eNOS, VEGF, PI3K/AKT signalling pathways (434, 435). Caveolins have also been suggested to aid chemotherapy internalisation and therefore their disruption could interfere with the therapeutic efficacy of drugs (434, 435). This tumour driver was expressed at significantly higher levels in EMT6, however, the context-dependent role of *Cav1* makes it challenging to draw valid conclusions.

Finally, the *Cks2* gene encodes the Cyclin-dependent kinases regulatory subunit 2 (CKS2), a kinase involved in regulation of the cell cycle (436). Its upregulation is usually associated with poor survival, larger tumour size and poorer differentiation in breast cancer patients (436). Due to its overexpression in many cancer types, it can be considered an oncogene (436). This gene was also expressed at significantly higher levels in EMT6 compared to 4T1, suggesting that despite its better responsiveness to IL-12 immunotherapy, EMT6 remains a highly aggressive model.

Overall, in this chapter, I have used the immunotypes as a classification system to determine the type of immune landscape that responds best to M-CBD-IL12 immunotherapy. Introducing M-CBD-IL12 into myeloid-enriched tumours with abundant collagen seems a promising strategy, which completely remodelled the TME. In T-cell-enriched collagen-depleted tumours, the opposite pattern was seen. Therefore, the immunotype classification is a useful tool for selection of suitable candidates for M-CBD-IL12 therapy, a tolerable alternative to toxic wild-type IL-12.

Chapter 4. The role of the *Kras^{G12D}* mutation in determining response of PDAC to IL-12-based therapy

4.1 Introduction

KRAS mutations are considered drivers of tumorigenesis since they are present in early forms of PDAC, such as pancreatic intraepithelial neoplasias (PanINs) and intraductal papillary mucinous neoplasms (IPMNs)(437). The crucial role of oncogenic *Kras* mutations in driving tumorigenesis has been demonstrated using genetic engineering of mouse models bearing pancreatic, colorectal and lung tumours (212, 438-440). Ischenko and colleagues specifically demonstrated a CRISPR-mediated *Kras^{G12D}* ablation to significantly delay PDAC tumour development and growth (212). They also observed the impact of the *Kras^{G12D}* ablation on cancer cells throughout different stages of tumour development; precancerous cells became non-proliferative colonies, whilst cell lines derived from established tumours were successful at forming ample viable colonies following *Kras^{G12D}* ablation (212). This highlights the concept of KRAS dependency and addiction and how they may differ at different stages of tumorigenesis (212). The ablation not only affected proliferation rates of cancer cells but also increased epithelial to mesenchymal transition (EMT) with increased expression of mesenchymal markers and TGFβ pathway upregulation, resulting in poorly differentiated tumours with large areas of necrosis (212). Interestingly, the authors found the MAPK/ERK pathway that operates downstream of KRAS to be unaffected by the ablation, which suggests *Kras^{G12D}* ablation alone may not be sufficient to suppress PDAC tumour burden (212).

Furthermore, not only the cancer cells themselves were impacted by this ablation, but the PDAC immune landscape was also affected (212). As described in the introduction, the PDAC TME is a highly dynamic and evolving system with a wide range of immune evasion mechanisms that lead to immunotherapy resistance. Ischenko and colleagues found *Kras^{G12D}* ablation to induce intratumoural immune ($CD4^+$ T-cells, $CD8^+$ T-cells, and myeloid cells) cell infiltration. Furthermore, they used a doxycycline-inducible *Kras^{G12D}* model to confirm these findings and found the withdrawal of doxycycline (no *Kras^{G12D}* expression) to induce immune cell infiltration, metastatic regression and

sensitisation to CPI therapy. In contrast, these were not the case in the presence of doxycycline (*Kras*^{G12D} expressed). These regressions were also not found in nude mice, highlighting the role of the immune system in suppressing tumour and metastatic burden.

Similar findings were yielded from the first pre-clinical studies using the recently discovered first KRAS G12D small molecule inhibitor MRTX1133 (213). Kemp and colleagues found the inhibitor to reduce tumour growth in two different PDAC models with unique immune landscapes (213). They also observed a complete modulation of the immune composition of these tumours with an increase in both $CD4^+$ and $CD8^+$ T-cells, as well as an increase in the M1/M2 macrophage ratio (213). However, the authors highlight that this T-cell infiltration was no longer evident after 7 days of MRTX1133 therapy (213). They also demonstrated the tumour regression following MRTX1133 therapy to be dependent on $CD8^+$ T-cell activity and that it was futile when they were exhausted, suggesting the need for combination with CPIs (213). These pivotal studies clearly highlight the role of the *KRAS*^{G12D} mutation as an immune evasion mechanism that may be partially responsible for the lack of success of immunotherapy in PDACs.

Immunotherapy clinical trials in PDAC have been extensively discussed in section 1.6.3 of the Introduction, yet very few of these clinical trials involve IL-12. Similarly, IL-12 studies in mouse models remain scarce. Localised intratumoural IL-12 as polylactic acid microspheres in combination with SBRT in preclinical mouse models resulted in a significant increase in intratumoural IFNγ and $CD8^+$ T-cells along with a significant prolongation in survival and suppression in tumour burden (441). Nash et al. have similarly used a cytokine delivery platform for localised administration of IL-12 cytokine factories (genetically engineered cells in polymers). Although their data is preliminary, this technique seems to reduce pan02 tumour burden by 80% in mice, along with an increase in intratumoural T-cells (442). A third group used intratumoural adenovirus-mediated co-expression of IL-12 and the costimulatory molecule B7.1. This too led to complete regressions in 80% of immune depleted PDAC mouse models. The adenovirus-mediated coexpression of IL-12 alone was however less efficacious (443). Unfortunately, intratumoural administration of compounds for PDAC patients is an invasive procedure for which most patients may be too unwell.

Nevertheless, an adenoviral vector encoding human IL-12 genes was trialled intratumourally in patients with liver cancer, CRC or PDAC (444). It resulted in some toxicity, in particular lymphopenia in 85% of patients, sweating and malaise in around 60% of patients, along with a pleural effusion, nausea and vomiting in 24% of patients, and intense oedema in a patient with a colostomy bag (444). Two of the PDAC patients passed away due to disease progression prior to assessing for clinical efficacy. Although some reduction in node metastases were observed, the overall clinical benefit was limited. A second trial was initiated more recently using intratumoural adenovirus-mediated suicide and IL-12 gene therapy along with oral chemotherapy in metastatic PDAC patients (445). The median survival of the 6 patients on the highest dose was 18.0 months, which is longer than what has been shown with standard of care chemotherapy (445). However, between the 12 enrolled patients, a total of 121 adverse events had been noted by day 21 of the study (445).

Overall, the success with IL-12 therapy in PDAC has been rather limited, even with intratumoural injection. This highlights the need for efficacious drug delivery mechanisms as well as improving our understanding of resistance mechanisms to IL-12 therapy. Here, my aim was to investigate the *Kras*^{G12D} mutation as a potential resistance mechanism to IL-12 therapy in PDAC mouse models. After observing differential responses to IL-12 therapy between the PDAC mouse models to be associated with differential KRAS G12D expression, I aimed to investigate the relationship between the two. I used co-culture systems, tumour-derived cell lines that were previously treated with IL-12 immunotherapy, and inducible *Kras* (*iKras*) cell lines to establish whether KRAS G12D inhibition may sensitise resistant models to IL-12 immunotherapy.

4.2 Results

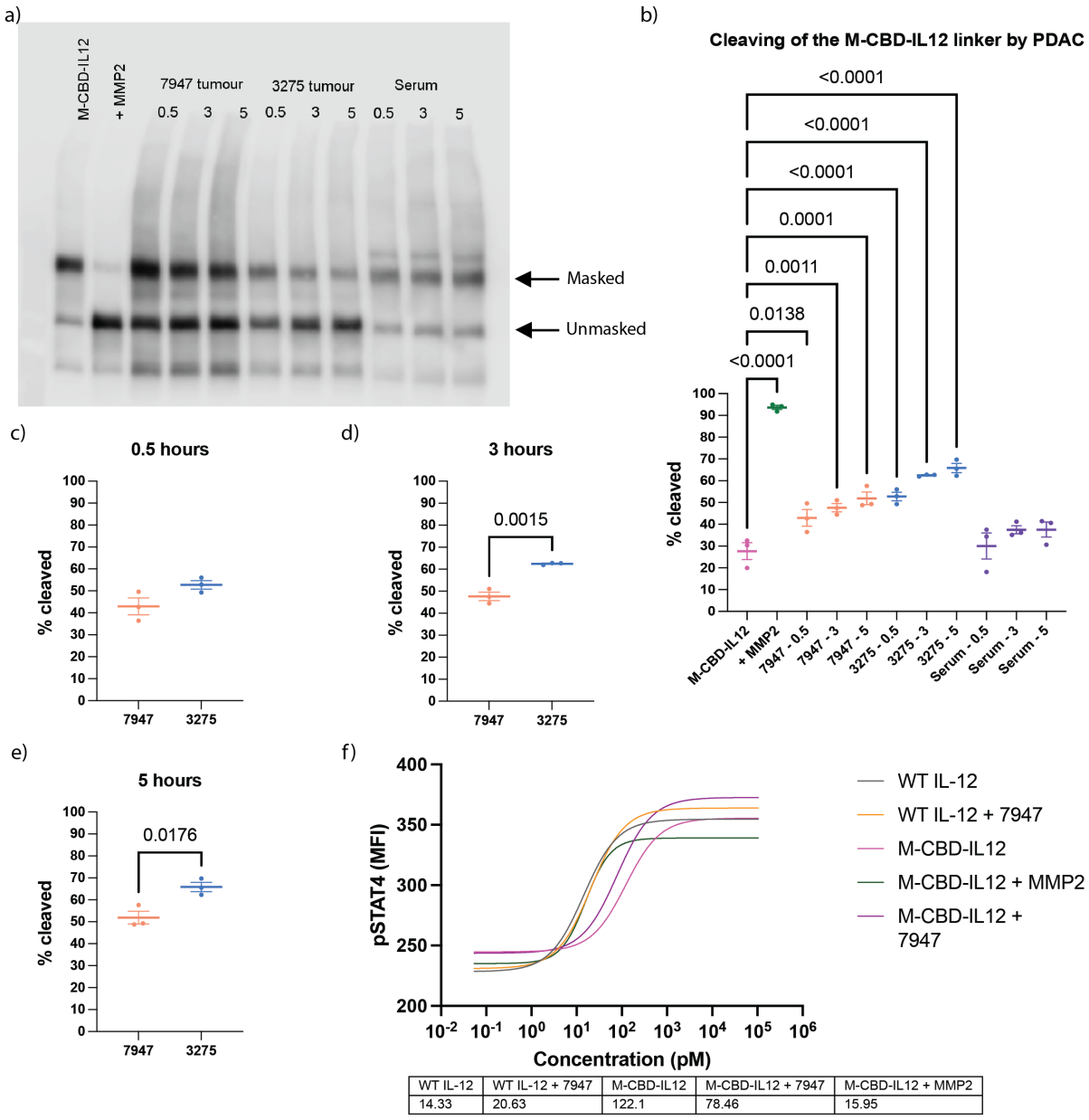
4.2.1 The M-CBD-IL12 linker is cleaved by two syngeneic PDAC mouse models, but not by their serum

In this chapter, I aimed to test the bioengineered IL-12 molecule M-CBD-IL12 in two orthotopic mouse models of PDAC: 7947 and 3275. Both these models have been widely used in the Sadanandam laboratory and are well characterised (446, 447). The former has a mesenchymal morphology, is immune-depleted and highly metastatic, whilst the latter is more heterogeneous with a mixture of epithelial and mesenchymal cancer cells. It is less metastatic than the 7949 model.

To predict whether these models would be capable of cleaving the M-CBD-IL12 linker, I once again performed a western blot on the incubation mixtures as described in the methodology section 2.13.1 (see Figure 4.1a). I observed no difference between the percentage of cleaved linker for untreated M-CBD-IL12 and the incubations with serum, suggesting the majority of the molecule remains masked in the bloodstream (see Figure 4.1b). In contrast, in the presence of recombinant murine MMP2, over 90% of the linker was cleaved, which was significantly more than the untreated M-CBD-IL12 ($p<0.0001$) (see Figure 4.1b). All tumour lysates at any of the time points cleaved significantly more linker compared to the untreated M-CBD-IL12 (see Figure 4.1b). Between the two tumour models, at the 30-minute time point, 3275 cleaved around 10% more of the linker than 7947, albeit not significant (see Figure 4.1c). However, from 3 hours onwards, 3275 cleaved significantly more of the M-CBD-IL12 linker than 7947 ($p=0.0015$ at 3 hours, $p=0.0176$ at 5 hours)(see Figure 4.1d,e).

As mentioned previously, phosphorylation of STAT4 can provide information on the biological activity of M-CBD-IL12 following removal of the mask. Similarly to my breast cancer experiments (see Figure 3.7f), I tested whether M-CBD-IL12 is not only unmasked but also biologically active following removal of the mask by PDAC tumours, as described in section 2.13.2 of the Methodology. In contrast with wild-type IL-12 therapy, M-CBD-IL12 had an EC50 that was almost 10-fold higher, which highlights the suppressive effect of the mask towards IL-12 signalling when the molecule is masked (see Figure 4.1f). Addition of recombinant MMP2 to M-CBD-IL12 restores the EC50 to

virtually the same as wild-type IL-12, suggesting when >90% of the linker is cleaved (see Figure 4.1b), IL-12's biological effects are fully restored (see Figure 4.1f). Finally, incubation with 7947 lysate reduced the EC50 to 78.46 (see Figure 4.1f). This suggests cleaving of the linker by tumour lysate partially restores the biological activity of M-CBD-IL12, yet it contains insufficient MMP2 to cleave all the linker.



WT IL-12	WT IL-12 + 7947	M-CBD-IL12	M-CBD-IL12 + 7947	M-CBD-IL12 + MMP2
14.33	20.63	122.1	78.46	15.95

Figure 4.1 The M-CBD-IL12 linker is cleaved by PDAC tissue lysate but not by mouse serum

a) Western blot of murine IL-12 representing the cleaving of the linker following incubation of M-CBD-IL12 with tumour lysates and serum for 0.5, 3 or 5 hours and 37

°C. Of the incubation mixtures, 10 µg of protein was loaded onto a gel, except for 0.0625 µg of untreated M-CBD-IL12 and 1 µg of the murine MMP2 mixture. The top band represents M-CBD-IL12 whilst the bottom band represents unmasked CBD-IL12. b) Three independent experiments were performed, and blots were quantified. c-e) Comparison of the cleaving of the linker at each of the time points for the different tumour lysates. f) Quantification of the *in vitro* activity of M-CBD-IL12 on pre-activated primary $CD8^+$ T-cells through measurements of pSTAT4 MFI using flow cytometry. EC50 values are presented in the table for each condition. This experiment was performed once to confirm *in vitro* biological activity following removal of the mask. Flow cytometry data was analysed using Flowjo. Statistical analyses were performed using a two-tailed student's t-test on GraphPad Prism.

4.2.2 M-CBD-IL12 is significantly less toxic than wild-type IL-12 in non-tumour bearing mice

IL-12-based toxicity is highly variable between different strains of mice, which makes it crucial to test toxicity of immunotherapies between different strains (448). For example, the C3H/Hej strain is highly sensitive to IL-12-mediated toxicity and will rapidly lose weight (448). Therefore, I tested the toxicity of M-CBD-IL12 and wild-type IL-12 in non-tumour bearing Fvb/NCrl mice (see Figure 4.2a). I however observed no impact on their body weight (see Figure 4.2b), similarly to the BALB/c mice in Figure 3.8. I also bled the mice from the tail vein on two separate occasions to be able to measure the toxicity marker plasma IFNγ. On day 2 after the first dose, wild-type IL-12-treated mice had significantly higher (250-fold higher) plasma IFNγ compared to the M-CBD-IL12 group ($p=0.0019$)(see Figure 4.2c). However, on day 6 (three days after the second dose), these levels started to normalise again and the difference between wild-type IL-12 and M-CBD-IL12 groups was not significant anymore (see Figure 4.2d). Therefore, wild-type IL-12, but not M-CBD-IL12 seems to induce plasma IFNγ production in non-tumour bearing Fvb/NCrl mice. These mice do however recover rapidly from the high plasma IFNγ levels.

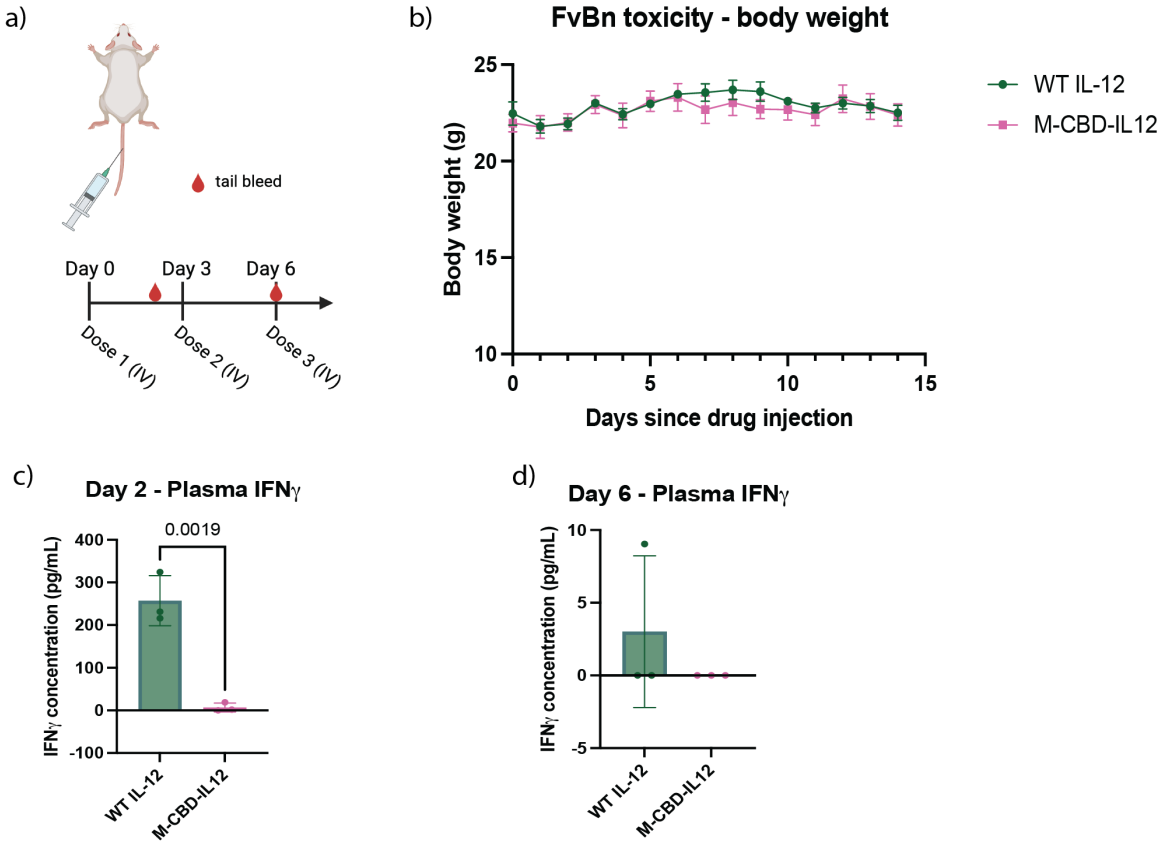


Figure 4.2 M-CBD-IL12 is significantly less toxic than wild-type IL-12 in non-tumour bearing Fvb/NCrl mice

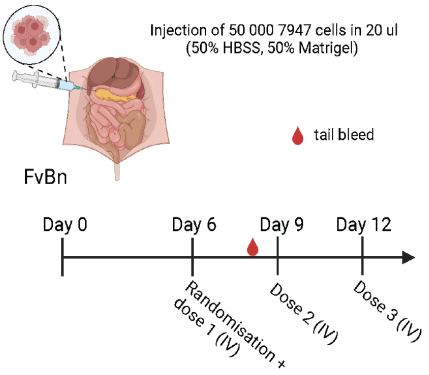
a) Study design of the tolerability study of wild-type IL-12 and M-CBD-IL12 in non-tumour bearing Fvb/NCrl mice. 6-7-week-old non-tumour-bearing Fvb/NCrl mice (n=3) were treated with 83 pmol of wild-type (WT) IL-12 or 250 pmol of M-CBD-IL12 intravenously (IV) on days 0, 3, and 6. b) The mice's body weight was recorded for 13 days following the first dose. Plasma IFNγ quantification through ELISA from days 2 c) and 6 d) following the first dose of the respective drugs. Mouse experiments and ELISAs were performed only once. Statistical tests were performed using a two-tailed student's t-test on Graphad prism. Schematics were designed on Biorender.com

4.2.3 The efficacy of wild-type IL-12 and M-CBD-IL12 differs in two immunologically distinct PDAC mouse models

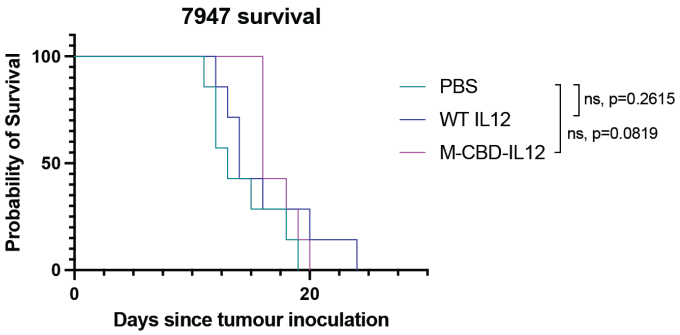
Next, I tested the effect of M-CBD-IL12 and wild-type IL-12 on the survival of the orthotopic syngeneic 7947 PDAC mouse model (see Figure 4.3a). M-CBD-IL12 moderately prolonged the survival of mice bearing orthotopic 7947 PDAC tumours compared to PBS controls, although this change was not significant (see Figure 4.3b). In contrast, wild-type IL-12 treated mice did not survive longer than the PBS group (see Figure 4.3b). Interestingly, despite the shorter survival, mice treated with wild-type IL-12 seemed to have smaller tumours than M-CBD-IL12 and PBS controls, although this change was not significant either (see Figure 4.3c). Little difference in liver and spleen weight was observed between treatment groups (see Figure 4.3d,e). Upon necropsy, mice treated with M-CBD-IL12 had less abdominal fluid (ascites) than the other groups (not significant) (see Figure 4.3f). Percentage change in body weight was showing an increasing trend for both the wild-type IL-12 mice and the M-CBD-IL12 mice compared to PBS, yet a lot of variation existed and this change was not significant (see Figure 4.3g,h). It is also important to highlight how ascites may mask any weight loss these animals may experience.

In the M-CBD-IL12-treated group, 5 out of 7 mice were liver metastasis-free, compared to only 1 out 7 in the wild-type IL-12 and PBS groups (see Figure 4.3i). This suggests M-CBD-IL12 therapy suppressed liver metastases, potentially contributing to the modest reduction in ascites volume and modestly prolonged survival in this group (see Figure 4.3b,f,i). In contrast, despite the wild-type IL-12 tumour volume being smaller than M-CBD-IL12, the survival of the mice in the wild-type IL-12 group was shorter than with M-CBD-IL12 (see Figure 4.3b,c). This means the wild-type IL-12-treated mice most likely succumbed to the effects of the liver metastases instead. Finally, I analysed the plasma from day 8 for mouse IFNγ using ELISA. I observed a significant difference in plasma IFNγ between the wild-type IL-12 group and both the PBS controls ($p<0.0001$) and the M-CBD-IL12 group ($p=0.0013$)(see Figure 4.3j). This suggests M-CBD-IL12 is also significantly less toxic than its wild-type counterpart in this mouse strain.

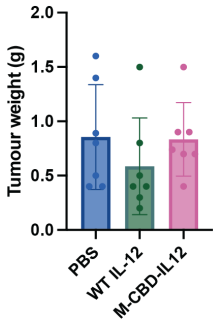
a)



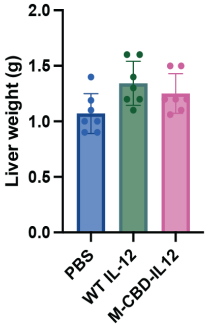
b)



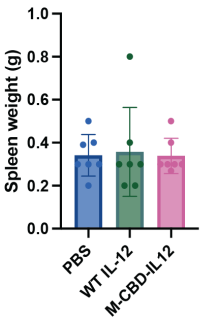
c)



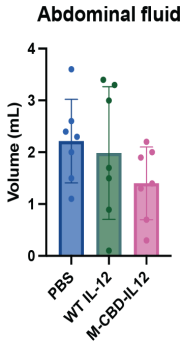
d)



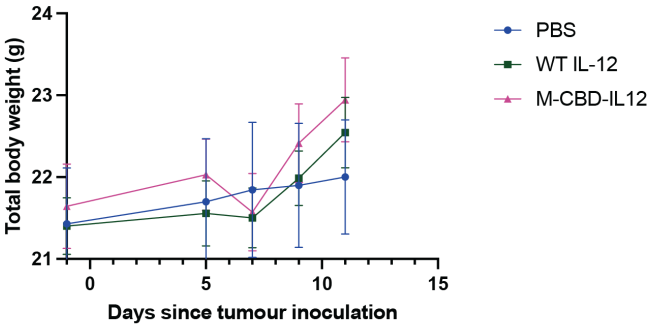
e)



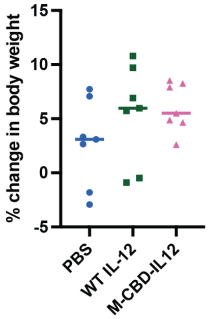
f)



g)



h)



i)

Animal Number	PBS	WT IL-12	masked CBD-IL12
1	0	+	0
2	++	+++++++	0
3	+++	+	0
4	++++	+	0
5	++	++	0
6	+	+	++
7	+	0	+++++

Liver metastases

Animal number	PBS	WT IL-12	masked CBD-IL12
1	+++++	+++++	+++
2	+++	++++	++++++
3	+++++	++++	+++++++
4	++++++	+++	+++++
5	+++++	++++	++++
6	+++++	+++++	++++
7	+++++	+++++++	+++

Spleen metastases

j)

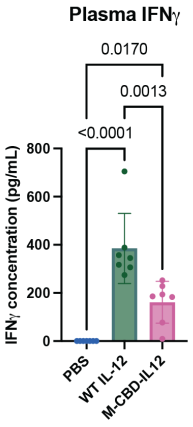


Figure 4.3 M-CBD-IL12 moderately prolongs survival of mice bearing orthotopic 7947 PDAC tumours

a) 6-7-week-old Fvb/NCrl mice (n=7) were orthotopically injected with 50 000 7947 PDAC cells into the pancreas. Mice then received either 83 pmol of wild-type (WT) IL-12 or 250 pmol of M-CBD-IL12 intravenously (IV) on days 6, 9, and 12. Mice were terminated once they reached the humane endpoint. The b) survival curve, c) tumour weights, d) liver weights, e) spleen weights, f) abdominal fluid volumes, g) body weight curves, and h) percentage body weight changes have been displayed. i) Liver and spleen metastases were visually counted upon necropsy. A '+' represents a single metastasis. j) Mice were bled from the tail vein on day 8 following tumour inoculation and plasma was analysed for murine IFNγ using ELISA. Each mouse experiment was performed only once. Statistical tests were performed using a one-way ANOVA with Tukey's multiple comparison tests or Mantel Cox test for Kaplan Meier survival on GraphPad Prism. Schematics were designed on Biorender.com

In the 3275 PDAC model, I applied the same treatment regimen whilst including some combination immunotherapy groups with either intraperitoneal anti-PD-1 or anti-PD-L1 to prevent IFNγ-mediated T-cell exhaustion in response to IL-12 immunotherapy (see Figure 4.4a). Since some of the mice became unwell rapidly, I decided to convert this into an intervention study, meaning all mice were culled simultaneously once the first mouse became unwell. The tumours of mice treated with wild-type IL-12 were significantly smaller than PBS controls (p=0.0004)(see Figure 4.4b-c). Meanwhile, tumours from mice treated with M-CBD-IL12 were borderline significantly smaller than PBS controls (p=0.0550)(see Figure 4.4b,d). Interestingly, the CPI combination therapy did not suppress tumour burden to the same extent (see Figure 4.4b). Therefore, this model may be intrinsically responsive to IL-12 without an increase in checkpoint expression to evade its effects.

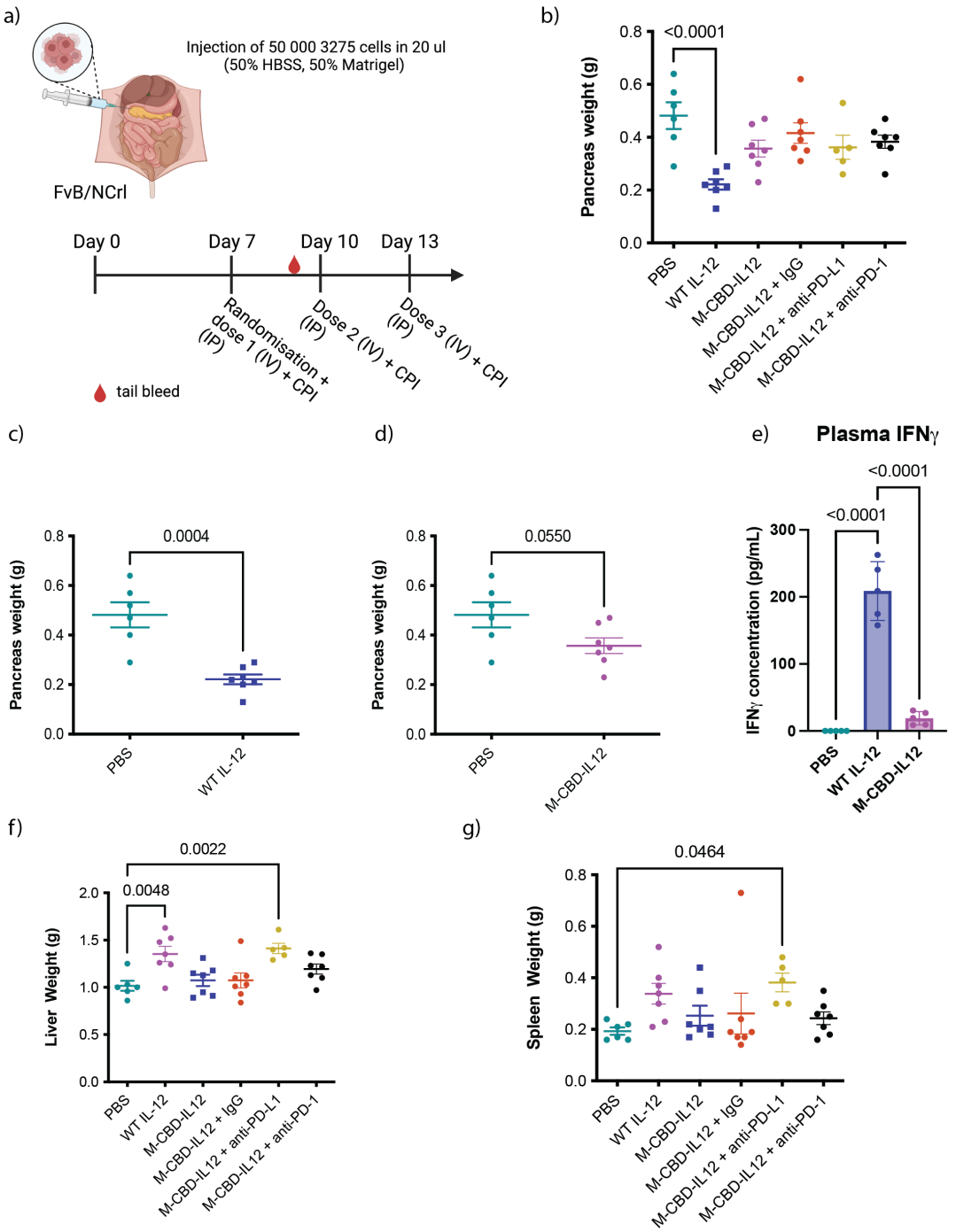


Figure 4.4 Wild-type IL-12 suppresses 3275 tumour burden to a larger extent than M-CBD-IL12

a) 6-7-week-old Fvb/NCrl mice (n=7 for all groups except n=6 for PBS and n=5 for M-CBD-IL12 + anti-PD-L1) were orthotopically injected with 50 000 3275 PDAC cells into the pancreas. a) Once tumours had developed, they were imaged using In Vivo Imaging System (IVIS). Mice then received either 83 pmol of wild-type (WT) IL-12 or 250 pmol of M-CBD-IL12 intravenously (IV) on days 7, 10, and 13 with 100 µg of the respective CPI or associated IgG control intraperitoneally (IP) on the indicated days. Mice were bled from the tail vein on day 9 following tumour inoculation and plasma was analysed for murine IFNγ using ELISA. Mice were terminated once the first

mouse reached the humane endpoint. The b-d) pancreas weights, e) plasma IFNγ, f) liver weights, g) spleen weights are displayed. Mouse experiments and ELISAs were performed only once. Statistical tests were performed using a two-tailed student's t-test or one-way ANOVA with Tukey's multiple comparison tests. Schematics were designed on Biorender.com.

However, as observed in the previous models, plasma IFNγ is again significantly lower with both M-CBD-IL12 and PBS compared to wild-type IL-12 (both $p<0.0001$)(see Figure 4.4e). The liver weights of the wild-type IL-12 ($p=0.0048$) and M-CBD-IL12 + anti-PD-L1 groups ($p=0.0022$) and the spleen weight of M-CBD-IL12 + anti-PD-L1 group ($p=0.0464$) were significantly raised compared to PBS suggesting the anti-PD-L1 in particular may be toxic (see Figure 4.4f,g). Similarly to what I observed in the EMT6 model in Chapter 3, although this tumour type responds to wild-type IL-12, its toxicity remains a problem. Whilst eradicating this toxicity, the mask and the CBD reduce some of the IL-12's efficacy.

Overall, both these PDAC models seem to respond differently to wild-type IL-12. The current M-CBD-IL12 dose seems to be too low to generate sufficient unmasked CBD-IL12 in either model. M-CBD-IL12 dose optimisation may help overcome these obstacles in future experiments. I however was interested in understanding the biological factors that contribute to this difference in sensitivity to IL-12 between the PDAC models. This would further my understanding of potential resistance mechanisms that limit the success of IL-12 immunotherapy in PDAC. Firstly, to allow for a like-for-like comparison between models, I performed a small intervention study on the orthotopic 7947 model including two treatment groups only: PBS and wild-type IL-12 (see Figure 4.5a). Similarly to the survival study, 7947 was more resistant to wild-type IL-12 in this intervention study, since tumour burden was only minimally reduced (see Figure 4.5b). However, the liver weight was once again significantly higher in the wild-type IL-12 groups compared to PBS ($p<0.0001$), most likely representing IL-12 induced toxicity (see Figure 4.5c). Spleen weight was also raised, but not significantly (see Figure 4.5d).

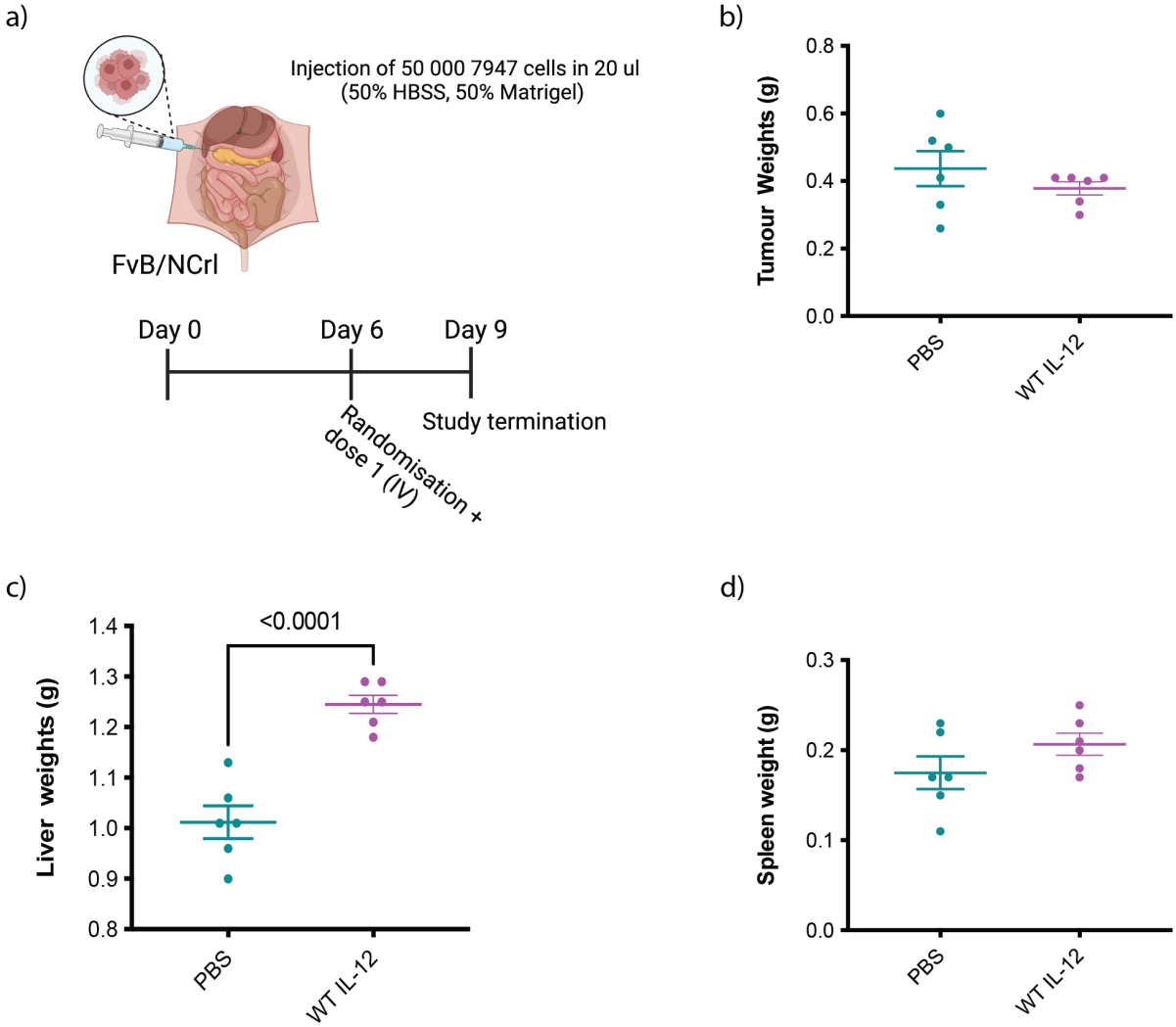


Figure 4.5 The 7947 orthotopic PDAC mouse model is resistant to wild-type IL-12

a) 6-7-week-old Fvb/NCrl mice (n=6) were orthotopically injected with 50 000 7947 PDAC cells into the pancreas. a) Once tumours had developed, they were imaged using In Vivo Imaging System (IVIS). Mice then received 83 pmol of wild-type (WT) IL-12 intravenously (IV) on day 6. All the mice were terminated on day 9, at which point the first mouse reached the humane endpoint. The b) tumour weights, c) liver weights and d) spleen weights are displayed. Mouse experiments were performed only once. Statistical tests were performed using a two-tailed student's t-test on GraphPad Prism and schematics were designed on Biorender.com.

4.2.4 7947 tumours upregulate KRAS G12D protein expression to evade immune responses

Due to the immunomodulatory role of the *KRAS*^{G12D} mutation in PDAC and its involvement in immune evasion (212), I decided to measure its expression in the harvested tumours from both intervention studies. I also included IL-12-treated tumours to visualise whether 7947 tumours were evading the effect of IL-12 therapy by upregulating KRAS G12D protein expression. 7947 tumours have borderline significantly higher KRAS G12D protein levels than 3275 tumours (p=0.0547)(see Figure 4.6a). This suggests 7947's high KRAS G12D protein levels may be partially responsible for its unresponsiveness to IL-12 therapy. Interestingly, IL-12 therapy did not further increase KRAS G12D protein levels in 7947, which may already have reached maximum and plateaued (see Figure 4.6b). However, in 3275, IL-12 therapy triggered an increasing trend in KRAS G12D protein expression, although this increase was not significant (see Figure 4.6c). However, despite this, KRAS G12D protein levels in 3275 were still not nearly as high as in 7947 tumours. I then decided to quantify the expression phosphorylated and total ERK as a component of a downstream KRAS signalling pathway (see Figure 4.6d). Despite a small non-significant increase in ERK phosphorylation in 7947 tumours (see Figure 4.6e), IL-12 therapy did not affect ERK phosphorylation in either model compared to PBS (see Figure 4.6e,f). Therefore, IL-12 therapy does not seem to affect downstream ERK phosphorylation in these PDAC models.

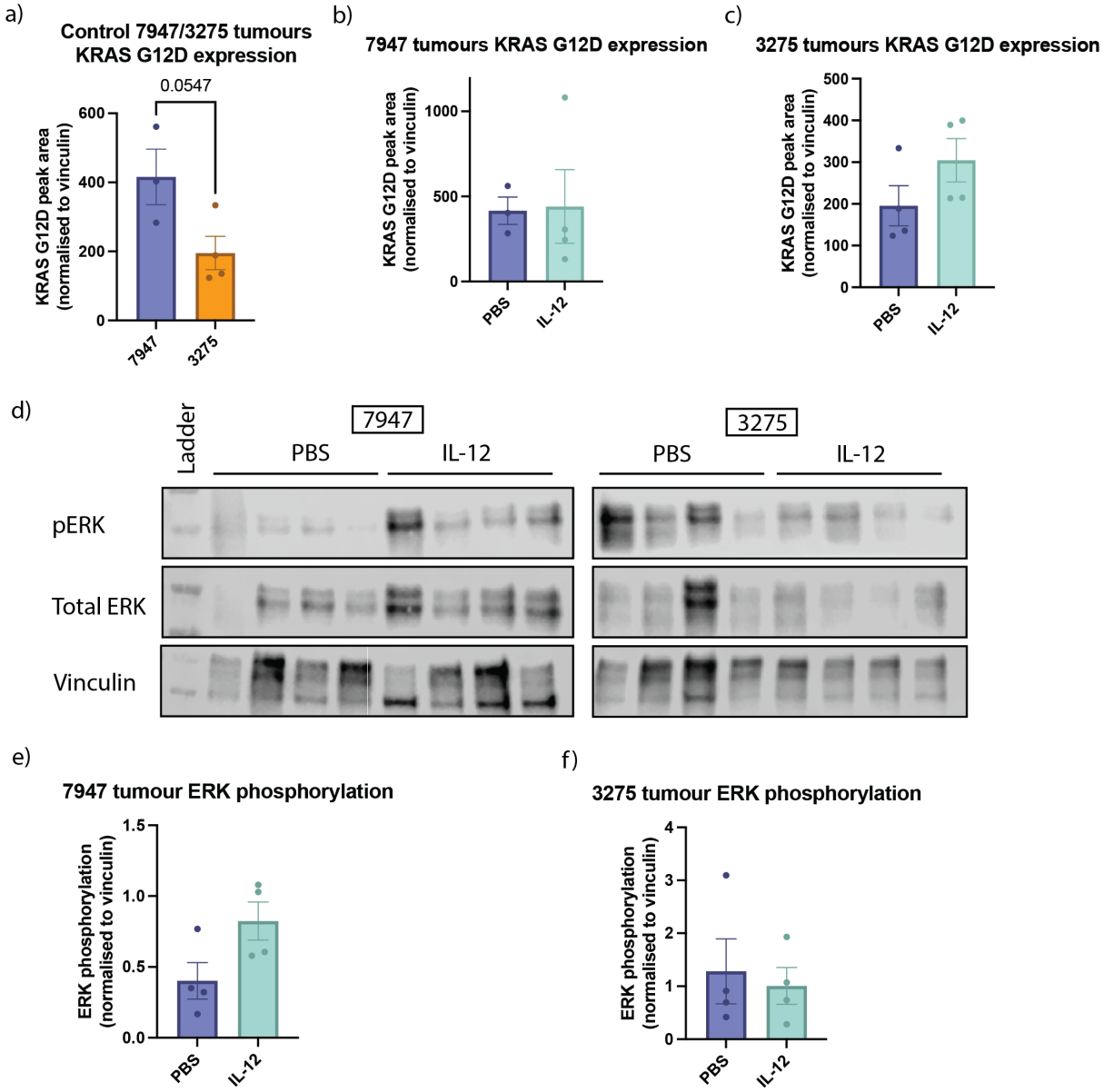


Figure 4.6 7947 tumours express higher KRAS G12D protein levels than 3275

a) Control and b/c) IL-12-treated (83 pmol intravenously) 7947 (from study described in Figure 4.5, n=3 PBS, n=4 IL-12) and 3275 (from study described in Figure 4.4, n=4) tumours were collected and homogenised. Protein concentration was determined, and the lysates were analysed for KRAS G12D protein expression using Wes Simple Western and d) for phosphorylated and total ERK using western blotting on 10 µg of protein (n=4). e/f) Signals from 4 different tumours per group were quantified and plotted on GraphPad Prism. Statistical analyses were performed using a two-tailed student's t-test on GraphPad Prism.

I then measured KRAS G12D protein expression in the parental cell lines the tumours originated from. This would demonstrate whether the tumorigenic PDAC TME is responsible for increasing KRAS G12D protein expression in 7947 tumours. In the cell lines, the opposite pattern in KRAS G12D protein expression was observed between the two cell lines; 3275-luc cells expressed significantly higher levels of KRAS G12D than 7947-luc ($p=0.0049$)(see Figure 4.7a). This may suggest that cancer cells within 7947 tumours upregulate KRAS G12D expression to evade the immune cells in the TME, whilst the 7947-luc cell line *in vitro* does not experience this pressure to evade. Therefore, KRAS G12D levels are low in the 7947-luc cell line. The effects of the TME may therefore cause these conflicting results between results from tumours and cell lines. This hypothesis is supported by the fact that 3275-luc cells (high KRAS G12D) proliferate faster than 7947-luc cells (low KRAS G12D) *in vitro* (see Figure 4.7c). In contrast, 7947 tumours (high KRAS G12D) grew faster than 3275 tumours (low KRAS G12D) *in vivo* (see Figure 4.4a, Figure 4.5a). This compensatory increase in KRAS G12D expression and consequently immune evasion may be driving 7947's resistance to IL-12 immunotherapy. Due to difficulties with total KRAS western blotting/simple western antibodies, I quantified total *Kras* using qRT-PCR. Total *Kras* was also higher in 3275-luc compared to 7947-luc, yet this difference was not significant (see Figure 4.7b).

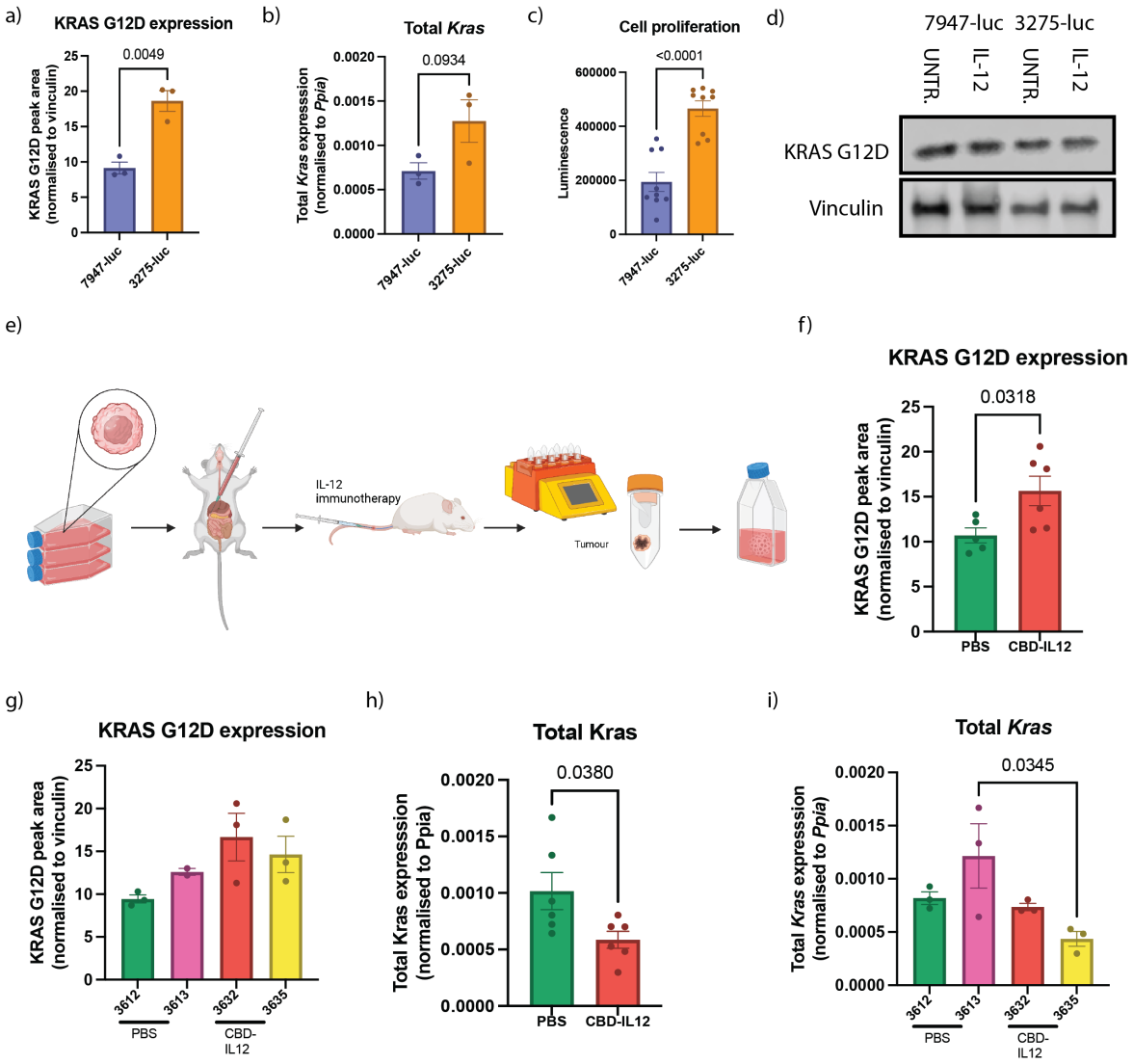


Figure 4.7 The TME and IL-12 therapy trigger an increase in KRAS G12D expression in 7947

7947-luc and 3275-luc cells were collected, homogenised and protein concentration was determined on three separate occasions. a) KRAS G12D protein expression was quantified using Wes Simple Western, whilst b) total *Kras* levels were quantified using qRT-PCR. Differences in cell proliferation between the two cell lines are displayed in c). 2500 cells were seeded per well of a 96-well cell culture plate and they were left to grow for 96 hours, at which point luminescence was measured using Cell Titer Glo. d) Cancer cells were treated with normal media or IL-12-containing media for 72 hours. The cancer cells were then collected and homogenised for western blotting using 30 µg of protein. This experiment was performed once. e) Schematic representing the development of CBD-IL12-treated cell lines. The protein was collected from these cell lines on three separate occasions and the expression of KRAS G12D in these cell lines was determined using Wes Simple Western. The results have been displayed in terms of treatment groups in f) or individual cell lines in g). Total *Kras* expression in the CBD-IL12 lines was quantified using qRT-PCR and the results have also been displayed in terms of treatment groups h) or as individual cell lines i). Statistical tests were performed using a two-tailed student's t-test or one-way ANOVA with Tukey's

multiple comparison tests on GraphPad Prism. Schematic was designed on Biorender.com.

4.2.5 Cancer cell lines generated from IL-12-treated 7947 tumours express significantly more KRAS G12D than from untreated 7947 tumours

I then attempted to visualise the relationship between the resistance to IL-12 immunotherapy and KRAS G12D expression *in vitro* (see Figure 4.7d). As expected, IL-12 therapy does not directly affect the KRAS G12D expression in cancer cells *in vitro* (see Figure 4.7d). I also used cell lines that were generated by my colleague Chanthirika Ragulan, who is working on CBD-IL12 in PDAC. These cell lines originate from 7947 tumours that had been treated with either PBS or CBD-IL12 *in vivo* (see Figure 4.7e). Following this therapy, the morphology of the cells and the expression of epithelial and mesenchymal markers had changed in comparison with the parent cell line. This data has not been included in this thesis since it is part of Chanthirika's thesis. These changes remain consistent, and the cell lines did not revert back to the parental, even after repetitive culturing. I therefore quantified the KRAS G12D protein expression using Wes Simple Western in two PBS-treated (3612, 3613) and two CBD-IL12-treated (3632, 3635) cell lines (see Figure 4.7f,g). I observed a significant increase in KRAS G12D expression in the CBD-IL12-treated lines compared to PBS ($p=0.0318$)(see Figure 4.7f,g). The opposite pattern is observed with total KRAS levels (see Figure 4.7h,i). These figures have been represented both as the individual cell lines as well as the treatment groups for clarity. This suggests that the IL-12 treatment in the 7947 tumours from which the cell lines originate caused them to upregulate KRAS G12D expression to evade the IL-12-induced immune response. The IL-12 therapy therefore does not directly induce KRAS G12D upregulation in cancer cells, but instead it indirectly promotes its upregulation by increasing the threat that the immune cells pose to cancer cells.

I also quantified the downstream phosphorylated and total ERK (see Figure 4.8a). I saw that ERK is phosphorylated considerably less in 7947-luc than 3275-luc cancer cells, although this is not significant (see Figure 4.8a,b). This corresponds with the KRAS G12D protein expression being higher in 3275-luc too. There seems to be no difference

in ERK phosphorylation between PBS-treated and IL-12-treated cell lines (see Figure 4.8c,d). However, these findings require confirmation in a larger number of cell lines.

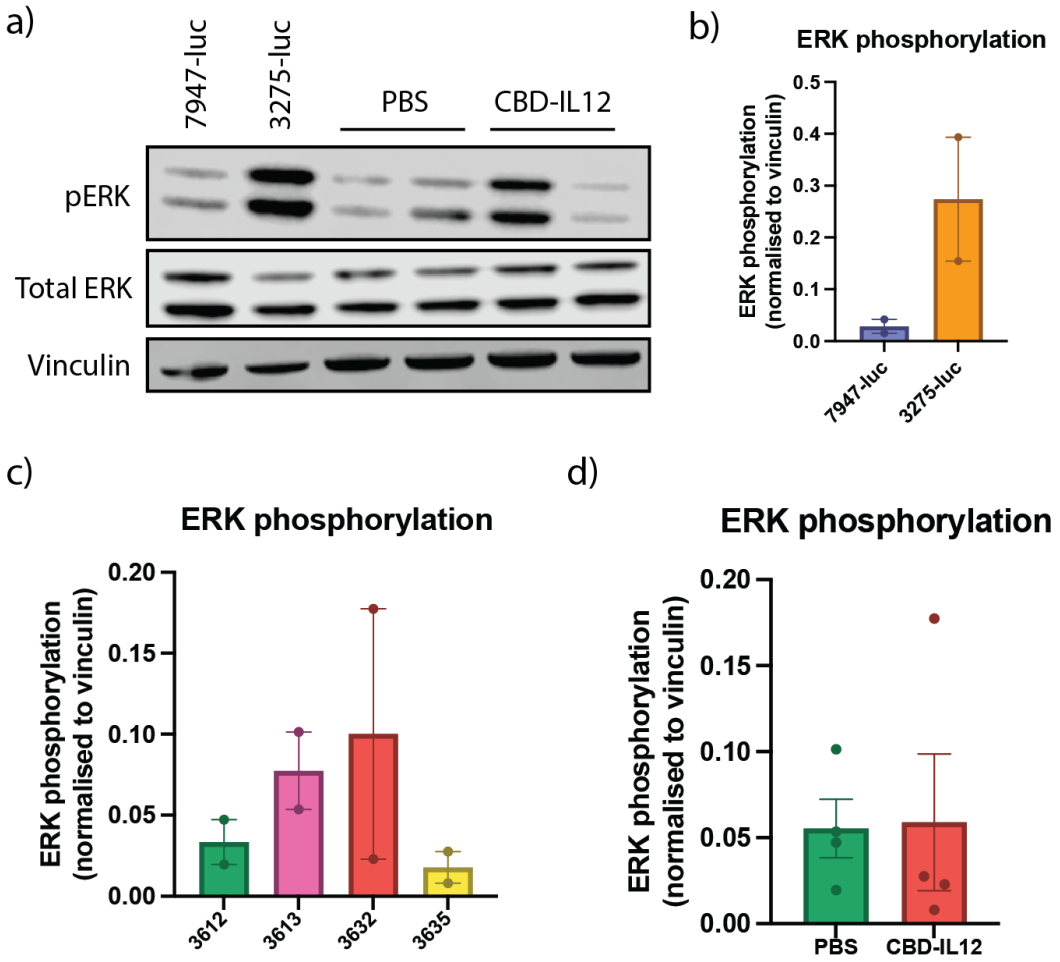


Figure 4.8 ERK phosphorylation does not differ between cell lines generated from IL-12-treated or PBS-treated 7947 tumours

7947-luc, 3275-luc cells and the CBD-IL12 cell lines were collected on two separate occasions and homogenised and protein concentration was determined. a) Western blots for phosphorylated and total ERK proteins were performed on 10 µg of protein. b) The signals of two independent experiments were quantified, normalised to vinculin signals, and plotted on GraphPad Prism. Statistical analyses were performed using a one-way ANOVA with Tukey's multiple comparison tests or two-tailed student's t-tests on GraphPad Prism.

4.2.6 The upregulated KRAS G12D expression following IL-12 therapy does not make 7947 more sensitive to MRTX1133 therapy

These findings demonstrate there seems to be an association between KRAS G12D expression in the cancer cells and response to IL-12 therapy. I therefore decided to use the KRAS G12D inhibitor MRTX1133 on the cell lines (see Figure 4.9a). In terms of the IC50s, little difference exists between 3275-luc and 7947-luc in response to MRTX1133 (see Figure 4.9b). I confirmed these findings both with 5% and 10% FBS in the cell culture media, since FBS contains some growth factors that may promote KRAS signalling and may influence the cell lines' sensitivity to MRTX1133 therapy (see Figure 4.9b,c). The IC50 however did not seem to be affected much by FBS (see Figure 4.9b,c). With the support of my colleague Chanthirika Ragulan, we performed the same MRTX1133 assay on the tumour-derived cell lines too (see Figure 4.9d). The IC50s of the PBS-treated and CBD-IL12 lines were similar to one other and to the parental. Therefore, despite IL-12 therapy triggering a compensatory raise in KRAS G12D expression in 7947 (see Figure 4.7f), it does not make these cells more KRAS G12D dependent (MRTX1133 is not sufficient to eliminate cancer cells). These findings confirm that KRAS G12D inhibition alone may not suffice for PDAC elimination.

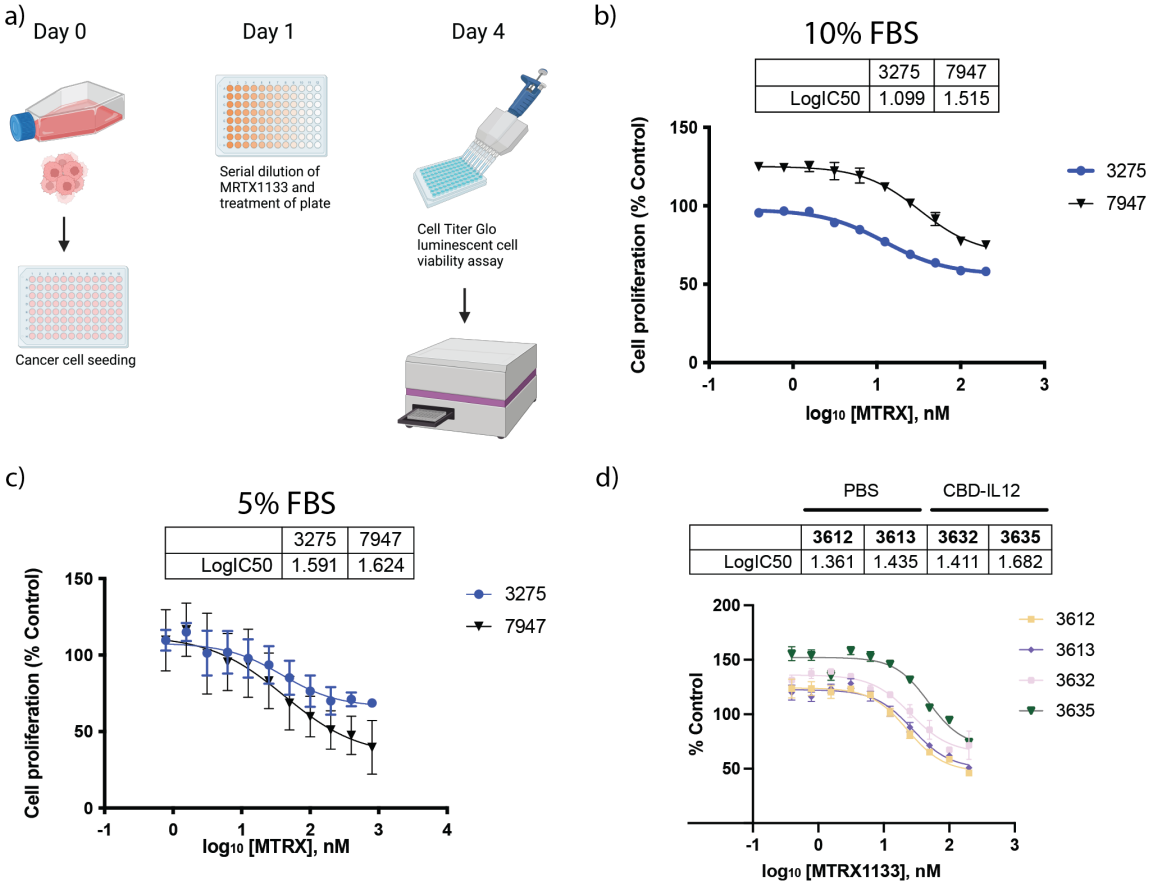


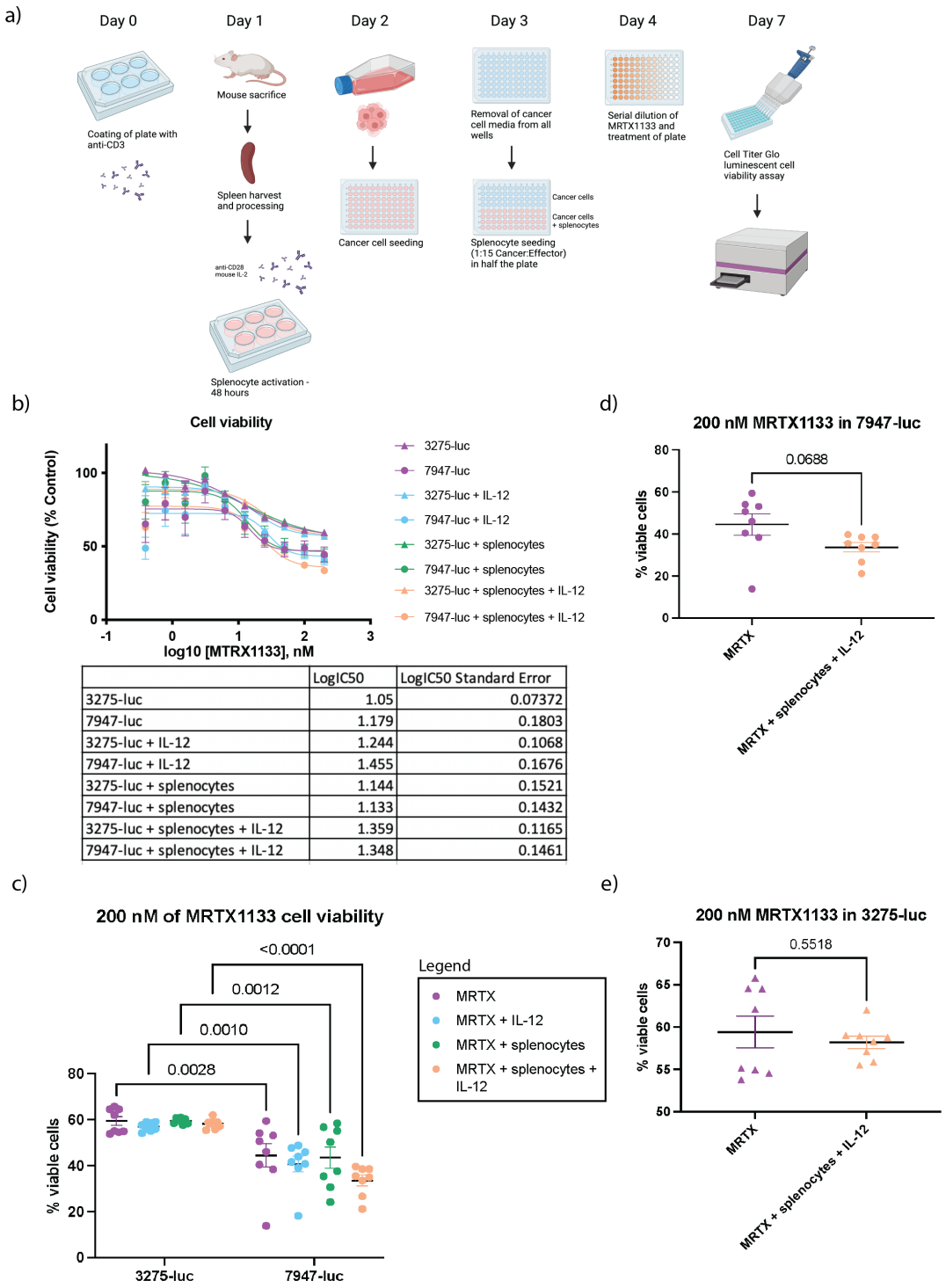
Figure 4.9 Both 7947 and 3275 respond similarly to KRAS G12D inhibition using MRTX1133 *in vitro*

a) Schematic representing the methodology for the MRTX1133 assay. This schematic was designed on Biorender.com. The dose response curve and IC50 of MRTX1133 on 7947-luc and 3275-luc cells in b) 10% FBS RPMI or c) 5% FBS RPMI. d) Dose response curves and IC50 of MRTX1133 on the tumour-derived cell lines. Experiments were performed twice. Curves were plotted on GraphPad Prism.

4.2.7 KRAS G12D inhibition in 7947 sensitises it to IL-12 therapy in the presence of immune cells

Since KRAS G12D is known to promote immune evasion (212), its inhibition could sensitise 7947 cells to IL-12 immunotherapy. Therefore, I proceeded to perform the same MRTX1133 assay yet in the presence of immune cells and IL-12 as part of a co-culture system (see Figure 4.10a). In terms of IC50s of the dose response curves, I only observed slight fluctuations between the different conditions and cell lines (see Figure 4.10b). However, a significant difference between the two cell lines could be seen at the maximum concentration of 200 nM of MRTX1133, particularly in the presence of

splenocytes and IL-12 ($p<0.0001$)(see Figure 4.10c); the cell viability of 7947-luc cells dropped to below 40% when normalised to the DMSO control at 200 nM (see Figure 4.10c). Only in 7947-luc, but not in 3275-luc, caused the addition of IL-12 and splenocytes to MRTX1133 a drop in cell survival compared to MRTX1133 monotherapy, although this change was not significant (see Figure 4.10d,e). This suggests that simultaneous KRAS G12D inhibition with IL-12 therapy may prevent 7947-luc from evading the IL-12-induced immune response.



	LogIC50	LogIC50 Standard Error
3275-luc	1.05	0.07372
7947-luc	1.179	0.1803
3275-luc + IL-12	1.244	0.1068
7947-luc + IL-12	1.455	0.1676
3275-luc + splenocytes	1.144	0.1521
7947-luc + splenocytes	1.133	0.1432
3275-luc + splenocytes + IL-12	1.359	0.1165
7947-luc + splenocytes + IL-12	1.348	0.1461

Figure 4.10 7947 is more responsive to simultaneous IL-12 therapy and KRAS G12D inhibition in the presence of immune cells *in vitro*

a) Design of the co-culture studies. Schematic was designed on Biorender.com. b) Dose response curves of the different co-culture conditions and their associated IC50s. These curves were plotted on GraphPad Prism. c-e) Comparison of the viability between the two cell lines in different conditions. Experiments were performed

three times. Statistical analyses were performed using a two-way ANOVA or two-tailed student's t-test on GraphPad Prism.

Due to the immunomodulatory role of KRAS G12D, I measured whether MRTX1133, and IL-12 affect the composition of adaptive immune cell populations in the splenocytes following co-culture. I therefore performed the same co-culture experiment but on a larger scale, collected the splenocytes from each condition, and analysed them through flow cytometry (see Figure 4.11). I measured whether inhibiting KRAS G12D through MRTX1133 to prevent immune evasion in the presence of IL-12 affects T-cell subsets. I therefore quantified the proportions of overall, $CD4^+$ and $CD8^+$ T-cells following co-culture with either 7947-luc (see Figure 4.11a/c) or 3275-luc (see Figure 4.11b/d). With either cell line, few changes in these subsets were observed, except for a slight increase in $CD8^+$ T-cells, and consequently decrease in $CD4^+$ T-cells, with MRTX+IL-12 compared to DMSO+IL-12 following co-culture with 7947-luc (see Figure 4.11c). This change was however not significant. When splenocytes are cultured alone (without cancer cells) and treated with IL-12 either in combination with DMSO or MRTX1133, little difference in number of overall, $CD4^+$ and $CD8^+$ T-cells exists between these conditions (see Figure 4.11e). This suggests that the KRAS G12D-driven immune evasive cancer cell effects do not directly affect these T-cell subsets.

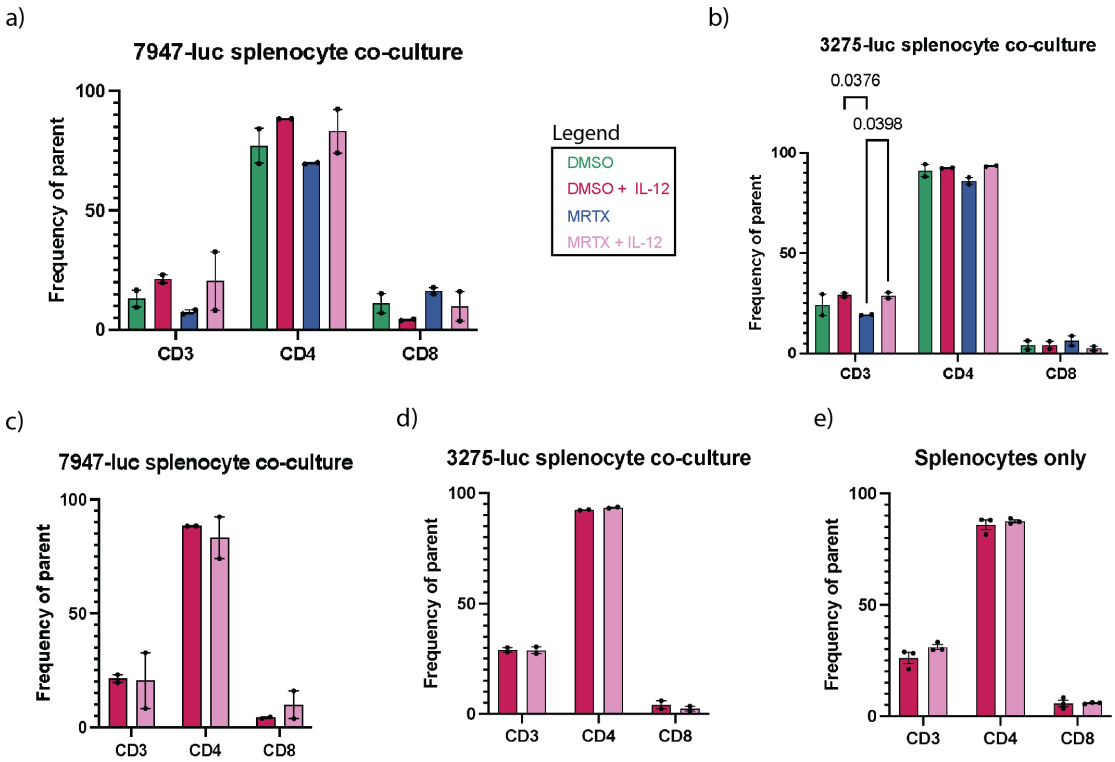
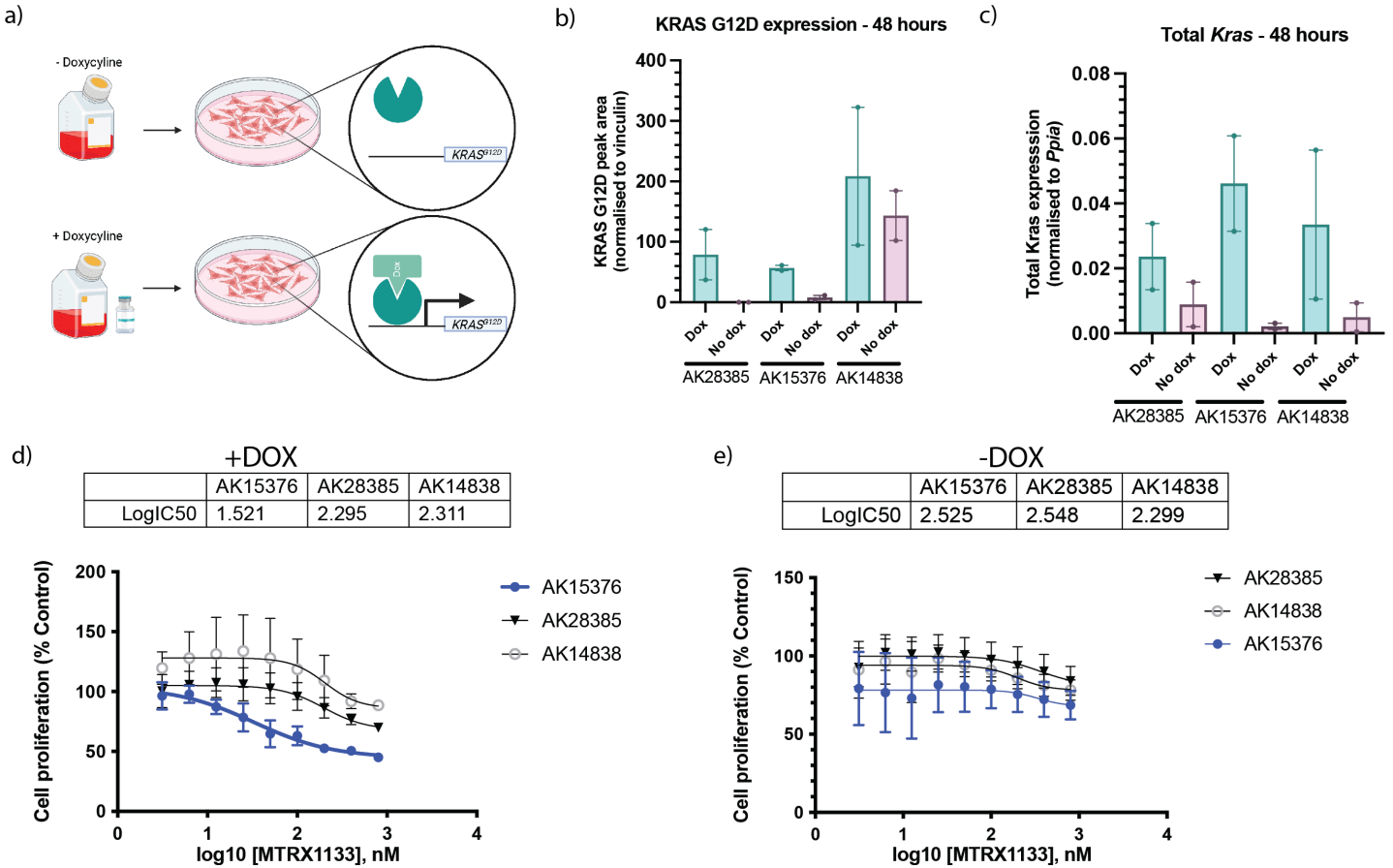


Figure 4.11 The proportions of adaptive immune cell populations within splenocytes are not affected by MRTX1133 and IL-12 in a co-culture setting

Following co-culture with either a/c) 7947-luc or b/d) 3275-luc cancer cells for 72 hours as described in Figure 4.10, splenocytes were collected, washed, and stained for flow cytometry. e) A plate of splenocytes cultured in the absence of cancer cells was also included. Two repeats of each condition were used in this experiment and it was performed once. The data was analysed on Flowjo and statistical analyses were performed using a two-way ANOVA on GraphPad Prism.

4.2.8 *iKras cell lines as an alternative to MRTX1133*

Due to difficulties with the material transfer agreement for MRTX1133 for *in vivo* use, I instead used three doxycycline *iKras* PDAC cell lines that express the $Kras^{G12D}$ mutation in the presence of doxycycline and do not in its absence (see Figure 4.12a). One of the lines (AK15376) was morphologically (mesenchymal, slower growing *in vitro*) similar to 7947-luc, whilst another (AK28385) was morphologically similar to 3275-luc (epithelial, very fast growing *in vitro*). I used a combination of both Wes Simple Western and qRT-PCR to confirm that the doxycycline-inducible system functioned (see Figure 4.12b,c). Similarly to 7947-luc and 3275-luc, I performed the MRTX1133 assay on these *iKras* lines both in the presence and absence of doxycycline (see Figure 4.12d,e). In this assay, I confirmed AK15376 to also respond similarly to MRTX1133 with virtually the same IC50 as 7947-luc (see Figure 4.12d). AK28385 and AK14838 were more resistant to KRAS G12D inhibition (see Figure 4.12d). As expected, performing assays in the absence of doxycycline obliterated the observed response in AK15376, whilst the other cell lines remain unchanged (see Figure 4.12e).



d) +DOX	AK15376	AK28385	AK14838
LogIC50	1.521	2.295	2.311

e) -DOX	AK15376	AK28385	AK14838
LogIC50	2.525	2.548	2.299

Figure 4.12 The AK15376 *iKras* cell line responds similarly to MRTX1133 as 7947-luc/3275-luc *in vitro*

a) Schematic representing the inducible *Kras* system in the presence and absence of doxycycline. b/c) the three *iKras* lines were plated in the presence or absence of doxycycline and were left for 48 hours. Cells were collected and homogenised on two separate occasions. Either RNA was extracted for total *Kras* qRT-PCR or protein concentration was measured for KRAS G12D Wes Simple Western. The MRTX1133 assay was performed on the three *iKras* lines in the d) presence or e) absence of doxycycline. This experiment was performed three times. Dose response curves were generated on Graphpad prism. Schematics were designed on Biorender.com

4.2.9 AK28385 and AK14838 mouse models respond to IL-12 in a similar manner as the 3275 mouse model

Together with Chanthirika Ragulan, I performed a small *in vivo* pilot study using these three *iKras* lines (see Figure 4.13a). All mice stayed on doxycycline drinking water throughout the study to test their baseline sensitivity to IL-12. We found the AK28385 (similar in morphology to 3275-luc) to fully respond to IL-12 therapy; the % change in tumour volume was significantly lower in the mice treated with IL-12 compared to PBS controls ($p=0.0012$)(see Figure 4.13b). In the case of AK14838, IL-12 partially suppressed tumour volume, yet it was not significantly different between the PBS mice and the IL-12-treated mice (see Figure 4.13c). Finally, AK15376 showed a modest response with a degree of resistance (see Figure 4.13d). Hence, AK15376 was not only similar to 7947 in terms of morphology and sensitivity to MRTX1133 *in vitro*, it also responded similarly to IL-12 *in vivo*. Therefore, my hypothesis was that KRAS G12D inhibition would sensitise this model to IL-12 immunotherapy.

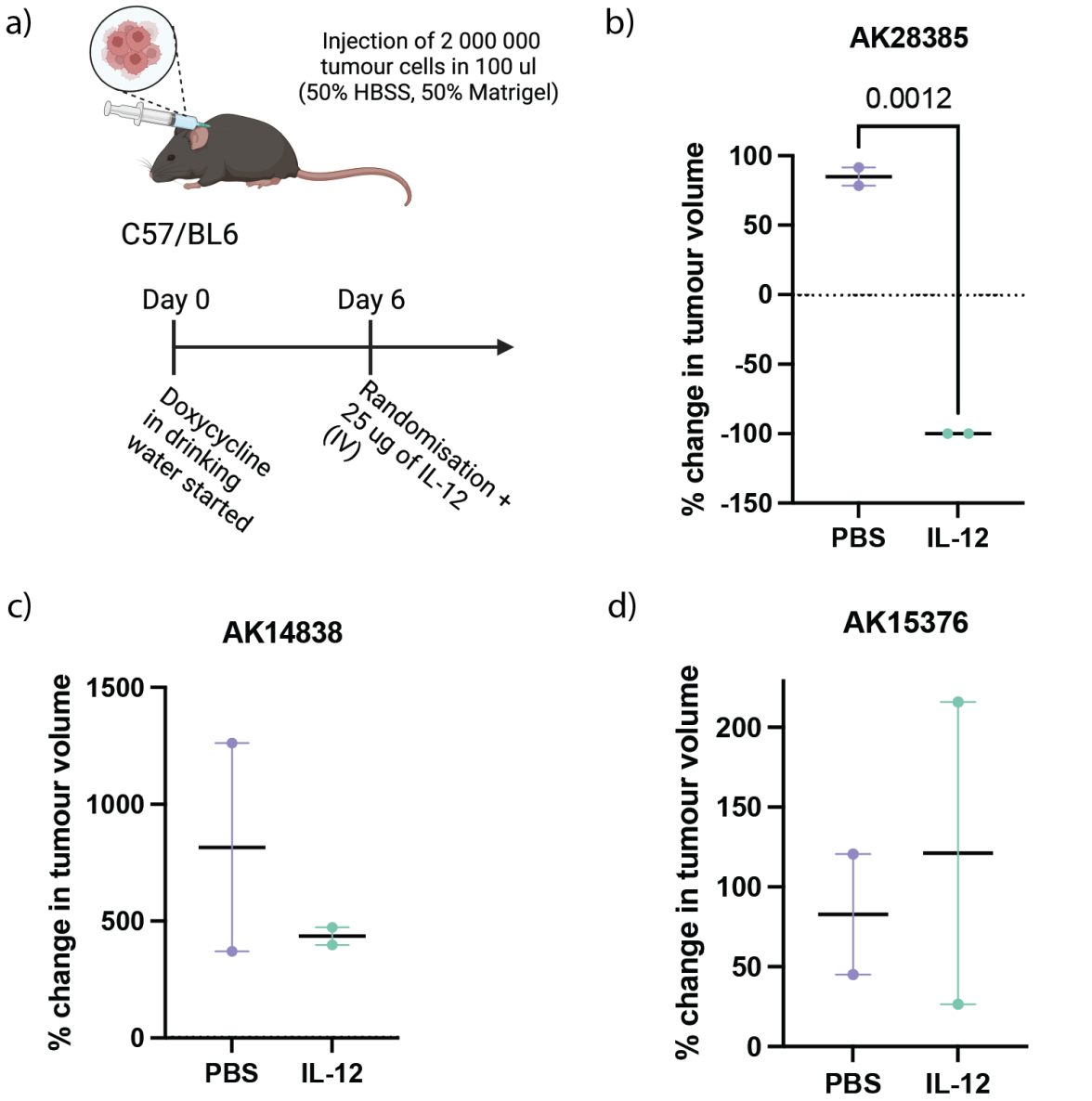


Figure 4.13 AK28385 *iKras* PDAC mouse model responds fully to IL-12 immunotherapy

a) C57/BL6 mice (n=4 per cell line, n=2 per condition) were inoculated with 2 000 000 *iKras* cancer cells subcutaneously and they were transitioned onto doxycycline drinking water (2g/L) supplemented with sucrose (30g/L). Two mice from each group were administered 25 µg of wild-type IL-12 intravenously (IV) on a single occasion. Tumour volumes were recorded throughout the study. For AK28385 and AK14838, the percentage change in tumour volume was done between days 6 (randomisation) and 20 following tumour inoculation, whilst for AK15376, it was done between days 6 (randomisation) and 15, since these mice were terminated earlier. This mouse experiment was performed only once. Statistical analyses were performed using a two-tailed student's t-test on Graphpad prism and the schematic was designed on Biorender.com.

Therefore, I tested IL-12 immunotherapy in the AK15376 mouse model with (*Kras*^{G12D} is expressed) or without (*Kras*^{G12D} is not expressed) doxycycline in their drinking water. All mice were put on doxycycline from the day of tumour inoculation to the day of randomisation and IL-12 administration. At this point, half of the mice remained on doxycycline and the other half was returned to normal drinking water (see Figure 4.14a). In the mice that remained on doxycycline (*Kras*^{G12D} is expressed), the PBS controls survived significantly less long that the IL-12-treated mice (p=0.006)(see Figure 4.14b). In the group on normal drinking water, all mice survived equally since the withdrawal of doxycycline reduced tumour burden in both the PBS and IL-12 groups (see Figure 4.14b). This explains why the survival is not significantly different between the NO DOX PBS group and the NO DOX IL-12 groups (see Figure 4.14b).

However, changes in tumour burden were clearly observed; the tumour volume of mice on doxycycline (*Kras*^{G12D} is expressed) was only slightly affected by IL-12 (see Figure 4.14c), as I previously demonstrated in Figure 4.13d. The difference in tumour volume between DOX PBS and DOX IL-12 was therefore not significant on day 13 following tumour inoculation (see Figure 4.14d,e). This suggests that in the presence of *Kras*^{G12D}, IL-12 in the AK15376 model is not capable of fully curing the tumours. For the mice returned to normal drinking water (*Kras*^{G12D} is not expressed), on day 13 there was a borderline significant difference between IL-12-treated mice and PBS controls (p=0.0611)(see Figure 4.14f). By day 15, this change had become significant (p=0.0106)(see Figure 4.14g). This suggests that the removal of doxycycline (*Kras*^{G12D} is not expressed) in combination with IL-12 immunotherapy causes the AK15376 tumours to rapidly disappear. Therefore, *Kras*^{G12D} may be partially responsible for resistance to IL-12 therapy in this mouse model.

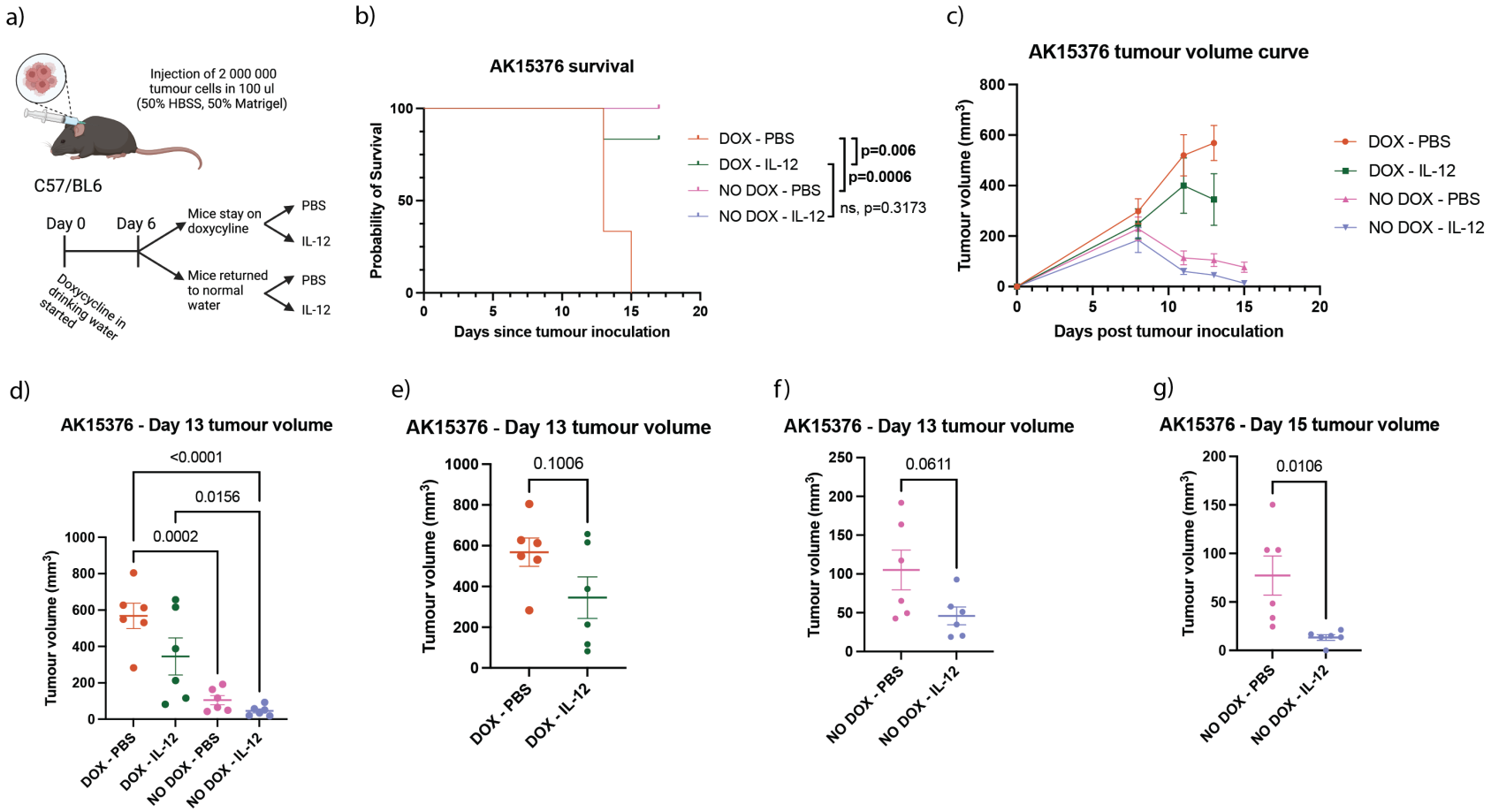


Figure 4.14 *Kras*^{G12D} withdrawal sensitises AK15376 PDAC mouse model to IL-12 therapy

6-7-week-old C57/BL6 mice (n=6) were started on doxycycline drinking water (2 g/L) and were injected subcutaneously with 2 000 000 cells. These mice then received 25 µg of wild-type IL-12 on day 6 following tumour inoculation as shown in the schematic in a). The b) survival curve and c) tumour volume curves of this study are presented. A comparison between the PBS and IL-12 groups in the presence e) or absence f) of doxycycline in the drinking water on day 13 is shown. A consecutive day 15 comparison for the mice on normal drinking water is shown in g). This mouse experiment was performed only once. Statistical analyses were performed using a one-way ANOVA or two-tailed student's t-test on Graphpad prism and the schematic was designed on Biorender.com.

4.3 Discussion

Immunotherapy has yielded limited success in PDAC and understanding the mechanisms behind this resistance will allow us to overcome it. The *Kras*^{G12D} mutation has been shown to play a key role in evading the immune system and therefore the effects of immunotherapy. Here, I have attempted to establish the role of the *Kras*^{G12D} mutation in responsiveness to IL-12 immunotherapy in two different PDAC mouse models that respond differently to IL-12. I found the 7947 mouse models (least responsive to IL-12) to express KRAS G12D more than the 3275 mouse model (most responsive to IL-12). In cell lines, I observed the exact opposite, highlighting the role of the TME in triggering an increase in KRAS G12D expression in the 7947 mouse model. Despite these expression differences, the sensitivity of the cell lines to KRAS G12D inhibition using MRTX1133 did not differ *in vitro*. However, in the presence of immune cells and IL-12 as part of a co-culture study, 7947-luc cells became more sensitive to MRTX1133, whilst 3275 did not. Using *iKras* cell lines, I demonstrated that the mesenchymal model (AK15376) resembling 7947 also only partially responded to IL-12 therapy in the presence of doxycycline, yielding no significant difference in tumour burden between PBS and IL-12 groups. However, when *Kras*^{G12D} was not expressed (no doxycycline), the tumour burden was significantly reduced with IL-12 therapy compared to the PBS group. Therefore, *Kras*^{G12D} may be driving unresponsiveness to IL-12 in this mouse model.

Data from genetically engineered mouse models (212), *iKras* models (214), as well as from MRTX1133 in mouse models (213) have demonstrated that PDAC tumour regression can be achieved by inactivation of KRAS. Using different techniques, Kemp et al., Ischenko et al., and Mahadevan et al. all highlighted the link between the *Kras*^{G12D} mutation and the immune landscapes of their PDAC mouse models (212-214). Data from all three of these studies suggest that a bidirectional relationship exists. On one hand, knocking out (KO) *Kras*^{G12D} in a mutant cancer cell line generated a slower growing tumour with a completely different immune composition, CAF profile and collagen content compared to its intact counterpart (212). This was because *Kras*^{G12D} KO tumours were less aggressive and were unable to evade the immune system resulting in anti-tumour immune responses (212). These immune responses contained tumour growth in immunocompetent mice (212). Conversely, depleting either $CD4^+$ T-

cells or $CD8^+$ T-cells obliterated this anti-tumour protection and restored the tumorigenic potential of the $Kras^{G12D}$ KO tumours (212).

Mahadevan et al. found, using the doxycycline-inducible *iKras* system, that PDAC tumours initiated upon doxycycline administration ($Kras^{G12D}$ is expressed) and that they retracted when doxycycline was removed ($Kras^{G12D}$ is not expressed) (214). They revealed $Kras^{G12D}$ elimination by doxycycline withdrawal to trigger T-cell infiltration (both $CD4^+$ and $CD8^+$) and a reduction in $CD11b^+$ myeloid cells, including granulocytic and monocytic MDSCs (214). The infiltrating $CD4^+$ T-cells largely included Tregs, Th2 and Th17 cells whilst the $CD8^+$ T-cells were mainly $Tbet^+$ (214). Expression of *Ifng* was raised across the T-cell subsets. Interestingly, intratumoural $CD86^+$ and $CD40^+$ dendritic cells and macrophages, who both act as antigen presenting cells, increased following $Kras^{G12D}$ elimination. Their MHC class II signalling was increased, whilst PD-L1 expression on the myeloid cells was reduced (214).

Using scRNA-seq, Mahadevan et al. demonstrated $Kras^{G12D}$ inhibition to lead to a reactivation of FAS-mediated cancer cell apoptosis (214). Under normal circumstances, FAS on cancer cells binds to FAS ligand on a variety of immune cells to induce apoptotic pathways in cancer cells (214). To circumvent this, $Kras^{G12D}$ normally methylates the promoter region of the FAS receptor on cancer cells, a form of epigenetic control which allows cancer cells to escape from this pathway. However, FAS expression on PDAC cells increased following $Kras^{G12D}$ elimination in a time-dependent manner and it remained raised even at 4 weeks following elimination (214). Therefore, $Kras^{G12D}$ elimination seems to restore the FAS apoptotic pathway. They also used one of the *iKras* cell lines I used in this chapter (AK14838) and found *Fas* transcripts to be low in the presence of doxycycline ($Kras^{G12D}$ is expressed) and to gradually increase upon its withdrawal ($Kras^{G12D}$ is not expressed) (214). They also used another *iKras* cell line (AK14837) where they suppressed *Fas* expression using a short hairpin RNA (ShRNA) called ShFas and its scrambled control (ShScr). When injected orthotopically into the pancreas of mice on doxycycline ($Kras^{G12D}$ is expressed), the *Fas* expression was low due to the methylating effects of $Kras^{G12D}$. Therefore, there was no survival difference between the parental, ShFas and ShScr-bearing mice (214). However, in the absence of doxycycline ($Kras^{G12D}$ is not expressed), the mice bearing parental and ShScr

tumours showed complete tumour regression, most likely due to the reactivation of FAS-mediated apoptosis. In contrast, those with ShFas progressed as usual (214).

They consequently verified whether this restoration of FAS-mediated apoptosis following *Kras*^{G12D} inhibition relies on CD4$^+$ T-cells or CD8$^+$ T-cells (214). The depletion of CD8$^+$ T-cells, but not CD4$^+$ T-cells, reversed the tumour regression that results from *Kras*^{G12D} inhibition and consequently increased FAS-mediated apoptosis (214). This suggests CD8$^+$ T-cells are a crucial mediator of the reduction in tumour burden. Since FAS ligand expression on immune cells is essential for FAS pathway activation, it is not surprising that they found it to be most abundant on CD8$^+$ T-cells, whilst to a much lesser extent on CD4$^+$ T-cells (214). Hence, the CD8$^+$ T-cells and their role in the FAS pathway may be the crucial link between *Kras*^{G12D} and the immune evasion that renders PDAC unresponsive to immunotherapy.

Another study found that the adoptive transfer of tumour-targeted engineered IL-12 expressing CD8$^+$ T-cells trigger an increase in FAS expression on MDSCs, dendritic cells and macrophages (449). This increase is not observed in mice that lack the IL-12 receptor. In return, the IL-12 induced FAS binding to FAS ligand on the transferred CD8$^+$ T-cells maintains the transferred CD8$^+$ T-cell population (449). In mice that lack FAS expression, these T-cells do not engraft properly (449). This co-stimulatory event is referred to as reverse signalling and the authors suggest this is a mechanism that results in the production of effector memory CD8$^+$ T-cells (449). Since both IL-12 and KRAS G12D inhibition seem to result in an upregulation of FAS as well as CD8$^+$ T-cell proliferation, they may have synergistically induced 7947-luc apoptosis in the co-culture studies. This is also in line with the slight increase in the proportion of CD8$^+$ T-cells within the splenocytes following co-culture with 7947-luc. However, further experiments are required to confirm these findings.

Although Ischenko et al. (212) and Mahadevan et al. (214) both found *Kras*^{G12D} elimination to induce the CD4$^+$ and CD8$^+$ T-cell infiltration that contributed to the suppression in tumour burden, Kemp et al. (213) found MRTX1133 to operate without relying on immune cells. Despite observing a similar immune cell infiltration upon MRTX1133 therapy, the reduction in tumour burden obtained through MRTX1133 was not affected by CD4$^+$ or CD8$^+$ T-cell depletion (213). However, when halting the course

of MRTX1133, T-cells were crucial in maintaining the effect of MRTX1133; their depletion caused mice to relapse rapidly whilst others with intact T-cell populations remained protected. Interestingly, in contrast with Ischenko et al. (212) where the *Kras*^{G12D} KO did not affect downstream phospho-ERK1/2 expression, MRTX1133 treatment caused a dose-dependent reduction in phosphor-ERK1/2 both *in vitro* and *in vivo* (213). Therefore, subtle differences exist between the two techniques of *Kras*^{G12D} elimination that may influence the role of the immune infiltration in suppressing tumour burden.

The relationship between *Kras*^{G12D} and PDAC regression that these studies have demonstrated closely align with the oncogene addiction theory. This theory states that certain cancer cells rely on a single oncogenic mutation to maintain their invasiveness and tumorigenic potential (450). In line with this, withdrawal of this oncogenic mutation should lead to cancer cell death and disappearance of the tumour. Hence, discoveries of small molecule inhibitors that counteract oncogenic mutation should result in complete tumour regressions. Although this concept is accurate to an extent, it may be overly simplistic due to a variety of reasons. PDAC tumorigenesis and progression is supported by and associated with multiple mutations, one of the hallmarks of cancer. These mutations, of which *Kras*^{G12D} is an example, occur sporadically and lead to consecutive disruptions in signalling pathways that sustain and drive tumorigenesis. This genetic instability is partially responsible for the extensive intratumoural and intertumoural heterogeneity within PDACs, which is for example reflected in the immunologically unique mouse models used in this chapter. Since these oncogenic mutations may not take place uniformly throughout the tumour, some areas will be genetically, metabolically, and immunologically distinct from others. In addition, some PDAC TMEs are highly dynamic and evolving systems that adapt to stimuli or stressors. I for example observed in my studies that KRAS G12D protein expression is much higher in 7947 tumours than the 7947 cell line. This suggests that the TME and its immune cells puts pressure on cancer cells resulting in increased KRAS G12D protein expression to evade immune cells. This suggests that inhibiting a singular oncoprotein in isolation in PDAC may most likely not be sufficient to provide patients with a long-term benefit.

To tackle this problem within PDAC, many have resorted to combination immunotherapy with the aim of targeting multiple immune evasive mechanisms simultaneously. Ischenko et all also used an *iKras* model treated with anti-PD-1 and anti-CTLA-4 to observe whether KRAS inhibition sensitises PDACs to CPI therapy (212). They found tumours to regress completely in the absence of doxycycline (*Kras*^{G12D} is not expressed) compared to in its presence. This suggests that by eliminating the *Kras*^{G12D}-mediated immune invasion, PDACs can be sensitised to immunotherapy. However, little evidence currently exists for other forms of immunotherapy in combination with *Kras*^{G12D} inhibition in PDAC, making the experiments in this chapter completely novel. Despite having demonstrated some concepts in my experiments, more extensive studies to optimise M-CBD-IL12 dose or linker variations that better suit the PDAC TME are required for translational purposes.

Chapter 5. Bioengineered murine IFNγ for tolerable PDAC immunotherapy

5.1 Introduction

Interferons are widely used for the treatment of a plethora of conditions; pegylated interferon IFNα for the treatment of hepatitis C (451) and for lymphomas (452), and β IFNs for multiple sclerosis (453). The three types of IFNs each have their unique sources, receptors, and modes of action; type I IFNs comprise of IFNα and β and are rapidly produced during the innate immune response by either virus-infected cells or plasmacytoid dendritic cells (12). They serve to induce an antimicrobial state and promote antigen presentation and adaptive immune response formation. Type II IFNs consist of IFNγ, produced by active T-cells, B-cells and NK cells (see Figure 1.4) (12). IFNλ is the single member of the type III IFNs and mainly signals at epithelial surfaces, rather than immune cells (12). Interferons signal through the JAK-STAT pathways that ultimately induce MHC, protein kinase R and other immunomodulators that aid the mounting of an adaptive immune response (12). The IFNs were originally named after their ability to interfere with viruses after Wheelock discovered in 1965 that IFNγ can suppress viral replication (454). Thirty years following this discovery, IFNγ emerged as a major regulator of cancer immune surveillance (455) and an immunomodulator that is a 100-10000-fold stronger than other IFNs (456). This was discovered when Meth A fibrosarcoma cells with defective IFNγ receptors (less sensitive to endogenous IFNγ) were more tumorigenic when implanted in mice than those sensitive to endogenous IFNγ (455). This and many other studies that followed (402, 457, 458) highlighted the modulatory impact of IFNγ on tumour progression.

IFNγ signalling triggers the expression of IFNγ-regulated genes with a variety of effects such as apoptosis, cell cycle regulation and immunomodulation. It is particularly well-known for its ability to upregulate MHC expression (459, 460), one of its earliest described effects. It was found to upregulate MHC class I and transporter associated with antigen processing (TAP) expression on PDAC cells *in vitro* (461). Since many tumours are known to downregulate MHC to remain invisible to $CD8^+$ T-cells (462), the ability of IFNγ to upregulate MHC is essential. Besides manipulating MHC class I

expression, it also governs cytotoxicity by inducing T-cell differentiation into cytotoxic $CD8^+$ T-cells (12, 463).

IFNγ also functions as part of a positive feedback loop; it is a product of a Th1 response, it directs Th1 effector mechanisms, maintains this Th1 lineage and prevents differentiation into Th2 cells (403). Apart from affecting the immune landscape, it also directly suppresses cancer cell proliferation through STAT1 which induces the cyclin-dependent kinase inhibitor p21 (464). IFNγ can also induce cancer cell apoptosis by upregulating caspase (465, 466) and FAS (ligand) (467) expression, as well as necroptosis through RIP1 (468). Finally, it suppresses angiogenesis by reducing the longevity of endothelial cells and it triggers ischaemia inside the tumour core (469-471), both of which have been shown to lead to enhanced tumour rejection (472). IFNγ has been tested in multiple clinical trials on glioblastomas, breast cancers, and ovarian cancers (NCT02550678, NCT03112590, NCT02948426, NCT02197169).

However, overall, IFNγ has not successfully been introduced into the clinic as a form of cancer immunotherapy. Unfortunately, the toxicity and off target effects of IFNγ mean that doses are often too low to obtain sufficient intratumoural IFNγ levels (473). IFNγ is unable to penetrate the dense stroma of solid tumours following intravenous administration (473). This means it either is rapidly cleared from the bloodstream with a half-life of only 25 to 35 minutes or it diffuses into healthy tissues where it triggers auto-immune-like effects (473). Such effects can include fever, fatigue and nausea (473). Therefore, in this chapter, I produced CBD-IFNγ, a bioengineered version of IFNγ. The CBD is the same as in M-CBD-IL12 as discussed in Chapters 3 and 4. It serves to prolong the half-life of IFNγ by increasing its molecular weight and causes it to accumulate in collagenous tumour stroma. I hypothesised that despite their closely linked signalling pathways, IFNγ may be more powerful than IL-12 as an immunostimulatory agent due to its ability to cause cancer cell apoptosis, whilst also triggering immune activation by for example enhancing antigen presentation. In contrast, IL-12 signalling is largely limited to T-cells and NK cells (as previously shown in Figure 1.4).

In this chapter, I tested the anti-tumour effects of CBD-IFNγ in a CRC and PDAC model. As monotherapy, CBD-IFNγ induced a significant prolongation of survival in CRC-

bearing mice, yet eventually the mice became resistant. This CRC model is known to respond well to IL-12 therapy, which I demonstrated in Chapter 3 Figure 3.8. I therefore decided to test CBD-IFNγ in this model as a pilot study to compare its biological activity to my IL-12-based molecules. Due to the observed resistance in the CRC model, I decided to combine CBD-IFNγ with anti-PD-1 therapy in the PDAC mouse study. Some studies have demonstrated that anti-PD-1 efficacy is dependent on the presence of tumour-infiltrating dendritic cells and IFNγ (474). The authors state that the IFNγ is produced by T-cells in response to anti-PD1 and acts on dendritic cells (474). In response to IFNγ, these dendritic cells can produce IL-12 which in itself triggers T-cell activity (474). This forms a positive feedback loop. I hypothesised that exogenous IFNγ could activate this feedback loop and augment the sensitivity of these PDAC tumours to anti-PD-1 therapy. I observed a slight modulation in the immune composition of PDAC tumours with CBD-IFNγ+anti-PD-1 therapy. However, resistance mechanisms such as overexpression of PD-L1 in the tumour stroma most likely allowed the tumours to eventually overcome the effects of IFNγ.

5.2 Results

5.2.1 Production of wild-type IFNγ and CBD-IFNγ

For the production of CBD-IFNγ, I initially trialled 293fectin as a transfection reagent (see Figure 5.1a). This yielded a 40 mAU UV absorbance peak on the immobilised metal affinity chromatogram (Figure 5.1a). I performed a murine IFNγ ELISA on this protein to confirm its identity and found the IFNγ concentration to be 1.56 µg/ml (see Figure 5.1b). This low yield led me to attempt the consecutive transfection with linear PEI (transfection grade, MW 25 000, 23966-1). From this transfection, I obtained a UV absorbance peak of 750 mAU on the metal affinity chromatography, making PEI the more suitable transfection reagent for CBD-IFNγ (see Figure 5.1c).

The size exclusion purification for this protein demonstrates a rather wide and heterogeneous split peak (see Figure 5.1d). I analysed the identity of each of its components on SDS-PAGE (see Figure 5.1e). Under both reducing and non-reducing conditions, murine wild-type IFNγ normally appears on SDS-PAGE as multiple bands between 15-25 kDa due to different glycosylation states (475). For CBD-IFNγ (38 kDa), I observed the same set of multiple bands at around 38 kDa which confirms the identity of CBD-IFNγ protein (see Figure 5.1e). However, in the later fractions of the peak, an additional set of bands was present at 75 kDa. Wild-type murine IFNγ functionally exists as a homodimer, suggesting two CBD-IFNγ molecules are expected to dimerise, yielding a molecule of around 75 kDa. Therefore, this band corresponds with a CBD-IFNγ homodimer, which is its biologically active form (see Figure 5.1e).

However, size exclusion purification usually elutes the proteins with a larger molecular weight into the earlier fractions of the peak. Since the SDS-PAGE reveals the dimer to be present exclusively in the later fractions, this suggests the dimerisation occurred following protein purification. Mouse IFNγ homodimers are formed by anti-parallel interlocking of the IFNγ monomers, which occurs through non-covalent interactions (476). The SDS and heating of the sample should normally denature the proteins and disrupt the CBD-IFNγ homodimers on SDS-PAGE. This occurs by rendering the amino acids negatively charged, which weakens the non-covalent bonds that hold the homodimer together. Despite the presence of SDS and the heating, the homodimers

remained visible on the SDS-PAGEs of all the CBD-IFNγ batches. I hypothesised this was most likely due to the nature of the sample buffer or insufficient heating of the sample leading to protein aggregation. Following the production of both CBD-IFNγ and wild-type IFNγ, I therefore ran an SDS-PAGE using a different sample buffer which contains 4% Lithium Dodecyl Sulfate (LDS) instead of the 8% SDS in the original sample buffer (see Figure 5.1f). In addition, I boiled the samples for an additional 2 minutes and stored them on ice for at least 5 minutes after boiling. This reduces their ability to re-aggregate when exposed to room temperature during gel loading. This technique significantly improved the formation of aggregates and confirmed that the observed bands at high molecular weight were the IFNγ dimers (see Figure 5.1f).

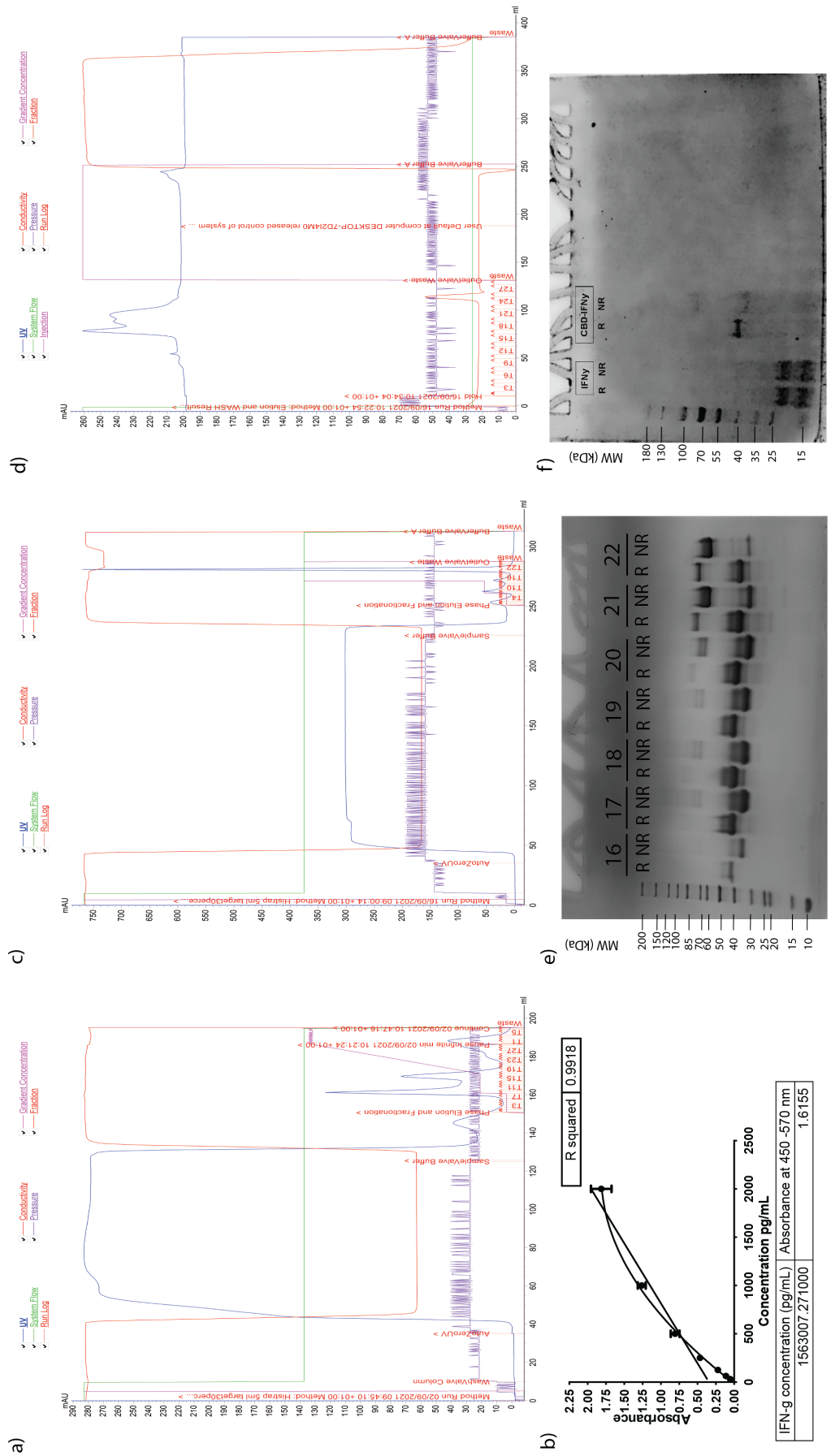


Figure 5.1 CBD-IFNγ was successfully produced using the HEK293F expression system

Batches 1and 2 of CBD-IFNγ were produced in HEK293F cells using 293fectin and PEI, respectively. The immobilised metal affinity chromatograms are displayed in a) for batch 1 and c) for batch 2. b) The peak was analysed using murine IFNγ ELISA. c) The size exclusion chromatogram of batch 2 is displayed in d). e) Fractions were then analysed on SDS-PAGE under reducing (R) and non-reducing (NR) conditions. f) 4% LDS sample buffer was used and samples were heated to 95 °C for 7 minutes.

Murine wild-type IFNγ was efficiently produced in Expi293F cells (see Figure 5.2). Similarly to CBD-IFNγ, I observed various glycosylation forms of IFNγ monomers on the SDS-PAGE, as well as the IFNγ homodimers (see Figure 5.2c,f).

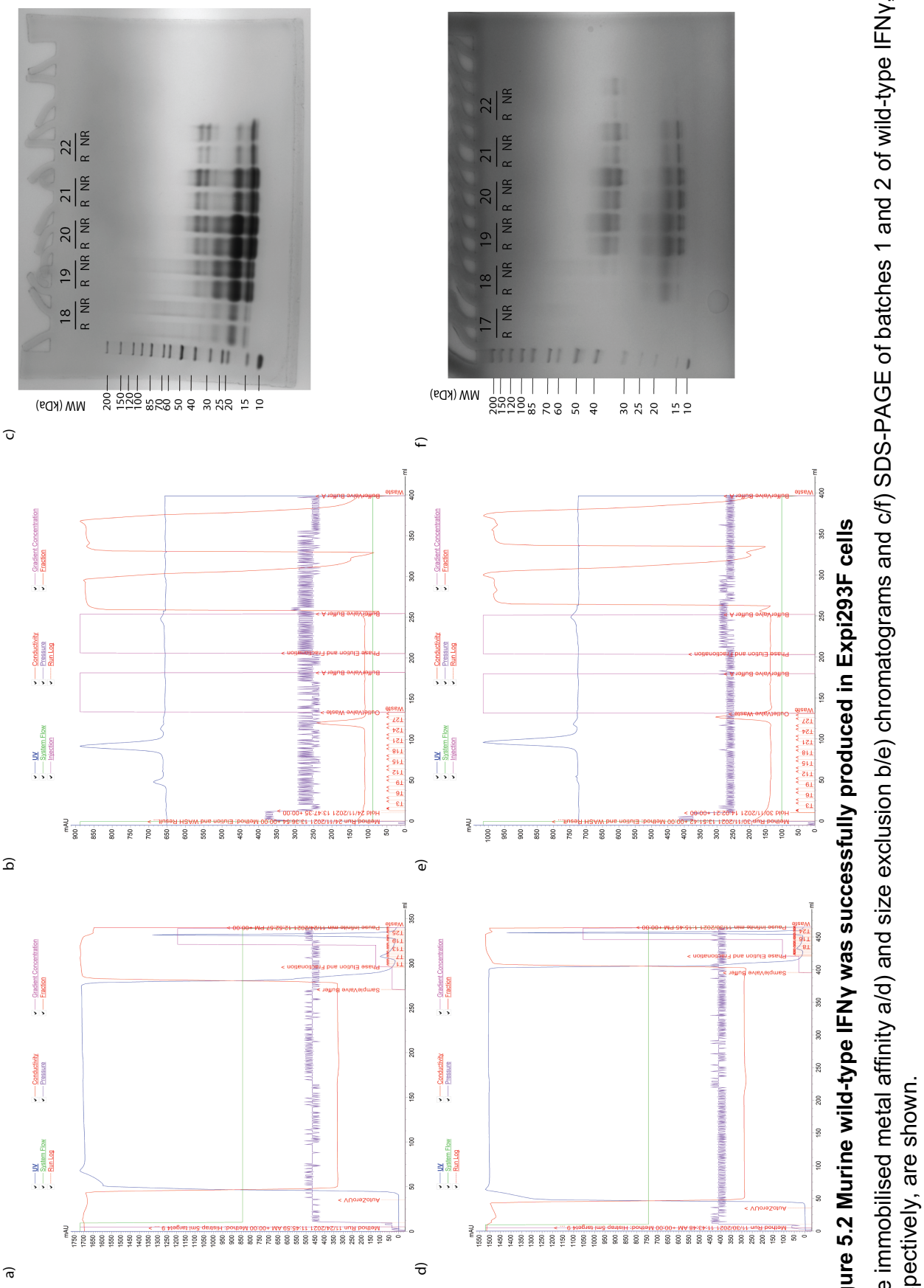


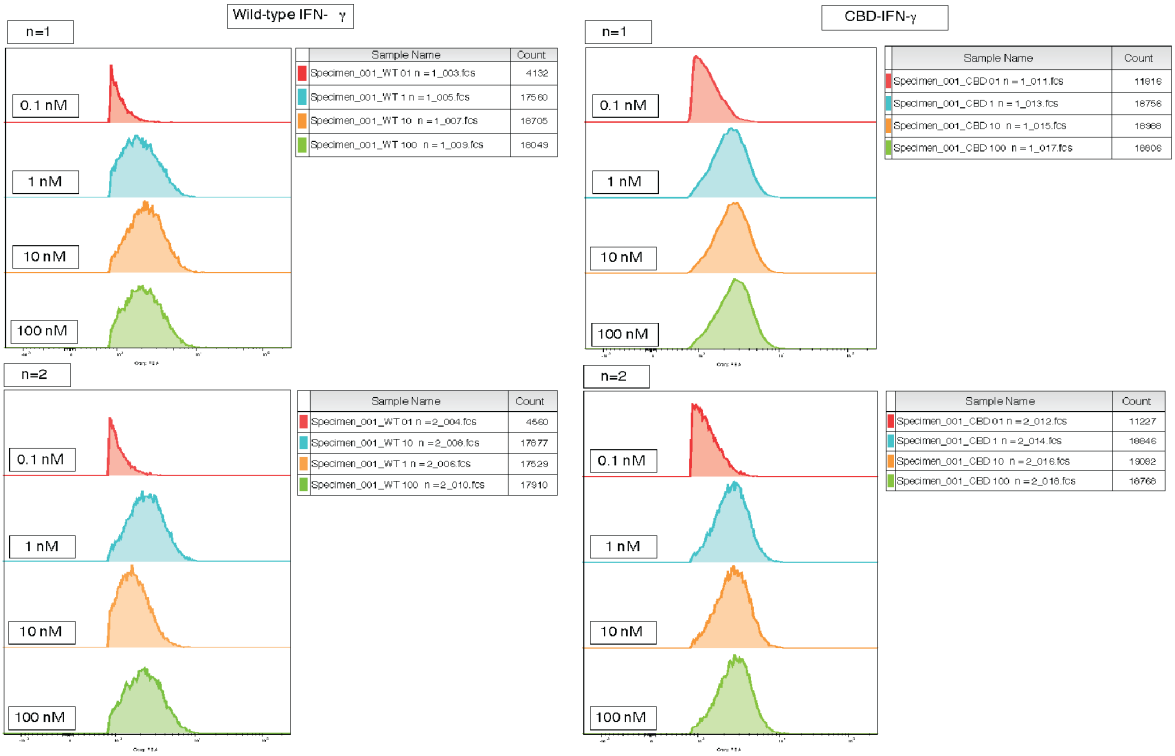
Figure 5.2 Murine wild-type IFNγ was successfully produced in Expi293F cells

The immobilised metal affinity a/d) and size exclusion b/e) chromatograms and c/f) SDS-PAGE of batches 1 and 2 of wild-type IFNγ, respectively, are shown.

5.2.2 Both wild-type IFNγ and CBD-IFNγ upregulate PD-L1 expression on cancer cells *in vitro*

IFNγ is known to upregulate PD-L1 expression on cancer cells (407). To test the biological activity of both murine wild-type IFNγ and CBD-IFNγ, and whether they differ, I treated Panc02 PDAC cancer cells with increasing concentration of either protein (see Figure 5.3). I then measured PD-L1 expression on the cancer cells through flow cytometry. In my pilot experiment to identify the correct concentration range, I observed a sharp increase between 0.1 and 1 nM with both molecules (see Figure 5.3a). At the higher concentrations, PD-L1 expression had reached a plateau, which meant the concentration range should be reduced. Therefore, I used a range of 0-10 nM and observed that both molecules trigger a gradual increase in PD-L1 expression with increasing concentrations, suggesting they have a similar biological activity towards cancer cells (see Figure 5.3b).

a)


Wild-type IFN- γ
CBD-IFN-γ
n=1
n=2
0.1 nM
1 nM
10 nM
100 nM
Sample Name
Count
Specimen_001_WT 01 n = 1_003.fcs 4132
Specimen_001_WT 1 n = 1_005.fcs 17560
Specimen_001_WT 10 n = 1_007.fcs 16705
Specimen_001_WT 100 n = 1_009.fcs 16049
Specimen_001_CBD 01 n = 1_011.fcs 11916
Specimen_001_CBD 1 n = 1_013.fcs 18756
Specimen_001_CBD 10 n = 1_015.fcs 18988
Specimen_001_CBD 100 n = 1_017.fcs 18606
Specimen_001_WT 01 n = 2_004.fcs 4560
Specimen_001_WT 10 n = 2_006.fcs 17677
Specimen_001_WT 1 n = 2_008.fcs 17529
Specimen_001_WT 100 n = 2_010.fcs 17910
Specimen_001_CBD 01 n = 2_012.fcs 11227
Specimen_001_CBD 1 n = 2_014.fcs 18846
Specimen_001_CBD 10 n = 2_016.fcs 19082
Specimen_001_CBD 100 n = 2_018.fcs 18766

b)

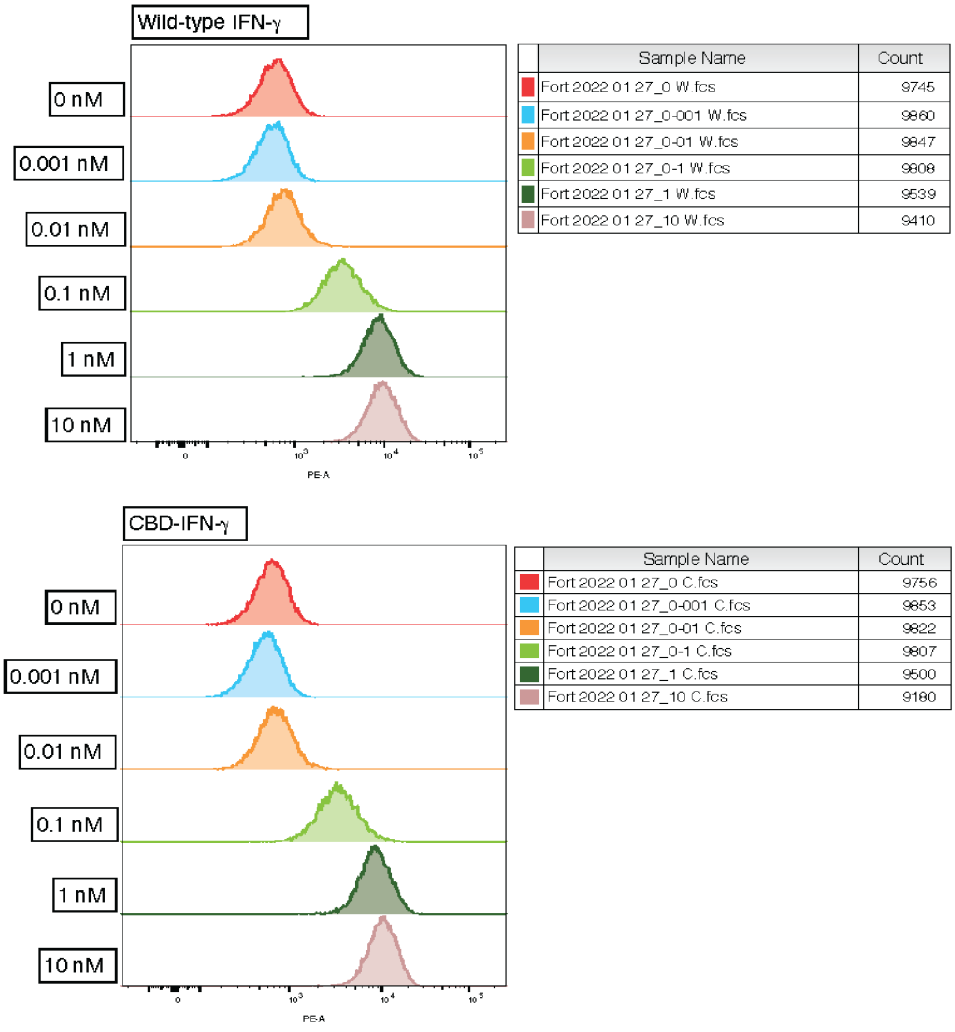

Wild-type IFN-γ
0 nM
0.001 nM
0.01 nM
0.1 nM
1 nM
10 nM
PE-A
Sample Name
Count
Fort 2022 01 27_0 W.fcs 9745
Fort 2022 01 27_0-001 W.fcs 9860
Fort 2022 01 27_0-01 W.fcs 9847
Fort 2022 01 27_0-1 W.fcs 9808
Fort 2022 01 27_1 W.fcs 9539
Fort 2022 01 27_10 W.fcs 9410
CBD-IFN-γ
Fort 2022 01 27_0 C.fcs 9756
Fort 2022 01 27_0-001 C.fcs 9853
Fort 2022 01 27_0-01 C.fcs 9822
Fort 2022 01 27_0-1 C.fcs 9807
Fort 2022 01 27_1 C.fcs 9500
Fort 2022 01 27_10 C.fcs 9180

Figure 5.3 Both murine wild-type IFNγ and CBD-IFNγ upregulate PD-L1 expression on PDAC cells

a) Pilot *in vitro* experiment to test the biological activity of wild-type IFNγ and CBD-IFNγ (0.1-100 nM) towards Panc02 PDAC cells. PD-L1 expression was quantified using flow cytometry 48 hours following treatment. b) Actual *in vitro* experiment using 0-10 nM of murine wild-type IFNγ and CBD-IFNγ on Panc02 cells. This experiment was performed twice, and data was analysed on Flowjo.

5.2.3 Wild-type IFNγ and CBD-IFNγ moderately prolong the survival of the MC38 CRC mouse model

Next, I tested this bioengineered molecule *in vivo* in a syngeneic MC38 colorectal cancer model (see Figure 5.4). As previously mentioned, IFNγ is a downstream effector molecule of IL-12. The MC38 CRC model fully responded to both wild-type IL-12 and M-CBD-IL12 therapy in a study performed by a collaborator Dr. Aslan Mansurov at the University of Chicago (see Figure 3.8f). Therefore, with the help of Dr. Charanjit Singh and Maria Nikolaidi, I used this model to initially trial CBD-IFNγ *in vivo* activity (see Figure 5.4a). Both wild-type IFNγ ($p=0.0399$) and CBD-IFNγ ($p=0.0439$) significantly prolonged survival compared to PBS controls (see Figure 5.4b). Although wild-type IFNγ-treated tumours grew slower than CBD-IFNγ, these mice were sacrificed earlier due to severe ulceration (see Figure 5.4c). On day 16 following tumour inoculation, both the wild-type IFNγ- and CBD-IFNγ-treated groups had smaller tumours compared to PBS controls, although this difference was not significant (see Figure 5.4d).

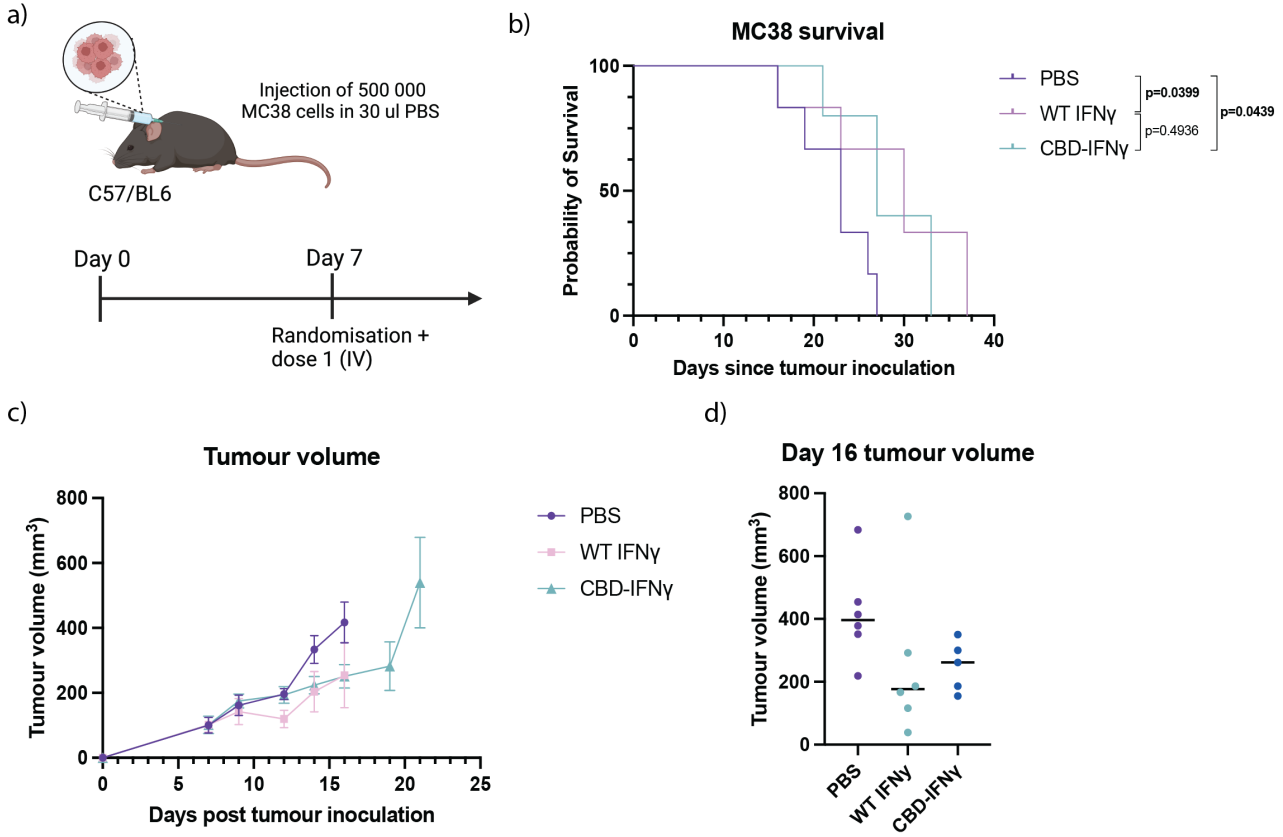


Figure 5.4 Wild-type IFNγ and CBD-IFNγ prolong survival of the MC38 CRC mouse model

C57/BL6 mice (n=6 except for CBD-IFNγ n=5) were injected with 500 000 MC38 cells in PBS subcutaneously on their back. On day 7, mice received either 25 µg of wild-type (WT) IFNγ or CBD-IFNγ intravenously (IV). The study design a), Kaplan Meier survival curve b), tumour growth curve c) are displayed. d) demonstrates differences in tumour volume between groups on day 16 following tumour inoculation. This mouse experiment was performed only once. Statistical analyses were performed with a one-way ANOVA with Tukey's multiple comparison tests or Mantel Cox test for Kaplan Meier survival curves. Schematics were designed on Biorender.com

5.2.4 CBD-IFNγ therapy remodels the TME of a syngeneic PDAC mouse model

I then proceeded to test CBD-IFNγ in the immune cold, mesenchymal orthotopic 7947 PDAC model as part of an intervention study with the kind support of Chanthirika Ragulan (see Figure 5.5a). To prevent immune evasion by the cancer cells upregulating the PD-L1/PD-1 axis in response to IFNγ, we included a combination immunotherapy group treated with CBD-IFNγ + anti-PD-1 (see Figure 5.5a). All mice were sacrificed once the first mouse reached the humane endpoint (see Figure 5.5a). I observed a slight decrease in tumour weight with the combination therapy, although a lot of variation existed, making this finding not statistically significant (see Figure 5.5b). Interestingly, mice treated with both CBD-IFNγ monotherapy and combination therapy maintained their body weight significantly better than PBS controls; on day 10 following tumour inoculation, I observed a significant difference in body weight between the CBD-IFNγ(+anti-PD-1) groups and the PBS controls (both $p<0.0001$)(see Figure 5.5c,d). This could suggest CBD-IFNγ may be reducing the cachexia that is normally observed in late-stage PDAC patients.

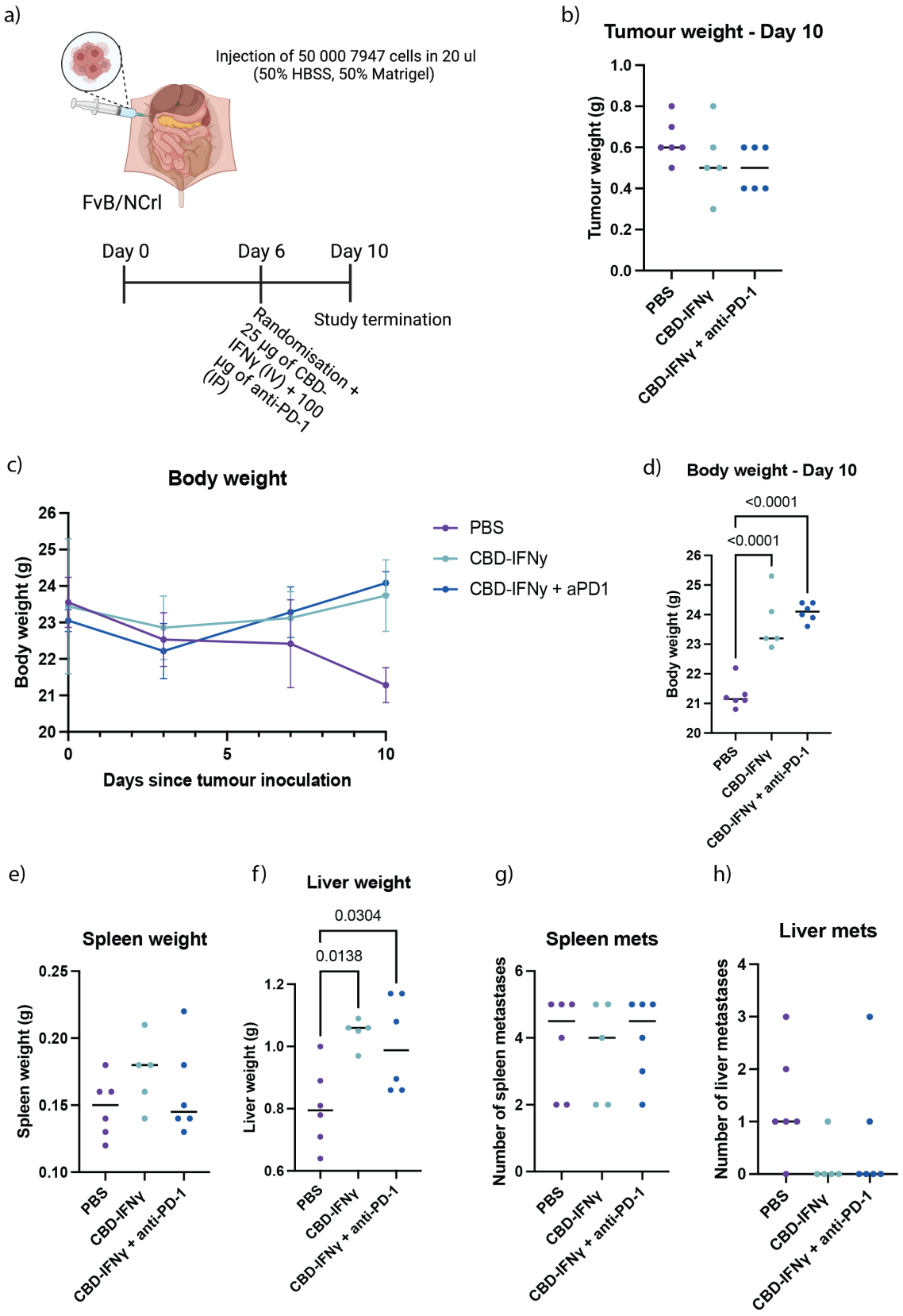


Figure 5.5 CBD-IFNγ therapy in a syngeneic metastatic PDAC mouse model

a) 6-7-week-old FVB/NCrl mice (n=6, except n=5 for CBD-IFNγ) were orthotopically injected with 50 000 PDAC cells into the pancreas through a laparotomy and mice received 25 µg of CBD-IFNγ intravenously (IV) with or without 100 µg of anti-PD-1 intraperitoneally (IP) on day 6 following tumour inoculation. All mice were culled once the first animal reached the humane endpoint. a) Study design, b) tumour weight at study termination, c) body weight curve and d) day 10 comparison, e) spleen weights and f) liver weights are displayed. Spleen g) and liver h) macrometastases were visually counted upon necropsy. This mouse experiment was performed only once. Statistical analyses were performed with a one-way ANOVA with Tukey's multiple comparison tests on GraphPad prism. Schematics were designed on Biorender.com.

Although a lot of variation was observed in the spleen weights (see Figure 5.5e), the liver weight was significantly higher in the mice treated with CBD-IFNγ (p=0.0138) and CBD-IFNγ+anti-PD-1 (p=0.0304) compared to PBS controls (see Figure 5.5f). Despite their higher liver weight, those mice had fewer liver macro-metastases than PBS controls, although this difference was not statistically significant (see Figure 5.5h). These metastases, as well as the spleen metastases, were counted visually when sacrificing the mice. CBD-IFNγ may therefore be suppressing the formation of liver metastases.

With the kind support of Chanthirika Ragulan, we analysed the tumours using flow cytometry (see Figure 5.6a-k). The overall number of immune cells was not gravely affected by either therapy (see Figure 5.6a). With the combination immunotherapy, I observed a significant increase in T-cells in the tumour compared to PBS controls (p=0.0099) (see Figure 5.6b). Within T-cells, $CD4^+$ T-cells and more specifically Tregs seem to show an increasing trend with the combination immunotherapy, albeit not significant (see Figure 5.6d,f). Due to a problem with the Foxp3 antibody in this experiment, Tregs were defined as $CD4^+$ $CD127^-$ T-cells (see Figure 5.6f). All T-cells following activation loose CD127 expression (477). Memory and effector T-cells regain CD127 expression whilst Foxp3+ Tregs remain CD127 negative, since Foxp3 interacts with the CD127 promoter whereby reducing its expression (477).

In the $CD8^+$ T-cells, CD127 expression is linked to active effector and memory T-cells. Although not significant, overall $CD8^+$ T-cells and memory $CD8^+$ T-cells show a decreasing trend with the combination immunotherapy (see Figure 5.6e,g), whilst dendritic cells are significantly reduced in this group compared to PBS (p=0.0499)(see Figure 5.6i). These findings collectively suggest there may be a degree of resistance

taking place to CBD-IFNγ therapy. This can most likely be attributed to the PD-L1 expression on both immune ($CD45^+$) ($p=0.0134$) and non-immune ($CD45^-$) ($p=0.0025$) cells being significantly increased with the combination immunotherapy compared to PBS, but not with the monotherapy (see Figure 5.6j,k). This finding was confirmed through western blotting of PD-L1 in tumour lysates; an increasing trend in PD-L1 was observed especially with combination immunotherapy, although a lot of variation was observed (see Figure 5.6l,m).This suggests anti-PD-1 therapy may cause cancer cells to compensate for the PD-1 inhibition by further upregulating PD-L1. Therefore, it may be useful to combine CBD-IFNγ therapy with both anti-PD-1 and anti-PD-L1 to counteract this in future studies.

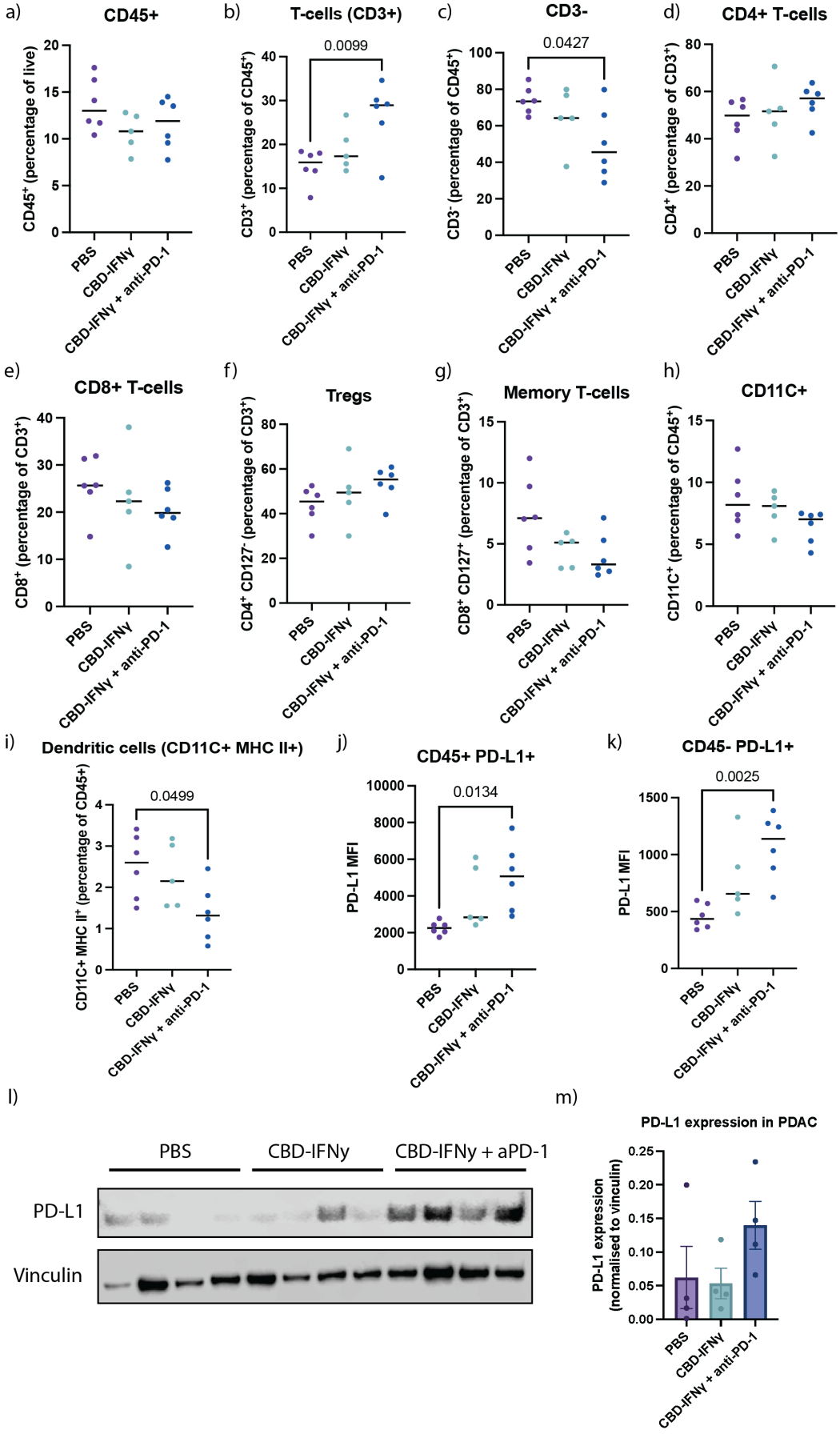

a)
CD45+
CD45+ (percentage of live)
b)
T-cells (CD3+)
0.0099
CD3+ (percentage of CD45+)
c)
CD3-
0.0427
CD3- (percentage of CD45+)
d)
CD4+ T-cells
CD4+ (percentage of CD3+)
e)
CD8+ T-cells
CD8+ (percentage of CD3+)
f)
Tregs
CD4+ CD127- (percentage of CD3+)
g)
Memory T-cells
CD8+ CD127+ (percentage of CD3+)
h)
CD11C+
CD11C+ (percentage of CD45+)
i)
Dendritic cells (CD11C+ MHC II+)
0.0499
CD11C+ MHC II+ (percentage of CD45+)
j)
CD45+ PD-L1+
0.0134
PD-L1 MFI
k)
CD45- PD-L1+
0.0025
PD-L1 MFI
PBS
CBD-IFNγ
CBD-IFNγ + anti-PD-1
l)
PBS
CBD-IFNγ
CBD-IFNγ + aPD-1
PD-L1
Vinculin
m)
PD-L1 expression in PDAC
PD-L1 expression (normalised to vinculin)

Figure 5.6 The combination of CBD-IFNγ + anti-PD-1 increases intratumoural T-cells and reduces dendritic cells in the 7947 PDAC mouse model

a) 6-7-week-old FVB/NCrl mice (n=6, except n=5 for CBD-IFNγ) were orthotopically injected with 50 000 PDAC cells into the pancreas through a laparotomy and mice received 25 µg of CBD-IFNγ intravenously (IV) with or without 100 µg of anti-PD-1 intraperitoneally (IP) on day 6 following tumour inoculation. All mice were culled once the first animal reached the humane endpoint. The tumours were processed and stained for flow cytometric analysis a-k) or snap frozen for protein analysis l-m). 10 µg of protein was then used for a PD-L1 western blot. Signals from four tumours per group were quantified and normalised to the loading control. This western blot was performed only once. Statistical analyses were performed with a one-way ANOVA with Tukey's multiple comparison tests on GraphPad prism.

5.3 Discussion

IFNγ is a potent inflammatory cytokine with pleiotropic effects. It has been heavily studied in multiple cancer types with varying results. A major limitation of this interferon is that it triggers severe toxicity. In this chapter, I have bioengineered IFNγ by conjugating it to CBD to improve its pharmacokinetics and prolong its tumour retention. I produced this molecule, as well as wild-type IFNγ using the HEK293F and Expi293 expression systems. I tested CBD-IFNγ in PDAC and CRC mouse model. In both models, the molecule seems to affect the TME but its ability to reduce tumour burden and prolonging survival were limited.

I initially trialled the efficacy of wild-type IFNγ and CBD-IFNγ in the MC38 model. Since others have found IFNγ to be incapable of inducing MC38 cell apoptosis *in vitro* (478), I hypothesised IFNγ would exert its effect by influencing the immune landscape of the tumour rather than directly inducing cancer cell apoptosis. Although both wild-type IFNγ and CBD-IFNγ significantly prolonged survival, no complete responses were observed, and mice eventually became resistant. In this same model, a colleague of mine Dr. Aslan Mansurov at the university of Chicago demonstrated wild-type IL-12 and M-CBD-IL12 to induce complete responses in all mice (see Figure 3.8f). This suggests the MC38 model is more responsive to IL-12 than IFNγ, despite their closely linked signalling pathways.

Similarly to what was demonstrated in this study, others have observed limited efficacy of IFNγ in different tumour types, outside of its pharmacokinetic challenges and limited

tumour penetration. This can be a result of multiple factors and remains a controversial topic to this day. IFNγ also plays a role in maintaining homeostasis and preventing tissue damage. For example, some studies have shown IFNγ to reduce the mortality of mice with autoimmune diseases such as autoimmune encephalomyelitis, suggesting IFNγ can also have anti-inflammatory effects (479). Secondly, early studies discovering the anti-tumour effects of IFNγ also highlighted that in certain human tumours, mutations in IFNγ signalling proteins have been found, which can be a source of unresponsiveness to IFNγ (402). Thirdly, IFNγ has been shown to induce the production of MDSCs that suppress dendritic cell (480) and T-cell (481) activity, and to upregulate immune checkpoints such as the PD-1/P-L1 axis (482). I observed the latter both *in vitro* using flow cytometry and in my *in vivo* PDAC study flow cytometry results.

Interestingly, others have found the combination of intratumoural IFNγ and intra-peritoneal anti-PD-L1 in the MC38 model to significantly prolong survival and suppress tumour burden (483). In contrast, IFNγ monotherapy performed significantly worse than PBS controls in MC38 in their study. In contrast, in my MC38 *in vivo* study both wild-type IFNγ and CBD-IFNγ prolonged the survival significantly of mice bearing MC38 tumours. However, some resistance still took place.

Since intratumoural injection is challenging to perform for CRC, a tumour-targeted form of IFNγ that allows for intravenous injection in combination with anti-PD-L1 may be efficacious in this mouse model. Dougan and colleagues combined tumour-targeted delivery of IFNγ through conjugation to CPIs to address the PD-L1 resistance mechanism (21). They conjugated a Variable Heavy domain of Heavy Chain (VHH) against PD-L1 to IFNγ (21). In CT26 as monotherapy, and in B16 in combination with the TA99 antibody, the conjugate significantly prolonged survival (21). KPC organoids, orthotopically implanted and treated with the VHH-IFNγ, were significantly smaller than controls (21). These mice also survived significantly longer, and the treated tumours harboured significantly fewer myeloid cells and significantly more $CD4^+$ and $CD8^+$ T-cells (21). In contrast, CBD-IFNγ in my trials did not suppress tumour burden to the same extent in any tumour model, even when combined with anti-PD-1 therapy. This could be attributed to multiple factors; the first one being the inhibitory effect of the VHH towards PD-L1, which would prevent interaction with PD-1 and thereby inhibit this axis. However, it is important to highlight the potential off-target effects of this PD-L1-

targeting VHH due to the widespread expression of PD-L1. This may therefore result in toxicity. Use of a VHH with affinity to a tumour-specific antigen would improve this problem. Instead of anti-PD-L1, I combined CBD-IFNγ therapy with anti-PD-1 in my PDAC mouse study since evidence suggests PDACs may rely on PD-1 expression more than PD-L1 for their tumorigenic potential (461). However, in my PDAC study, inhibition of PD-1 along with CBD-IFNγ therapy does not seem to have the same desired effect as the PD-L1-targeting VHH. This is most likely related to the immunological nature of the PDAC model. As described in the introduction of this chapter, anti-PD-1 efficacy relies on the presence of T-cells and dendritic cells in the tumour stroma. The PDAC model I chose to treat is mesenchymal and immunologically 'cold' meaning it harbours few T-cells and antigen presenting cells for the anti-PD-1 to act on. In contrast, PD-L1 is more widely expressed on cancer cells and myeloid cells (407) and therefore its efficacy does not depend on the presence of T-cells in the tumour stroma. I predicted IFNγ to have a chemotactic effect on T-cells, similarly to IL-12, which could sensitise these tumours to anti-PD-1. Nevertheless, anti-PD-L1 therapy in combination with IFNγ may be a more suitable alternative for immunologically cold PDAC models.

Overall, I produced a novel bioengineered IFNγ immunotherapy and tested its efficacy *in vitro* and *in vivo*. *In vitro*, the molecule performed similarly to its wild-type counterpart. *In vivo*, as monotherapy CBD-IFNγ did not perform as well as M-CBD-IL12 in the MC38, suggesting despite their linked signalling pathways, they still operate differently within the same mouse models. In the PDAC mouse models, CBD-IFNγ in combination with CPIs somewhat remodelled the TME, yet only modestly suppressed tumour burden and prolonged survival.

Chapter 6. Discussion and future directions

The therapeutic options for challenging-to-treat cancer types are usually limited because of their complex TME. Exogenous cytokines can remodel tumours either as monotherapy or in synergy with other immunotherapy such as CPIs. They have however been largely disregarded in the clinic due to their toxicity. In this PhD, I bioengineered two pro-inflammatory cytokines to increase their safety and enhance their efficacy: IL-12 and IFNγ. I used a combination of collagen anchoring and masking to achieve this. I tested the molecules in immunologically distinct mouse models of TNBC and PDAC; orthotopic EMT6 tumours respond well to M-CBD-IL12 (4 out 6 complete responses), and even better to wild-type IL-12 (7 out of 7 complete responses). Both molecules significantly prolonged survival, prevented relapse and completely remodelled the TME, yet M-CBD-IL12 did so with considerably less toxicity. The 4T1 model responded less well to both wild-type IL-12 and M-CBD-IL12, potentially due to a combination of its significantly higher TGFβ levels and low collagen content in comparison with EMT6. In both the PDAC mouse models, response to M-CBD-IL12 was modest. However, orthotopic 3275 tumours shrank significantly with wild-type IL-12 therapy. The same cannot be said for 7947, suggesting this model exhibits evasive characteristics towards IL-12. I found 7947 tumours, but not cells, to express significantly higher KRAS G12D protein than 3275, which is known to promote immune evasion and lead to unresponsiveness to immunotherapy. Using a co-culture system, I demonstrated that the combination of MRTX1133 therapy (KRAS G12D small molecule inhibitor) and IL-12 to lead to reduced cancer cell viability in the presence of splenocytes. The efficacy of IL-12 therapy in the AK15376 *iKras* mouse model was enhanced by the elimination $Kras^{G12D}$ through the withdrawal of doxycycline. Finally, CBD-IFNγ as monotherapy or combination (anti-PD-1) therapy also remodelled the TME of 7947 tumours yet did not suppress tumour burden either.

6.1 The fine balance between IL-12 and IFNγ efficacy and toxicity

Recombinant human IL-12 was heavily studied as cancer therapy around two decades ago (484-487). In a phase I study on multiple advanced cancers in 1997, intravenous recombinant human IL-12 however triggered a wide range of adverse events including

nausea, chills, fever, neutropenia, and hyperbilirubinemia (487). They identified the maximum tolerated dose to be 500 ng/kg (487). However, at this dose, three patients still had deranged liver tests and another patient passed away due to *Clostridia perfringens* septicaemia, potentially unrelated to the IL-12 (487). The other patients tolerated 500 ng/kg well (487). In a phase II trial, this same dose of IL-12 was toxic in 12 out of 17 patients and unfortunately two participants passed away (485). This led to the FDA temporarily halting all IL-12 clinical trials (485). Later on, these were fortunately resumed but the IL-12 toxicity remains a challenge to this day (485). It is however important to highlight that within toxicity, objective measurements exists (such as deranged liver tests and neutropenia) whilst others are reported by patients (malaise, sweating) and can be considered subjective. Manipulating the route of administration of IL-12 to suppress toxicity unfortunately also reduced efficacy; in a phase II trial on IL-12 therapy in non-Hodgkin's lymphoma, 40% of patients treated intravenously had either partial or complete responses whilst in patients treated subcutaneously, this was only 7% (488). This suggests that reducing toxicity by altering the route of administration is not an option for IL-12.

IFNγ was found to be a major culprit of IL-12 toxicity; even at low doses of IL-12, IFNγ expression in blood is raised (486). Interestingly, after repeated IL-12 injections, IFNγ production gradually declines (486, 489). I was able to confirm this in my toxicity studies on both FvB/NCrl and BALB/c non-tumour bearing mice; plasma IFNγ dropped considerably between the first and second dose of wild-type IL-12. In contrast, M-CBD-IL12 triggered virtually undetectable levels of plasma IFNγ, highlighting the ability of the mask to suppress toxicity.

Although this reduction in IFNγ is useful in terms of toxicity, Gollob et al. demonstrated in a phase I clinical trial on intravenous IL-12 therapy for metastatic renal cell carcinoma or melanoma, that IL-12 clinical benefit depended on sustained IFNγ secretion (490). Similar findings were confirmed by Bekaii-Saab et al. (491). I demonstrated intratumoural IFNγ levels were raised in the EMT6 tumours in both wild-type IL-12 and M-CBD-IL12 groups in Chapter 3. Interestingly, the M-CBD-IL12-treated mice remained protected for 248 days following tumour inoculation. A population of memory T-cells was most likely formed that protected the mice long-term even after IFNγ was cleared from the tumour. However, due to the treated tumours disappearing rapidly following

therapy, I was not able to confirm whether this IFNγ response was maintained intratumourally. Plasma IFNγ increased cumulatively with multiple doses of wild-type IL-12 and to a lesser extent with M-CBD-IL12 too. Therefore, in contrast with the findings from the aforementioned clinical trials, I did not find plasma IFNγ nor the clinical benefit to reduce following multiple doses of IL-12 in the EMT6 model. However, murine biology often does not translate into clinical trials and vice versa.

6.2 Finetuning the immunosuppressive cytokines and their effect on IL-12 immunotherapy

In the PDAC models and the 4T1 model, there are most likely compensatory mechanisms that induce resistance to IL-12 therapy over time. An example is that repetitive IL-12 signalling can also lead to a negative feedback loop, frequently mediated by IL-10 (486, 489). Although this can be a source of resistance to IL-12 therapy, evidently, some models are more prone to this type of resistance than others. For example, I showed in Chapter 3 that in EMT6, IL-12 treated tumours, but not M-CBD-IL12-treated tumours, have significantly higher intratumoural IL-10 and TNFα than PBS controls. Exactly why IL-12 triggers this over M-CBD-IL12 remains elusive, yet it is most likely associated with their pharmacokinetics; unmodified IL-12 signalling is more powerful and diffuse than M-CBD-IL12, potentially leading to the activation of this negative feedback loop at an earlier time point. However, despite the raised IL-10 levels, wild-type IL-12 still performed better than M-CBD-IL12 in prolonging survival, suggesting this IL-10-mediated loop has little immunosuppressive effect in the EMT6 model. In future studies, measuring the IL-10 in the other models, as well as other immunosuppressive cytokines, may help explain resistance to IL-12 therapy.

Besides IL-10, other immunosuppressive cytokines can play a role in reducing the efficacy of IL-12. TGFβ is an immunosuppressive cytokine that was significantly less abundant in the IL-12-responsive EMT6 model compared to the 4T1 model in which both wild-type IL-12 and M-CBD-IL12 had little effect. Interestingly, with both wild-type IL-12 and M-CBD-IL12, the already low TGFβ1 levels in EMT6 tumours further significantly decreased compared to PBS control mice. This suggests that in EMT6, IL-12 suppresses the TGFβ1 levels, whilst 4T1 may be exhibiting resistance to IL-12 due

to its excessively high TGFβ1. These conflicting results fit within a much larger ongoing debate regarding the association between IL-12 and TGFβ1 (492). As previously mentioned, one of TGFβ1's tumorigenic effects is to direct T-cell differentiation towards Tregs and Th17 cells (492). This helps explain why 4T1 as an immunotype 1 tumour is TGFβ1-enriched and heavily infiltrated with Tregs and Th17 cells (see Figure 3.2, see Figure 3.22). These TGFβ-induced T-cell differentiation programs are counteracted by the effects of IL-12 and its downstream effector IFNγ (492); IL-12 has even been shown to inhibit the expression of the Treg transcription factor Foxp3 and the Th17 transcription factor RORγt *in vitro* (492). Cells treated with both IL-12 and TGFβ simultaneously start to display Th1 characteristics (Tbet expression, IFNγ/IL-2 production) and they are capable of triggering nitric oxide production by macrophages, suggesting IL-12 reverses or counteracts the effects of TGFβ (492). However, other research has shown TGFβ to suppress the IFNγ response of lymphocytes to IL-12 signalling (493, 494). TGFβ also seems to inhibit JAK2 and TYK2 phosphorylation as well as the phosphorylation of STAT4, all crucial components of the IL-12 signalling pathway (494). These findings support the use of TGFβ inhibitors in combination with IL-12 therapy in models like 4T1.

Although controversial, the use of IL-12 in combination with TGFβ inhibitors has become increasingly more common, unfortunately with mixed outcomes. More specifically, the combination of the NHS-IL12 immuno-cytokine (histone-targeting antibody + two human IL-12 heterodimers) and bintrafusp alfa (TGFβ trap consisting of a component of the TGFβRII fused to an anti-PD-L1 antibody), both of which were explained in the introduction in section 1.3.1. The NHS-IL12 antibody was found to be safe and to trigger some immune remodelling of the TME of patients with metastatic solid tumours (NCT01417546) (495).

In EMT6 and MC38 mouse models, murine NHS-IL12 in combination with the anti-PD-L1 antibody avelumab performed better than either therapy alone (496); the combination triggered complete responses in 7 out of 8 mice with EMT6 tumours, whilst the NHS-IL12 as monotherapy at both 2 μg and 10 μg barely delayed tumour progression. This suggests the anti-tumour effects of NHS-IL12 as monotherapy are less powerful than M-CBD-IL12 in the EMT6 model (496). Their combination-treated and cured mice resisted an EMT6 rechallenge yet were not protected from inoculation with 4T1 tumours (496). They however did not trial the combination in 4T1-bearing mice.

In MC38, whilst the NHS-IL12 and avelumab monotherapies did not significantly suppress tumour burden, the combination treatment did, and simultaneously prolonged survival significantly (496). Similarly to EMT6, M-CBD-IL12 also had an outstanding performance in MC38 as monotherapy, suggesting EMT6 and MC38 models respond similarly to IL-12 therapy (496). The findings of this study caused NHS-IL12+avelumab to progress to a phase Ib trial (NCT02994953) in patients with advanced solid tumours, which confirmed the safety of the combination (497). Recently, a second phase Ib trial was performed on patients with advanced solid tumours using this combination and a dose expansion was performed on a subset of patients with advanced urothelial carcinoma (498). Unfortunately, the dose expansion part did not meet the pre-defined criteria required for stage 2 (≥ 3 confirmed objective responses) (498).

Bintrafusp alfa (TGFβ trap) demonstrated promising effects in mouse models (499) and early clinical trials (29, 500-502) (see Table 1.8). In combination with NHS-IL12, it was studied in MC38, EMT6 and 4T1 mouse models (503). In MC38, the monotherapies already significantly suppressed tumour burden, yet this response was further enhanced when both were combined. Two out of the eight mice treated with the combination had complete responses and these mice were protected from a rechallenge (503). In contrast, no complete responses were observed with NHS-IL12 monotherapy and isotype controls and a single complete response for bintrafusp alfa monotherapy.

In EMT6, a similar pattern was observed; both monotherapies and the combination significantly suppressed tumour burden and prolonged survival, yet the response was stronger with the combination (503). In 4T1, bintrafusp alfa as monotherapy and in combination with NHS-IL12 significantly reduced lung metastases, whilst NHS-IL12 as monotherapy had little effect (503). Due to these promising results, this combination also progressed to clinical trials; in patients with metastatic genitourinary malignancies bintrafusp alfa, SBRT and NHS-IL12 triggered an ORR of 36.4% (504). Interestingly, in PDAC, bintrafusp alfa in combination with gemcitabine or with NHS-IL12 and SBRT was unsuccessful; a clinical trial was terminated prematurely due to a worsening risk to benefit ratio (NCT04327986) (see Table 1.8), highlighting the uniqueness of the PDAC TME yet again.

Evidently, the combination of TGFβ with IL-12 has been heavily studied but its effects observed in mice have not translated well into patients. Due to the high levels of TGFβ1 in the 4T1 TME, investigating the combination of M-CBD-IL12 with TGFβ inhibition in this model may be a promising future strategy. In contrast, due to the failure of TGFβ inhibition in PDAC (see Table 1.8), the same cannot be said for 7947 and 3275.

6.3 Immune suppression at a genetic level may reduce the efficacy of IL-12 immunotherapy

The production of these immunosuppressive cytokines that lead to resistance to IL-12 can be driven by oncogenic driver mutations. As discussed in Chapter 4, associations between the *Kras*^{G12D} mutation and immunotherapy resistance exist, yet pinpointing the exact mechanism through which this takes place remains elusive. In addition to IL-10 and TGFβ, resistance to immunotherapy may originate from *Kras*^{G12D}-induced GM-CSF production (505). The authors describe the *Kras*^{G12D} mutant cells to produce more GM-CSF into cell culture media than wild-type cells (505). Inhibition of the PI3K or MAPK pathways obliterated this cytokine production (505). Although GM-CSF is known to induce proliferation of monocytes and dendritic cells, it also recruits immunosuppressive Gr1^{+}CD11b^{+} myeloid cells (505). GM-CSF was found to induce their differentiation, which led to a reduction in T-cell proliferation, highlighting their immunosuppressive effects (505). Interestingly, GM-CSF suppression through an shRNA in *Kras*^{G12D} mutant PDAC cells resulted in reduced tumour formation and smaller tumour sizes compared to the scrambled control. These tumours also harboured a large CD8^{+} T-cell population and raised apoptosis, whilst the scrambled shRNA tumours were completely CD8^{+} T-cell depleted (505). Depleting CD8^{+} T-cells in the GM-CSF shRNA knockdown mouse model restored the tumorigenic potential of the cancer cells and led to tumour formation. This suggests that *Kras*^{G12D} mutant, but not wild-type *Kras* PDAC cells rely on GM-CSF and Gr1^{+}CD11b^{+} myeloid cells to escape from CD8^{+} T-cells to form tumours (505). Therefore, GM-CSF production is a second plausible mechanism, besides the FAS pathway described in chapter 4, through which *Kras*^{G12D} can promote immune evasion and unresponsiveness to immunotherapy in PDAC.

In addition, in other cancer types, other *Kras*^{G12D}-mediated immune evasive mechanisms have been described that operate through cytokines. For example, in NSCLC, unresponsiveness to CPIs has been attributed to the *KRAS*^{G12D} mutation, since *KRAS*^{G12D} mutant NSCLCs expressed less PD-L1 (surrogate biomarker for CPI efficacy) and less CXCL10/CXCL11 (506). Further, they found the mutation to actively suppress PD-L1 expression through the P70S6K/PI3K/AKT axis and CXCL10/CXCL11 expression through downregulation of high mobility group protein A2 (506). In mouse models, paclitaxel therapy restored CXCL10/CXCL11 secretion, and in combination with an anti-PD-L1 antibody, it therefore suppressed tumour growth compared to anti-PD-L1 monotherapy (506). However, conflicting evidence exists on whether *KRAS* mutation status affects response to CPI in NSCLC (507-509).

Overall, a clear association exists between the *Kras*^{G12D} mutation, CD8^{+} T-cells, and immunotherapy response within PDAC. Unfortunately, the research on IL-12 in PDAC is currently limited. Despite having established an association between *Kras*^{G12D} and IL-12 therapy in my experiments, more work is required to identify the mechanism of action through which *Kras*^{G12D} exerts its effects between different PDAC mouse models.

6.4 Limitations and future directions

Some limitations have reduced the validity of certain findings in this PhD thesis, the first one being the nature of certain *in vitro* experiments. More specifically, the assay representing the cleaving of the M-CBD-IL12 linker through western blotting, which uses tumour lysates. Although these lysates were used to capture the ability of proteases in the TME in its entirety to cleave the linker, this unfortunately also meant that certain intracellular proteases were released during tissue homogenisation that may have contributed to linker cleaving. In future experiments, it may be useful to include an additional condition. More specifically, after generating a single cell suspension from an established tumour model, homogenising these cells could visualise the extent of cleaving induced by the intracellular lysates. In addition, although this experiment was aimed at demonstrating linker cleaving, demonstrating the cleaving *in vivo* could help understand the tumour-specific activation of the M-CBD-IL12 molecule. This could potentially be achieved by injecting the M-CBD-IL12 molecule in tumour-bearing mice

and sacrificing mice at different timepoints (3 hours, 6 hours, 9 hours, and 24 hours after intravenous injection). The tumour as well as multiple other organs could be homogenised for protein analysis. An IL-12 western blot or Wes Simple western could demonstrate both the biodistribution of the molecule between organs, as well as the degree of linker cleaving.

In Chapter 3, the bioengineered cytokines I produced triggered some complete responses, especially in the EMT6 TNBC model. This suggests that the findings in this thesis have helped identify an immune landscape that is likely to respond to a bioengineered tolerable IL-12 molecule. Such associations may be very valuable in a translational context, yet require confirmation in a much larger number of TNBC mouse models. Despite having analysed changes in the TME following therapy, identifying the cell-to-cell interactions that generated this response requires further work. This could be achieved by depleting different immune cell types and observing whether this obliterates or enhances the observed effects of IL-12. For example, I identified raised TGFβ1 expression in 4T1 as a potential resistance mechanism that may have reduced the efficacy of M-CBD-IL12 in this model. Therefore, inhibiting TGFβ1 through a monoclonal antibody would offer insight into the link between a tumour's immune landscape and how this contributes to resistance to IL-12 immunotherapy. Similarly, to pinpoint the cell population that is largely responsible for the disappearance of EMT6 tumours following M-CBD-IL12 therapy, I would aim to perform $CD8^+$ T-cell depletion studies. In addition, to confirm whether the observed response in EMT6-bearing mice was of a long-lasting nature because of a population of memory cytotoxic T-cells, a rechallenge study would need to be performed. Finally, validation of the immunological changes following therapy using a technique other than flow cytometry such as immunohistochemistry could increase the validity of my findings. However, the tissues available for analysis in the treated groups are very limited due to the tumours disappearing, suggesting the animal studies would need to be repeated multiple times to achieve this.

In Chapter 4, I demonstrated a relationship between the $Kras^{G12D}$ mutation and response to IL-12 therapy in *iKras* PDAC mouse models. Although the immunomodulatory role of this mutation was previously established, few have explored its role in reducing the efficacy of IL-12. Therefore, the findings in this thesis may

contribute to the identification of a crucial resistance mechanism leading to the low immunotherapy efficacy in PDAC clinical trials. Building on these findings, it would be interesting to confirm whether the KRAS G12D inhibitor MRTX1133 can suppress immune evasive mechanisms in the less IL-12 responsive 7947 model to sensitise it to IL-12. In addition, I would aim to establish whether differences in immune landscape between the 7947 and 3275 mouse models are driven by their differential KRAS G12D levels. Finally, further work would be required to optimise the linker sequence of M-CBD-IL12 for PDACs. The sequence can be adjusted according to the most abundantly expressed proteases in the tumour to enhance removal of the mask exclusively in the tumour.

As described above, a major barrier that limits the success of many therapeutic agents in both TNBC and PDAC is the heterogeneity. Throughout this PhD, I have attempted account for intratumoural heterogeneity by using multiple immunologically distinct mouse models of the same cancer type where possible. Where applicable, tumours were also inoculated orthotopically either into the pancreas or the 4th nipple mammary fat pad. Although I demonstrated some responses to the bioengineered cytokines in different mouse models, these studies have been performed under highly controlled conditions and on rather small samples (n=6-7). An ongoing issue with mouse studies is that the data often does not translate into clinical trials, where environmental factors and genetics cause an even larger degree of heterogeneity. The implantation of Patient-Derived Xenografts (PDX) into immunocompromised or humanised mice, are used by many to bridge the gap between mouse and human. However, for immunotherapy to be successful, immunocompetent humanised mice are required. Producing a humanised version of the bioengineered cytokines and testing them in such models would make my findings more generalisable to patients. However, the cost of these models as well as obtaining patient samples are barriers that prevented me from achieving this throughout my PhD.

6.5 Conclusion

Overall, cancer types with challenging TMEs require combination therapy without the associated cumulative toxicity. Bioengineered tolerable anti-tumour cytokines as

monotherapy suffice for some mouse models, yet others demonstrate resistance through a variety of different pathways. This highlights the importance of addressing heterogeneity through patient classification to enable for selection of the most suitable immunotherapy agents. Consequently, delving into the different resistance mechanisms between models has helped me identify potential ways in which future research could pre-empt them.

Reference List

1. Zhang Y, Zhang Z. The history and advances in cancer immunotherapy: understanding the characteristics of tumor-infiltrating immune cells and their therapeutic implications. Cellular & Molecular Immunology. 2020;17(8):807-21.
2. Coley WB. The treatment of malignant tumors by repeated inoculations of erysipelas. With a report of ten original cases. 1893. Clin Orthop Relat Res. 1991(262):3-11.
3. Eno J. Immunotherapy Through the Years. J Adv Pract Oncol. 2017;8(7):747-53.
4. Liu X, Yin L, Shen S, Hou Y. Inflammation and cancer: paradoxical roles in tumorigenesis and implications in immunotherapies. Genes & Diseases. 2023;10(1):151-64.
5. Hanahan D. Hallmarks of Cancer: New Dimensions. Cancer Discovery. 2022;12(1):31-46.
6. Bremnes RM, Dønnem T, Al-Saad S, Al-Shibli K, Andersen S, Sirera R, et al. The role of tumor stroma in cancer progression and prognosis: emphasis on carcinoma-associated fibroblasts and non-small cell lung cancer. J Thorac Oncol. 2011;6(1):209-17.
7. Anderson NM, Simon MC. The tumor microenvironment. Curr Biol. 2020;30(16):R921-r5.
8. Ho WJ, Jaffee EM, Zheng L. The tumour microenvironment in pancreatic cancer - clinical challenges and opportunities. Nat Rev Clin Oncol. 2020;17(9):527-40.
9. Jiang B, Zhou L, Lu J, Wang Y, Liu C, You L, et al. Stroma-Targeting Therapy in Pancreatic Cancer: One Coin With Two Sides? Front Oncol. 2020;10:576399.
10. Marin-Acevedo JA, Kimbrough EO, Lou Y. Next generation of immune checkpoint inhibitors and beyond. Journal of Hematology & Oncology. 2021;14(1):45.
11. Zhang JM, An J. Cytokines, inflammation, and pain. Int Anesthesiol Clin. 2007;45(2):27-37.
12. Castro F, Cardoso AP, Gonçalves RM, Serre K, Oliveira MJ. Interferon-Gamma at the Crossroads of Tumor Immune Surveillance or Evasion. Front Immunol. 2018;9:847.
13. Berraondo P, Sanmamed MF, Ochoa MC, Etxeberria I, Aznar MA, Pérez-Gracia JL, et al. Cytokines in clinical cancer immunotherapy. British Journal of Cancer. 2019;120(1):6-15.
14. Keegan AD, Leonard WJ, Zhu J. Recent advances in understanding the role of IL-4 signaling. Fac Rev. 2021;10:71.
15. Zídek Z, Anzenbacher P, Kmoníčková E. Current status and challenges of cytokine pharmacology. Br J Pharmacol. 2009;157(3):342-61.
16. Lasek W, Zagożdżon R, Jakobisiak M. Interleukin 12: still a promising candidate for tumor immunotherapy? Cancer Immunol Immunother. 2014;63(5):419-35.
17. Nguyen KG, Vrabel MR, Mantooth SM, Hopkins JJ, Wagner ES, Gabaldon TA, et al. Localized Interleukin-12 for Cancer Immunotherapy. Frontiers in Immunology. 2020;11.
18. O'Reilly EM, Oh DY, Dhani N, Renouf DJ, Lee MA, Sun W, et al. Durvalumab With or Without Tremelimumab for Patients With Metastatic Pancreatic Ductal Adenocarcinoma: A Phase 2 Randomized Clinical Trial. JAMA Oncol. 2019;5(10):1431-8.
19. Wainberg ZA, Hochster HS, Kim EJ, George B, Kaylan A, Chiorean EG, et al. Open-label, Phase I Study of Nivolumab Combined with nab-Paclitaxel Plus Gemcitabine in Advanced Pancreatic Cancer. Clinical Cancer Research. 2020;26(18):4814-22.
20. Neri D, Sondel PM. Immunocytokines for cancer treatment: past, present and future. Curr Opin Immunol. 2016;40:96-102.
21. Dougan M, Ingram JR, Jeong HJ, Mosaheb MM, Bruck PT, Ali L, et al. Targeting Cytokine Therapy to the Pancreatic Tumor Microenvironment Using PD-L1-Specific VHHs. Cancer Immunol Res. 2018;6(4):389-401.

22. Waldhauer I, Gonzalez-Nicolini V, Freimoser-Grundschober A, Nayak TK, Fahrni L, Hosse RJ, et al. Simlukafusp alfa (FAP-IL2v) immunocytokine is a versatile combination partner for cancer immunotherapy. mAbs. 2021;13(1):1913791.
23. Shi M, Yu DH, Chen Y, Zhao CY, Zhang J, Liu QH, et al. Expression of fibroblast activation protein in human pancreatic adenocarcinoma and its clinicopathological significance. World J Gastroenterol. 2012;18(8):840-6.
24. Liu F, Qi L, Liu B, Liu J, Zhang H, Che D, et al. Fibroblast activation protein overexpression and clinical implications in solid tumors: a meta-analysis. PLoS One. 2015;10(3):e0116683.
25. Klein C, Waldhauer I, Nicolini VG, Freimoser-Grundschober A, Nayak T, Vugts DJ, et al. Cergutuzumab amunaleukin (CEA-IL2v), a CEA-targeted IL-2 variant-based immunocytokine for combination cancer immunotherapy: Overcoming limitations of aldesleukin and conventional IL-2-based immunocytokines. Oncoimmunology. 2017;6(3):e1277306.
26. Wagner K, Schulz P, Scholz A, Wiedenmann B, Menrad A. The targeted immunocytokine L19-IL2 efficiently inhibits the growth of orthotopic pancreatic cancer. Clin Cancer Res. 2008;14(15):4951-60.
27. Rekers NH, Olivo Pimentel V, Yaromina A, Lieuwes NG, Biemans R, Zegers CML, et al. The immunocytokine L19-IL2: An interplay between radiotherapy and long-lasting systemic anti-tumour immune responses. Oncoimmunology. 2018;7(4):e1414119.
28. Johannsen M, Spitaleri G, Curigliano G, Roigas J, Weikert S, Kempkensteffen C, et al. The tumour-targeting human L19-IL2 immunocytokine: Preclinical safety studies, phase I clinical trial in patients with solid tumours and expansion into patients with advanced renal cell carcinoma. European Journal of Cancer. 2010;46(16):2926-35.
29. Strauss J, Heery CR, Schlom J, Madan RA, Cao L, Kang Z, et al. Phase I Trial of M7824 (MSB0011359C), a Bifunctional Fusion Protein Targeting PD-L1 and TGFβ, in Advanced Solid Tumors. Clin Cancer Res. 2018;24(6):1287-95.
30. Principe DR, Timbers KE, Atia LG, Koch RM, Rana A. TGFbeta Signaling in the Pancreatic Tumor Microenvironment. Cancers (Basel). 2021;13(20).
31. Greiner JW, Morillon YM, 2nd, Schlom J. NHS-IL12, a Tumor-Targeting Immunocytokine. Immunotargets Ther. 2021;10:155-69.
32. Lee C-k, Jung M, Park S, Kwon WS, Kim KH, Hong M, et al. Bintrafusp alfa plus paclitaxel for advanced gastric cancer as a second-line treatment: An open label, single-arm, phase Ib/II study. Journal of Clinical Oncology. 2023;41(4_suppl):374-.
33. Spira A, Awada A, Isambert N, Estellés DL, Nemunaitis J, Penel N, et al. Abstract P3-09-06: Bintrafusp alfa (M7824), a bifunctional fusion protein targeting transforming growth factor-β and programmed death ligand 1, in advanced triple-negative breast cancer: Preliminary results from a phase 1 cohort. Cancer Research. 2020;80(4_Supplement):P3-09-6-P3--6.
34. Cho BC, Daste A, Ravaud A, Salas S, Isambert N, McClay EF, et al. Long-term follow-up of bintrafusp alfa, a bifunctional fusion protein targeting TGF-β and PD-L1, in advanced squamous cell carcinoma of the head and neck (SCCHN). Journal of Clinical Oncology. 2021;39(15_suppl):6020-.
35. Paz-Ares L, Kim TM, Vicente D, Felip E, Lee DH, Lee KH, et al. Bintrafusp Alfa, a Bifunctional Fusion Protein Targeting TGF-β and PD-L1, in Second-Line Treatment of Patients With NSCLC: Results From an Expansion Cohort of a Phase 1 Trial. J Thorac Oncol. 2020;15(7):1210-22.
36. Tan B, Khattak A, Felip E, Kelly K, Rich P, Wang D, et al. Bintrafusp Alfa, a Bifunctional Fusion Protein Targeting TGF-β and PD-L1, in Patients with Esophageal Adenocarcinoma: Results from a Phase 1 Cohort. Target Oncol. 2021;16(4):435-46.
37. Feng J, Tang D, Wang J, Zhou Q, Peng J, Lou H, et al. SHR-1701, a Bifunctional Fusion Protein Targeting PD-L1 and TGFβ, for Recurrent or Metastatic Cervical Cancer: A Clinical Expansion Cohort of a Phase I Study. Clin Cancer Res. 2022;28(24):5297-305.

38. Zhou J, Yu X, Li Z, Zhou Y, Li J, Xue R, et al. A phase 1b/2 trial of SHR-1701 in combination with gemcitabine and nab-paclitaxel in patients with untreated locally advanced or metastatic pancreatic cancer. Journal of Clinical Oncology. 2022;40(16_suppl):e16264-e.
39. Li Z, Wang M, Yao X, Luo W, Qu Y, Yu D, et al. Development of a Novel EGFR-Targeting Antibody-Drug Conjugate for Pancreatic Cancer Therapy. Target Oncol. 2019;14(1):93-105.
40. Li Z, Wang M, Yu D, Luo W, Fang J, Huang C, et al. Monomethyl auristatin E-conjugated anti-EGFR antibody inhibits the growth of human EGFR-positive non-small cell lung cancer. Cancer Chemotherapy and Pharmacology. 2019;84(1):61-72.
41. McDaid WJ, Greene MK, Johnston MC, Pollheimer E, Smyth P, McLaughlin K, et al. Repurposing of Cetuximab in antibody-directed chemotherapy-loaded nanoparticles in EGFR therapy-resistant pancreatic tumours. Nanoscale. 2019;11(42):20261-73.
42. Duwa R, Banstola A, Emami F, Jeong J-H, Lee S, Yook S. Cetuximab conjugated temozolomide-loaded poly (lactic-co-glycolic acid) nanoparticles for targeted nanomedicine in EGFR overexpressing cancer cells. Journal of Drug Delivery Science and Technology. 2020;60:101928.
43. Hassan R, Blumenschein GR, Jr., Moore KN, Santin AD, Kindler HL, Nemunaitis JJ, et al. First-in-Human, Multicenter, Phase I Dose-Escalation and Expansion Study of Anti-Mesothelin Antibody-Drug Conjugate Anetumab Ravtansine in Advanced or Metastatic Solid Tumors. J Clin Oncol. 2020;38(16):1824-35.
44. Adjei AA, Bekaii-Saab TS, Berlin J, Philip PA, Mercade TM, Walter A, et al. Phase 1b multi-indication study of the antibody drug conjugate anetumab ravtansine in patients with mesothelin-expressing advanced or recurrent malignancies. Journal of Clinical Oncology. 2018;36(15_suppl):TPS2607-TPS.
45. Santin AD, Vergote I, González-Martín A, Moore K, Oaknin A, Romero I, et al. Safety and activity of anti-mesothelin antibody-drug conjugate anetumab ravtansine in combination with pegylated-liposomal doxorubicin in platinum-resistant ovarian cancer: multicenter, phase Ib dose escalation and expansion study. Int J Gynecol Cancer. 2023;33(4):562-70.
46. Momin N, Mehta NK, Bennett NR, Ma L, Palmeri JR, Chinn MM, et al. Anchoring of intratumorally administered cytokines to collagen safely potentiates systemic cancer immunotherapy. Sci Transl Med. 2019;11(498).
47. Saenger YM, Li Y, Chiou KC, Chan B, Rizzuto G, Terzulli SL, et al. Improved tumor immunity using anti-tyrosinase related protein-1 monoclonal antibody combined with DNA vaccines in murine melanoma. Cancer Res. 2008;68(23):9884-91.
48. Pérez-Lorenzo R, Erjavec SO, Christiano AM, Clynes R. Improved therapeutic efficacy of unmodified anti-tumor antibodies by immune checkpoint blockade and kinase targeted therapy in mouse models of melanoma. Oncotarget. 2021;12(2):66-80.
49. Yeow YL, Kotamraju VR, Wang X, Chopra M, Azme N, Wu J, et al. Immune-mediated ECM depletion improves tumour perfusion and payload delivery. EMBO Mol Med. 2019;11(12):e10923.
50. Ishihara J, Ishihara A, Sasaki K, Lee SS, Williford JM, Yasui M, et al. Targeted antibody and cytokine cancer immunotherapies through collagen affinity. Sci Transl Med. 2019;11(487).
51. Mansurov A, Ishihara J, Hosseinchi P, Potin L, Marchell TM, Ishihara A, et al. Collagen-binding IL-12 enhances tumour inflammation and drives the complete remission of established immunologically cold mouse tumours. Nature Biomedical Engineering. 2020;4(5):531-43.
52. Williford JM, Ishihara J, Ishihara A, Mansurov A, Hosseinchi P, Marchell TM, et al. Recruitment of CD103(+) dendritic cells via tumor-targeted chemokine delivery enhances efficacy of checkpoint inhibitor immunotherapy. Sci Adv. 2019;5(12):eaay1357.
53. Veronese FM, Mero A. The impact of PEGylation on biological therapies. BioDrugs. 2008;22(5):315-29.

54. Autio K, Oft M. Pegylated Interleukin-10: Clinical Development of an Immunoregulatory Cytokine for Use in Cancer Therapeutics. Current Oncology Reports. 2019;21(2):19.
55. Herndon TM, Demko SG, Jiang X, He K, Gootenberg JE, Cohen MH, et al. U.S. Food and Drug Administration Approval: peginterferon-alfa-2b for the adjuvant treatment of patients with melanoma. Oncologist. 2012;17(10):1323-8.
56. Mumm JB, Emmerich J, Zhang X, Chan I, Wu L, Mauze S, et al. IL-10 elicits IFNγ-dependent tumor immune surveillance. Cancer Cell. 2011;20(6):781-96.
57. Hecht JR, Naing A, Falchook GS, Patel MR, Infante JR, Aljumaily R, et al. Overall survival of PEGylated human IL-10 (AM0010) with 5-FU/LV and oxaliplatin (FOLFOX) in metastatic pancreatic adenocarcinoma (PDAC). Journal of Clinical Oncology. 2018;36(4_suppl):374-.
58. Hecht JR, Papadopoulos KP, Falchook GS, Patel MR, Infante JR, Aljumaily R, et al. Immunologic and tumor responses of pegilodecakin with 5-FU/LV and oxaliplatin (FOLFOX) in pancreatic ductal adenocarcinoma (PDAC). Invest New Drugs. 2021;39(1):182-92.
59. Naing A, Wong DJ, Infante JR, Korn WM, Aljumaily R, Papadopoulos KP, et al. Pegilodecakin combined with pembrolizumab or nivolumab for patients with advanced solid tumours (IVY): a multicentre, multicohort, open-label, phase 1b trial. Lancet Oncol. 2019;20(11):1544-55.
60. Naing A, Papadopoulos KP, Autio KA, Ott PA, Patel MR, Wong DJ, et al. Safety, Antitumor Activity, and Immune Activation of Pegylated Recombinant Human Interleukin-10 (AM0010) in Patients With Advanced Solid Tumors. J Clin Oncol. 2016;34(29):3562-9.
61. Hecht JR, Lonardi S, Bendell J, Sim HW, Macarulla T, Lopez CD, et al. Randomized Phase III Study of FOLFOX Alone or With Pegilodecakin as Second-Line Therapy in Patients With Metastatic Pancreatic Cancer That Progressed After Gemcitabine (SEQUOIA). J Clin Oncol. 2021;39(10):1108-18.
62. Agarwal Y, Milling LE, Chang JYH, Santollani L, Sheen A, Lutz EA, et al. Intratumourally injected alum-tethered cytokines elicit potent and safer local and systemic anticancer immunity. Nature Biomedical Engineering. 2022;6(2):129-43.
63. Pio R, Ajona D, Ortiz-Espinosa S, Mantovani A, Lambris JD. Complementing the Cancer-Immunity Cycle. Frontiers in Immunology. 2019;10.
64. Gill S, Brudno JN. CAR T-Cell Therapy in Hematologic Malignancies: Clinical Role, Toxicity, and Unanswered Questions. American Society of Clinical Oncology Educational Book. 2021(41):e246-e65.
65. Yang C-Y, Fan MH, Miao CH, Liao YJ, Yuan R-H, Liu CL. Engineering Chimeric Antigen Receptor T Cells against Immune Checkpoint Inhibitors PD-1/PD-L1 for Treating Pancreatic Cancer. Molecular Therapy - Oncolytics. 2020;17:571-85.
66. Yeo D, Giardina C, Saxena P, Rasko JEJ. The next wave of cellular immunotherapies in pancreatic cancer. Molecular Therapy - Oncolytics. 2022;24:561-76.
67. Haas AR, Tanyi JL, O'Hara MH, Gladney WL, Lacey SF, Torigian DA, et al. Phase I Study of Lentiviral-Transduced Chimeric Antigen Receptor-Modified T Cells Recognizing Mesothelin in Advanced Solid Cancers. Mol Ther. 2019;27(11):1919-29.
68. Beatty GL, Haas AR, Maus MV, Torigian DA, Soulen MC, Plesa G, et al. Mesothelin-Specific Chimeric Antigen Receptor mRNA-Engineered T Cells Induce Antitumor Activity in Solid Malignancies. Cancer Immunology Research. 2014;2(2):112-20.
69. Beatty GL, O'Hara MH, Lacey SF, Torigian DA, Nazimuddin F, Chen F, et al. Activity of Mesothelin-Specific Chimeric Antigen Receptor T Cells Against Pancreatic Carcinoma Metastases in a Phase 1 Trial. Gastroenterology. 2018;155(1):29-32.
70. Reusch U, Sundaram M, Davol PA, Olson SD, Davis JB, Demel K, et al. Anti-CD3 × Anti-Epidermal Growth Factor Receptor (EGFR) Bispecific Antibody Redirects T-Cell Cytolytic Activity to EGFR-Positive Cancers In vitro and in an Animal Model. Clinical Cancer Research. 2006;12(1):183-90.

71. Lum LG, Thakur A, Choi M, Deol A, Kondadasula V, Schalk D, et al. Clinical and immune responses to anti-CD3 x anti-EGFR bispecific antibody armed activated T cells (EGFR BATs) in pancreatic cancer patients. Oncoimmunology. 2020;9(1):1773201.
72. Wang H, Hou Y, Hu Y, Dou J, Shen Y, Wang Y, et al. Enzyme-Activatable Interferon–Poly(α-amino acid) Conjugates for Tumor Microenvironment Potentiation. Biomacromolecules. 2019;20(8):3000-8.
73. Mansurov A, Hosseinchi P, Chang K, Lauterbach AL, Gray LT, Alpar AT, et al. Masking the immunotoxicity of interleukin-12 by fusing it with a domain of its receptor via a tumour-protease-cleavable linker. Nature Biomedical Engineering. 2022;6(7):819-29.
74. Xue D, Moon B, Liao J, Guo J, Zou Z, Han Y, et al. A tumor-specific pro-IL-12 activates preexisting cytotoxic T cells to control established tumors. Science Immunology. 2022;7(67):eabi6899.
75. Sung H, Ferlay J, Siegel RL, Laversanne M, Soerjomataram I, Jemal A, et al. Global Cancer Statistics 2020: GLOBOCAN Estimates of Incidence and Mortality Worldwide for 36 Cancers in 185 Countries. CA: A Cancer Journal for Clinicians. 2021;71(3):209-49.
76. Karim AM, Eun Kwon J, Ali T, Jang J, Ullah I, Lee Y-G, et al. Triple-negative breast cancer: epidemiology, molecular mechanisms, and modern vaccine-based treatment strategies. Biochemical Pharmacology. 2023;212:115545.
77. Trivers KF, Lund MJ, Porter PL, Liff JM, Flagg EW, Coates RJ, et al. The epidemiology of triple-negative breast cancer, including race. Cancer Causes & Control. 2009;20(7):1071-82.
78. Yang XR, Chang-Claude J, Goode EL, Couch FJ, Nevanlinna H, Milne RL, et al. Associations of Breast Cancer Risk Factors With Tumor Subtypes: A Pooled Analysis From the Breast Cancer Association Consortium Studies. JNCI: Journal of the National Cancer Institute. 2010;103(3):250-63.
79. Noruzinia M, Coupier I, Pujol P. Is BRCA1/BRCA2-related breast carcinogenesis estrogen dependent? Cancer. 2005;104(8):1567-74.
80. Makki J. Diversity of Breast Carcinoma: Histological Subtypes and Clinical Relevance. Clin Med Insights Pathol. 2015;8:23-31.
81. Sgroi DC. Preinvasive breast cancer. Annu Rev Pathol. 2010;5:193-221.
82. Perou CM, Sørlie T, Eisen MB, van de Rijn M, Jeffrey SS, Rees CA, et al. Molecular portraits of human breast tumours. Nature. 2000;406(6797):747-52.
83. Sørlie T, Perou CM, Tibshirani R, Aas T, Geisler S, Johnsen H, et al. Gene expression patterns of breast carcinomas distinguish tumor subclasses with clinical implications. Proc Natl Acad Sci U S A. 2001;98(19):10869-74.
84. Sotiriou C, Neo SY, McShane LM, Korn EL, Long PM, Jazaeri A, et al. Breast cancer classification and prognosis based on gene expression profiles from a population-based study. Proc Natl Acad Sci U S A. 2003;100(18):10393-8.
85. van 't Veer LJ, Dai H, van de Vijver MJ, He YD, Hart AA, Mao M, et al. Gene expression profiling predicts clinical outcome of breast cancer. Nature. 2002;415(6871):530-6.
86. Hu Z, Fan C, Oh DS, Marron JS, He X, Qaqish BF, et al. The molecular portraits of breast tumors are conserved across microarray platforms. BMC Genomics. 2006;7:96.
87. Stevens KN, Vachon CM, Couch FJ. Genetic Susceptibility to Triple-Negative Breast Cancer. Cancer Research. 2013;73(7):2025-30.
88. Korlimarla A, Ps H, Prabhu J, Ragulan C, Patil Y, Vp S, et al. Comprehensive characterization of immune landscape of Indian and Western triple negative breast cancers. Transl Oncol. 2022;25:101511.
89. Dias K, Dvorkin-Gheva A, Hallett RM, Wu Y, Hassell J, Pond GR, et al. Claudin-Low Breast Cancer; Clinical & Pathological Characteristics. PLoS One. 2017;12(1):e0168669.
90. Obidiro O, Battogtokh G, Akala EO. Triple Negative Breast Cancer Treatment Options and Limitations: Future Outlook. Pharmaceutics. 2023;15(7).

91. Shimelis H, LaDuca H, Hu C, Hart SN, Na J, Thomas A, et al. Triple-Negative Breast Cancer Risk Genes Identified by Multigene Hereditary Cancer Panel Testing. JNCI: Journal of the National Cancer Institute. 2018;110(8):855-62.
92. Ragupathi A, Singh M, Perez AM, Zhang D. Targeting the BRCA1/2 deficient cancer with PARP inhibitors: Clinical outcomes and mechanistic insights. Front Cell Dev Biol. 2023;11:1133472.
93. Ashworth A. A Synthetic Lethal Therapeutic Approach: Poly(ADP) Ribose Polymerase Inhibitors for the Treatment of Cancers Deficient in DNA Double-Strand Break Repair. Journal of Clinical Oncology. 2008;26(22):3785-90.
94. Robson M, Im SA, Senkus E, Xu B, Domchek SM, Masuda N, et al. Olaparib for Metastatic Breast Cancer in Patients with a Germline BRCA Mutation. N Engl J Med. 2017;377(6):523-33.
95. Litton JK, Rugo HS, Ettl J, Hurvitz SA, Gonçalves A, Lee KH, et al. Talazoparib in Patients with Advanced Breast Cancer and a Germline BRCA Mutation. N Engl J Med. 2018;379(8):753-63.
96. Han Y, Yu X, Li S, Tian Y, Liu C. New Perspectives for Resistance to PARP Inhibitors in Triple-Negative Breast Cancer. Front Oncol. 2020;10:578095.
97. Barchiesi G, Roberto M, Verrico M, Vici P, Tomao S, Tomao F. Emerging Role of PARP Inhibitors in Metastatic Triple Negative Breast Cancer. Current Scenario and Future Perspectives. Front Oncol. 2021;11:769280.
98. Marra A, Trapani D, Viale G, Criscitiello C, Curigliano G. Practical classification of triple-negative breast cancer: intratumoral heterogeneity, mechanisms of drug resistance, and novel therapies. npj Breast Cancer. 2020;6(1):54.
99. Juric D, Rodon J, Tabernero J, Janku F, Burris HA, Schellens JHM, et al. Phosphatidylinositol 3-Kinase α-Selective Inhibition With Alpelisib (BYL719) in PIK3CA-Altered Solid Tumors: Results From the First-in-Human Study. J Clin Oncol. 2018;36(13):1291-9.
100. Kim SB, Dent R, Im SA, Espié M, Blau S, Tan AR, et al. Ipatasertib plus paclitaxel versus placebo plus paclitaxel as first-line therapy for metastatic triple-negative breast cancer (LOTUS): a multicentre, randomised, double-blind, placebo-controlled, phase 2 trial. Lancet Oncol. 2017;18(10):1360-72.
101. Schmid P, Abraham J, Chan S, Wheatley D, Brunt AM, Nemsadze G, et al. Capivasertib Plus Paclitaxel Versus Placebo Plus Paclitaxel As First-Line Therapy for Metastatic Triple-Negative Breast Cancer: The PAKT Trial. J Clin Oncol. 2020;38(5):423-33.
102. Harris LG, Pannell LK, Singh S, Samant RS, Shevde LA. Increased vascularity and spontaneous metastasis of breast cancer by hedgehog signaling mediated upregulation of cyr61. Oncogene. 2012;31(28):3370-80.
103. Kwon YJ, Hurst DR, Steg AD, Yuan K, Vaidya KS, Welch DR, et al. Gli1 enhances migration and invasion via up-regulation of MMP-11 and promotes metastasis in ERα negative breast cancer cell lines. Clin Exp Metastasis. 2011;28(5):437-49.
104. Sims-Mourtada J, Opdenaker LM, Davis J, Arnold KM, Flynn D. Taxane-induced hedgehog signaling is linked to expansion of breast cancer stem-like populations after chemotherapy. Mol Carcinog. 2015;54(11):1480-93.
105. Sekulic A, Migden MR, Oro AE, Dirix L, Lewis KD, Hainsworth JD, et al. Efficacy and safety of vismodegib in advanced basal-cell carcinoma. N Engl J Med. 2012;366(23):2171-9.
106. Robinson GW, Orr BA, Wu G, Gururangan S, Lin T, Qaddoumi I, et al. Vismodegib Exerts Targeted Efficacy Against Recurrent Sonic Hedgehog-Subgroup Medulloblastoma: Results From Phase II Pediatric Brain Tumor Consortium Studies PBTC-025B and PBTC-032. J Clin Oncol. 2015;33(24):2646-54.
107. Berlin J, Bendell JC, Hart LL, Firdaus I, Gore I, Hermann RC, et al. A randomized phase II trial of vismodegib versus placebo with FOLFOX or FOLFIRI and bevacizumab in

patients with previously untreated metastatic colorectal cancer. Clin Cancer Res. 2013;19(1):258-67.
108. Kim EJ, Sahai V, Abel EV, Griffith KA, Greenson JK, Takebe N, et al. Pilot clinical trial of hedgehog pathway inhibitor GDC-0449 (vismodegib) in combination with gemcitabine in patients with metastatic pancreatic adenocarcinoma. Clin Cancer Res. 2014;20(23):5937-45.
109. Belani CP, Dahlberg SE, Rudin CM, Fleisher M, Chen HX, Takebe N, et al. Vismodegib or cixutumumab in combination with standard chemotherapy for patients with extensive-stage small cell lung cancer: A trial of the ECOG-ACRIN Cancer Research Group (E1508). Cancer. 2016;122(15):2371-8.
110. Ruiz-Borrego M, Jimenez B, Antolín S, García-Saenz JA, Corral J, Jerez Y, et al. A phase Ib study of sonidegib (LDE225), an oral small molecule inhibitor of smoothened or Hedgehog pathway, in combination with docetaxel in triple negative advanced breast cancer patients: GEICAM/2012-12 (EDALINE) study. Invest New Drugs. 2019;37(1):98-108.
111. Niewiadomski P, Niedziółka SM, Markiewicz Ł, Uśpieński T, Baran B, Chojnowska K. Gli Proteins: Regulation in Development and Cancer. Cells. 2019;8(2).
112. Yang L, Wu X, Wang Y, Zhang K, Wu J, Yuan YC, et al. FZD7 has a critical role in cell proliferation in triple negative breast cancer. Oncogene. 2011;30(43):4437-46.
113. DeAlmeida VI, Miao L, Ernst JA, Koeppen H, Polakis P, Rubinfeld B. The Soluble Wnt Receptor Frizzled8CRD-hFc Inhibits the Growth of Teratocarcinomas In vivo. Cancer Research. 2007;67(11):5371-9.
114. Traina TA, Miller K, Yardley DA, Eakle J, Schwartzberg LS, O'Shaughnessy J, et al. Enzalutamide for the Treatment of Androgen Receptor-Expressing Triple-Negative Breast Cancer. J Clin Oncol. 2018;36(9):884-90.
115. Gucalp A, Tolaney S, Isakoff SJ, Ingle JN, Liu MC, Carey LA, et al. Phase II trial of bicalutamide in patients with androgen receptor-positive, estrogen receptor-negative metastatic Breast Cancer. Clin Cancer Res. 2013;19(19):5505-12.
116. Bonnefoi H, Grellety T, Tredan O, Saghatchian M, Dalenc F, Mailliez A, et al. A phase II trial of abiraterone acetate plus prednisone in patients with triple-negative androgen receptor positive locally advanced or metastatic breast cancer (UCBG 12-1). Ann Oncol. 2016;27(5):812-8.
117. Schmid P, Rugo HS, Adams S, Schneeweiss A, Barrios CH, Iwata H, et al. Atezolizumab plus nab-paclitaxel as first-line treatment for unresectable, locally advanced or metastatic triple-negative breast cancer (IMpassion130): updated efficacy results from a randomised, double-blind, placebo-controlled, phase 3 trial. Lancet Oncol. 2020;21(1):44-59.
118. (NICE) NIfHaCE. Atezolizumab with nab- paclitaxel for untreated PD-L1-positive, locally advanced or metastatic, triple-negative breast cancer (TA639) 2020 [
119. Cortes J, Cescon DW, Rugo HS, Nowecki Z, Im S-A, Yusof MM, et al. Pembrolizumab plus chemotherapy versus placebo plus chemotherapy for previously untreated locally recurrent inoperable or metastatic triple-negative breast cancer (KEYNOTE-355): a randomised, placebo-controlled, double-blind, phase 3 clinical trial. The Lancet. 2020;396(10265):1817-28.
120. Cortes J, Rugo HS, Cescon DW, Im S-A, Yusof MM, Gallardo C, et al. Pembrolizumab plus Chemotherapy in Advanced Triple-Negative Breast Cancer. New England Journal of Medicine. 2022;387(3):217-26.
121. (NICE) NIfHaCE. Pembrolizumab plus chemotherapy for untreated, triple-negative, locally recurrent unresectable or metastatic breast cancer (TA801) 2022 [
122. (NICE) NIfHaCE. Pembrolizumab for neoadjuvant and adjuvant treatment of triple-negative early or locally advanced breast cancer (TA851) 2022 [
123. Li L, Zhang F, Liu Z, Fan Z. Immunotherapy for Triple-Negative Breast Cancer: Combination Strategies to Improve Outcome. Cancers (Basel). 2023;15(1).

124. Nanda R, Chow LQ, Dees EC, Berger R, Gupta S, Geva R, et al. Pembrolizumab in Patients With Advanced Triple-Negative Breast Cancer: Phase Ib KEYNOTE-012 Study. J Clin Oncol. 2016;34(21):2460-7.
125. Adams S, Schmid P, Rugo HS, Winer EP, Loirat D, Awada A, et al. Pembrolizumab monotherapy for previously treated metastatic triple-negative breast cancer: cohort A of the phase II KEYNOTE-086 study. Ann Oncol. 2019;30(3):397-404.
126. Adams S, Loi S, Toppmeyer D, Cescon DW, De Laurentiis M, Nanda R, et al. Pembrolizumab monotherapy for previously untreated, PD-L1-positive, metastatic triple-negative breast cancer: cohort B of the phase II KEYNOTE-086 study. Ann Oncol. 2019;30(3):405-11.
127. Winer EP, Lipatov O, Im SA, Goncalves A, Muñoz-Couselo E, Lee KS, et al. Pembrolizumab versus investigator-choice chemotherapy for metastatic triple-negative breast cancer (KEYNOTE-119): a randomised, open-label, phase 3 trial. Lancet Oncol. 2021;22(4):499-511.
128. Vinayak S, Tolaney SM, Schwartzberg L, Mita M, McCann G, Tan AR, et al. Open-label Clinical Trial of Niraparib Combined With Pembrolizumab for Treatment of Advanced or Metastatic Triple-Negative Breast Cancer. JAMA Oncol. 2019;5(8):1132-40.
129. Dirix LY, Takacs I, Jerusalem G, Nikolinakos P, Arkenau HT, Forero-Torres A, et al. Avelumab, an anti-PD-L1 antibody, in patients with locally advanced or metastatic breast cancer: a phase 1b JAVELIN Solid Tumor study. Breast Cancer Res Treat. 2018;167(3):671-86.
130. Yap TA, Bardia A, Dvorkin M, Galsky MD, Beck JT, Wise DR, et al. Avelumab Plus Talazoparib in Patients With Advanced Solid Tumors: The JAVELIN PARP Medley Nonrandomized Controlled Trial. JAMA Oncol. 2023;9(1):40-50.
131. Emens LA, Cruz C, Eder JP, Braiteh F, Chung C, Tolaney SM, et al. Long-term Clinical Outcomes and Biomarker Analyses of Atezolizumab Therapy for Patients With Metastatic Triple-Negative Breast Cancer: A Phase 1 Study. JAMA Oncol. 2019;5(1):74-82.
132. Tolaney SM, Kalinsky K, Kaklamani VG, D'Adamo DR, Aktan G, Tsai ML, et al. Eribulin Plus Pembrolizumab in Patients with Metastatic Triple-Negative Breast Cancer (ENHANCE 1): A Phase Ib/II Study. Clin Cancer Res. 2021;27(11):3061-8.
133. Miles D, Gligorov J, André F, Cameron D, Schneeweiss A, Barrios C, et al. Primary results from IMpassion131, a double-blind, placebo-controlled, randomised phase III trial of first-line paclitaxel with or without atezolizumab for unresectable locally advanced/metastatic triple-negative breast cancer. Ann Oncol. 2021;32(8):994-1004.
134. Cortés J, André F, Gonçalves A, Kümmel S, Martín M, Schmid P, et al. IMpassion132 Phase III trial: atezolizumab and chemotherapy in early relapsing metastatic triple-negative breast cancer. Future Oncology. 2019;15(17):1951-61.
135. Schmid P, Salgado R, Park YH, Muñoz-Couselo E, Kim SB, Sohn J, et al. Pembrolizumab plus chemotherapy as neoadjuvant treatment of high-risk, early-stage triple-negative breast cancer: results from the phase 1b open-label, multicohort KEYNOTE-173 study. Annals of Oncology. 2020;31(5):569-81.
136. Loibl S, Untch M, Burchardi N, Huober J, Sinn BV, Blohmer JU, et al. A randomised phase II study investigating durvalumab in addition to an anthracycline taxane-based neoadjuvant therapy in early triple-negative breast cancer: clinical results and biomarker analysis of GeparNuevo study. Annals of Oncology. 2019;30(8):1279-88.
137. Chen L, Jiang YZ, Wu SY, Wu J, Di GH, Liu GY, et al. Famitinib with Camrelizumab and Nab-Paclitaxel for Advanced Immunomodulatory Triple-Negative Breast Cancer (FUTURE-C-Plus): An Open-Label, Single-Arm, Phase II Trial. Clin Cancer Res. 2022;28(13):2807-17.
138. Kuemmel S, Campone M, Loirat D, Lopez RL, Beck JT, De Laurentiis M, et al. A Randomized Phase II Study of Anti-CSF1 Monoclonal Antibody Lacnotuzumab (MCS110) Combined with Gemcitabine and Carboplatin in Advanced Triple-Negative Breast Cancer. Clinical Cancer Research. 2022;28(1):106-15.

139. Bachelot T, Filleron T, Bieche I, Arnedos M, Campone M, Dalenc F, et al. Durvalumab compared to maintenance chemotherapy in metastatic breast cancer: the randomized phase II SAFIR02-BREAST IMMUNO trial. Nature Medicine. 2021;27(2):250-5.
140. Adams S, Diamond JR, Hamilton E, Pohlmann PR, Tolaney SM, Chang CW, et al. Atezolizumab Plus nab-Paclitaxel in the Treatment of Metastatic Triple-Negative Breast Cancer With 2-Year Survival Follow-up: A Phase 1b Clinical Trial. JAMA Oncol. 2019;5(3):334-42.
141. Brufsky A, Kim SB, Zvirbule Ž, Eniu A, Mebis J, Sohn JH, et al. A phase II randomized trial of cobimetinib plus chemotherapy, with or without atezolizumab, as first-line treatment for patients with locally advanced or metastatic triple-negative breast cancer (COLET): primary analysis. Annals of Oncology. 2021;32(5):652-60.
142. Liu J, Liu Q, Li Y, Li Q, Su F, Yao H, et al. Efficacy and safety of camrelizumab combined with apatinib in advanced triple-negative breast cancer: an open-label phase II trial. J Immunother Cancer. 2020;8(1).
143. Santa-Maria CA, Kato T, Park JH, Kiyotani K, Rademaker A, Shah AN, et al. A pilot study of durvalumab and tremelimumab and immunogenomic dynamics in metastatic breast cancer. Oncotarget. 2018;9(27):18985-96.
144. Hecht JR, Raman SS, Chan A, Kalinsky K, Baurain JF, Jimenez MM, et al. Phase Ib study of talimogene laherparepvec in combination with atezolizumab in patients with triple negative breast cancer and colorectal cancer with liver metastases. ESMO Open. 2023;8(2):100884.
145. Pusztai L, Yau C, Wolf DM, Han HS, Du L, Wallace AM, et al. Durvalumab with olaparib and paclitaxel for high-risk HER2-negative stage II/III breast cancer: Results from the adaptively randomized I-SPY2 trial. Cancer Cell. 2021;39(7):989-98.e5.
146. Nanda R, Liu MC, Yau C, Shatsky R, Pusztai L, Wallace A, et al. Effect of Pembrolizumab Plus Neoadjuvant Chemotherapy on Pathologic Complete Response in Women With Early-Stage Breast Cancer: An Analysis of the Ongoing Phase 2 Adaptively Randomized I-SPY2 Trial. JAMA Oncol. 2020;6(5):676-84.
147. Jiang Z, Ouyang Q, Sun T, Zhang Q, Teng Y, Cui J, et al. TORCHLIGHT: A randomized, double-blind, phase III trial of toripalimab versus placebo, in combination with nab-paclitaxel(nab-P) for patients with metastatic or recurrent triple-negative breast cancer (TNBC). Journal of Clinical Oncology. 2023;41(17_suppl):LBA1013-LBA.
148. O'Day SJ, Borges VF, Chmielowski B, Rao RD, Abu-Khalaf M, Stopeck A, et al. Abstract CT073: IMPRIME 1 (NCT02981303): A novel phase 2 study in second-line +, metastatic triple negative breast cancer patients shows promising clinical benefit for the combination of the immune checkpoint inhibitor, pembrolizumab (pembro), with the novel innate immune activator, Imprime PGG. Cancer Research. 2020;80(16_Supplement):CT073-CT.
149. Røssevold AH, Andresen NK, Bjerre CA, Gilje B, Jakobsen EH, Raj SX, et al. Atezolizumab plus anthracycline-based chemotherapy in metastatic triple-negative breast cancer: the randomized, double-blind phase 2b ALICE trial. Nat Med. 2022;28(12):2573-83.
150. Schmid P, Cortes J, Dent R, Pusztai L, McArthur H, Kümmel S, et al. Event-free Survival with Pembrolizumab in Early Triple-Negative Breast Cancer. New England Journal of Medicine. 2022;386(6):556-67.
151. Sharma P, Stecklein SR, Yoder R, Staley JM, Schwensen K, O'Dea A, et al. Clinical and Biomarker Findings of Neoadjuvant Pembrolizumab and Carboplatin Plus Docetaxel in Triple-Negative Breast Cancer: NeoPACT Phase 2 Clinical Trial. JAMA Oncology. 2024;10(2):227-35.
152. Gianni L, Huang CS, Egle D, Bermejo B, Zamagni C, Thill M, et al. Pathologic complete response (pCR) to neoadjuvant treatment with or without atezolizumab in triple-negative, early high-risk and locally advanced breast cancer: NeoTRIP Michelangelo randomized study[☆]. Annals of Oncology. 2022;33(5):534-43.

153. Mittendorf EA, Zhang H, Barrios CH, Saji S, Jung KH, Hegg R, et al. Neoadjuvant atezolizumab in combination with sequential nab-paclitaxel and anthracycline-based chemotherapy versus placebo and chemotherapy in patients with early-stage triple-negative breast cancer (IMpassion031): a randomised, double-blind, phase 3 trial. The Lancet. 2020;396(10257):1090-100.
154. Im S-A, Lee K-H, Min A, Lee D, Kim TY, Ryu HS, et al. Abstract PD15-08: Window of opportunity trial of neoadjuvant olaparib and durvalumab for triple negative or low ER-positive breast cancer. Cancer Research. 2022;82(4_Supplement):PD15-08-PD15-08.
155. Tan TJ, Sammons S, Im YH, She L, Mundy K, Bigelow R, et al. Phase II DORA Study of Olaparib with or without Durvalumab as a Chemotherapy-Free Maintenance Strategy in Platinum-Pretreated Advanced Triple-Negative Breast Cancer. Clin Cancer Res. 2024.
156. McArthur HL, Barker CA, Gucalp A, Lebron Zapata L, Wen YH, Phung A, et al. 247P - A single-arm, phase ii study assessing the efficacy of pembrolizumab (pembro) plus radiotherapy (RT) in metastatic triple negative breast cancer (mTNBC). Annals of Oncology. 2017;28:v79.
157. Han H, Diab S, Alemany C, Basho R, Brown-Glaberman U, Meisel J, et al. Abstract PD1-06: Open label phase 1b/2 study of ladiratuzumab vedotin in combination with pembrolizumab for first-line treatment of patients with unresectable locally-advanced or metastatic triple-negative breast cancer. Cancer Research. 2020;80(4_Supplement):PD1-06-PD1-.
158. Buisseret L, Loirat D, Aftimos P, Maurer C, Punie K, Debien V, et al. Paclitaxel plus carboplatin and durvalumab with or without oleclumab for women with previously untreated locally advanced or metastatic triple-negative breast cancer: the randomized SYNERGY phase I/II trial. Nat Commun. 2023;14(1):7018.
159. Li Q, Liu J, Zhang Q, Ouyang Q, Zhang Y, Liu Q, et al. The anti-PD-L1/CTLA-4 bispecific antibody KN046 in combination with nab-paclitaxel in first-line treatment of metastatic triple-negative breast cancer: a multicenter phase II trial. Nat Commun. 2024;15(1):1015.
160. David S, Savas P, Siva S, White M, Neeson MW, White S, et al. Abstract PD10-02: A randomised phase II trial of single fraction or multi-fraction SABR (stereotactic ablative body radiotherapy) with atezolizumab in patients with advanced triple negative breast cancer (AZTEC trial). Cancer Research. 2022;82(4_Supplement):PD10-02-PD10-02.
161. Nguyen VP, Campbell KM, Nowicki TS, Elumalai N, Medina E, Baselga-Carretero I, et al. A Pilot Study of Neoadjuvant Nivolumab, Ipilimumab, and Intralesional Oncolytic Virotherapy for HER2-negative Breast Cancer. Cancer Res Commun. 2023;3(8):1628-37.
162. Liu J, Wang Y, Tian Z, Lin Y, Li H, Zhu Z, et al. Multicenter phase II trial of Camrelizumab combined with Apatinib and Eribulin in heavily pretreated patients with advanced triple-negative breast cancer. Nat Commun. 2022;13(1):3011.
163. Yam C, Mittendorf EA, Garber HR, Sun R, Damodaran S, Murthy RK, et al. A phase II study of neoadjuvant atezolizumab and nab-paclitaxel in patients with anthracycline-resistant early-stage triple-negative breast cancer. Breast Cancer Research and Treatment. 2023;199(3):457-69.
164. Tutt ANJ, Garber JE, Kaufman B, Viale G, Fumagalli D, Rastogi P, et al. Adjuvant Olaparib for Patients with BRCA1- or BRCA2-Mutated Breast Cancer. N Engl J Med. 2021;384(25):2394-405.
165. Domchek SM, Postel-Vinay S, Im SA, Park YH, Delord JP, Italiano A, et al. Olaparib and durvalumab in patients with germline BRCA-mutated metastatic breast cancer (MEDIOLA): an open-label, multicentre, phase 1/2, basket study. Lancet Oncol. 2020;21(9):1155-64.
166. Diab A, Hurwitz ME, Cho DC, Papadimitrakopoulou V, Curti BD, Tykodi SS, et al. NKTR-214 (CD122-biased agonist) plus nivolumab in patients with advanced solid tumors:

Preliminary phase 1/2 results of PIVOT. Journal of Clinical Oncology. 2018;36(15_suppl):3006-.
167. Yuan Y, Lee JS, Yost SE, Frankel PH, Ruel C, Egelston CA, et al. A Phase II Clinical Trial of Pembrolizumab and Enobosarm in Patients with Androgen Receptor-Positive Metastatic Triple-Negative Breast Cancer. Oncologist. 2021;26(2):99-e217.
168. Tutt A, Nowecki Z, Szoszkiewicz R, Im SA, Arkenau HT, Armstrong A, et al. 161O VIOLETTE: Randomised phase II study of olaparib (ola) + ceralasertib (cer) or adavosertib (ada) vs ola alone in patients (pts) with metastatic triple-negative breast cancer (mTNBC). Annals of Oncology. 2022;33:S194-S5.
169. Schmid P, Turner NC, Barrios CH, Isakoff SJ, Kim SB, Sablin MP, et al. First-Line Ipatasertib, Atezolizumab, and Taxane Triplet for Metastatic Triple-Negative Breast Cancer: Clinical and Biomarker Results. Clin Cancer Res. 2024;30(4):767-78.
170. Aguilar LK, Shirley LA, Chung VM, Marsh CL, Walker J, Coyle W, et al. Gene-mediated cytotoxic immunotherapy as adjuvant to surgery or chemoradiation for pancreatic adenocarcinoma. Cancer Immunology, Immunotherapy. 2015;64(6):727-36.
171. Ferrucci PF, Pala L, Conforti F, Cocorocchio E. Talimogene Laherparepvec (T-VEC): An Intralesional Cancer Immunotherapy for Advanced Melanoma. Cancers (Basel). 2021;13(6).
172. Woo Y, Zhang Z, Yang A, Chaurasiya S, Park AK, Lu J, et al. Novel Chimeric Immuno-Oncolytic Virus CF33-hNIS-antiPDL1 for the Treatment of Pancreatic Cancer. J Am Coll Surg. 2020;230(4):709-17.
173. Bardia A, Hurvitz SA, Tolaney SM, Loirat D, Punie K, Oliveira M, et al. Sacituzumab Govitecan in Metastatic Triple-Negative Breast Cancer. New England Journal of Medicine. 2021;384(16):1529-41.
174. Mathews DV, Dong Y, Higginbotham LB, Kim SC, Breeden CP, Stobert EA, et al. CD122 signaling in CD8+ memory T cells drives costimulation-independent rejection. J Clin Invest. 2018;128(10):4557-72.
175. Gan HK, Coward J, Mislang ARA, Cosman R, Nagrial A, Jin X, et al. Safety of AK117, an anti-CD47 monoclonal antibody, in patients with advanced or metastatic solid tumors in a phase I study. Journal of Clinical Oncology. 2021;39(15_suppl):2630-.
176. Saxena M, van der Burg SH, Melief CJM, Bhardwaj N. Therapeutic cancer vaccines. Nature Reviews Cancer. 2021;21(6):360-78.
177. Nooka AK, Wang ML, Yee AJ, Kaufman JL, Bae J, Peterkin D, et al. Assessment of Safety and Immunogenicity of PVX-410 Vaccine With or Without Lenalidomide in Patients With Smoldering Multiple Myeloma: A Nonrandomized Clinical Trial. JAMA Oncol. 2018;4(12):e183267.
178. McCarthy PM, Clifton GT, Vreeland TJ, Adams AM, O'Shea AE, Peoples GE. AE37: a HER2-targeted vaccine for the prevention of breast cancer recurrence. Expert Opin Investig Drugs. 2021;30(1):5-11.
179. Raimondo MG, Biggioggero M, Crotti C, Becciolini A, Favalli EG. Profile of sarilumab and its potential in the treatment of rheumatoid arthritis. Drug Des Devel Ther. 2017;11:1593-603.
180. Algazi A, Bhatia S, Agarwala S, Molina M, Lewis K, Faries M, et al. Intratumoral delivery of tavokinogene telseplasmid yields systemic immune responses in metastatic melanoma patients. Annals of Oncology. 2020;31(4):532-40.
181. Nathan MR, Schmid P. The emerging world of breast cancer immunotherapy. The Breast. 2018;37:200-6.
182. Zhang Q, Le K, Xu M, Zhou J, Xiao Y, Yang W, et al. Combined MEK inhibition and tumor-associated macrophages depletion suppresses tumor growth in a triple-negative breast cancer mouse model. Int Immunopharmacol. 2019;76:105864.
183. Zhang WJ, Wang XH, Gao ST, Chen C, Xu XY, Sun Q, et al. Tumor-associated macrophages correlate with phenomenon of epithelial-mesenchymal transition and

contribute to poor prognosis in triple-negative breast cancer patients. J Surg Res. 2018;222:93-101.
184. Kumar S, Wilkes DW, Samuel N, Blanco MA, Nayak A, Alicea-Torres K, et al. ΔNp63-driven recruitment of myeloid-derived suppressor cells promotes metastasis in triple-negative breast cancer. J Clin Invest. 2018;128(11):5095-109.
185. Piranlioglu R, Lee E, Ouzounova M, Bollag RJ, Vinyard AH, Arbab AS, et al. Primary tumor-induced immunity eradicates disseminated tumor cells in syngeneic mouse model. Nat Commun. 2019;10(1):1430.
186. Zareinejad M, Mehdipour F, Roshan-Zamir M, Faghih Z, Ghaderi A. Dual Functions of T Lymphocytes in Breast Carcinoma: From Immune Protection to Orchestrating Tumor Progression and Metastasis. Cancers (Basel). 2023;15(19).
187. Walker JA, McKenzie ANJ. TH2 cell development and function. Nature Reviews Immunology. 2018;18(2):121-33.
188. Hong CC, Yao S, McCann SE, Dolnick RY, Wallace PK, Gong Z, et al. Pretreatment levels of circulating Th1 and Th2 cytokines, and their ratios, are associated with ER-negative and triple negative breast cancers. Breast Cancer Res Treat. 2013;139(2):477-88.
189. Shibabaw T, Teferi B, Ayelign B. The role of Th-17 cells and IL-17 in the metastatic spread of breast cancer: As a means of prognosis and therapeutic target. Front Immunol. 2023;14:1094823.
190. Yang L, Qi Y, Hu J, Tang L, Zhao S, Shan B. Expression of Th17 cells in breast cancer tissue and its association with clinical parameters. Cell Biochem Biophys. 2012;62(1):153-9.
191. Faucheux L, Grandclaudon M, Perrot-Dockès M, Sirven P, Berger F, Hamy AS, et al. A multivariate Th17 metagene for prognostic stratification in T cell non-inflamed triple negative breast cancer. Oncoimmunology. 2019;8(9):e1624130.
192. Zheng H, Siddharth S, Parida S, Wu X, Sharma D. Tumor Microenvironment: Key Players in Triple Negative Breast Cancer Immunomodulation. Cancers (Basel). 2021;13(13).
193. Taylor NA, Vick SC, Iglesia MD, Brickey WJ, Midkiff BR, McKinnon KP, et al. Treg depletion potentiates checkpoint inhibition in claudin-low breast cancer. J Clin Invest. 2017;127(9):3472-83.
194. Jamiyan T, Kuroda H, Yamaguchi R, Nakazato Y, Noda S, Onozaki M, et al. Prognostic impact of a tumor-infiltrating lymphocyte subtype in triple negative cancer of the breast. Breast Cancer. 2020;27(5):880-92.
195. Rosemblit C, Datta J, Lowenfeld L, Xu S, Basu A, Kodumudi K, et al. Oncodriver inhibition and CD4 + Th1 cytokines cooperate through Stat1 activation to induce tumor senescence and apoptosis in HER2+ and triple negative breast cancer: implications for combining immune and targeted therapies. Oncotarget. 2018;9(33).
196. Shang L, Zhong Y, Yao Y, Liu C, Wang L, Zhang W, et al. Subverted macrophages in the triple-negative breast cancer ecosystem. Biomedicine & Pharmacotherapy. 2023;166:115414.
197. Oshi M, Asaoka M, Tokumaru Y, Yan L, Matsuyama R, Ishikawa T, et al. CD8 T Cell Score as a Prognostic Biomarker for Triple Negative Breast Cancer. Int J Mol Sci. 2020;21(18).
198. Thacker G, Henry S, Nandi A, Debnath R, Singh S, Nayak A, et al. Immature natural killer cells promote progression of triple-negative breast cancer. Sci Transl Med. 2023;15(686):eabl4414.
199. Juliá EP, Mordoh J, Levy EM. Cetuximab and IL-15 Promote NK and Dendritic Cell Activation In Vitro in Triple Negative Breast Cancer. Cells. 2020;9(7):1573.
200. Siegel RL, Miller KD, Jemal A. Cancer Statistics, 2017. CA Cancer J Clin. 2017;67(1):7-30.
201. Kannan S, Shaik Syed Ali P, Sheeza A. Short report - Lethal and aggressive pancreatic cancer: molecular pathogenesis, cellular heterogeneity, and biomarkers of pancreatic ductal adenocarcinoma. Eur Rev Med Pharmacol Sci. 2022;26(3):1017-9.

202. Ushio J, Kanno A, Ikeda E, Ando K, Nagai H, Miwata T, et al. Pancreatic Ductal Adenocarcinoma: Epidemiology and Risk Factors. Diagnostics (Basel). 2021;11(3).
203. Groot VP, Gemenetzis G, Blair AB, Ding D, Javed AA, Burkhart RA, et al. Implications of the Pattern of Disease Recurrence on Survival Following Pancreatectomy for Pancreatic Ductal Adenocarcinoma. Ann Surg Oncol. 2018;25(8):2475-83.
204. Ratnayake B, Savastyuk AY, Nayar M, Wilson CH, Windsor JA, Roberts K, et al. Recurrence Patterns for Pancreatic Ductal Adenocarcinoma after Upfront Resection Versus Resection Following Neoadjuvant Therapy: A Comprehensive Meta-Analysis. J Clin Med. 2020;9(7).
205. Fang YT, Yang WW, Niu YR, Sun YK. Recent advances in targeted therapy for pancreatic adenocarcinoma. World J Gastrointest Oncol. 2023;15(4):571-95.
206. Collisson EA, Sadanandam A, Olson P, Gibb WJ, Truitt M, Gu S, et al. Subtypes of pancreatic ductal adenocarcinoma and their differing responses to therapy. Nature Medicine. 2011;17(4):500-3.
207. Bailey P, Chang DK, Nones K, Johns AL, Patch A-M, Gingras M-C, et al. Genomic analyses identify molecular subtypes of pancreatic cancer. Nature. 2016;531(7592):47-52.
208. Moffitt RA, Marayati R, Flate EL, Volmar KE, Loeza SGH, Hoadley KA, et al. Virtual microdissection identifies distinct tumor- and stroma-specific subtypes of pancreatic ductal adenocarcinoma. Nature Genetics. 2015;47(10):1168-78.
209. Shen H, Lundy J, Strickland AH, Harris M, Swan M, Desmond C, et al. KRAS G12D Mutation Subtype in Pancreatic Ductal Adenocarcinoma: Does It Influence Prognosis or Stage of Disease at Presentation? Cells. 2022;11(19).
210. Colicelli J. Human RAS superfamily proteins and related GTPases. Sci STKE. 2004;2004(250):Re13.
211. Buscail L, Bournet B, Cordelier P. Role of oncogenic KRAS in the diagnosis, prognosis and treatment of pancreatic cancer. Nature Reviews Gastroenterology & Hepatology. 2020;17(3):153-68.
212. Ischenko I, D'Amico S, Rao M, Li J, Hayman MJ, Powers S, et al. KRAS drives immune evasion in a genetic model of pancreatic cancer. Nature Communications. 2021;12(1):1482.
213. Kemp SB, Cheng N, Markosyan N, Sor R, Kim IK, Hallin J, et al. Efficacy of a Small-Molecule Inhibitor of KrasG12D in Immunocompetent Models of Pancreatic Cancer. Cancer Discov. 2023;13(2):298-311.
214. Mahadevan KK, LeBleu VS, Ramirez EV, Chen Y, Li B, Sockwell AM, et al. Elimination of oncogenic KRAS in genetic mouse models eradicates pancreatic cancer by inducing FAS-dependent apoptosis by CD8+ T cells. Developmental Cell. 2023;58(17):1562-77.e8.
215. Macdonald JS, McCoy S, Whitehead RP, Iqbal S, Wade JL, 3rd, Giguere JK, et al. A phase II study of farnesyl transferase inhibitor R115777 in pancreatic cancer: a Southwest oncology group (SWOG 9924) study. Invest New Drugs. 2005;23(5):485-7.
216. Skoulidis F, Li BT, Dy GK, Price TJ, Falchook GS, Wolf J, et al. Sotorasib for Lung Cancers with KRAS p.G12C Mutation. New England Journal of Medicine. 2021;384(25):2371-81.
217. Wei D, Wang L, Zuo X, Maitra A, Bresalier RS. A Small Molecule with Big Impact: MRTX1133 Targets the KRASG12D Mutation in Pancreatic Cancer. Clinical Cancer Research. 2024;30(4):655-62.
218. Ullah R, Yin Q, Snell AH, Wan L. RAF-MEK-ERK pathway in cancer evolution and treatment. Semin Cancer Biol. 2022;85:123-54.
219. Rinehart J, Adjei AA, Lorusso PM, Waterhouse D, Hecht JR, Natale RB, et al. Multicenter phase II study of the oral MEK inhibitor, CI-1040, in patients with advanced non-small-cell lung, breast, colon, and pancreatic cancer. J Clin Oncol. 2004;22(22):4456-62.
220. Bodoky G, Timcheva C, Spigel DR, La Stella PJ, Ciuleanu TE, Pover G, et al. A phase II open-label randomized study to assess the efficacy and safety of selumetinib

(AZD6244 [ARRY-142886]) versus capecitabine in patients with advanced or metastatic pancreatic cancer who have failed first-line gemcitabine therapy. Invest New Drugs. 2012;30(3):1216-23.
221. Van Cutsem E, Hidalgo M, Canon JL, Macarulla T, Bazin I, Poddubskaya E, et al. Phase I/II trial of pimasertib plus gemcitabine in patients with metastatic pancreatic cancer. Int J Cancer. 2018;143(8):2053-64.
222. Infante JR, Somer BG, Park JO, Li CP, Scheulen ME, Kasubhai SM, et al. A randomised, double-blind, placebo-controlled trial of trametinib, an oral MEK inhibitor, in combination with gemcitabine for patients with untreated metastatic adenocarcinoma of the pancreas. Eur J Cancer. 2014;50(12):2072-81.
223. van Brummelen EMJ, Huijberts S, van Herpen C, Desar I, Opdam F, van Geel R, et al. Phase I Study of Afatinib and Selumetinib in Patients with KRAS-Mutated Colorectal, Non-Small Cell Lung, and Pancreatic Cancer. Oncologist. 2021;26(4):290-e545.
224. Chung V, McDonough S, Philip PA, Cardin D, Wang-Gillam A, Hui L, et al. Effect of Selumetinib and MK-2206 vs Oxaliplatin and Fluorouracil in Patients With Metastatic Pancreatic Cancer After Prior Therapy: SWOG S1115 Study Randomized Clinical Trial. JAMA Oncol. 2017;3(4):516-22.
225. Yamamoto S, Tomita Y, Hoshida Y, Morooka T, Nagano H, Dono K, et al. Prognostic significance of activated Akt expression in pancreatic ductal adenocarcinoma. Clin Cancer Res. 2004;10(8):2846-50.
226. Fei HR, Chen G, Wang JM, Wang FZ. Perifosine induces cell cycle arrest and apoptosis in human hepatocellular carcinoma cell lines by blockade of Akt phosphorylation. Cytotechnology. 2010;62(5):449-60.
227. Wolpin BM, Hezel AF, Abrams T, Blaszkowsky LS, Meyerhardt JA, Chan JA, et al. Oral mTOR inhibitor everolimus in patients with gemcitabine-refractory metastatic pancreatic cancer. J Clin Oncol. 2009;27(2):193-8.
228. Kordes S, Klümpen HJ, Weterman MJ, Schellens JH, Richel DJ, Wilmink JW. Phase II study of capecitabine and the oral mTOR inhibitor everolimus in patients with advanced pancreatic cancer. Cancer Chemother Pharmacol. 2015;75(6):1135-41.
229. Maddalena M, Mallel G, Nataraj NB, Shreberk-Shaked M, Hassin O, Mukherjee S, et al. TP53 missense mutations in PDAC are associated with enhanced fibrosis and an immunosuppressive microenvironment. Proc Natl Acad Sci U S A. 2021;118(23).
230. Valsecchi ME, McDonald M, Brody JR, Hyslop T, Freydin B, Yeo CJ, et al. Epidermal growth factor receptor and insulinlike growth factor 1 receptor expression predict poor survival in pancreatic ductal adenocarcinoma. Cancer. 2012;118(14):3484-93.
231. Moore MJ, Goldstein D, Hamm J, Figer A, Hecht JR, Gallinger S, et al. Erlotinib plus gemcitabine compared with gemcitabine alone in patients with advanced pancreatic cancer: a phase III trial of the National Cancer Institute of Canada Clinical Trials Group. J Clin Oncol. 2007;25(15):1960-6.
232. Kelley RK, Ko AH. Erlotinib in the treatment of advanced pancreatic cancer. Biologics. 2008;2(1):83-95.
233. Schultheis B, Reuter D, Ebert MP, Siveke J, Kerkhoff A, Berdel WE, et al. Gemcitabine combined with the monoclonal antibody nimotuzumab is an active first-line regimen in KRAS wildtype patients with locally advanced or metastatic pancreatic cancer: a multicenter, randomized phase IIb study. Ann Oncol. 2017;28(10):2429-35.
234. Qin S, Bai Y, Wang Z, Chen Z, Xu R, Xu J, et al. Nimotuzumab combined with gemcitabine versus gemcitabine in K-RAS wild-type locally advanced or metastatic pancreatic cancer: A prospective, randomized-controlled, double-blinded, multicenter, and phase III clinical trial. Journal of Clinical Oncology. 2022;40(17_suppl):LBA4011-LBA.
235. Graeven U, Kremer B, Südhoff T, Killing B, Rojo F, Weber D, et al. Phase I study of the humanised anti-EGFR monoclonal antibody matuzumab (EMD 72000) combined with gemcitabine in advanced pancreatic cancer. Br J Cancer. 2006;94(9):1293-9.

236. Halfdanarson TR, Foster NR, Kim GP, Meyers JP, Smyrk TC, McCullough AE, et al. A Phase II Randomized Trial of Panitumumab, Erlotinib, and Gemcitabine Versus Erlotinib and Gemcitabine in Patients with Untreated, Metastatic Pancreatic Adenocarcinoma: North Central Cancer Treatment Group Trial N064B (Alliance). Oncologist. 2019;24(5):589-e160.
237. Philip PA, Benedetti J, Corless CL, Wong R, O'Reilly EM, Flynn PJ, et al. Phase III study comparing gemcitabine plus cetuximab versus gemcitabine in patients with advanced pancreatic adenocarcinoma: Southwest Oncology Group-directed intergroup trial S0205. J Clin Oncol. 2010;28(22):3605-10.
238. Mihaljevic A, Büchler P, Harder J, Hofheinz R, Gregor M, Kanzler S, et al. A prospective, non-randomized phase II trial of Trastuzumab and Capecitabine in patients with HER2 expressing metastasized pancreatic cancer. BMC Surg. 2009;9:1.
239. Haas M, Waldschmidt DT, Stahl M, Reinacher-Schick A, Freiberg-Richter J, Fischer von Weikersthal L, et al. Afatinib plus gemcitabine versus gemcitabine alone as first-line treatment of metastatic pancreatic cancer: The randomised, open-label phase II ACCEPT study of the Arbeitsgemeinschaft Internistische Onkologie with an integrated analysis of the 'burden of therapy' method. Eur J Cancer. 2021;146:95-106.
240. Mutgan AC, Besikcioglu HE, Wang S, Friess H, Ceyhan GO, Demir IE. Insulin/IGF-driven cancer cell-stroma crosstalk as a novel therapeutic target in pancreatic cancer. Mol Cancer. 2018;17(1):66.
241. Fuchs CS, Azevedo S, Okusaka T, Van Laethem JL, Lipton LR, Riess H, et al. A phase 3 randomized, double-blind, placebo-controlled trial of ganitumab or placebo in combination with gemcitabine as first-line therapy for metastatic adenocarcinoma of the pancreas: the GAMMA trial. Ann Oncol. 2015;26(5):921-7.
242. Abdel-Wahab R, Varadhachary GR, Bhosale PR, Wang X, Fogelman DR, Shroff RT, et al. Randomized, phase I/II study of gemcitabine plus IGF-1R antagonist (MK-0646) versus gemcitabine plus erlotinib with and without MK-0646 for advanced pancreatic adenocarcinoma. J Hematol Oncol. 2018;11(1):71.
243. Kuehn R, Lelkes PI, Bloechle C, Niendorf A, Izbicki JR. Angiogenesis, angiogenic growth factors, and cell adhesion molecules are upregulated in chronic pancreatic diseases: angiogenesis in chronic pancreatitis and in pancreatic cancer. Pancreas. 1999;18(1):96-103.
244. Van Cutsem E, Vervenne WL, Bennouna J, Humblet Y, Gill S, Van Laethem JL, et al. Phase III trial of bevacizumab in combination with gemcitabine and erlotinib in patients with metastatic pancreatic cancer. J Clin Oncol. 2009;27(13):2231-7.
245. Ko AH, Venook AP, Bergsland EK, Kelley RK, Korn WM, Dito E, et al. A phase II study of bevacizumab plus erlotinib for gemcitabine-refractory metastatic pancreatic cancer. Cancer Chemother Pharmacol. 2010;66(6):1051-7.
246. Pàez-Ribes M, Allen E, Hudock J, Takeda T, Okuyama H, Viñals F, et al. Antiangiogenic therapy elicits malignant progression of tumors to increased local invasion and distant metastasis. Cancer Cell. 2009;15(3):220-31.
247. Taeger J, Moser C, Hellerbrand C, Mycielska ME, Glockzin G, Schlitt HJ, et al. Targeting FGFR/PDGFR/VEGFR impairs tumor growth, angiogenesis, and metastasis by effects on tumor cells, endothelial cells, and pericytes in pancreatic cancer. Mol Cancer Ther. 2011;10(11):2157-67.
248. Rougier P, Riess H, Manges R, Karasek P, Humblet Y, Barone C, et al. Randomised, placebo-controlled, double-blind, parallel-group phase III study evaluating aflibercept in patients receiving first-line treatment with gemcitabine for metastatic pancreatic cancer. Eur J Cancer. 2013;49(12):2633-42.
249. Gonçalves A, Gilabert M, François E, Dahan L, Perrier H, Lamy R, et al. BAYPAN study: a double-blind phase III randomized trial comparing gemcitabine plus sorafenib and gemcitabine plus placebo in patients with advanced pancreatic cancer. Ann Oncol. 2012;23(11):2799-805.

250. Han B, Li K, Wang Q, Zhang L, Shi J, Wang Z, et al. Effect of Anlotinib as a Third-Line or Further Treatment on Overall Survival of Patients With Advanced Non-Small Cell Lung Cancer: The ALTER 0303 Phase 3 Randomized Clinical Trial. JAMA Oncol. 2018;4(11):1569-75.
251. de Mestier L, Danset JB, Neuzillet C, Rebours V, Cros J, Soufir N, et al. Pancreatic ductal adenocarcinoma in BRCA2 mutation carriers. Endocr Relat Cancer. 2016;23(10):T57-67.
252. Kaufman B, Shapira-Frommer R, Schmutzler RK, Audeh MW, Friedlander M, Balmaña J, et al. Olaparib monotherapy in patients with advanced cancer and a germline BRCA1/2 mutation. J Clin Oncol. 2015;33(3):244-50.
253. Golan T, Hammel P, Reni M, Van Cutsem E, Macarulla T, Hall MJ, et al. Maintenance Olaparib for Germline BRCA-Mutated Metastatic Pancreatic Cancer. N Engl J Med. 2019;381(4):317-27.
254. Lowery MA, Kelsen DP, Capanu M, Smith SC, Lee JW, Stadler ZK, et al. Phase II trial of veliparib in patients with previously treated BRCA-mutated pancreas ductal adenocarcinoma. Eur J Cancer. 2018;89:19-26.
255. Shroff RT, Hendifar A, McWilliams RR, Geva R, Epelbaum R, Rolfe L, et al. Rucaparib Monotherapy in Patients With Pancreatic Cancer and a Known Deleterious BRCA Mutation. JCO Precis Oncol. 2018;2018.
256. Venkatasubbarao K, Peterson L, Zhao S, Hill P, Cao L, Zhou Q, et al. Inhibiting signal transducer and activator of transcription-3 increases response to gemcitabine and delays progression of pancreatic cancer. Mol Cancer. 2013;12(1):104.
257. Beatty GL, Shahda S, Beck T, Uppal N, Cohen SJ, Donehower R, et al. A Phase Ib/II Study of the JAK1 Inhibitor, Itacitinib, plus nab-Paclitaxel and Gemcitabine in Advanced Solid Tumors. Oncologist. 2019;24(1):14-e0.
258. De Jesus-Acosta A, Laheru D, Maitra A, Arcaroli J, Rudek MA, Dasari A, et al. A phase II study of the gamma secretase inhibitor RO4929097 in patients with previously treated metastatic pancreatic adenocarcinoma. Invest New Drugs. 2014;32(4):739-45.
259. Cook N, Basu B, Smith DM, Gopinathan A, Evans J, Steward WP, et al. A phase I trial of the γ-secretase inhibitor MK-0752 in combination with gemcitabine in patients with pancreatic ductal adenocarcinoma. Br J Cancer. 2018;118(6):793-801.
260. Hu ZI, Bendell JC, Bullock A, LoConte NK, Hatoum H, Ritch P, et al. A randomized phase II trial of nab-paclitaxel and gemcitabine with tarextumab or placebo in patients with untreated metastatic pancreatic cancer. Cancer Med. 2019;8(11):5148-57.
261. Gaspar NJ, Li L, Kapoun AM, Medicherla S, Reddy M, Li G, et al. Inhibition of transforming growth factor beta signaling reduces pancreatic adenocarcinoma growth and invasiveness. Mol Pharmacol. 2007;72(1):152-61.
262. Schlingensiepen KH, Jaschinski F, Lang SA, Moser C, Geissler EK, Schlitt HJ, et al. Transforming growth factor-beta 2 gene silencing with trabedersen (AP 12009) in pancreatic cancer. Cancer Sci. 2011;102(6):1193-200.
263. Melisi D, Garcia-Carbonero R, Macarulla T, Pezet D, Deplanque G, Fuchs M, et al. Galunisertib plus gemcitabine vs. gemcitabine for first-line treatment of patients with unresectable pancreatic cancer. Br J Cancer. 2018;119(10):1208-14.
264. Melisi D, Oh DY, Hollebecque A, Calvo E, Varghese A, Borazanci E, et al. Safety and activity of the TGFβ receptor I kinase inhibitor galunisertib plus the anti-PD-L1 antibody durvalumab in metastatic pancreatic cancer. J Immunother Cancer. 2021;9(3).
265. Olive KP, Jacobetz MA, Davidson CJ, Gopinathan A, McIntyre D, Honess D, et al. Inhibition of Hedgehog signaling enhances delivery of chemotherapy in a mouse model of pancreatic cancer. Science. 2009;324(5933):1457-61.
266. Rhim AD, Oberstein PE, Thomas DH, Mirek ET, Palermo CF, Sastra SA, et al. Stromal elements act to restrain, rather than support, pancreatic ductal adenocarcinoma. Cancer Cell. 2014;25(6):735-47.

267. Lafaro KJ, Melstrom LG. The Paradoxical Web of Pancreatic Cancer Tumor Microenvironment. Am J Pathol. 2019;189(1):44-57.
268. Ko AH, LoConte N, Tempero MA, Walker EJ, Kate Kelley R, Lewis S, et al. A Phase I Study of FOLFIRINOX Plus IPI-926, a Hedgehog Pathway Inhibitor, for Advanced Pancreatic Adenocarcinoma. Pancreas. 2016;45(3):370-5.
269. Catenacci DV, Junttila MR, Karrison T, Bahary N, Horiba MN, Nattam SR, et al. Randomized Phase Ib/II Study of Gemcitabine Plus Placebo or Vismodegib, a Hedgehog Pathway Inhibitor, in Patients With Metastatic Pancreatic Cancer. J Clin Oncol. 2015;33(36):4284-92.
270. De Jesus-Acosta A, Sugar EA, O'Dwyer PJ, Ramanathan RK, Von Hoff DD, Rasheed Z, et al. Phase 2 study of vismodegib, a hedgehog inhibitor, combined with gemcitabine and nab-paclitaxel in patients with untreated metastatic pancreatic adenocarcinoma. Br J Cancer. 2020;122(4):498-505.
271. Tahkola K, Ahtiainen M, Mecklin J-P, Kellokumpu I, Laukkarinen J, Tammi M, et al. Stromal hyaluronan accumulation is associated with low immune response and poor prognosis in pancreatic cancer. Scientific Reports. 2021;11(1):12216.
272. Hingorani SR, Zheng L, Bullock AJ, Seery TE, Harris WP, Sigal DS, et al. HALO 202: Randomized Phase II Study of PEGPH20 Plus Nab-Paclitaxel/Gemcitabine Versus Nab-Paclitaxel/Gemcitabine in Patients With Untreated, Metastatic Pancreatic Ductal Adenocarcinoma. J Clin Oncol. 2018;36(4):359-66.
273. Ramanathan RK, McDonough SL, Philip PA, Hingorani SR, Lacy J, Kortmansky JS, et al. Phase IB/II Randomized Study of FOLFIRINOX Plus Pegylated Recombinant Human Hyaluronidase Versus FOLFIRINOX Alone in Patients With Metastatic Pancreatic Adenocarcinoma: SWOG S1313. J Clin Oncol. 2019;37(13):1062-9.
274. Ko AH, Kim KP, Siveke JT, Lopez CD, Lacy J, O'Reilly EM, et al. Atezolizumab Plus PEGPH20 Versus Chemotherapy in Advanced Pancreatic Ductal Adenocarcinoma and Gastric Cancer: MORPHEUS Phase Ib/II Umbrella Randomized Study Platform. Oncologist. 2023;28(6):553-e472.
275. Piperigkou Z, Kyriakopoulou K, Koutsakis C, Mastronikolis S, Karamanos NK. Key Matrix Remodeling Enzymes: Functions and Targeting in Cancer. Cancers (Basel). 2021;13(6).
276. Bramhall SR, Rosemurgy A, Brown PD, Bowry C, Buckels JA. Marimastat as first-line therapy for patients with unresectable pancreatic cancer: a randomized trial. J Clin Oncol. 2001;19(15):3447-55.
277. Bramhall SR, Schulz J, Nemunaitis J, Brown PD, Baillet M, Buckels JA. A double-blind placebo-controlled, randomised study comparing gemcitabine and marimastat with gemcitabine and placebo as first line therapy in patients with advanced pancreatic cancer. Br J Cancer. 2002;87(2):161-7.
278. Moore MJ, Hamm J, Dancey J, Eisenberg PD, Dagenais M, Fields A, et al. Comparison of gemcitabine versus the matrix metalloproteinase inhibitor BAY 12-9566 in patients with advanced or metastatic adenocarcinoma of the pancreas: a phase III trial of the National Cancer Institute of Canada Clinical Trials Group. J Clin Oncol. 2003;21(17):3296-302.
279. Bendell J, Sharma S, Patel MR, Windsor KS, Wainberg ZA, Gordon M, et al. Safety and Efficacy of Andecaliximab (GS-5745) Plus Gemcitabine and Nab-Paclitaxel in Patients with Advanced Pancreatic Adenocarcinoma: Results from a Phase I Study. Oncologist. 2020;25(11):954-62.
280. Neuzillet C, Tijeras-Raballand A, Ragulan C, Cros J, Patil Y, Martinet M, et al. Inter- and intra-tumoural heterogeneity in cancer-associated fibroblasts of human pancreatic ductal adenocarcinoma. J Pathol. 2019;248(1):51-65.
281. Poudel P, Nyamundanda G, Ragulan C, Lawlor RT, Das K, Tan P, et al. Revealing unidentified heterogeneity in different epithelial cancers using heterocellular subtype classification. bioRxiv. 2017:175505.

282. Liudahl SM, Betts CB, Sivagnanam S, Morales-Oyarvide V, da Silva A, Yuan C, et al. Leukocyte Heterogeneity in Pancreatic Ductal Adenocarcinoma: Phenotypic and Spatial Features Associated with Clinical Outcome. Cancer Discov. 2021;11(8):2014-31.
283. Borghaei H, Paz-Ares L, Horn L, Spigel DR, Steins M, Ready NE, et al. Nivolumab versus Docetaxel in Advanced Nonsquamous Non-Small-Cell Lung Cancer. N Engl J Med. 2015;373(17):1627-39.
284. Motzer RJ, Escudier B, McDermott DF, George S, Hammers HJ, Srinivas S, et al. Nivolumab versus Everolimus in Advanced Renal-Cell Carcinoma. N Engl J Med. 2015;373(19):1803-13.
285. Sharma P, Callahan MK, Bono P, Kim J, Spiliopoulou P, Calvo E, et al. Nivolumab monotherapy in recurrent metastatic urothelial carcinoma (CheckMate 032): a multicentre, open-label, two-stage, multi-arm, phase 1/2 trial. Lancet Oncol. 2016;17(11):1590-8.
286. Robert C, Long GV, Brady B, Dutriaux C, Maio M, Mortier L, et al. Nivolumab in previously untreated melanoma without BRAF mutation. N Engl J Med. 2015;372(4):320-30.
287. Royal RE, Levy C, Turner K, Mathur A, Hughes M, Kammula US, et al. Phase 2 trial of single agent Ipilimumab (anti-CTLA-4) for locally advanced or metastatic pancreatic adenocarcinoma. J Immunother. 2010;33(8):828-33.
288. Herpels M, Ishihara J, Sadanandam A. The clinical terrain of immunotherapies in heterogeneous pancreatic cancer: unravelling challenges and opportunities. J Pathol. 2023;260(5):533-50.
289. Brahmer JR, Tykodi SS, Chow LQ, Hwu WJ, Topalian SL, Hwu P, et al. Safety and activity of anti-PD-L1 antibody in patients with advanced cancer. N Engl J Med. 2012;366(26):2455-65.
290. Aglietta M, Barone C, Sawyer MB, Moore MJ, Miller WH, Jr., Bagalà C, et al. A phase I dose escalation trial of tremelimumab (CP-675,206) in combination with gemcitabine in chemotherapy-naive patients with metastatic pancreatic cancer. Ann Oncol. 2014;25(9):1750-5.
291. Kamath SD, Kalyan A, Kircher S, Nimeiri H, Fought AJ, Benson A, 3rd, et al. Ipilimumab and Gemcitabine for Advanced Pancreatic Cancer: A Phase Ib Study. Oncologist. 2020;25(5):e808-e15.
292. Kalyan A, Kircher SM, Mohindra NA, Nimeiri HS, Maurer V, Rademaker A, et al. Ipilimumab and gemcitabine for advanced pancreas cancer: A phase Ib study. Journal of Clinical Oncology. 2016;34(15_suppl):e15747-e.
293. Mohindra NA, Kircher SM, Nimeiri HS, Benson AB, Rademaker A, Alonso E, et al. Results of the phase Ib study of ipilimumab and gemcitabine for advanced pancreas cancer. Journal of Clinical Oncology. 2015;33(15_suppl):e15281-e.
294. Weiss GJ, Waypa J, Blaydorn L, Coats J, McGahey K, Sangal A, et al. A phase Ib study of pembrolizumab plus chemotherapy in patients with advanced cancer (PembroPlus). British Journal of Cancer. 2017;117(1):33-40.
295. Weiss GJ, Blaydorn L, Beck J, Bornemann-Kolatzki K, Urnovitz H, Schütz E, et al. Phase Ib/II study of gemcitabine, nab-paclitaxel, and pembrolizumab in metastatic pancreatic adenocarcinoma. Investigational New Drugs. 2018;36(1):96-102.
296. Marabelle A, Le DT, Ascierto PA, Di Giacomo AM, De Jesus-Acosta A, Delord JP, et al. Efficacy of Pembrolizumab in Patients With Noncolorectal High Microsatellite Instability/Mismatch Repair-Deficient Cancer: Results From the Phase II KEYNOTE-158 Study. J Clin Oncol. 2020;38(1):1-10.
297. Hong D, Rasco D, Veeder M, Luke JJ, Chandler J, Balmanoukian A, et al. A Phase 1b/2 Study of the Bruton Tyrosine Kinase Inhibitor Ibrutinib and the PD-L1 Inhibitor Durvalumab in Patients with Pretreated Solid Tumors. Oncology. 2019;97(2):102-11.
298. Rahma OE, Katz MHG, Wolpin BM, Dias-Costa A, Nowak J, Rodig SJ, et al. Randomized multicenter phase Ib/II study of neoadjuvant chemoradiation therapy (CRT)

alone or in combination with pembrolizumab in patients with resectable or borderline resectable pancreatic cancer. Journal of Clinical Oncology. 2021;39(15_suppl):4128-.
299. Parikh AR, Szabolcs A, Allen JN, Clark JW, Wo JY, Raabe M, et al. Radiation therapy enhances immunotherapy response in microsatellite stable colorectal and pancreatic adenocarcinoma in a phase II trial. Nature Cancer. 2021;2(11):1124-35.
300. Xie C, Duffy AG, Brar G, Fioravanti S, Mabry-Hrones D, Walker M, et al. Immune Checkpoint Blockade in Combination with Stereotactic Body Radiotherapy in Patients with Metastatic Pancreatic Ductal Adenocarcinoma. Clinical Cancer Research. 2020;26(10):2318-26.
301. Karamitopoulou E, Andreou A, Wenning AS, Gloor B, Perren A. High tumor mutational burden (TMB) identifies a microsatellite stable pancreatic cancer subset with prolonged survival and strong anti-tumor immunity. European Journal of Cancer. 2022;169:64-73.
302. Imamura T, Ashida R, Ohshima K, Uesaka K, Sugiura T, Ohgi K, et al. Characterization of pancreatic cancer with ultra-low tumor mutational burden. Scientific Reports. 2023;13(1):4359.
303. McGranahan N, Furness AJ, Rosenthal R, Ramskov S, Lyngaa R, Saini SK, et al. Clonal neoantigens elicit T cell immunoreactivity and sensitivity to immune checkpoint blockade. Science. 2016;351(6280):1463-9.
304. Eroglu Z, Zaretsky JM, Hu-Lieskovan S, Kim DW, Algazi A, Johnson DB, et al. High response rate to PD-1 blockade in desmoplastic melanomas. Nature. 2018;553(7688):347-50.
305. Rizvi NA, Hellmann MD, Snyder A, Kvistborg P, Makarov V, Havel JJ, et al. Mutational landscape determines sensitivity to PD-1 blockade in non–small cell lung cancer. Science. 2015;348(6230):124-8.
306. Tumeh PC, Harview CL, Yearley JH, Shintaku IP, Taylor EJ, Robert L, et al. PD-1 blockade induces responses by inhibiting adaptive immune resistance. Nature. 2014;515(7528):568-71.
307. Le DT, Durham JN, Smith KN, Wang H, Bartlett BR, Aulakh LK, et al. Mismatch repair deficiency predicts response of solid tumors to PD-1 blockade. Science. 2017;357(6349):409-13.
308. Cohen AD, Diab A, Perales MA, Wolchok JD, Rizzuto G, Merghoub T, et al. Agonist anti-GITR antibody enhances vaccine-induced CD8(+) T-cell responses and tumor immunity. Cancer Res. 2006;66(9):4904-12.
309. Bartkowiak T, Curran MA. 4-1BB Agonists: Multi-Potent Potentiators of Tumor Immunity. Front Oncol. 2015;5:117.
310. O'Hara MH, O'Reilly EM, Varadhachary G, Wolff RA, Wainberg ZA, Ko AH, et al. CD40 agonistic monoclonal antibody APX005M (sotigalimab) and chemotherapy, with or without nivolumab, for the treatment of metastatic pancreatic adenocarcinoma: an open-label, multicentre, phase 1b study. Lancet Oncol. 2021;22(1):118-31.
311. Padrón LJ, Maurer DM, O'Hara MH, O'Reilly EM, Wolff RA, Wainberg ZA, et al. Sotigalimab and/or nivolumab with chemotherapy in first-line metastatic pancreatic cancer: clinical and immunologic analyses from the randomized phase 2 PRINCE trial. Nat Med. 2022;28(6):1167-77.
312. Dalgleish AG, Stebbing J, Adamson DJ, Arif SS, Bidoli P, Chang D, et al. Randomised, open-label, phase II study of gemcitabine with and without IMM-101 for advanced pancreatic cancer. Br J Cancer. 2016;115(7):789-96.
313. Noel M, O'Reilly EM, Wolpin BM, Ryan DP, Bullock AJ, Britten CD, et al. Phase 1b study of a small molecule antagonist of human chemokine (C-C motif) receptor 2 (PF-04136309) in combination with nab-paclitaxel/gemcitabine in first-line treatment of metastatic pancreatic ductal adenocarcinoma. Invest New Drugs. 2020;38(3):800-11.
314. Nywening TM, Wang-Gillam A, Sanford DE, Belt BA, Panni RZ, Cusworth BM, et al. Targeting tumour-associated macrophages with CCR2 inhibition in combination with

FOLFIRINOX in patients with borderline resectable and locally advanced pancreatic cancer: a single-centre, open-label, dose-finding, non-randomised, phase 1b trial. Lancet Oncol. 2016;17(5):651-62.
315. Beatty GL, Chiorean EG, Fishman MP, Saboury B, Teitelbaum UR, Sun W, et al. CD40 agonists alter tumor stroma and show efficacy against pancreatic carcinoma in mice and humans. Science. 2011;331(6024):1612-6.
316. Beatty GL, Torigian DA, Chiorean EG, Saboury B, Brothers A, Alavi A, et al. A phase I study of an agonist CD40 monoclonal antibody (CP-870,893) in combination with gemcitabine in patients with advanced pancreatic ductal adenocarcinoma. Clin Cancer Res. 2013;19(22):6286-95.
317. Wang-Gillam A, Plambeck-Suess S, Goedegebuure P, Simon PO, Mitchem JB, Hornick JR, et al. A phase I study of IMP321 and gemcitabine as the front-line therapy in patients with advanced pancreatic adenocarcinoma. Invest New Drugs. 2013;31(3):707-13.
318. Doi T, Muro K, Ishii H, Kato T, Tsushima T, Takenoyama M, et al. A Phase I Study of the Anti-CC Chemokine Receptor 4 Antibody, Mogamulizumab, in Combination with Nivolumab in Patients with Advanced or Metastatic Solid Tumors. Clinical Cancer Research. 2019;25(22):6614-22.
319. Bockorny B, Semenisty V, Macarulla T, Borazanci E, Wolpin BM, Stemmer SM, et al. BL-8040, a CXCR4 antagonist, in combination with pembrolizumab and chemotherapy for pancreatic cancer: the COMBAT trial. Nature Medicine. 2020;26(6):878-85.
320. Hidalgo M, Semenisty V, Bockorny B, Borazanci E, von Hoff DD, Feliu J, et al. A Multi-Center Phase IIA Trial to Assess the Safety and Efficacy of BL-8040 (a CXCR4 Inhibitor) in Combination with Pembrolizumab and Chemotherapy in Patients with Metastatic Pancreatic Adenocarcinoma (PDAC). Annals of Oncology. 2019;30:xi33.
321. Aoki T, Matsushita H, Hoshikawa M, Hasegawa K, Kokudo N, Kakimi K. Adjuvant combination therapy with gemcitabine and autologous γδ T-cell transfer in patients with curatively resected pancreatic cancer. Cytotherapy. 2017;19(4):473-85.
322. Kumai T, Mizukoshi E, Hashiba T, Nakagawa H, Kitahara M, Miyashita T, et al. Effect of adoptive T-cell immunotherapy on immunological parameters and prognosis in patients with advanced pancreatic cancer. Cytotherapy. 2021;23(2):137-45.
323. Thistlethwaite FC, Gilham DE, Guest RD, Rothwell DG, Pillai M, Burt DJ, et al. The clinical efficacy of first-generation carcinoembryonic antigen (CEACAM5)-specific CAR T cells is limited by poor persistence and transient pre-conditioning-dependent respiratory toxicity. Cancer Immunol Immunother. 2017;66(11):1425-36.
324. Katz SC, Moody AE, Guha P, Hardaway JC, Prince E, LaPorte J, et al. HITM-SURE: Hepatic immunotherapy for metastases phase Ib anti-CEA CAR-T study utilizing pressure enabled drug delivery. J Immunother Cancer. 2020;8(2).
325. Netsrithong R, Wattanapanitch M. Advances in Adoptive Cell Therapy Using Induced Pluripotent Stem Cell-Derived T Cells. Frontiers in Immunology. 2021;12.
326. Rozenbaum M, Meir A, Aharony Y, Itzhaki O, Schachter J, Bank I, et al. Gamma-Delta CAR-T Cells Show CAR-Directed and Independent Activity Against Leukemia. Front Immunol. 2020;11:1347.
327. Holmen Olofsson G, Idorn M, Carnaz Simões AM, Aehnlich P, Skadborg SK, Noessner E, et al. Vγ9Vδ2 T Cells Concurrently Kill Cancer Cells and Cross-Present Tumor Antigens. Frontiers in Immunology. 2021;12.
328. Lum LG, Thakur A, Al-Kadhimi Z, Colvin GA, Cummings FJ, Legare RD, et al. Targeted T-cell Therapy in Stage IV Breast Cancer: A Phase I Clinical Trial. Clin Cancer Res. 2015;21(10):2305-14.
329. Rojas LA, Sethna Z, Soares KC, Olcese C, Pang N, Patterson E, et al. Personalized RNA neoantigen vaccines stimulate T cells in pancreatic cancer. Nature. 2023.
330. Yanagimoto H, Shiomi H, Satoi S, Mine T, Toyokawa H, Yamamoto T, et al. A phase II study of personalized peptide vaccination combined with gemcitabine for non-resectable pancreatic cancer patients. Oncol Rep. 2010;24(3):795-801.

331. Bernhardt SL, Gjertsen MK, Trachsel S, Møller M, Eriksen JA, Meo M, et al. Telomerase peptide vaccination of patients with non-resectable pancreatic cancer: a dose escalating phase I/II study. British Journal of Cancer. 2006;95(11):1474-82.
332. Middleton G, Silcocks P, Cox T, Valle J, Wadsley J, Propper D, et al. Gemcitabine and capecitabine with or without telomerase peptide vaccine GV1001 in patients with locally advanced or metastatic pancreatic cancer (TeloVac): an open-label, randomised, phase 3 trial. The Lancet Oncology. 2014;15(8):829-40.
333. Zheng L, Ding D, Edil BH, Judkins C, Durham JN, Thomas DL, 2nd, et al. Vaccine-Induced Intratumoral Lymphoid Aggregates Correlate with Survival Following Treatment with a Neoadjuvant and Adjuvant Vaccine in Patients with Resectable Pancreatic Adenocarcinoma. Clin Cancer Res. 2021;27(5):1278-86.
334. Laheru D, Lutz E, Burke J, Biedrzycki B, Solt S, Onners B, et al. Allogeneic granulocyte macrophage colony-stimulating factor-secreting tumor immunotherapy alone or in sequence with cyclophosphamide for metastatic pancreatic cancer: a pilot study of safety, feasibility, and immune activation. Clin Cancer Res. 2008;14(5):1455-63.
335. Jaffee EM, Hruban RH, Biedrzycki B, Laheru D, Schepers K, Sauter PR, et al. Novel allogeneic granulocyte-macrophage colony-stimulating factor-secreting tumor vaccine for pancreatic cancer: a phase I trial of safety and immune activation. J Clin Oncol. 2001;19(1):145-56.
336. Lutz E, Yeo CJ, Lillemoe KD, Biedrzycki B, Kobrin B, Herman J, et al. A lethally irradiated allogeneic granulocyte-macrophage colony stimulating factor-secreting tumor vaccine for pancreatic adenocarcinoma. A Phase II trial of safety, efficacy, and immune activation. Ann Surg. 2011;253(2):328-35.
337. Le DT, Brockstedt DG, Nir-Paz R, Hampl J, Mathur S, Nemunaitis J, et al. A live-attenuated Listeria vaccine (ANZ-100) and a live-attenuated Listeria vaccine expressing mesothelin (CRS-207) for advanced cancers: phase I studies of safety and immune induction. Clin Cancer Res. 2012;18(3):858-68.
338. Le DT, Wang-Gillam A, Picozzi V, Greten TF, Crocenzi T, Springett G, et al. Safety and survival with GVAX pancreas prime and Listeria Monocytogenes-expressing mesothelin (CRS-207) boost vaccines for metastatic pancreatic cancer. J Clin Oncol. 2015;33(12):1325-33.
339. Le DT, Picozzi VJ, Ko AH, Wainberg ZA, Kindler H, Wang-Gillam A, et al. Results from a Phase IIb, Randomized, Multicenter Study of GVAX Pancreas and CRS-207 Compared with Chemotherapy in Adults with Previously Treated Metastatic Pancreatic Adenocarcinoma (ECLIPSE Study). Clin Cancer Res. 2019;25(18):5493-502.
340. Tsujikawa T, Crocenzi T, Durham JN, Sugar EA, Wu AA, Onners B, et al. Evaluation of Cyclophosphamide/GVAX Pancreas Followed by Listeria-Mesothelin (CRS-207) with or without Nivolumab in Patients with Pancreatic Cancer. Clin Cancer Res. 2020;26(14):3578-88.
341. Wu AA, Bever KM, Ho WJ, Fertig EJ, Niu N, Zheng L, et al. A Phase II Study of Allogeneic GM-CSF-Transfected Pancreatic Tumor Vaccine (GVAX) with Ipilimumab as Maintenance Treatment for Metastatic Pancreatic Cancer. Clin Cancer Res. 2020;26(19):5129-39.
342. Le DT, Lutz E, Uram JN, Sugar EA, Onners B, Solt S, et al. Evaluation of ipilimumab in combination with allogeneic pancreatic tumor cells transfected with a GM-CSF gene in previously treated pancreatic cancer. J Immunother. 2013;36(7):382-9.
343. Lee V, Ding D, Rodriguez C, Onners B, Narang A, Meyer J, et al. A phase 2 study of cyclophosphamide (CY), GVAX, pembrolizumab (Pembro), and stereotactic body radiation (SBRT) in patients (pts) with locally advanced pancreas cancer (LAPC). Journal of Clinical Oncology. 2021;39(15_suppl):4134-.
344. Geynisman DM, Zha Y, Kunnavakkam R, Aklilu M, Catenacci DV, Polite BN, et al. A randomized pilot phase I study of modified carcinoembryonic antigen (CEA) peptide

(CAP1-6D)/montanide/GM-CSF-vaccine in patients with pancreatic adenocarcinoma. Journal for ImmunoTherapy of Cancer. 2013;1(1):8.
345. Wedén S, Klemp M, Gladhaug IP, Møller M, Eriksen JA, Gaudernack G, et al. Long-term follow-up of patients with resected pancreatic cancer following vaccination against mutant K-ras. International Journal of Cancer. 2011;128(5):1120-8.
346. Abou-Alfa GK, Chapman PB, Feilchenfeldt J, Brennan MF, Capanu M, Gansukh B, et al. Targeting Mutated K-ras in Pancreatic Adenocarcinoma Using an Adjuvant Vaccine. American Journal of Clinical Oncology. 2011;34(3):321-5.
347. Mutated Ras-Transfected, EBV-Transformed Lymphoblastoid Cell Lines as a Model Tumor Vaccine for Boosting T-Cell Responses Against Pancreatic Cancer: A Pilot Trial. Human Gene Therapy. 2012;23(12):1224-36.
348. Palmer DH, Valle JW, Ma YT, Faluyi O, Neoptolemos JP, Jensen Gjertsen T, et al. TG01/GM-CSF and adjuvant gemcitabine in patients with resected RAS-mutant adenocarcinoma of the pancreas (CT TG01-01): a single-arm, phase 1/2 trial. Br J Cancer. 2020;122(7):971-7.
349. Bassani-Sternberg M, Digklia A, Huber F, Wagner D, Sempoux C, Stevenson BJ, et al. A Phase Ib Study of the Combination of Personalized Autologous Dendritic Cell Vaccine, Aspirin, and Standard of Care Adjuvant Chemotherapy Followed by Nivolumab for Resected Pancreatic Adenocarcinoma-A Proof of Antigen Discovery Feasibility in Three Patients. Front Immunol. 2019;10:1832.
350. Bauer C, Dauer M, Saraj S, Schnurr M, Bauernfeind F, Sterzik A, et al. Dendritic cell-based vaccination of patients with advanced pancreatic carcinoma: results of a pilot study. Cancer Immunology, Immunotherapy. 2011;60(8):1097-107.
351. Kimura Y, Tsukada J, Tomoda T, Takahashi H, Imai K, Shimamura K, et al. Clinical and Immunologic Evaluation of Dendritic Cell–Based Immunotherapy in Combination With Gemcitabine and/or S-1 in Patients With Advanced Pancreatic Carcinoma. Pancreas. 2012;41(2):195-205.
352. Yutani S, Komatsu N, Yoshitomi M, Matsueda S, Yonemoto K, Mine T, et al. A phase II study of a personalized peptide vaccination for chemotherapy-resistant advanced pancreatic cancer patients. Oncol Rep. 2013;30(3):1094-100.
353. Qiu Y, Yun MM, Xu MB, Wang YZ, Yun S. Pancreatic carcinoma-specific immunotherapy using synthesised alpha-galactosyl epitope-activated immune responders: findings from a pilot study. International Journal of Clinical Oncology. 2013;18(4):657-65.
354. Lin M, Yuan Y-Y, Liu S-P, Shi J-J, Long X-A, Niu L-Z, et al. Prospective study of the safety and efficacy of a pancreatic cancer stem cell vaccine. Journal of Cancer Research and Clinical Oncology. 2015;141(10):1827-33.
355. Zhang L, Zhu W, Li J, Yang X, Ren Y, Niu J, et al. Clinical outcome of immunotherapy with dendritic cell vaccine and cytokine-induced killer cell therapy in hepatobiliary and pancreatic cancer. Mol Clin Oncol. 2016;4(1):129-33.
356. Mehrotra S, Britten CD, Chin S, Garrett-Mayer E, Cloud CA, Li M, et al. Vaccination with poly(IC:LC) and peptide-pulsed autologous dendritic cells in patients with pancreatic cancer. J Hematol Oncol. 2017;10(1):82.
357. Asahara S, Takeda K, Yamao K, Maguchi H, Yamaue H. Phase I/II clinical trial using HLA-A24-restricted peptide vaccine derived from KIF20A for patients with advanced pancreatic cancer. J Transl Med. 2013;11:291.
358. Suzuki N, Hazama S, Ueno T, Matsui H, Shindo Y, Iida M, et al. A phase I clinical trial of vaccination with KIF20A-derived peptide in combination with gemcitabine for patients with advanced pancreatic cancer. J Immunother. 2014;37(1):36-42.
359. Suzuki N, Hazama S, Iguchi H, Uesugi K, Tanaka H, Hirakawa K, et al. Phase II clinical trial of peptide cocktail therapy for patients with advanced pancreatic cancer: VENUS-PC study. Cancer Sci. 2017;108(1):73-80.
360. Miyazawa M, Ohsawa R, Tsunoda T, Hirono S, Kawai M, Tani M, et al. Phase I clinical trial using peptide vaccine for human vascular endothelial growth factor receptor 2

in combination with gemcitabine for patients with advanced pancreatic cancer. Cancer Sci. 2010;101(2):433-9.
361. Miyazawa M, Katsuda M, Maguchi H, Katanuma A, Ishii H, Ozaka M, et al. Phase II clinical trial using novel peptide cocktail vaccine as a postoperative adjuvant treatment for surgically resected pancreatic cancer patients. Int J Cancer. 2017;140(4):973-82.
362. Yamaue H, Tsunoda T, Tani M, Miyazawa M, Yamao K, Mizuno N, et al. Randomized phase II/III clinical trial of elpamotide for patients with advanced pancreatic cancer: PEGASUS-PC Study. Cancer Sci. 2015;106(7):883-90.
363. Kameshima H, Tsuruma T, Kutomi G, Shima H, Iwayama Y, Kimura Y, et al. Immunotherapeutic benefit of α-interferon (IFNα) in survivin2B-derived peptide vaccination for advanced pancreatic cancer patients. Cancer Sci. 2013;104(1):124-9.
364. Shima H, Tsurita G, Wada S, Hirohashi Y, Yasui H, Hayashi H, et al. Randomized phase II trial of survivin 2B peptide vaccination for patients with HLA-A24-positive pancreatic adenocarcinoma. Cancer Sci. 2019;110(8):2378-85.
365. Rong Y, Qin X, Jin D, Lou W, Wu L, Wang D, et al. A phase I pilot trial of MUC1-peptide-pulsed dendritic cells in the treatment of advanced pancreatic cancer. Clinical and Experimental Medicine. 2012;12(3):173-80.
366. Kaida M, Morita-Hoshi Y, Soeda A, Wakeda T, Yamaki Y, Kojima Y, et al. Phase 1 trial of Wilms tumor 1 (WT1) peptide vaccine and gemcitabine combination therapy in patients with advanced pancreatic or biliary tract cancer. J Immunother. 2011;34(1):92-9.
367. Nishida S, Koido S, Takeda Y, Homma S, Komita H, Takahara A, et al. Wilms tumor gene (WT1) peptide-based cancer vaccine combined with gemcitabine for patients with advanced pancreatic cancer. J Immunother. 2014;37(2):105-14.
368. Nishida S, Ishikawa T, Egawa S, Koido S, Yanagimoto H, Ishii J, et al. Combination Gemcitabine and WT1 Peptide Vaccination Improves Progression-Free Survival in Advanced Pancreatic Ductal Adenocarcinoma: A Phase II Randomized Study. Cancer Immunol Res. 2018;6(3):320-31.
369. Koido S, Homma S, Okamoto M, Takakura K, Mori M, Yoshizaki S, et al. Treatment with chemotherapy and dendritic cells pulsed with multiple Wilms' tumor 1 (WT1)-specific MHC class I/II-restricted epitopes for pancreatic cancer. Clin Cancer Res. 2014;20(16):4228-39.
370. Mayanagi S, Kitago M, Sakurai T, Matsuda T, Fujita T, Higuchi H, et al. Phase I pilot study of Wilms tumor gene 1 peptide-pulsed dendritic cell vaccination combined with gemcitabine in pancreatic cancer. Cancer Sci. 2015;106(4):397-406.
371. Yanagisawa R, Koizumi T, Koya T, Sano K, Koido S, Nagai K, et al. WT1-pulsed Dendritic Cell Vaccine Combined with Chemotherapy for Resected Pancreatic Cancer in a Phase I Study. Anticancer Res. 2018;38(4):2217-25.
372. Hanada S, Tsuruta T, Haraguchi K, Okamoto M, Sugiyama H, Koido S. Long-term survival of pancreatic cancer patients treated with multimodal therapy combined with WT1-targeted dendritic cell vaccines. Hum Vaccin Immunother. 2019;15(2):397-406.
373. NAGAI K, ADACHI T, HARADA H, EGUCHI S, SUGIYAMA H, MIYAZAKI Y. Dendritic Cell-based Immunotherapy Pulsed With Wilms Tumor 1 Peptide and Mucin 1 as an Adjuvant Therapy for Pancreatic Ductal Adenocarcinoma After Curative Resection: A Phase I/IIa Clinical Trial. Anticancer Research. 2020;40(10):5765-76.
374. Hardacre JM, Mulcahy M, Small W, Talamonti M, Obel J, Krishnamurthi S, et al. Addition of algenpantucel-L immunotherapy to standard adjuvant therapy for pancreatic cancer: a phase 2 study. J Gastrointest Surg. 2013;17(1):94-100; discussion p. -1.
375. Hewitt DB, Nissen N, Hatoum H, Musher B, Seng J, Coveler AL, et al. A Phase 3 Randomized Clinical Trial of Chemotherapy With or Without Algenpantucel-L (HyperAcute-Pancreas) Immunotherapy in Subjects With Borderline Resectable or Locally Advanced Unresectable Pancreatic Cancer. Ann Surg. 2022;275(1):45-53.
376. Lee J-c, Shin DW, Park H, Kim J, Youn Y, Kim JH, et al. Tolerability and safety of EUS-injected adenovirus-mediated double-suicide gene therapy with chemotherapy in

locally advanced pancreatic cancer: a phase 1 trial. Gastrointestinal Endoscopy. 2020;92(5):1044-52.e1.
377. Musher BL, Smaglo BG, Abidi W, Othman M, Patel K, Jawaid S, et al. A phase I/II study of LOAd703, a TMZ-CD40L/4-1BBL-armed oncolytic adenovirus, combined with nab-paclitaxel and gemcitabine in advanced pancreatic cancer. Journal of Clinical Oncology. 2022;40(16_suppl):4138-.
378. Bazan-Peregrino M, Garcia-Carbonero R, Laquente B, Álvarez R, Mato-Berciano A, Gimenez-Alejandre M, et al. VCN-01 disrupts pancreatic cancer stroma and exerts antitumor effects. J Immunother Cancer. 2021;9(11).
379. Garcia-Carbonero R, Bazan-Peregrino M, Gil-Martín M, Álvarez R, Macarulla T, Riesco-Martinez MC, et al. Phase I, multicenter, open-label study of intravenous VCN-01 oncolytic adenovirus with or without nab-paclitaxel plus gemcitabine in patients with advanced solid tumors. J Immunother Cancer. 2022;10(3).
380. Nakao A, Kasuya H, Sahin TT, Nomura N, Kanzaki A, Misawa M, et al. A phase I dose-escalation clinical trial of intraoperative direct intratumoral injection of HF10 oncolytic virus in non-resectable patients with advanced pancreatic cancer. Cancer Gene Therapy. 2011;18(3):167-75.
381. Kasuya H, Kodera Y, Nakao A, Yamamura K, Gewen T, Zhiwen W, et al. Phase I Dose-escalation Clinical Trial of HF10 Oncolytic Herpes Virus in 17 Japanese Patients with Advanced Cancer. Hepatogastroenterology. 2014;61(131):599-605.
382. Hirooka Y, Kasuya H, Ishikawa T, Kawashima H, Ohno E, Villalobos IB, et al. A Phase I clinical trial of EUS-guided intratumoral injection of the oncolytic virus, HF10 for unresectable locally advanced pancreatic cancer. BMC Cancer. 2018;18(1):596.
383. Hashimoto Y, Ueno M, Tanaka M, Ikeda M. Results from phase I study of the oncolytic viral immunotherapy agent canerpaturev (C-REV) in combination with gemcitabine plus nab-paclitaxel for unresectable pancreatic cancer. Journal of Clinical Oncology. 2019;37(4_suppl):325-.
384. Noonan AM, Farren MR, Geyer SM, Huang Y, Tahiri S, Ahn D, et al. Randomized Phase 2 Trial of the Oncolytic Virus Pelareorep (Reolysin) in Upfront Treatment of Metastatic Pancreatic Adenocarcinoma. Mol Ther. 2016;24(6):1150-8.
385. Mahalingam D, Goel S, Aparo S, Patel Arora S, Noronha N, Tran H, et al. A Phase II Study of Pelareorep (REOLYSIN(®)) in Combination with Gemcitabine for Patients with Advanced Pancreatic Adenocarcinoma. Cancers (Basel). 2018;10(6).
386. Mahalingam D, Wilkinson GA, Eng KH, Fields P, Raber P, Moseley JL, et al. Pembrolizumab in Combination with the Oncolytic Virus Pelareorep and Chemotherapy in Patients with Advanced Pancreatic Adenocarcinoma: A Phase Ib Study. Clin Cancer Res. 2020;26(1):71-81.
387. Bian J, Almhanna K. Pancreatic cancer and immune checkpoint inhibitors-still a long way to go. Transl Gastroenterol Hepatol. 2021;6:6.
388. Ying H, Kimmelman AC, Lyssiotis CA, Hua S, Chu GC, Fletcher-Sananikone E, et al. Oncogenic Kras maintains pancreatic tumors through regulation of anabolic glucose metabolism. Cell. 2012;149(3):656-70.
389. Ragulan C, Eason K, Fontana E, Nyamundanda G, Tarazona N, Patil Y, et al. Analytical Validation of Multiplex Biomarker Assay to Stratify Colorectal Cancer into Molecular Subtypes. Sci Rep. 2019;9(1):7665.
390. Carpen L, Falvo P, Orecchioni S, Mitola G, Hillje R, Mazzara S, et al. A single-cell transcriptomic landscape of innate and adaptive intratumoral immunity in triple negative breast cancer during chemo- and immunotherapies. Cell Death Discovery. 2022;8(1):106.
391. Han HS, Vikas P, Costa RLB, Jahan N, Taye A, Stringer-Reasor EM. Early-Stage Triple-Negative Breast Cancer Journey: Beginning, End, and Everything in Between. American Society of Clinical Oncology Educational Book. 2023(43):e390464.

392. Lehmann BD, Bauer JA, Chen X, Sanders ME, Chakravarthy AB, Shyr Y, et al. Identification of human triple-negative breast cancer subtypes and preclinical models for selection of targeted therapies. J Clin Invest. 2011;121(7):2750-67.
393. Lehmann BD, Jovanović B, Chen X, Estrada MV, Johnson KN, Shyr Y, et al. Refinement of Triple-Negative Breast Cancer Molecular Subtypes: Implications for Neoadjuvant Chemotherapy Selection. PLoS One. 2016;11(6):e0157368.
394. Burstein MD, Tsimelzon A, Poage GM, Covington KR, Contreras A, Fuqua SA, et al. Comprehensive genomic analysis identifies novel subtypes and targets of triple-negative breast cancer. Clin Cancer Res. 2015;21(7):1688-98.
395. Jiang YZ, Ma D, Suo C, Shi J, Xue M, Hu X, et al. Genomic and Transcriptomic Landscape of Triple-Negative Breast Cancers: Subtypes and Treatment Strategies. Cancer Cell. 2019;35(3):428-40.e5.
396. Hu S, Qu X, Jiao Y, Hu J, Wang B. Immune Classification and Immune Landscape Analysis of Triple-Negative Breast Cancer. Frontiers in Genetics. 2021;12.
397. He Y, Jiang Z, Chen C, Wang X. Classification of triple-negative breast cancers based on Immunogenomic profiling. Journal of Experimental & Clinical Cancer Research. 2018;37(1):327.
398. Gruosso T, Gigoux M, Manem VSK, Bertos N, Zuo D, Perlitch I, et al. Spatially distinct tumor immune microenvironments stratify triple-negative breast cancers. J Clin Invest. 2019;129(4):1785-800.
399. Font-Clos F, Zapperi S, La Porta CAM. Classification of triple negative breast cancer by epithelial mesenchymal transition and the tumor immune microenvironment. Scientific Reports. 2022;12(1):9651.
400. [TA639] NTag. Atezolizumab with nab-paclitaxel for untreated PD-L1-positive, locally advanced or metastatic, triple-negative breast cancer 2020 [
401. [TA851] NTag. Pembrolizumab for neoadjuvant and adjuvant treatment of triple-negative early or locally advanced breast cancer 2022 [
402. Kaplan DH, Shankaran V, Dighe AS, Stockert E, Aguet M, Old LJ, et al. Demonstration of an interferon gamma-dependent tumor surveillance system in immunocompetent mice. Proc Natl Acad Sci U S A. 1998;95(13):7556-61.
403. Oriss TB, McCarthy SA, Morel BF, Campana MA, Morel PA. Crossregulation between T helper cell (Th)1 and Th2: inhibition of Th2 proliferation by IFN-gamma involves interference with IL-1. J Immunol. 1997;158(8):3666-72.
404. Yoon C, Johnston SC, Tang J, Stahl M, Tobin JF, Somers WS. Charged residues dominate a unique interlocking topography in the heterodimeric cytokine interleukin-12. Embo j. 2000;19(14):3530-41.
405. Lee YG, Yang N, Chun I, Porazzi P, Carturan A, Paruzzo L, et al. Apoptosis: a Janus bifrons in T-cell immunotherapy. J Immunother Cancer. 2023;11(4).
406. Silva F, Padín-Iruegas ME, Caponio VCA, Lorenzo-Pouso AI, Saavedra-Nieves P, Chamorro-Petronacci CM, et al. Caspase 3 and Cleaved Caspase 3 Expression in Tumorogenesis and Its Correlations with Prognosis in Head and Neck Cancer: A Systematic Review and Meta-Analysis. Int J Mol Sci. 2022;23(19).
407. Cheng X, Zhao Z, Ventura E, Gran B, Shindler KS, Rostami A. The PD-1/PD-L pathway is up-regulated during IL-12-induced suppression of EAE mediated by IFN-gamma. J Neuroimmunol. 2007;185(1-2):75-86.
408. Fang P, Li X, Dai J, Cole L, Camacho JA, Zhang Y, et al. Immune cell subset differentiation and tissue inflammation. Journal of Hematology & Oncology. 2018;11(1):97.
409. Kumar A, Taghi Khani A, Sanchez Ortiz A, Swaminathan S. GM-CSF: A Double-Edged Sword in Cancer Immunotherapy. Front Immunol. 2022;13:901277.
410. Chiu JW, Binte Hanafi Z, Chew LCY, Mei Y, Liu H. IL-1α Processing, Signaling and Its Role in Cancer Progression. Cells. 2021;10(1).
411. Rébé C, Ghiringhelli F. Interleukin-1β and Cancer. Cancers (Basel). 2020;12(7).

412. Carlini V, Noonan DM, Abdalalem E, Goletti D, Sansone C, Calabrone L, et al. The multifaceted nature of IL-10: regulation, role in immunological homeostasis and its relevance to cancer, COVID-19 and post-COVID conditions. Frontiers in Immunology. 2023;14.
413. Wang X, Lin Y. Tumor necrosis factor and cancer, buddies or foes? Acta Pharmacol Sin. 2008;29(11):1275-88.
414. Jang DI, Lee AH, Shin HY, Song HR, Park JH, Kang TB, et al. The Role of Tumor Necrosis Factor Alpha (TNF-α) in Autoimmune Disease and Current TNF-α Inhibitors in Therapeutics. Int J Mol Sci. 2021;22(5).
415. Yang J, Zhang L, Yu C, Yang X-F, Wang H. Monocyte and macrophage differentiation: circulation inflammatory monocyte as biomarker for inflammatory diseases. Biomarker Research. 2014;2(1):1.
416. Chen Daniel S, Mellman I. Oncology Meets Immunology: The Cancer-Immunity Cycle. Immunity. 2013;39(1):1-10.
417. Ingersoll MA, Spanbroek R, Lottaz C, Gautier EL, Frankenberger M, Hoffmann R, et al. Comparison of gene expression profiles between human and mouse monocyte subsets. Blood. 2010;115(3):e10-e9.
418. Ong S-M, Teng K, Newell E, Chen H, Chen J, Loy T, et al. A Novel, Five-Marker Alternative to CD16–CD14 Gating to Identify the Three Human Monocyte Subsets. Frontiers in Immunology. 2019;10.
419. Wong KL, Yeap WH, Tai JJY, Ong SM, Dang TM, Wong SC. The three human monocyte subsets: implications for health and disease. Immunologic Research. 2012;53(1):41-57.
420. Subimerb C, Pinlaor S, Lulitanond V, Khuntikeo N, Okada S, McGrath MS, et al. Circulating CD14(+) CD16(+) monocyte levels predict tissue invasive character of cholangiocarcinoma. Clin Exp Immunol. 2010;161(3):471-9.
421. Patysheva M, Larionova I, Stakheyeva M, Grigoryeva E, Iamshchikov P, Tarabanovskaya N, et al. Effect of Early-Stage Human Breast Carcinoma on Monocyte Programming. Frontiers in Oncology. 2022;11.
422. Nathan CF, Murray HW, Wiebe ME, Rubin BY. Identification of interferon-gamma as the lymphokine that activates human macrophage oxidative metabolism and antimicrobial activity. J Exp Med. 1983;158(3):670-89.
423. Herrero C, Hu X, Li WP, Samuels S, Sharif MN, Kotenko S, et al. Reprogramming of IL-10 activity and signaling by IFN-gamma. J Immunol. 2003;171(10):5034-41.
424. Nagineni CN, Cherukuri KS, Kutty V, Detrick B, Hooks JJ. Interferon-gamma differentially regulates TGF-beta1 and TGF-beta2 expression in human retinal pigment epithelial cells through JAK-STAT pathway. J Cell Physiol. 2007;210(1):192-200.
425. Derynck R, Turley SJ, Akhurst RJ. TGFβ biology in cancer progression and immunotherapy. Nat Rev Clin Oncol. 2021;18(1):9-34.
426. Hanley CJ, Henriet E, Sirka OK, Thomas GJ, Ewald AJ. Tumor-Resident Stromal Cells Promote Breast Cancer Invasion through Regulation of the Basal Phenotype. Mol Cancer Res. 2020;18(11):1615-22.
427. Cheung KJ, Gabrielson E, Werb Z, Ewald AJ. Collective invasion in breast cancer requires a conserved basal epithelial program. Cell. 2013;155(7):1639-51.
428. Panse J, Friedrichs K, Marx A, Hildebrandt Y, Luetkens T, Barrels K, et al. Chemokine CXCL13 is overexpressed in the tumour tissue and in the peripheral blood of breast cancer patients. Br J Cancer. 2008;99(6):930-8.
429. Schmidt M, Weyer-Elberich V, Hengstler JG, Heimes A-S, Almstedt K, Gerhold-Ay A, et al. Prognostic impact of CD4-positive T cell subsets in early breast cancer: a study based on the FinHer trial patient population. Breast Cancer Research. 2018;20(1):15.
430. Ma Q, Chen Y, Qin Q, Guo F, Wang YS, Li D. CXCL13 expression in mouse 4T1 breast cancer microenvironment elicits antitumor immune response by regulating immune cell infiltration. Precis Clin Med. 2021;4(3):155-67.

431. Ma YJ, Hein E, Munthe-Fog L, Skjoedt M-O, Bayarri-Olmos R, Romani L, et al. Soluble Collectin-12 (CL-12) Is a Pattern Recognition Molecule Initiating Complement Activation via the Alternative Pathway. The Journal of Immunology. 2015;195(7):3365-73.
432. Gu C, Gu X, Wang Y, Yao Z, Zhou C. Construction and Validation of a Novel Immunosignature for Overall Survival in Uveal Melanoma. Frontiers in Cell and Developmental Biology. 2021;9.
433. Akter J, Takatori A, Hossain MS, Ozaki T, Nakazawa A, Ohira M, et al. Expression of NLRR3 orphan receptor gene is negatively regulated by MYCN and Miz-1, and its downregulation is associated with unfavorable outcome in neuroblastoma. Clin Cancer Res. 2011;17(21):6681-92.
434. Qian XL, Pan YH, Huang QY, Shi YB, Huang QY, Hu ZZ, et al. Caveolin-1: a multifaceted driver of breast cancer progression and its application in clinical treatment. Onco Targets Ther. 2019;12:1539-52.
435. Godina C, Indira Chandran V, Barbachowska M, Tryggvadottir H, Nodin B, Visse E, et al. Interplay between Caveolin-1 and body and tumor size affects clinical outcomes in breast cancer. Translational Oncology. 2022;22:101464.
436. Wang J, Xu L, Liu Y, Chen J, Jiang H, Yang S, et al. Expression of cyclin kinase subunit 2 in human breast cancer and its prognostic significance. Int J Clin Exp Pathol. 2014;7(12):8593-601.
437. Delpu Y, Hanoun N, Lulka H, Sicard F, Selves J, Buscail L, et al. Genetic and epigenetic alterations in pancreatic carcinogenesis. Curr Genomics. 2011;12(1):15-24.
438. Collins MA, Bednar F, Zhang Y, Brisset JC, Galbán S, Galbán CJ, et al. Oncogenic Kras is required for both the initiation and maintenance of pancreatic cancer in mice. J Clin Invest. 2012;122(2):639-53.
439. Boutin AT, Liao WT, Wang M, Hwang SS, Karpinets TV, Cheung H, et al. Oncogenic Kras drives invasion and maintains metastases in colorectal cancer. Genes Dev. 2017;31(4):370-82.
440. Fisher GH, Wellen SL, Klimstra D, Lenczowski JM, Tichelaar JW, Lizak MJ, et al. Induction and apoptotic regression of lung adenocarcinomas by regulation of a K-Ras transgene in the presence and absence of tumor suppressor genes. Genes Dev. 2001;15(24):3249-62.
441. Mills BN, Connolly KA, Ye J, Murphy JD, Uccello TP, Han BJ, et al. Stereotactic Body Radiation and Interleukin-12 Combination Therapy Eradicates Pancreatic Tumors by Repolarizing the Immune Microenvironment. Cell Rep. 2019;29(2):406-21.e5.
442. Nash A, Aghlara-Fotovat S, Hernandez A, Ghani S, Joshi I, Ira D, et al. 1095 IL-12-based cytokine factories modulate tumor microenvironment to eradicate pancreatic tumors in mice and are well tolerated in non-human primates. Journal for ImmunoTherapy of Cancer. 2022;10(Suppl 2):A1138-A.
443. Pützer BM, Rödicker F, Hitt MM, Stiewe T, Esche H. Improved Treatment of Pancreatic Cancer by IL-12 and B7.1 Costimulation: Antitumor Efficacy and Immunoregulation in a Nonimmunogenic Tumor Model. Molecular Therapy. 2002;5(4):405-12.
444. Sangro B, Mazzolini G, Ruiz J, Herraiz M, Quiroga J, Herrero I, et al. Phase I Trial of Intratumoral Injection of an Adenovirus Encoding Interleukin-12 for Advanced Digestive Tumors. Journal of Clinical Oncology. 2004;22(8):1389-97.
445. Barton KN, Siddiqui F, Pompa R, Freytag SO, Khan G, Dobrosotskaya I, et al. Phase I trial of oncolytic adenovirus-mediated cytotoxic and interleukin-12 gene therapy for the treatment of metastatic pancreatic cancer. Mol Ther Oncolytics. 2021;20:94-104.
446. Ragulan C, Lawrence PV, Ps H, Desai K, Ishihara J, Sadanandam A. Abstract PO-020: Heating up immune cold pancreatic adenocarcinoma with bioengineered immunotherapy remodels tumor microenvironment and prevents metastasis in vivo. Cancer Research. 2021;81(22_Supplement):PO-020-PO-.

447. Ragulan C, Desai K, Lawrence PV, Ikami Y, Aalam MM, Ps H, et al. Context-specific GITR agonism potentiates anti-PD-L1 and CD40-based immuno-chemotherapy combination in heterogeneous pancreatic tumors. bioRxiv. 2023:2023.06.16.545301.
448. Leonard JP, Sherman ML, Fisher GL, Buchanan LJ, Larsen G, Atkins MB, et al. Effects of Single-Dose Interleukin-12 Exposure on Interleukin-12–Associated Toxicity and Interferon-γ Production. Blood. 1997;90(7):2541-8.
449. Kerkar SP, Leonardi AJ, van Panhuys N, Zhang L, Yu Z, Crompton JG, et al. Collapse of the tumor stroma is triggered by IL-12 induction of Fas. Mol Ther. 2013;21(7):1369-77.
450. Pagliarini R, Shao W, Sellers WR. Oncogene addiction: pathways of therapeutic response, resistance, and road maps toward a cure. EMBO Rep. 2015;16(3):280-96.
451. Rong L, Perelson AS. Treatment of hepatitis C virus infection with interferon and small molecule direct antivirals: viral kinetics and modeling. Crit Rev Immunol. 2010;30(2):131-48.
452. Zhang L, Tai YT, Ho MZG, Qiu L, Anderson KC. Interferon-alpha-based immunotherapies in the treatment of B cell-derived hematologic neoplasms in today's treat-to-target era. Exp Hematol Oncol. 2017;6:20.
453. Filipi M, Jack S. Interferons in the Treatment of Multiple Sclerosis: A Clinical Efficacy, Safety, and Tolerability Update. Int J MS Care. 2020;22(4):165-72.
454. Wheelock EF. Interferon-Like Virus-Inhibitor Induced in Human Leukocytes by Phytohemagglutinin. Science. 1965;149(3681):310-1.
455. Dighe AS, Richards E, Old LJ, Schreiber RD. Enhanced in vivo growth and resistance to rejection of tumor cells expressing dominant negative IFN gamma receptors. Immunity. 1994;1(6):447-56.
456. M A Farrar a, Schreiber RD. The Molecular Cell Biology of Interferon-gamma and its Receptor. Annual Review of Immunology. 1993;11(1):571-611.
457. Street SE, Cretney E, Smyth MJ. Perforin and interferon-gamma activities independently control tumor initiation, growth, and metastasis. Blood. 2001;97(1):192-7.
458. Street SE, Trapani JA, MacGregor D, Smyth MJ. Suppression of lymphoma and epithelial malignancies effected by interferon gamma. J Exp Med. 2002;196(1):129-34.
459. Shirayoshi Y, Burke PA, Appella E, Ozato K. Interferon-induced transcription of a major histocompatibility class I gene accompanies binding of inducible nuclear factors to the interferon consensus sequence. Proc Natl Acad Sci U S A. 1988;85(16):5884-8.
460. Amaldi I, Reith W, Berte C, Mach B. Induction of HLA class II genes by IFN-gamma is transcriptional and requires a trans-acting protein. J Immunol. 1989;142(3):999-1004.
461. Stifter K, Krieger J, Ruths L, Gout J, Mulaw M, Lechel A, et al. IFN-γ treatment protocol for MHC-I(lo)/PD-L1(+) pancreatic tumor cells selectively restores their TAP-mediated presentation competence and CD8 T-cell priming potential. J Immunother Cancer. 2020;8(2).
462. Garrido F, Aptsiauri N, Doorduijn EM, Garcia Lora AM, van Hall T. The urgent need to recover MHC class I in cancers for effective immunotherapy. Curr Opin Immunol. 2016;39:44-51.
463. Curtsinger JM, Agarwal P, Lins DC, Mescher MF. Autocrine IFN-γ promotes naive CD8 T cell differentiation and synergizes with IFN-α to stimulate strong function. J Immunol. 2012;189(2):659-68.
464. Chin YE, Kitagawa M, Su WC, You ZH, Iwamoto Y, Fu XY. Cell growth arrest and induction of cyclin-dependent kinase inhibitor p21 WAF1/CIP1 mediated by STAT1. Science. 1996;272(5262):719-22.
465. Fulda S, Debatin KM. IFNgamma sensitizes for apoptosis by upregulating caspase-8 expression through the Stat1 pathway. Oncogene. 2002;21(15):2295-308.
466. Chin YE, Kitagawa M, Kuida K, Flavell RA, Fu XY. Activation of the STAT signaling pathway can cause expression of caspase 1 and apoptosis. Mol Cell Biol. 1997;17(9):5328-37.

467. Xu X, Fu XY, Plate J, Chong AS. IFN-gamma induces cell growth inhibition by Fas-mediated apoptosis: requirement of STAT1 protein for up-regulation of Fas and FasL expression. Cancer Res. 1998;58(13):2832-7.
468. Thapa RJ, Basagoudanavar SH, Nogusa S, Irrinki K, Mallilankaraman K, Slifker MJ, et al. NF-kappaB protects cells from gamma interferon-induced RIP1-dependent necroptosis. Mol Cell Biol. 2011;31(14):2934-46.
469. Beatty G, Paterson Y. IFN-gamma-dependent inhibition of tumor angiogenesis by tumor-infiltrating CD4+ T cells requires tumor responsiveness to IFN-gamma. J Immunol. 2001;166(4):2276-82.
470. Kammertoens T, Friese C, Arina A, Idel C, Briesemeister D, Rothe M, et al. Tumour ischaemia by interferon-γ resembles physiological blood vessel regression. Nature. 2017;545(7652):98-102.
471. Hayakawa Y, Takeda K, Yagita H, Smyth MJ, Van Kaer L, Okumura K, et al. IFN-gamma-mediated inhibition of tumor angiogenesis by natural killer T-cell ligand, alpha-galactosylceramide. Blood. 2002;100(5):1728-33.
472. Briesemeister D, Sommermeyer D, Loddenkemper C, Loew R, Uckert W, Blankenstein T, et al. Tumor rejection by local interferon gamma induction in established tumors is associated with blood vessel destruction and necrosis. Int J Cancer. 2011;128(2):371-8.
473. Kurzrock R, Rosenblum MG, Sherwin SA, Rios A, Talpaz M, Quesada JR, et al. Pharmacokinetics, single-dose tolerance, and biological activity of recombinant gamma-interferon in cancer patients. Cancer Res. 1985;45(6):2866-72.
474. Garris CS, Arlauckas SP, Kohler RH, Trefny MP, Garren S, Piot C, et al. Successful Anti-PD-1 Cancer Immunotherapy Requires T Cell-Dendritic Cell Crosstalk Involving the Cytokines IFN-γ and IL-12. Immunity. 2018;49(6):1148-61.e7.
475. Gray PW, Goeddel DV. Cloning and expression of murine immune interferon cDNA. Proc Natl Acad Sci U S A. 1983;80(19):5842-6.
476. Bhat MY, Solanki HS, Advani J, Khan AA, Keshava Prasad TS, Gowda H, et al. Comprehensive network map of interferon gamma signaling. J Cell Commun Signal. 2018;12(4):745-51.
477. Liu W, Putnam AL, Xu-yu Z, Szot GL, Lee MR, Zhu S, et al. CD127 expression inversely correlates with FoxP3 and suppressive function of human CD4+ T reg cells. Journal of Experimental Medicine. 2006;203(7):1701-11.
478. Boulch M, Cazaux M, Cuffel A, Guerin MV, Garcia Z, Alonso R, et al. Tumor-intrinsic sensitivity to the pro-apoptotic effects of IFN-γ is a major determinant of CD4+ CAR T-cell antitumor activity. Nature Cancer. 2023;4(7):968-83.
479. Willenborg DO, Fordham S, Bernard CC, Cowden WB, Ramshaw IA. IFN-gamma plays a critical down-regulatory role in the induction and effector phase of myelin oligodendrocyte glycoprotein-induced autoimmune encephalomyelitis. J Immunol. 1996;157(8):3223-7.
480. Greifenberg V, Ribechini E, Rössner S, Lutz MB. Myeloid-derived suppressor cell activation by combined LPS and IFN-gamma treatment impairs DC development. Eur J Immunol. 2009;39(10):2865-76.
481. Shime H, Maruyama A, Yoshida S, Takeda Y, Matsumoto M, Seya T. Toll-like receptor 2 ligand and interferon-γ suppress anti-tumor T cell responses by enhancing the immunosuppressive activity of monocytic myeloid-derived suppressor cells. Oncoimmunology. 2017;7(1):e1373231.
482. Abiko K, Matsumura N, Hamanishi J, Horikawa N, Murakami R, Yamaguchi K, et al. IFN-γ from lymphocytes induces PD-L1 expression and promotes progression of ovarian cancer. Br J Cancer. 2015;112(9):1501-9.
483. Gao H, Wu Y, Shi J, Zhang X, Liu T, Hu B, et al. Nuclear imaging-guided PD-L1 blockade therapy increases effectiveness of cancer immunotherapy. J Immunother Cancer. 2020;8(2).

484. Lenzi R, Edwards R, June C, Seiden MV, Garcia ME, Rosenblum M, et al. Phase II study of intraperitoneal recombinant interleukin-12 (rhIL-12) in patients with peritoneal carcinomatosis (residual disease < 1 cm) associated with ovarian cancer or primary peritoneal carcinoma. J Transl Med. 2007;5:66.
485. Cohen J. IL-12 deaths: explanation and a puzzle. Science. 1995;270(5238):908.
486. Haicheur N, Escudier B, Dorval T, Negrier S, De Mulder PH, Dupuy JM, et al. Cytokines and soluble cytokine receptor induction after IL-12 administration in cancer patients. Clin Exp Immunol. 2000;119(1):28-37.
487. Atkins MB, Robertson MJ, Gordon M, Lotze MT, DeCoste M, DuBois JS, et al. Phase I evaluation of intravenous recombinant human interleukin 12 in patients with advanced malignancies. Clin Cancer Res. 1997;3(3):409-17.
488. Younes A, Pro B, Robertson MJ, Flinn IW, Romaguera JE, Hagemeister F, et al. Phase II clinical trial of interleukin-12 in patients with relapsed and refractory non-Hodgkin's lymphoma and Hodgkin's disease. Clin Cancer Res. 2004;10(16):5432-8.
489. Portielje JE, Lamers CH, Kruit WH, Sparreboom A, Bolhuis RL, Stoter G, et al. Repeated administrations of interleukin (IL)-12 are associated with persistently elevated plasma levels of IL-10 and declining IFN-gamma, tumor necrosis factor-alpha, IL-6, and IL-8 responses. Clin Cancer Res. 2003;9(1):76-83.
490. Gollob JA, Mier JW, Veenstra K, McDermott DF, Clancy D, Clancy M, et al. Phase I trial of twice-weekly intravenous interleukin 12 in patients with metastatic renal cell cancer or malignant melanoma: ability to maintain IFN-gamma induction is associated with clinical response. Clin Cancer Res. 2000;6(5):1678-92.
491. Bekaii-Saab TS, Roda JM, Guenterberg KD, Ramaswamy B, Young DC, Ferketich AK, et al. A phase I trial of paclitaxel and trastuzumab in combination with interleukin-12 in patients with HER2/neu-expressing malignancies. Mol Cancer Ther. 2009;8(11):2983-91.
492. Prochazkova J, Pokorna K, Holan V. IL-12 inhibits the TGF-β-dependent T cell developmental programs and skews the TGF-β-induced differentiation into a Th1-like direction. Immunobiology. 2012;217(1):74-82.
493. Xu H, Zhang GX, Wysocka M, Wu CY, Trinchieri G, Rostami A. The suppressive effect of TGF-beta on IL-12-mediated immune modulation specific to a peptide Ac1-11 of myelin basic protein (MBP): a mechanism involved in inhibition of both IL-12 receptor beta1 and beta2. J Neuroimmunol. 2000;108(1-2):53-63.
494. Pardoux C, Ma X, Gobert S, Pellegrini S, Mayeux P, Gay F, et al. Downregulation of interleukin-12 (IL-12) responsiveness in human T cells by transforming growth factor-beta: relationship with IL-12 signaling. Blood. 1999;93(5):1448-55.
495. Strauss J, Heery CR, Kim JW, Jochems C, Donahue RN, Montgomery AS, et al. First-in-Human Phase I Trial of a Tumor-Targeted Cytokine (NHS-IL12) in Subjects with Metastatic Solid Tumors. Clin Cancer Res. 2019;25(1):99-109.
496. Xu C, Zhang Y, Rolfe PA, Hernández VM, Guzman W, Kradjian G, et al. Combination Therapy with NHS-muIL12 and Avelumab (anti-PD-L1) Enhances Antitumor Efficacy in Preclinical Cancer Models. Clinical Cancer Research. 2017;23(19):5869-80.
497. Strauss J, Vugmeyster Y, Sznol M, Pachynski RK, Trang K, Chennoufi S, et al. 1224P - Phase Ib, open-label, dose-escalation study of M9241 (NHS-IL12) plus avelumab in patients (pts) with advanced solid tumours. Annals of Oncology. 2019;30:v500-v1.
498. Strauss J, Deville JL, Sznol M, Ravaud A, Maruzzo M, Pachynski RK, et al. First-in-human phase Ib trial of M9241 (NHS-IL12) plus avelumab in patients with advanced solid tumors, including dose expansion in patients with advanced urothelial carcinoma. J Immunother Cancer. 2023;11(5).
499. Lan Y, Zhang D, Xu C, Hance KW, Marelli B, Qi J, et al. Enhanced preclinical antitumor activity of M7824, a bifunctional fusion protein simultaneously targeting PD-L1 and TGF-β. Sci Transl Med. 2018;10(424).
500. Khasraw M, Weller M, Lorente D, Kolibaba K, Lee CK, Gedye C, et al. Bintrafusp alfa (M7824), a bifunctional fusion protein targeting TGF-β and PD-L1: results from a phase

I expansion cohort in patients with recurrent glioblastoma. Neurooncol Adv. 2021;3(1):vdab058.
501. Lin CC, Doi T, Muro K, Hou MM, Esaki T, Hara H, et al. Bintrafusp Alfa, a Bifunctional Fusion Protein Targeting TGFβ and PD-L1, in Patients with Esophageal Squamous Cell Carcinoma: Results from a Phase 1 Cohort in Asia. Target Oncol. 2021;16(4):447-59.
502. Cho BC, Daste A, Ravaud A, Salas S, Isambert N, McClay E, et al. Bintrafusp alfa, a bifunctional fusion protein targeting TGF-β and PD-L1, in advanced squamous cell carcinoma of the head and neck: results from a phase I cohort. J Immunother Cancer. 2020;8(2).
503. Xu C, Marelli B, Qi J, Qin G, Yu H, Wang H, et al. NHS-IL12 and bintrafusp alfa combination therapy enhances antitumor activity in preclinical cancer models. Transl Oncol. 2022;16:101322.
504. Simon NI, Niglio SA, Chandran E, Iannantuono GM, Boudjadi S, Banday R, et al. A phase I study of bintrafusp alfa and NHS-IL12 (M9241) alone and in combination with stereotactic body radiation therapy (SBRT) in patients with metastatic genitourinary (GU) malignancies. Journal of Clinical Oncology. 2023;41(16_suppl):4571-.
505. Pylayeva-Gupta Y, Lee KE, Hajdu CH, Miller G, Bar-Sagi D. Oncogenic Kras-induced GM-CSF production promotes the development of pancreatic neoplasia. Cancer Cell. 2012;21(6):836-47.
506. Liu C, Zheng S, Wang Z, Wang S, Wang X, Yang L, et al. KRAS-G12D mutation drives immune suppression and the primary resistance of anti-PD-1/PD-L1 immunotherapy in non-small cell lung cancer. Cancer Commun (Lond). 2022;42(9):828-47.
507. Jeanson A, Tomasini P, Souquet-Bressand M, Brandone N, Boucekine M, Grangeon M, et al. Efficacy of Immune Checkpoint Inhibitors in KRAS-Mutant Non-Small Cell Lung Cancer (NSCLC). J Thorac Oncol. 2019;14(6):1095-101.
508. Arbour KC, Rizvi H, Plodkowski AJ, Hellmann MD, Knezevic A, Heller G, et al. Treatment Outcomes and Clinical Characteristics of Patients with KRAS-G12C-Mutant Non-Small Cell Lung Cancer. Clin Cancer Res. 2021;27(8):2209-15.
509. Sun L, Hsu M, Cohen RB, Langer CJ, Mamtani R, Aggarwal C. Association Between KRAS Variant Status and Outcomes With First-line Immune Checkpoint Inhibitor-Based Therapy in Patients With Advanced Non-Small-Cell Lung Cancer. JAMA Oncol. 2021;7(6):937-9.

Appendix

6.6 Permission to reprint

A licence that permits reprint of Table 1.7, Table 1.8, and Table 1.9 from the publication described below has been attached in this appendix:

- Herpels, M., et al. (2023). "The clinical terrain of immunotherapies in heterogeneous pancreatic cancer: unravelling challenges and opportunities." J Pathol 260(5): 533-550.

CCC Marketplace

This is a License Agreement between Melanie Herpels ("User") and Copyright Clearance Center, Inc. ("CCC") on behalf of the Rightsholder identified in the order details below. The license consists of the order details, the Marketplace Permissions General Terms and Conditions below, and any Rightsholder Terms and Conditions which are included below.

All payments must be made in full to CCC in accordance with the Marketplace Permissions General Terms and Conditions below.

Order Date	01-May-2024
Order License ID	1479309-1
ISSN	1096-9896
Type of Use	Republish in a thesis/dissertation
Publisher	JOHN WILEY & SONS LTD.
Portion	Chart/graph/table/figure

LICENSED CONTENT

Publication Title	The Journal of pathology
Article Title	The clinical terrain of immunotherapies in heterogeneous pancreatic cancer: unravelling challenges and opportunities
Author/Editor	Wiley InterScience (Online service), Pathological Society of Great Britain and Ireland.
Date	01/01/1969
Language	English
Country	United Kingdom of Great Britain and Northern Ireland
Rightsholder	John Wiley & Sons - Books
Publication Type	e-Journal
Start Page	533
End Page	550
Issue	5
Volume	260
URL	http://www3.interscience.wiley.com/cgi-bin/jhome/110526247

REQUEST DETAILS

Portion Type	Chart/graph/table/figure
Number of Charts / Graphs / Tables / Figures Requested	3
Format (select all that apply)	Print, Electronic
Who Will Republish the Content?	Academic institution
Duration of Use	Life of current and all future editions
Lifetime Unit Quantity	Up to 500,000
Rights Requested	Main product
Distribution	Worldwide
Translation	Original language of publication
Copies for the Disabled?	No
Minor Editing Privileges?	Yes
Incidental Promotional Use?	No
Currency	GBP

NEW WORK DETAILS

Title	Bioengineered tumour-targeted cytokines for tolerable immunotherapy combinations in solid tumours
Instructor Name	Melanie Herpels
Institution Name	Imperial College London
Expected Presentation Date	2024-06-18

ADDITIONAL DETAILS

The Requesting Person / Organization to Appear on the License	Melanie Herpels

REQUESTED CONTENT DETAILS

Title, Description or Numeric Reference of the Portion(s)	Tables 1-3
Editor of Portion(s)	Herpels, Melanie; Ishihara, Jun; Sadanandam, Anguraj
Volume / Edition	260
Page or Page Range of Portion	533-550
Title of the Article / Chapter the Portion Is From	The clinical terrain of immunotherapies in heterogeneous pancreatic cancer: unravelling challenges and opportunities
Author of Portion(s)	Herpels, Melanie; Ishihara, Jun; Sadanandam, Anguraj
Publication Date of Portion	2023-08-27

RIGHTSHOLDER TERMS AND CONDITIONS

No right, license or interest to any trademark, trade name, service mark or other branding ("Marks") of WILEY or its licensors is granted hereunder, and you agree that you shall not assert any such right, license or interest with respect thereto. You may not alter, remove or suppress in any manner any copyright, trademark or other notices displayed by the Wiley material. This Agreement will be void if the Type of Use, Format, Circulation, or Requestor Type was misrepresented during the licensing process. In no instance may the total amount of Wiley Materials used in any Main Product, Compilation or Collective work comprise more than 5% (if figures/tables) or 15% (if full articles/chapters) of the (entirety of the) Main Product, Compilation or Collective Work. Some titles may be available under an Open Access license. It is the Licensors' responsibility to identify the type of Open Access license on which the requested material was published, and comply fully with the terms of that license for the type of use specified Further details can be found on Wiley Online Library http://olabout.wiley.com/WileyCDA/Section/id-410895.html.

Marketplace Permissions General Terms and Conditions

The following terms and conditions ("General Terms"), together with any applicable Publisher Terms and Conditions, govern User's use of Works pursuant to the Licenses granted by Copyright Clearance Center, Inc. ("CCC") on behalf of the applicable Rightsholders of such Works through CCC's applicable Marketplace transactional licensing services (each, a "Service").

1) **Definitions.** For purposes of these General Terms, the following definitions apply:

"License" is the licensed use the User obtains via the Marketplace platform in a particular licensing transaction, as set forth in the Order Confirmation.

"Order Confirmation" is the confirmation CCC provides to the User at the conclusion of each Marketplace transaction. "Order Confirmation Terms" are additional terms set forth on specific Order Confirmations not set forth in the General Terms that can include terms applicable to a particular CCC transactional licensing service and/or any Rightsholder-specific terms.

"Rightsholder(s)" are the holders of copyright rights in the Works for which a User obtains licenses via the Marketplace platform, which are displayed on specific Order Confirmations.

"Terms" means the terms and conditions set forth in these General Terms and any additional Order Confirmation Terms collectively.

"User" or "you" is the person or entity making the use granted under the relevant License. Where the person accepting the Terms on behalf of a User is a freelancer or other third party who the User authorized to accept the General Terms on the User's behalf, such person shall be deemed jointly a User for purposes of such Terms.

"Work(s)" are the copyright protected works described in relevant Order Confirmations.

2) **Description of Service.** CCC's Marketplace enables Users to obtain Licenses to use one or more Works in accordance with all relevant Terms. CCC grants Licenses as an agent on behalf of the copyright rightsholder identified in the relevant Order Confirmation.

3) **Applicability of Terms.** The Terms govern User's use of Works in connection with the relevant License. In the event of any conflict between General Terms and Order Confirmation Terms, the latter shall govern. User acknowledges that Rightsholders have complete discretion whether to grant any permission, and whether to place any limitations on any grant, and that CCC has no right to supersede or to modify any such discretionary act by a Rightsholder.

4) **Representations; Acceptance.** By using the Service, User represents and warrants that User has been duly authorized by the User to accept, and hereby does accept, all Terms.

5) **Scope of License; Limitations and Obligations.** All Works and all rights therein, including copyright rights, remain the sole and exclusive property of the Rightsholder. The License provides only those rights expressly set forth in the terms and conveys no other rights in any Works

6) **General Payment Terms.** User may pay at time of checkout by credit card or choose to be invoiced. If the User chooses to be invoiced, the User shall: (i) remit payments in the manner identified on specific invoices, (ii) unless otherwise specifically stated in an Order Confirmation or separate written agreement, Users shall remit payments upon receipt of the relevant invoice from CCC, either by delivery or notification of availability of the invoice via the Marketplace platform, and (iii) if the User does not pay the invoice within 30 days of receipt, the User may incur a service charge of 1.5% per month or the maximum rate allowed by applicable law, whichever is less. While User may exercise the rights in the License immediately upon receiving the Order Confirmation, the License is automatically revoked and is null and void, as if it had never been issued, if CCC does not receive complete payment on a timely basis.

7) **General Limits on Use.** Unless otherwise provided in the Order Confirmation, any grant of rights to User (i) involves only the rights set forth in the Terms and does not include subsequent or additional uses, (ii) is non-exclusive and non-transferable, and (iii) is subject to any and all limitations and restrictions (such as, but not limited to, limitations on duration of use or circulation) included in the Terms. Upon completion of the licensed use as set forth in the Order Confirmation, User shall either secure a new permission for further use of the Work(s) or immediately cease any new use of the Work(s) and shall render inaccessible (such as by deleting or by removing or severing links or other locators) any further copies of the Work. User may only make alterations to the Work if and as expressly set forth in the Order Confirmation. No Work may be used in any way that is unlawful, including without limitation if such use would violate applicable sanctions laws or regulations, would be defamatory, violate the rights of third parties (including such third parties' rights of copyright, privacy, publicity, or other tangible or intangible property), or is otherwise illegal, sexually explicit, or obscene. In addition, User may not conjoin a Work with any other material that may result in damage to the reputation of the Rightsholder. Any unlawful use will render any licenses hereunder null and void. User agrees to inform CCC if it becomes aware of any infringement of any rights in a Work and to cooperate with any reasonable request of CCC or the Rightsholder in connection therewith.

8) **Third Party Materials.** In the event that the material for which a License is sought includes third party materials (such as photographs, illustrations, graphs, inserts and similar materials) that are identified in such material as having been used by permission (or a similar indicator), User is responsible for identifying, and seeking separate licenses (under this Service, if available, or otherwise) for any of such third party materials; without a separate license, User may not use such third party materials via the License.

9) **Copyright Notice.** Use of proper copyright notice for a Work is required as a condition of any License granted under the Service. Unless otherwise provided in the Order Confirmation, a proper copyright notice will read substantially as follows: "Used with permission of [Rightsholder's name], from [Work's title, author, volume, edition number and year of copyright]; permission conveyed through Copyright Clearance Center, Inc." Such notice must be provided in a reasonably legible font size and must be placed either on a cover page or in another location that any person, upon gaining access to the material which is the subject of a permission, shall see, or in the case of republication Licenses, immediately adjacent to the Work as used (for example, as part of a by-line or footnote) or in the place where substantially all other credits or notices for the new work containing the republished Work are located. Failure to include the required notice results in loss to the Rightsholder and CCC, and the User shall be liable to pay liquidated damages for each such failure equal to twice the use fee specified in the Order Confirmation, in addition to the use fee itself and any other fees and charges specified.

10) **Indemnity.** User hereby indemnifies and agrees to defend the Rightsholder and CCC, and their respective employees and directors, against all claims, liability, damages, costs, and expenses, including legal fees and expenses, arising out of any use of a Work beyond the scope of the rights granted herein and in the Order Confirmation, or any use of a Work which has been altered in any unauthorized way by User, including claims of defamation or infringement of rights of copyright, publicity, privacy, or other tangible or intangible property.

11) **Limitation of Liability.** UNDER NO CIRCUMSTANCES WILL CCC OR THE RIGHTSHOLDER BE LIABLE FOR ANY DIRECT, INDIRECT, CONSEQUENTIAL, OR INCIDENTAL DAMAGES (INCLUDING WITHOUT LIMITATION DAMAGES FOR LOSS OF BUSINESS PROFITS OR INFORMATION, OR FOR BUSINESS INTERRUPTION) ARISING OUT OF THE USE OR INABILITY TO USE A WORK, EVEN IF ONE OR BOTH OF THEM HAS BEEN ADVISED OF THE POSSIBILITY OF SUCH DAMAGES. In any event, the total liability of the Rightsholder and CCC (including their respective employees and directors) shall not exceed the total amount actually paid by User for the relevant License. User assumes full liability for the actions and omissions of its principals, employees, agents, affiliates, successors, and assigns.

12) **Limited Warranties.** THE WORK(S) AND RIGHT(S) ARE PROVIDED "AS IS." CCC HAS THE RIGHT TO GRANT TO USER THE RIGHTS GRANTED IN THE ORDER CONFIRMATION DOCUMENT. CCC AND THE RIGHTSHOLDER DISCLAIM ALL OTHER WARRANTIES RELATING TO THE WORK(S) AND RIGHT(S), EITHER EXPRESS OR IMPLIED, INCLUDING WITHOUT LIMITATION IMPLIED WARRANTIES OF MERCHANTABILITY OR FITNESS FOR A PARTICULAR PURPOSE. ADDITIONAL RIGHTS MAY BE REQUIRED TO USE ILLUSTRATIONS, GRAPHS, PHOTOGRAPHS, ABSTRACTS, INSERTS, OR OTHER PORTIONS OF THE WORK (AS OPPOSED TO THE ENTIRE WORK) IN A MANNER CONTEMPLATED BY USER; USER UNDERSTANDS AND AGREES THAT NEITHER CCC NOR THE RIGHTSHOLDER MAY HAVE SUCH ADDITIONAL RIGHTS TO GRANT.

13) **Effect of Breach.** Any failure by User to pay any amount when due, or any use by User of a Work beyond the scope of the License set forth in the Order Confirmation and/or the Terms, shall be a material breach of such License. Any breach not cured within 10 days of written notice thereof shall result in immediate termination of such License without further notice. Any unauthorized (but licensable) use of a Work that is terminated immediately upon notice thereof may be liquidated by payment of the Rightsholder's ordinary license price therefor; any unauthorized (and unlicensable) use that is not terminated immediately for any reason (including, for example, because materials containing the Work cannot reasonably be recalled) will be subject to all remedies available at law or in equity, but in no event to a payment of less than three times the Rightsholder's ordinary license price for the most closely analogous licensable use plus Rightsholder's and/or CCC's costs and expenses incurred in collecting such payment.

14) **Additional Terms for Specific Products and Services.** If a User is making one of the uses described in this Section 14, the additional terms and conditions apply:

a) ***Print Uses of Academic Course Content and Materials (photocopies for academic coursepacks or classroom handouts).*** For photocopies for academic coursepacks or classroom handouts the following additional terms apply:

i) The copies and anthologies created under this License may be made and assembled by faculty members individually or at their request by on-campus bookstores or copy centers, or by off-campus copy shops and other similar entities.

ii) No License granted shall in any way: (i) include any right by User to create a substantively non-identical copy of the Work or to edit or in any other way modify the Work (except by means of deleting material immediately preceding or following the entire portion of the Work copied) (ii) permit "publishing ventures" where any particular anthology would be systematically marketed at multiple institutions.

iii) Subject to any Publisher Terms (and notwithstanding any apparent contradiction in the Order Confirmation arising from data provided by User), any use authorized under the academic pay-per-use service is limited as follows:

A) any License granted shall apply to only one class (bearing a unique identifier as assigned by the institution, and thereby including all sections or other subparts of the class) at one institution;

B) use is limited to not more than 25% of the text of a book or of the items in a published collection of essays, poems or articles;

C) use is limited to no more than the greater of (a) 25% of the text of an issue of a journal or other periodical or (b) two articles from such an issue;

D) no User may sell or distribute any particular anthology, whether photocopied or electronic, at more than one institution of learning;

E) in the case of a photocopy permission, no materials may be entered into electronic memory by User except in order to produce an identical copy of a Work before or during the academic term (or analogous period) as to which any particular permission is granted. In the event that User shall choose to retain materials that are the subject of a photocopy permission in electronic memory for purposes of producing identical copies more than one day after such retention (but still within the scope of any permission granted), User must notify CCC of such fact in the applicable permission request and such retention shall constitute one copy actually sold for purposes of calculating permission fees due; and

F) any permission granted shall expire at the end of the class. No permission granted shall in any way include any right by User to create a substantively non-identical copy of the Work or to edit or in any other way modify the Work (except by means of deleting material immediately preceding or following the entire portion of the Work copied).

iv) Books and Records; Right to Audit. As to each permission granted under the academic pay-per-use Service, User shall maintain for at least four full calendar years books and records sufficient for CCC to determine the numbers of copies made by User under such permission. CCC and any representatives it may designate shall have the right to audit such books and records at any time during User's ordinary business hours, upon two days' prior notice. If any such audit shall determine that User shall have underpaid for, or underreported, any photocopies sold or by three percent (3%) or more, then User shall bear all the costs of any such audit; otherwise, CCC shall bear the costs of any such audit. Any amount determined by such audit to have been underpaid by User shall immediately be paid to CCC by User, together with interest thereon at the rate of 10% per annum from the date such amount was originally due. The provisions of this paragraph shall survive the termination of this License for any reason.

b) ***Digital Pay-Per-Uses of Academic Course Content and Materials (e-coursepacks, electronic reserves, learning management systems, academic institution intranets).*** For uses in e-coursepacks, posts in electronic reserves, posts in learning management systems, or posts on academic institution intranets, the following additional terms apply:

i) The pay-per-uses subject to this Section 14(b) include:

A) **Posting e-reserves, course management systems, e-coursepacks for text-based content,** which grants authorizations to import requested material in electronic format, and allows electronic access to this material to members of a designated college or university class, under the direction of an instructor designated by the college or university, accessible only under appropriate electronic controls (e.g., password);

B) **Posting e-reserves, course management systems, e-coursepacks for material consisting of photographs or other still images not embedded in text,** which grants not only the authorizations described in Section 14(b)(i)(A) above, but also the following authorization: to include the requested material in course materials for use consistent with Section 14(b)(i)(A) above, including any necessary resizing, reformatting or modification of the resolution of such requested material (provided that such modification does not alter the underlying editorial content or meaning of the requested material, and provided that the resulting modified content is used solely within the scope of, and in a manner consistent with, the particular authorization described in the Order Confirmation and the Terms), but not including any other form of manipulation, alteration or editing of the requested material;

C) **Posting e-reserves, course management systems, e-coursepacks or other academic distribution for audiovisual content,** which grants not only the authorizations described in Section 14(b)(i)(A) above, but also the following authorizations: (i) to include the requested material in course materials for use consistent with Section 14(b)(i)(A) above; (ii) to display and perform the requested material to such members of such class in the physical classroom or remotely by means of streaming media or other video formats; and (iii) to "clip" or reformat the requested material for purposes of time or content management or ease of delivery, provided that such "clipping" or reformatting does not alter the underlying editorial content or meaning of the requested material and that the resulting material is used solely within the scope of, and in a manner consistent with, the particular authorization described in the Order Confirmation and the Terms. Unless expressly set forth in the relevant Order Conformation, the License does not authorize any other form of manipulation, alteration or editing of the requested material.

ii) Unless expressly set forth in the relevant Order Confirmation, no License granted shall in any way: (i) include any right by User to create a substantively non-identical copy of the Work or to edit or in any other way modify the Work (except by means of deleting material immediately preceding or following the entire portion of the Work copied or, in the case of Works subject to Sections 14(b)(1)(B) or (C) above, as described in such Sections) (ii) permit "publishing ventures" where any particular course materials would be systematically marketed at multiple institutions.

iii) Subject to any further limitations determined in the Rightsholder Terms (and notwithstanding any apparent contradiction in the Order Confirmation arising from data provided by User), any use authorized under the electronic course content pay-per-use service is limited as follows:

A) any License granted shall apply to only one class (bearing a unique identifier as assigned by the institution, and thereby including all sections or other subparts of the class) at one institution;

B) use is limited to not more than 25% of the text of a book or of the items in a published collection of essays, poems or articles;

C) use is limited to not more than the greater of (a) 25% of the text of an issue of a journal or other periodical or (b) two articles from such an issue;

D) no User may sell or distribute any particular materials, whether photocopied or electronic, at more than one institution of learning;

E) electronic access to material which is the subject of an electronic-use permission must be limited by means of electronic password, student identification or other control permitting access solely to students and instructors in the class;

F) User must ensure (through use of an electronic cover page or other appropriate means) that any person, upon gaining electronic access to the material, which is the subject of a permission, shall see:

- a proper copyright notice, identifying the Rightsholder in whose name CCC has granted permission,
- a statement to the effect that such copy was made pursuant to permission,
- a statement identifying the class to which the material applies and notifying the reader that the material has been made available electronically solely for use in the class, and
- a statement to the effect that the material may not be further distributed to any person outside the class, whether by copying or by transmission and whether electronically or in paper form, and User must also ensure that such cover page or other means will print out in the event that the person accessing the material chooses to print out the material or any part thereof.

G) any permission granted shall expire at the end of the class and, absent some other form of authorization, User is thereupon required to delete the applicable material from any electronic storage or to block electronic access to the applicable material.

iv) Uses of separate portions of a Work, even if they are to be included in the same course material or the same university or college class, require separate permissions under the electronic course content pay-per-use Service. Unless otherwise provided in the Order Confirmation, any grant of rights to User is limited to use completed no later than the end of the academic term (or analogous period) as to which any particular permission is granted.

v) Books and Records; Right to Audit. As to each permission granted under the electronic course content Service, User shall maintain for at least four full calendar years books and records sufficient for CCC to determine the numbers of copies made by User under such permission. CCC and any representatives it may designate shall have the right to audit such books and records at any time during User's ordinary business hours, upon two days' prior notice. If any such audit shall determine that User shall have underpaid for, or underreported, any electronic copies used by three percent (3%) or more, then User shall bear all the costs of any such audit; otherwise, CCC shall bear the costs of any such audit. Any amount determined by such audit to have been underpaid by User shall immediately be paid to CCC by User, together with interest thereon at the rate of 10% per annum from the date such amount was originally due. The provisions of this paragraph shall survive the termination of this license for any reason.

c) ***Pay-Per-Use Permissions for Certain Reproductions (Academic photocopies for library reserves and interlibrary loan reporting) (Non-academic internal/external business uses and commercial document delivery).*** The License expressly excludes the uses listed in Section (c)(i)-(v) below (which must be subject to separate license from the applicable Rightsholder) for: academic photocopies for library reserves and interlibrary loan reporting; and non-academic internal/external business uses and commercial document delivery.

i) electronic storage of any reproduction (whether in plain-text, PDF, or any other format) other than on a transitory basis;

ii) the input of Works or reproductions thereof into any computerized database;

iii) reproduction of an entire Work (cover-to-cover copying) except where the Work is a single article;

iv) reproduction for resale to anyone other than a specific customer of User;

v) republication in any different form. Please obtain authorizations for these uses through other CCC services or directly from the rightsholder.

Any license granted is further limited as set forth in any restrictions included in the Order Confirmation and/or in these Terms.

d) ***Electronic Reproductions in Online Environments (Non-Academic-email, intranet, internet and extranet).*** For "electronic reproductions", which generally includes e-mail use (including instant messaging or other electronic transmission to a defined group of recipients) or posting on an intranet, extranet or Intranet site (including any display or performance incidental thereto), the following additional terms apply:

i) Unless otherwise set forth in the Order Confirmation, the License is limited to use completed within 30 days for any use on the Internet, 60 days for any use on an intranet or extranet and one year for any other use, all as measured from the "republication date" as identified in the Order Confirmation, if any, and otherwise from the date of the Order Confirmation.

ii) User may not make or permit any alterations to the Work, unless expressly set forth in the Order Confirmation (after request by User and approval by Rightsholder); provided, however, that a Work consisting of photographs or other still images not embedded in text may, if necessary, be resized, reformatted or have its resolution modified without additional express permission, and a Work consisting of audiovisual content may, if necessary, be "clipped" or reformatted for purposes of time or content management or ease of delivery (provided that any such resizing, reformatting, resolution modification or "clipping" does not alter the underlying editorial content or meaning of the Work used, and that the resulting material is used solely within the scope of, and in a manner consistent with, the particular License described in the Order Confirmation and the Terms.

15) **Miscellaneous.**

a) User acknowledges that CCC may, from time to time, make changes or additions to the Service or to the Terms, and that Rightsholder may make changes or additions to the Rightsholder Terms. Such updated Terms will replace the prior terms and conditions in the order workflow and shall be effective as to any subsequent Licenses but shall not apply to Licenses already granted and paid for under a prior set of terms.

b) Use of User-related information collected through the Service is governed by CCC's privacy policy, available online at www.copyright.com/about/privacy-policy/.

c) The License is personal to User. Therefore, User may not assign or transfer to any other person (whether a natural person or an organization of any kind) the License or any rights granted thereunder; provided, however, that, where applicable, User may assign such License in its entirety on written notice to CCC in the event of a transfer of all or substantially all of User's rights in any new material which includes the Work(s) licensed under this Service.

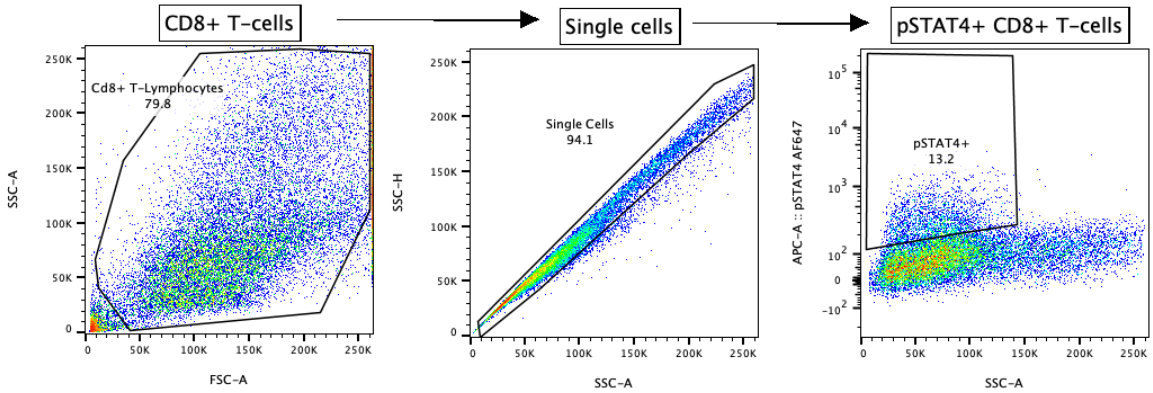
d) No amendment or waiver of any Terms is binding unless set forth in writing and signed by the appropriate parties, including, where applicable, the Rightsholder. The Rightsholder and CCC hereby object to any terms contained in any writing prepared by or on behalf of the User or its principals, employees, agents or affiliates and purporting to govern or otherwise relate to the License described in the Order Confirmation, which terms are in any way inconsistent with any Terms set forth in the Order Confirmation, and/or in CCC's standard operating procedures, whether such writing is prepared prior to, simultaneously with or subsequent to the Order Confirmation, and whether such writing appears on a copy of the Order Confirmation or in a separate instrument.

e) The License described in the Order Confirmation shall be governed by and construed under the law of the State of New York, USA, without regard to the principles thereof of conflicts of law. Any case, controversy, suit, action, or proceeding arising out of, in connection with, or related to such License shall be brought, at CCC's sole discretion, in any federal or state court located in the County of New York, State of New York, USA, or in any federal or state court whose geographical jurisdiction covers the location of the Rightsholder set forth in the Order Confirmation. The parties expressly submit to the personal jurisdiction and venue of each such federal or state court.

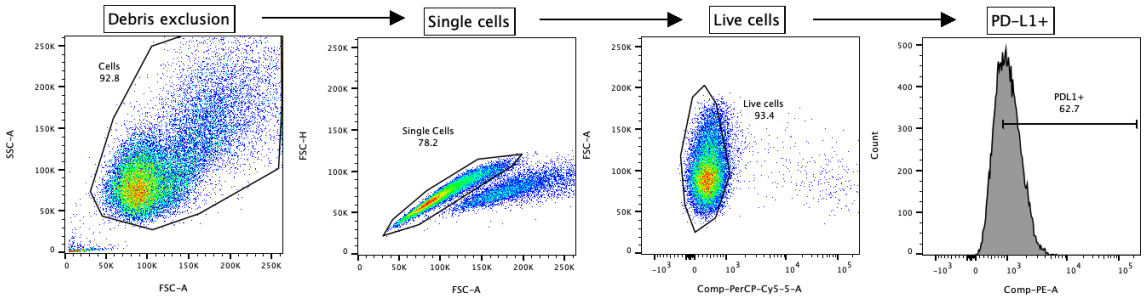
Privacy - Terms

Last updated October 2022

6.7 Gating strategy pSTAT4 experiment on CD8$^+$ T-cells

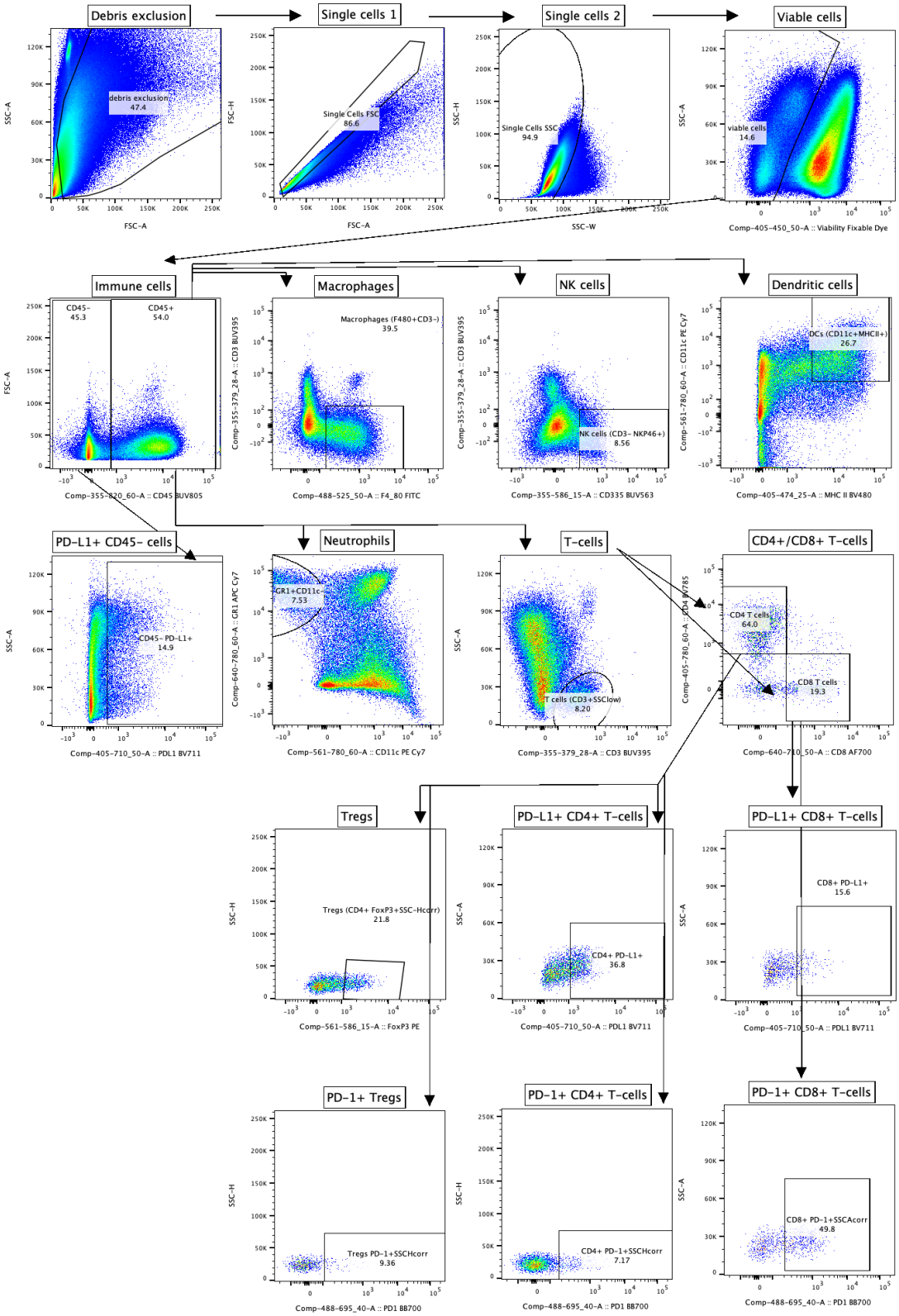


6.8 Gating strategy PD-L1 expression on PDAC cells following CBD-IFNγ treatment *in vitro*



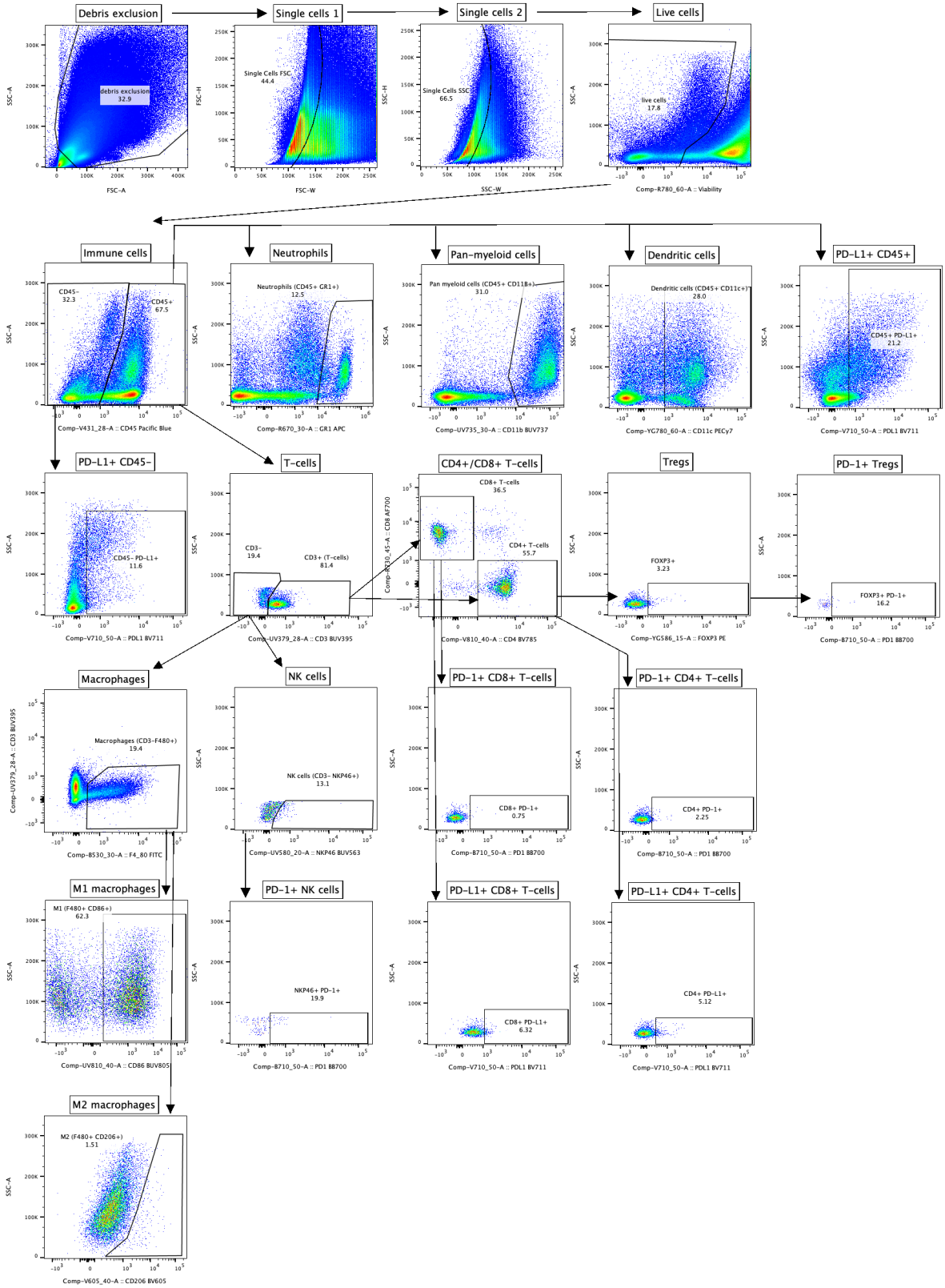
6.9 Gating strategy EMT6 intervention study 1

Applies to: Figure 3.9, Figure 3.10, Figure 3.11, Figure 3.12



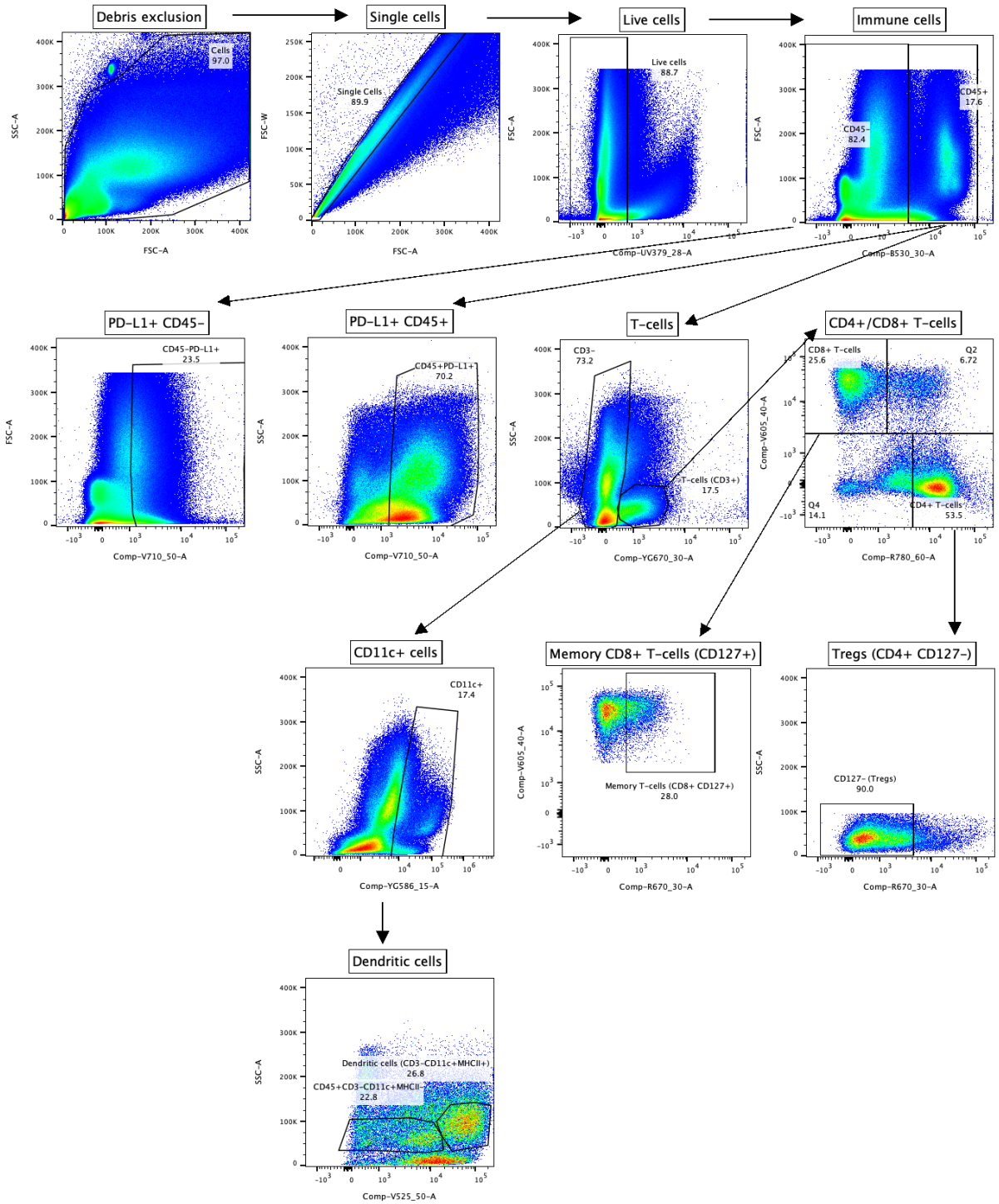
6.10 Gating strategy EMT6 intervention study 2

Applies to: Figure 3.15, Figure 3.16, Figure 3.17, Figure 3.18



6.11 Gating strategy 7947 CBD-IFNγ study

Applies to: Figure 5.6



Publications and awards

Papers:

- Herpels, M., et al. (2023). "The clinical terrain of immunotherapies in heterogeneous pancreatic cancer: unravelling challenges and opportunities." J Pathol 260(5): 533-550.

Abstracts and poster presentations:

- Oral presentation and poster presentation at the Cancer Research UK Convergence Science Centre Symposium 2024

- Herpels, M., et al. (2023). 1212 Bioengineered tumour-targeted interleukin-12 selectively cures murine triple-negative breast cancer (TNBC).
  Presented poster at SITC 2023, San Diego, United States

- Herpels, M., et al. (2022). "37P Synthetic tumour-infiltrating interleukin (IL)-12 for targeted and tolerable immunotherapy reduces metastasis in pancreatic cancer." Immuno-Oncology and Technology 16: 100142.
  Presented poster at ESMO Immuno-Oncology Congress 2022, Geneva, Switzerland

Awards:

- SITC Young Investigator Travel Award, 2023
- ESMO Merit Travel Grant, 2022
- Imperial College Graduate School Summer showcase, second prize, 2022